Balgacyclamides: Efforts towards total synthesis and applications into solving complex biological problems

by

Prathibha Kaushaki Desman

B.Sc., University of Colombo, Sri Lanka, 2011

AN ABSTRACT OF A DISSERTATION

submitted in partial fulfillment of the requirements for the degree

DOCTOR OF PHILOSOPHY

Department of Chemistry
College of Arts and Sciences

KANSAS STATE UNIVERSITY
Manhattan, Kansas

2020

Abstract

Balgacyclamides are a group of natural products isolated from freshwater cyanobacteria *Microcystis aeruginosa* EAWAG 251 Gademann and co-workers in 2014. They are macrocyclic polypeptides that can also be identified as cyanobactins. Three natural products that belongs to this family have been reported so far; namely balgacyclamide A-C. Balgacyclamide A and B have reported toxicity towards a chloroquine resistant strain of the malarial parasite *Plasmodium falciparum* K1 and possessed moderate cytotoxicity towards rat myoblasts with implied capability of penetration into lung and colon cancer cells. Given the interesting cellular penetration ability of balgacyclamides, our laboratory embarked on a journey for the first total synthesis of balgacyclamide A, and B in a convergent synthetic approach to access both the natural products in the same route. A synthetic route was established for accessing the two natural products and two other analogs using commercially available amino acids. Establishing the synthesis route for the two natural product analogs served as a model system for the synthetic route of the actual natural products. Due to the ability of balgacyclamides to penetrate into lung and colon cancer cells, it is envisioned to utilize these molecules to conjugate them with available anticancer drugs with the aim of lowering off-target side effects. Also, a small molecule library has been synthesized using an intermediate of balgacyclamide A, and B synthesis to study their ability to penetrate Gram-negative bacteria through porins. This study reveals many unprecedented properties of small molecules that aid penetration of molecules through porins; the most interesting finding being how the three-dimensional orientation of the molecules affect porin-mediated penetration of small molecules despite having approximately the same physicochemical properties.

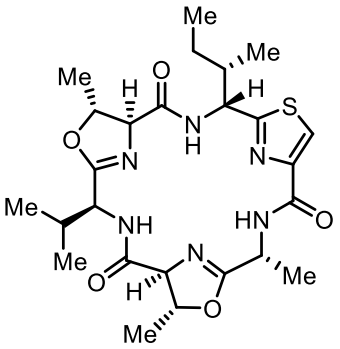

Balgacyclamide A

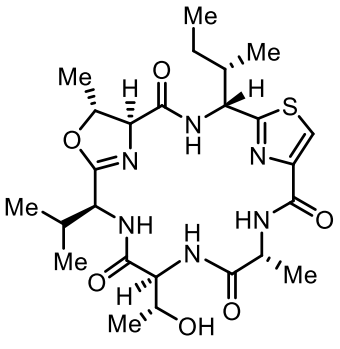

Balgacyclamide B

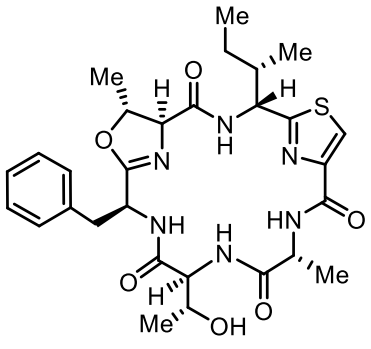

Balgacyclamide C

Balgacyclamides: Efforts towards total synthesis and applications into solving complex biological problems

by

Prathibha Kaushaki Desman

B.Sc., University of Colombo, 2011

A DISSERTATION

submitted in partial fulfillment of the requirements for the degree

DOCTOR OF PHILOSOPHY

Department of Chemistry
College of Arts and Sciences

KANSAS STATE UNIVERSITY
Manhattan, Kansas

2020

Approved by:

Major Professor
Dr. Ryan J. Rafferty

Copyright

Abstract

Balgacyclamides are a group of natural products isolated from freshwater cyanobacteria *Microcystis aeruginosa* EAWAG 251 Gademann and co-workers in 2014. They are macrocyclic polypeptides that can also be identified as cyanobactins. Three natural products that belongs to this family have been reported so far; namely balgacyclamide A-C. Balgacyclamide A and B have reported toxicity towards a chloroquine resistant strain of the malarial parasite *Plasmodium falciparum* K1 and possessed moderate cytotoxicity towards rat myoblasts with implied capability of penetration into lung and colon cancer cells. Given the interesting cellular penetration ability of balgacyclamides, our laboratory embarked on a journey for the first total synthesis of balgacyclamide A, and B in a convergent synthetic approach to access both the natural products in the same route. A synthetic route was established for accessing the two natural products and two other analogs using commercially available amino acids. Establishing the synthesis route for the two natural product analogs served as a model system for the synthetic route of the actual natural products. Due to the ability of balgacyclamides to penetrate into lung and colon cancer cells, it is envisioned to utilize these molecules to conjugate them with available anticancer drugs with the aim of lowering off-target side effects. Also, a small molecule library has been synthesized using an intermediate of balgacyclamide A, and B synthesis to study their ability to penetrate Gram-negative bacteria through porins. This study reveals many unprecedented properties of small molecules that aid penetration of molecules through porins; the most interesting finding being how the three-dimensional orientation of the molecules affect porin-mediated penetration of small molecules despite having approximately the same physicochemical properties (PCPs).

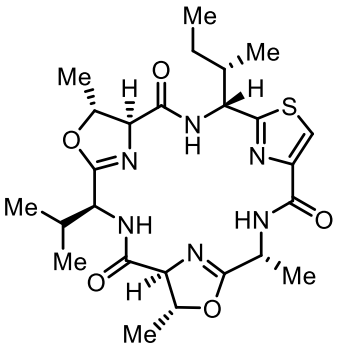

Balgacyclamide A

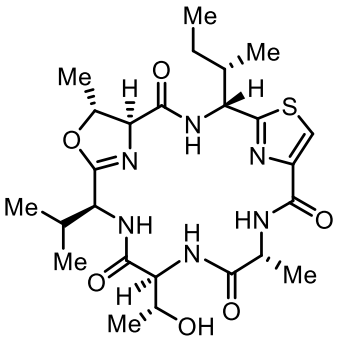

Balgacyclamide B

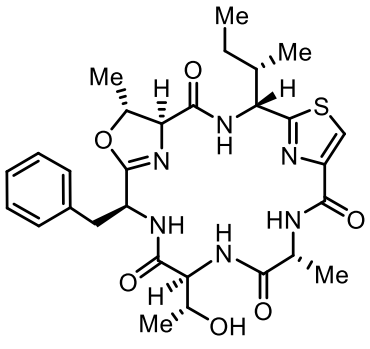

Balgacyclamide C

Table of Contents

List of Figures

List of Schemes

List of Tables

List of Abbreviations

Boc	tert-Butyloxycarbonyl
Boc_2O	Boc anhydride
BOPCl	Bis(2-oxo-3-oxazolidinyl)phosphinic chloride
Cbz	Carboxybenzyl
CD_3OD	Deuterated methanol
$CDCl_3$	Deuterated chloroform
CSL	Chemical Screening Library
DAST	Diethylaminosulfur trifluoride
DBU	1,8-Diazabicyclo[5.4.0]undec-7-ene
DCM/CH_2Cl_2	Dichloromethane/ methylene chloride
DEAD	Diethyl azodicarboxylate
DIPEA	Diisopropylethylamine
DMAP	4-Dimethylaminopyridine
EDC•HX	N-(3-dimethylaminopropyl)-N′-ethylcarbodiimide hydrohalide
Et_3N/TEA	Triethylamine
Et_3SiH	Triethylsilane
EtOAc	Ethyl acetate
EtOH	Ethanol
GNbac	Gram-Negative bacteria
GPbac	Gram-Positive bacteria
HBTU	Hexafluorophosphate Benzotriazole Tetramethyl Uronium

HOBt	1-Hydroxybenzotriazole hydrate
LPS	Lipopolysaccharide
MeOH	Methanol
NMR	Nuclear Magnetic Resonance
NP(s)	Natural products
PCP	Physicochemical Property
PG	Protecting group
PyBOP	Benzotriazol-1-yl-oxytripyrrolidinophosphonium hexafluorophosphate
RT	Room temperature
SAR	Structure–Activity Relationship
THF	Tetrahydrofuran

Acknowledgements

First and foremost, I would like to thank Dr. Ryan Rafferty, my Ph.D. advisor for being such an amazing PI. Dr. Rafferty, I have no words to explain what a blessing you have been in my life. You were a great teacher, mentor, and a wonderful person in general. You believed in me when I was falling and failing and encouraged me to get back up and run this race to reach the finish line victoriously. Thank you very much for being such a caring PI who constantly encourages me. You definitely have made me fall in love with organic chemistry and taught me to be a life-long learner.

I would like to acknowledge my committee members: Dr. Paul Smith, Dr. Jeffrey Comer, Dr. Santosh Aryal, and Dr. Duy Hua (former member), as well as Dr. Thu Nguyen (outside-chair). I am truly grateful for your guidance and support throughout my Ph.D. journey.

My heartfelt gratitude goes to all the current and past Rafferty lab members. All of you were such a blessing to me. I am so thankful to you for being so encouraging and loving group of people who made lab life enjoyable. You all will always have a special place in my heart as dear friends who helped me become a better person.

I would like to thank Kansas State University for giving me the opportunity to study and work for my Ph.D. And my special thanks go to the Department of Chemistry that became my home for the last five year. The faculty and staff have been really welcoming and created a very welcoming environment. I would especially like to acknowledge our Department Head, the organic faculty, Dr. Simon Sham who is our NMR director, Dr. Leila Maurman who is our former NMR director, Mr. Michael Hiton and Dr. Abhijeet Sinha who oversee teaching laboratories, for their support and guidance. I also thank Mr. Ron Jackson, Mr. Tobe Eggers, and our wonderful scientific glassblower Mr. James Hodgson for their technical support.

My deepest love and gratitude go to my loving parents: Mr. K.P. Desman (my father) and Mrs. K.D.C.A. Padmini (my mother). I will never have enough words to say thank you for the dedication both of you have towards me. I am so privileged to have you as my parents and whatever the success achieve in my life is based on what you raised me to be. Thank you very much for having my back during all the seasons of my life. And thank you for all the sacrifices you have done in your lives for me.

My sincere gratitude goes to all my teachers who taught me not only subject material, but also life. I would like to thank Rev. Sr. Hubert Marie and the teachers of Mary Immaculate convent, Tudella, Ja-Ela, Sri Lanka where I had my schooling from grade 1-13. I most fondly thank Mr. Susantha Palliyaguru, my chemistry teacher, who had the biggest impact on my life to choose chemistry as my career. Thank you, sir, for your commitment to teaching your students and laying down a firm foundation of chemistry fundamentals and basics with passion. And I would like to thank all the professors who taught me at University of Colombo, Sri Lanka, during my undergraduate program. Also, I would like to thank General Sir John Kotelawala Defense University, Sri Lanka where I worked, as its environment encouraged me to pursue my higher studies.

I would like to thank the endless list of my friends who were very supportive and cheered for during all the tough times, and my relatives who have helped me in many ways. A special thank goes to people involved with Bridges International, a campus ministry at K-State, and Faith Evangelical Free Church, for being my community, my support system, and feeding me spiritually during my 5 years in Manhattan.

My utmost respect goes to everyone who helped me in many ways, though I have missed many names here. Finally, according to my faith as a Christian I am so grateful to God for all the blessings in my life.

Dedication

To my loving parents, who gave me wings to fly and roots to come back to.

Chapter 1 - Introduction

1.1 Introduction

Disclosed herein are the efforts towards the total synthesis of balgacyclamide family of natural products (NPs); and synthetic analogs accessed en route. Emphasis will be given to optimizing the synthesis routes to access each identified fragment of the family members, their assembly in their linear system, and efforts at the macrocyclization to the final NPs. Scope of possible applications this family of NPs will also be explored. Apart from possible future applications of the final compounds, emphasis is given to utilizing an interesting intermediate of the synthesis to create a small molecule chemical screening library (CSL) for applications into biological investigations. The CSL assembled, consisting of derivatives of this intermediate, was employed to probe the effects of PCPs and their orientation upon the penetration of into Gram-Negative bacteria (GNbac) also will be discussed.

1.2 NPs in Drug Discovery

NPs have been used across cultures throughout the world to remedy ailments for thousands of years. Most NPs are secondary metabolites produced by biological organisms to perform specific secondary function beyond survival, such as: cell communication, self-defense, and stress responses.[1,2] While each of these are of importance to the organism, they can be exploited for therapeutic properties in mammals. Ayurveda (a system of traditional Indian medicine), and traditional Chinese medicine are great examples of medicine modalities alive to date that heavily use herbal medications to harness the medicinal properties of NPs found in various natural sources. With the advancement of science, and the emergence of Western medicine, we have leaned

towards a more regulated use of medicine that comes to the marked as approved therapy after rigorous testing. However, NPs still play a major role in drug discovery process.

According to the most recent statistics on approved drugs abstracted from 1981-2019 (Figure 1), 3.8% of them are unaltered NPs, 18.9% are NP derivatives, 3.2% are synthetic drugs with a NP pharmacophore, and 11.5% are synthetic drugs that are NP mimics.[3] It can also be said that the role of NPs in drug discovery are essential and have been the corner stone in therapeutic agent discovery. Therefore, not only isolating and identifying NPs from natural sources but also total synthesis of NPs can contribute immensely towards the drug discovery process.

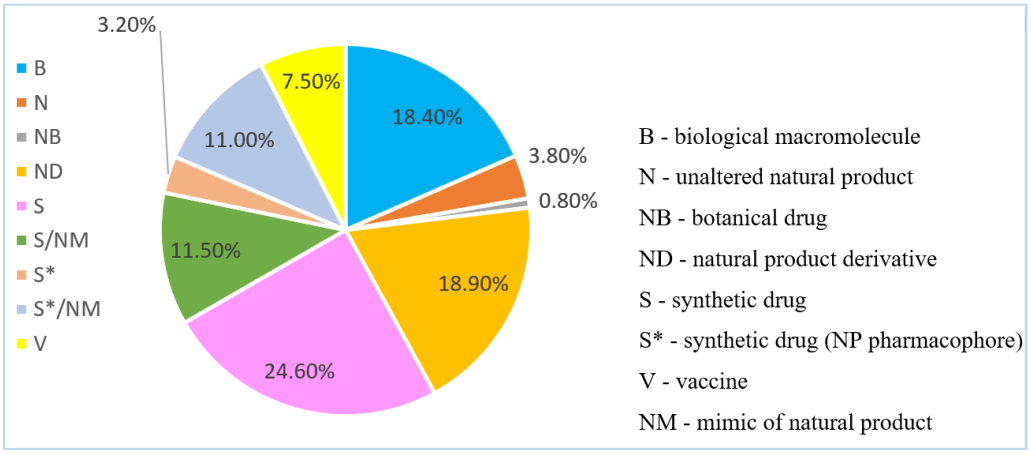

Figure 1: New drugs approved from 1981 to 2019

Few examples of approved drugs that are NPs are illustrated in Figure 2. Paclitaxel (Taxol) is an anticancer drug isolated from pacific yew tree. Digoxin is a cardiac glycoside isolated from foxglove plant and is used to treat various cardiac conditions. Codeine and morphine isolated from the sap of poppy plant are strong analgesics. Quinine that is isolated from the bark of cinchona tree is a widely used antimalarial drug. Vincristine isolated from rosy periwinkle is an anticancer drug, and atropine isolated from belladonna plant is an anticholinergic drug. In addition to NPs

themselves the synthetic intermediates accessed within the total synthesis routes also can act as valuable tools in understanding and solving complex biological problems.

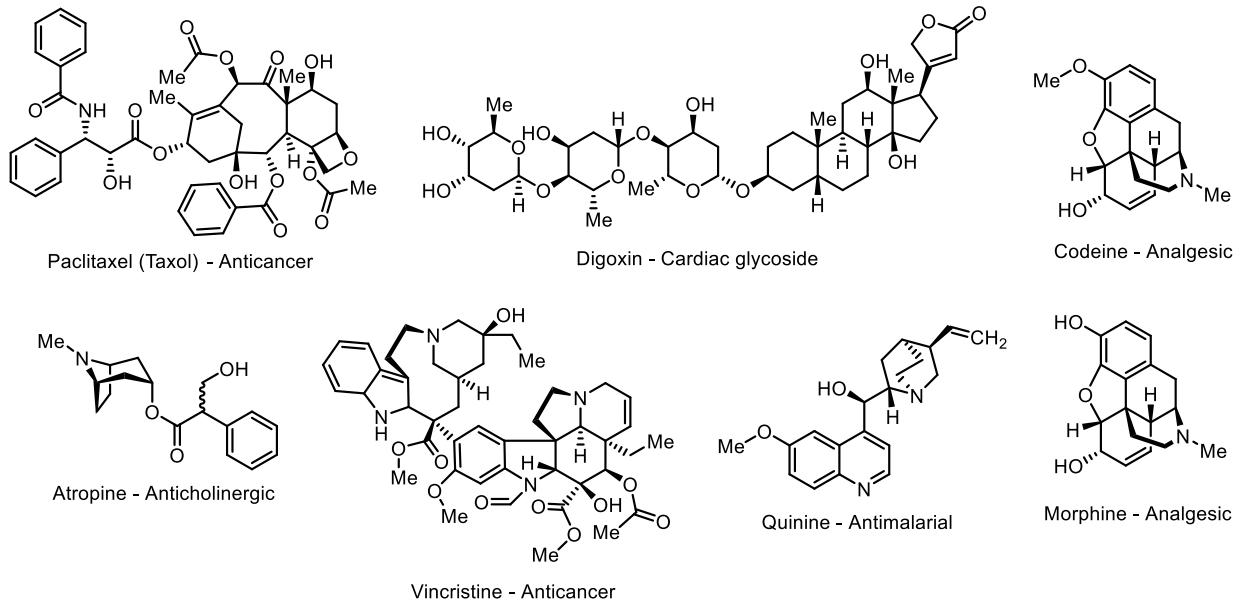

Figure 2: Examples of approved drugs that are NPs

1.3 Balgacyclamides

1.3.1 Cyanobactins:

Balgacyclamides are a group of NPs identified as cyanobactins,[4] which are a group of cyclic peptides produced by cyanobacteria where the peptides have undergone further post-translational modifications;[5,6] a few examples of cyanobactins are shown in Figure 3.[7,8,9,10,11] These post-translational modifications involved with the formation of cyanobactins include, but not limited to: heterocyclizations, prenylations, and oxidations of amino acids.[12] Most of them are suggested to be biosynthesized via ribosomal pathways, while a minority could be synthesized non-ribosomally as well. During post-translational modifications heterocyclases mediate oxazoline/oxazole (color-coded in green in Figure 3) as well as thiazoline/thiazole (color-coded in purple in Figure 3) formations, and prenyltransferases called F enzymes mediate prenylations (prenyls: color-coded in yellow in Figure 3).[13] All the isolated cyanobactins have not shown

bioactivity for their tested aspects. However, there are many cyanobactins that have possessed metal chelation ability, anticancer activity, multidrug resistance reversing ability, antimalarial activity, as well as ability to block P-glycoproteins and potassium channels.[12] However, while this class of NPs possesses interesting biological effects, the natural role(s) of cyanobactins remain unclear to date.[6] Apart from cyanobacteria, cyanobactins are found in other marine organisms as well (e.g., ascidians, sponges and mollusks).[6] With the recent expansion of explorations into marine sources for NPs, many isolated cyanobactins are being reported with interesting biological activity. That increases the possibility of discovering more cyanobactins as well. One such example of a group of cyanobactins from a marine source is the focus of this thesis, which are the balgacyclamides.

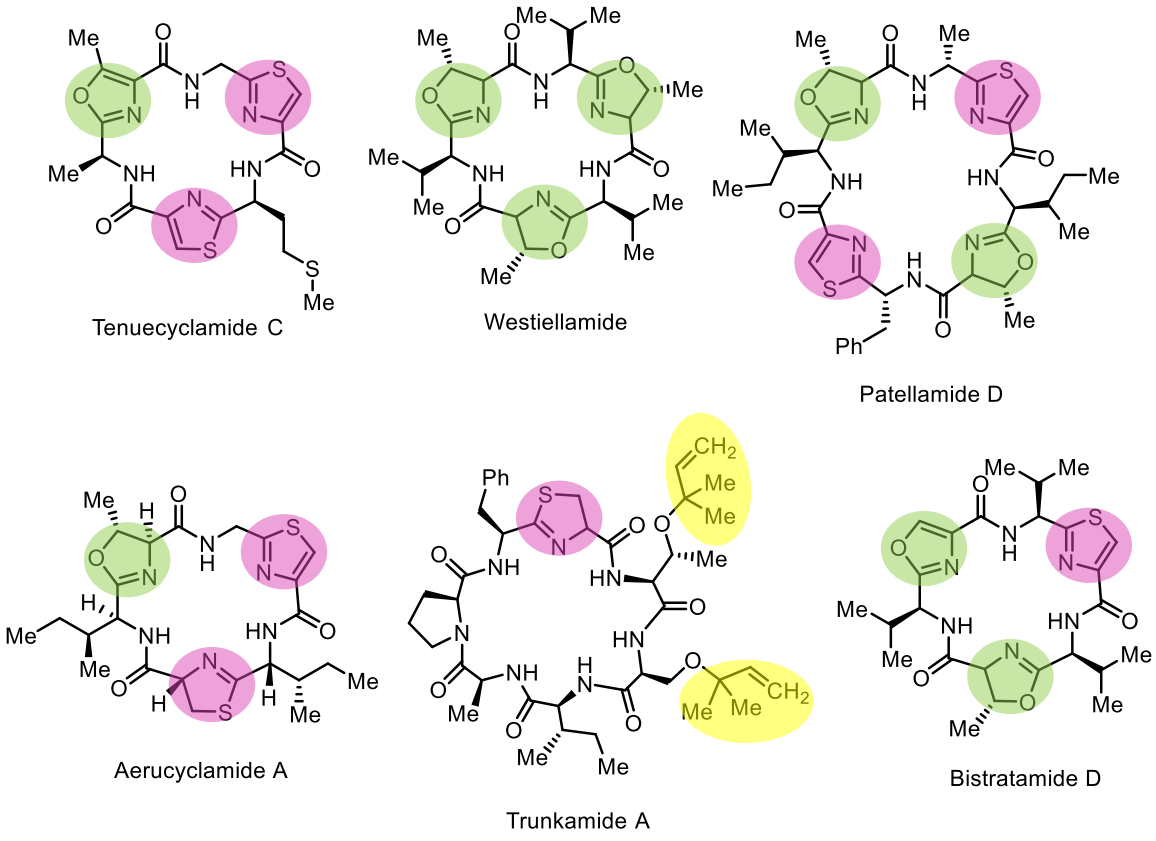

Figure 3: Few examples of reported cyanobactins

1.3.2 Isolation and Structure Elucidation of Balgacyclamides

Balgacyclamides are a group of cyclic peptides isolated from freshwater cyanobacteria *Microcystis aeruginosa* EAWAG 251. The isolation of balgacyclamides A, B, and C (Figure 4) were reported by Gademann and co-workers in 2014.[4] These macrocyclic peptides contain oxazoline and thiazole rings as key characteristic structural motifs of cyanobactins. Structural comparison of the three balgacyclamides revealed some interesting differences and similarities. Both balgacyclamide A and B share the same core except for the difference of having an oxazoline (color-coded in purple in Figure 4) versus an open dipeptide (color-coded in orange in Figure 4), respectively. Balgacyclamide B and C share the same open dipeptide with the rest of the similar structure except for having an isopropyl (color-coded in gray in Figure 4) in balgacyclamide B versus a benzyl group (color-coded in blue in Figure 4) in balgacyclamide C. As reported by the isolation chemists, the structure elucidation process of balgacyclamides has been a challenging task due to the low isolation yields. For balgacyclamide A, B, and C, the isolation yields have been as low as 0.55 mg, 0.15 mg, and 0.80 mg respectively, per 15 L of the cynobacterium culture. [4]

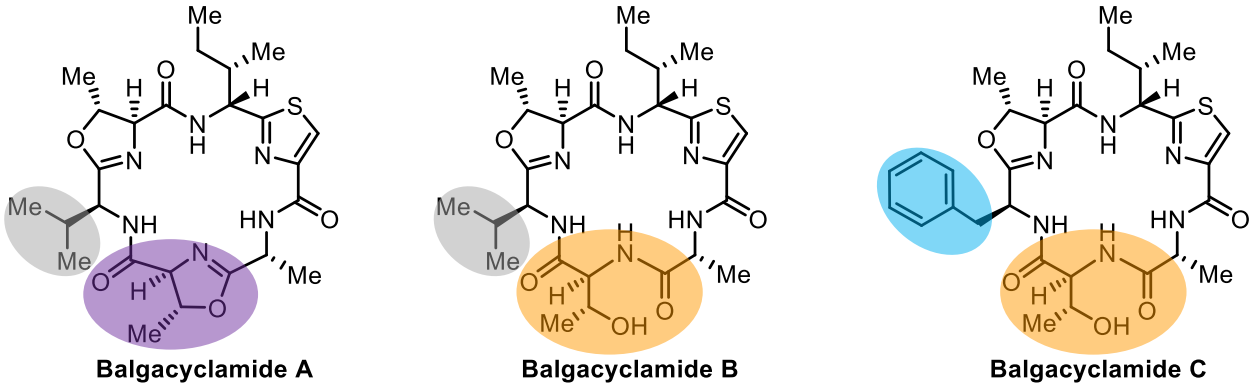

Figure 4: Balgacyclamide family isolated in 2014 from *Microcystis aeruginosa* EAWAG 251

Microcystis aeruginosa EAWAG 251, of which the balgacyclamide family of NPs were isolated, was obtained by the isolation chemists from Swiss Federal Institute of Aquatic Science and Technology. Multiple methanolic extractions were performed on the cyanobacterium cultures and

the extracts were lyophilized to obtain a dry powder. The resultant powder was reconstituted into an 80% methanolic solution and separated using a C_{18} SPE column and multiple runs on a C_{18} RP-HPLC. Isolated compounds were extensively analyzed using NMR (^{1}H, ^{13}C, 2D), IR, and mass spectrometry with aid from ozonolysis, hydrolysis, and Marfey's analysis on the compounds.

1.3.3 Bioactivity of Balgacyclamides: Need for Total Synthesis of Balgacyclamides and Scope for Drug Development

Balgacyclamide A and B have reported toxicity towards a chloroquine resistant strain of the malarial parasite *Plasmodium falciparum* K1 with reported IC_{50} values of 9.0 and 8.2 μM, respectively. Antiparasitic activities of balgacyclamide A and B against few other parasites also have been tested (Table 1). It is reported that both balgacyclamide A and B have moderate toxicity towards *Trypanosoma brucei*, and balgacyclamide B has moderate toxicity towards *Leishmania donovani*. When balgacyclamide A and B are compared, there is no significant difference in their biological activities. It implies that the presence of an oxazoline ring (color-code in purple in Figure 4) in balgacyclamide A compared to having an open peptide (color-code in orange in Figure 4) has not affected the biological activity of the two molecules. This family of compounds have possessed comparable IC_{50} values to other cyanobactin families such as venturamides and aerucyclmides.

Table 1:Antiparacytic activity of balgacyclamide A & B (IC_{50} values in μM)

	P. f.	*T. b. rhod.*	*T. cruz.*	*L. don.*
Balgacyclamide A	9.0	59	>150	>150
Balgacyclamide B	8.2	51	>150	28

P. f. - *Plasmodium falciparum* K1; *T. b. rhod.*: - *Trypanosoma brucei rhodesiens* STIB 900; *T. cruz.* - *Trypanosoma cruzi* Tulahuen C4; *L. don.* - *Leishmania donovani* MHOM-ET-67/L82

Interestingly, balgacyclamides were also shown to possess penetration into lung and colon cancer cells. The ability to penetrate to lung and colon cancer cells can be a very important property of these molecules as this property could potentially allow balgacyclamides to be used as a drug delivery vehicle to deliver anticancer drugs to target cells selectively. When most of the currently available anticancer drugs are considered, they are plagued with unselective toxicity as they penetrate to non-cancerous cells as well as cancerous cells and cause off target cytotoxicity. For example, commonly used anticancer drugs paclitaxel and doxorubicin cause side effects such as loss of blood count, nausea, vomiting, loss of appetite, hair loss, and even death. Our lab is interested in exploring 6-thiopurine (6TP), mainly used to treat acute lymphocytic leukemia. However, 6TP has many side effects, with one of the most severe being hepatotoxicity leading to jaundice. Therefore, drug delivery systems can be of great use to selectively deliver these potent drugs to their targets and get their maximum benefit. One such example would be carbohydrate-conjugated anticancer drugs that uses Warburg effect to sneak into cancer cells more rapidly than non-cancerous cells. Potential of using balgacyclamides for such purposes will be further discussed later.

1.4 Small Molecule Libraries Based on NPs to Facilitate the Process of Drug Discovery

While developing a total synthesis route to a NP does contribute to the advancement of organic synthetic methodology, it also provides a robust, scalable, and reliable method in accessing biologically active compounds. Total synthesis of NPs allows further exploration into the NPs, through SAR analysis of the derivatized NPs which can lead to small molecules with interesting biological properties useful in drug discovery. The Hergenrother group has sown the applications of derivatizing commercially available NPs for the construction of small CSLs which can be used

in the drug discovery process (Figure 5-A).[14] However, when the final NP is modified, most of the time the innate bioactivity of the parent NP does not change though its potency may change. Therefore, our laboratory focuses on constructing small molecule libraries from the intermediates of total synthesis route as well without constraining derivatization to the final NP (Figure 5-B). We envision that this method may allow us to discover small molecules that have different biological activities compared to the parent NP.

Up until the 1980's the role of NPs in drug discovery was nearly unmatched, however, in the 80's and the advancement of robotics in the drug discovery process a future "pitfall" in the field of drug discovery was born.[15] High-throughput screening (HTS), born in this era, is a method in which a collection of compounds, stored in cell culture plates ranging from 48 to 1536 wells per plate, could be screening in a rapid fashion for the discovery of new drug lead scaffold/therapeutic discovery or in the investigations into other biological pursuits; such as transport across complex biological barriers.[16,17] Prior to the discovery of HTS, screening collections were primarily populated in NPs and/or extracts from natural sources. With the enhanced speed of HTS, the need for the population of screening plates was a large issue in the late 1980's to present day.

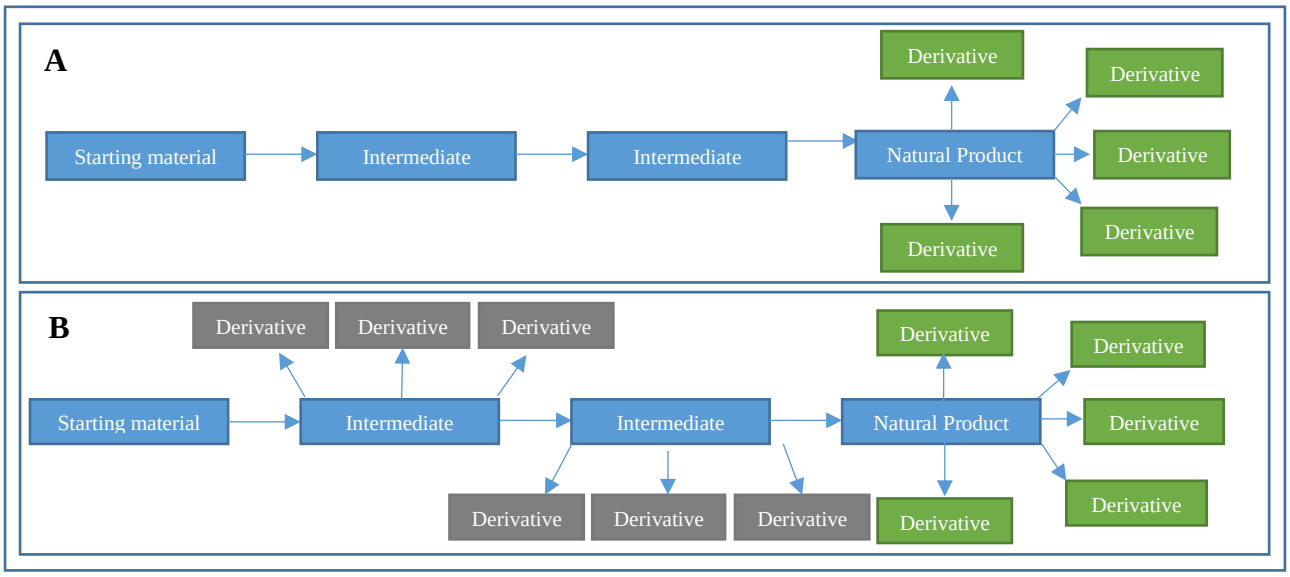

Figure 5: (A) Derivatizing only the final NP. (B) Derivatizing the final NP as well as other complex intermediates of the synthesis route

While NPs remain the best choice for the population of CSL collections, the discovery of new potent NPs has been on the decline over the past decade. Given this, along with the need to populate CSL plates, a solution was desperately needed. CSL plates were then populated with semi-synthetic NP moieties, marginal analog NPs that were constructed, other small molecules from failed total synthesis routes, and other total synthesis inspired compounds. However, this did not solve the population problem, as such, the use of sp^2-hydridized carbon-carbon bond form was employed; such as Suzuki, Stille and other organometallic reactions. In these efforts in the mid to late 1990's hundreds of thousands of small compounds were accessed via this coupling strategy. This strategy has continued, and one of the biggest CSL sources on the market today are those sold by ChemBridge, whose libraries are primarily synthesized via a platform-based synthesis. In platform-based synthesis, a large number of different molecules can be synthesized in a short period of time using automated methods.[18] In this, the libraries are composed of mainly small molecules that are flat (as evaluated by the percentage/fraction of sp^3-hybridized atoms in the

compound) and lacking a large percentage of stereocenters. Multiple drugs have been discovered and approved by the FDA employing the ChemBridge library. A large percentage of these drugs act as kinase inhibitors, and also cause many off target side effects. Kinases are very common enzymes that play vital roles in cell growth and metabolism, though the overexpression of kinases can be observed in some disease conditions such as cancer. Therefore, the inhibition of kinases can cause various side effects due to their inhibition of undesired targets. Therefore, discovering bioactive molecules with higher degree of complexity is crucial in drug discovery research to have higher efficiency with lower side effects. Quantifying molecular complexity is no easy task and has been done in a variety of means. One such metric to assess molecular complexity can be performed by assessment of the percentage/fraction of sp^3 hybridized carbons (Fsp^3) and the number of stereo centers. Together, Fsp^3 and the number of stereocenters can be an indicator of three-dimensional shape of molecules.[19] In additional to molecular complexity, lipophilicity is also another major point of consideration for library design. Lipophilicity is commonly quantified by cLogP, which explains the absorption and the permeation of the molecule.[20] The complexity and the lipophilicity of molecules directly affect the probability of finding drug candidates, which have higher potency and selectivity towards a particular protein target. Therefore, screening libraries with higher Fsp^3 /stereo centers and lower cLogP values have higher probability of finding drug like molecules. Small molecules in Chembridge library have the average Fsp^3 of 0.23, whereas the average Fsp^3 of FDA approved drugs is 0.47 (Figure 6-A). The average number of stereocenters in FDA approved drugs and the Chembridge library are 4.94 and 0.24, respectively (Figure 6-B).[21] ChemBridge has been used to discover most of the compounds found in the FDA. However, Fsp^3 of the large percentage of molecules having antibacterial and anticancer activities is significantly higher than the Fsp^3 of the molecules in ChemBridge library (Figure 6-C). Moreover, the number of stereocenters of molecules having anticancer and antibacterial activities is significantly higher

than that of ChemBridge library (Figure 6-D). This means that there is a gap (shown in green boxes) in ChemBridge library that needs to be filled with molecules with higher degree of complexity. Therefore, it is beneficial to construct small molecule screening libraries with higher Fsp^3 and higher number of stereocenters to increase the probability of discovering molecules with drug like properties.

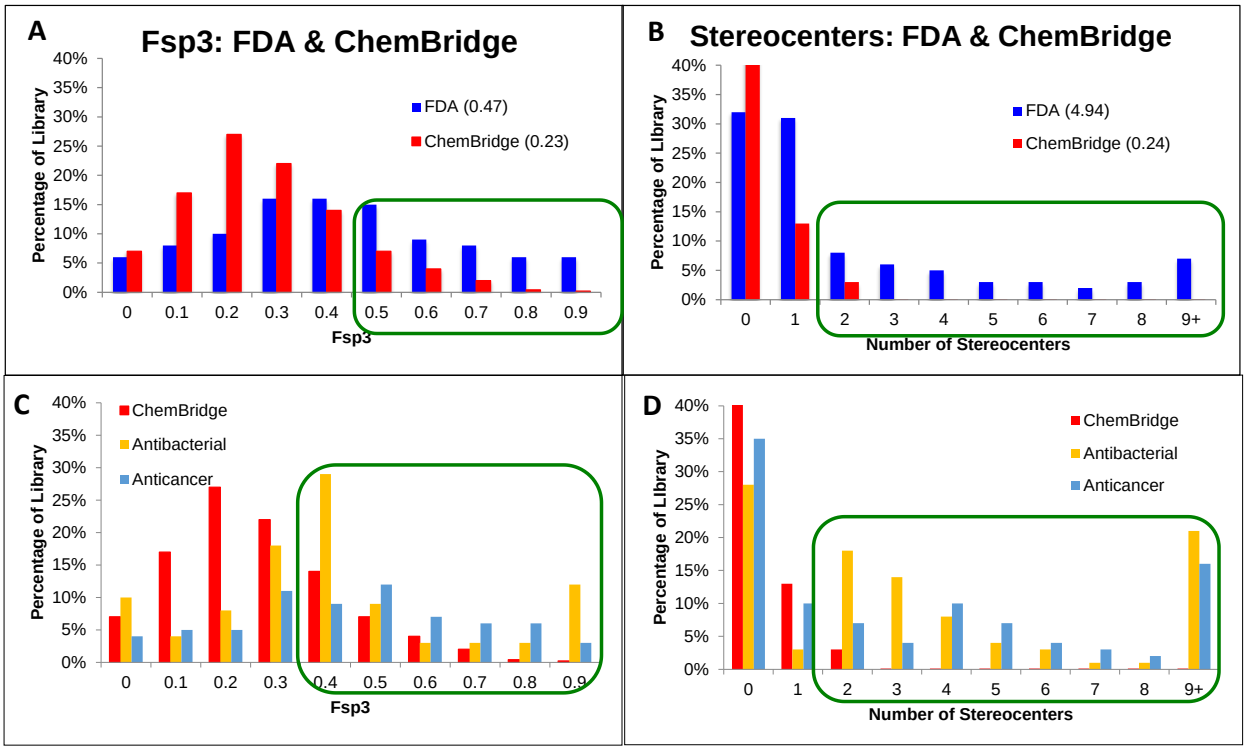

Figure 6: Fsp3 and Stereocenters of Small Molecules in ChemBridge Library[14]

To overcome the problem of the lack of structural complexity of the commercially available screening libraries, there should be more NPs and NP-like molecules that are more drug-like employed in the screening libraries. Also, such screening libraries could be used not only for direct screening to finds hits in drug discovery, but also, they can be employed in investigating different biological problems. For example, investigating the PCPs of molecules that could penetrate complex barriers such as the blood-brain-barrier, or GNbac cell wall. Complex molecules that are or would mimic NPs could be exploited extensively to systematically analyze such properties. As

such, our laboratory focuses on utilizing small molecule libraries based on NPs and intermediates of NPs to investigate small molecular penetration through GNbac cell wall through porin-mediated transport.

1.5 Porin-Mediated Small Molecule Transportation into GNbac

1.5.1 Bacterial Infections and GNbac

Bacterial and viral infections have caused epidemics and pandemics throughout the history that have costed millions of lives and fear of death for the rest of the world who survived. For example, currently we are dealing with COVID-19 caused by the novel corona virus SARS-CoV-2, and bacterial pandemics, such as the cholera and bubonic plague have consumed thousands of lives in the history of mankind. Antibiotics have saved an unimaginable number of lives from bacterial infections since the discovery of penicillin. Currently, hundreds of different antibiotics that belong to various chemical classes with different modes of action have come into the market as approved drugs. Though these antibiotics serve to fight and inhibit bacteria, emergence of bacterial resistance to the available antibiotics poses barriers for treating bacterial infections.[22,23]

Antibiotic resistance is caused when bacterial strains mutate and create mechanisms that negate or prevent antibacterial agents from elucidating their action. Such examples are increasing the number of efflux pumps in the cell membrane, possessing enzymes to hydrolyze antibiotics or altering the receptors.[24,25] The main cause of antibiotic resistance development is the irrational use of antibiotics. When a bacterial strain becomes resistant to one antibiotic it might be resistant to all the antibiotics that go after the same target as well. Current statistics alarm us of emergence of bacterial infections to be a leading cause of death in the future.[26] With all these, it is evident that there is a high demand for novel antibiotics that can combat bacteria that are resistant to currently available antibiotics. Despite this enormous demand, the number of antibiotics that comes to the

market has drastically decreased over the last few decades (Figure 7)[27] and all the major pharmaceutical companies have shut down their antibiotic research arms, leaving the discovery of novel antibiotics to the academic research groups.

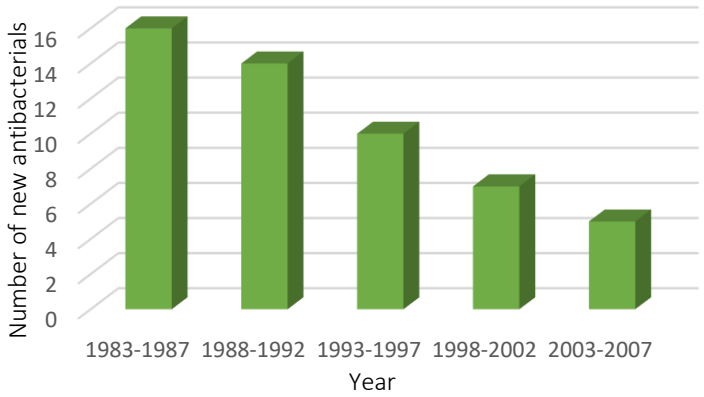

Figure 7: New systemic antibacterials approved by the US FDA

Antibiotics that are currently available have various different mechanisms of action and act upon various targets that are on the cell wall as well as on the targets in the bacterial cytoplasm. Most antibiotics need to penetrate through the cell wall into the bacterial cytoplasm to be effective. Hence, understanding the nature of the bacterial cell wall is essential in developing molecules with antibacterial properties. Also, mechanisms that allow penetration of small molecules through bacterial cell wall as well as the PCPs and characteristics of the small molecules that could penetrate bacteria need to be understood well. Therefore, key features of bacterial cell wall structure and mechanisms of small molecular penetration through it will be discussed herein.

The structural differences (Figure 8 and 9) between GNbac and Gram-Positive bacteria (GPbac), specifically in their outer membrane comparison allows for unique and different mechanism of action of resistance towards antibiotics. The evolution of GNbac has resulted in the formation of one of the most complex biological barriers that efficiently prevents the accumulation of foreign substances in the cytoplasm and periplasm (Figure 9).[28] The dual membrane system, 35-40 nm

wide, is responsible for this remarkably restrictive characteristic due to the outer membrane's composition and its ability to remove foreign substances from the interior efficiently and rapidly. Presence of an additional outer membrane acts as the main barrier for molecular penetration. It is the reason why many of the antibiotics that act upon intra-cellular targets are inherently inactive against GNbac due to their inability to reach those targets. The outer membrane of GNbac is composed of an unusual saturated lipopolysaccharide (LPS) layer [29, 30] composed of metal binding motifs[31] and multiple fatty acids chains per unit. As such, these components of the LPS make the GNbac less fluid-like,[32] and as such restrict the rate of movement of molecules to one-fiftieth to one-hundredth of that of simple membranes (phospholipid bilayers). Transport via LPS destabilization can only be accomplished via cation ion removal, an approach not commonly seen as feasible. Given the highly restrictive nature of the outer membrane, the movement of essential nutrients is governed by specific transporters that allow passage into the periplasm, where passive diffusion across the inner membrane can occur. To allow the movement of other nutrients, given that there are not specific transports for all, porin channels are present in the outer membrane to allow self-promoted uptake.[33]

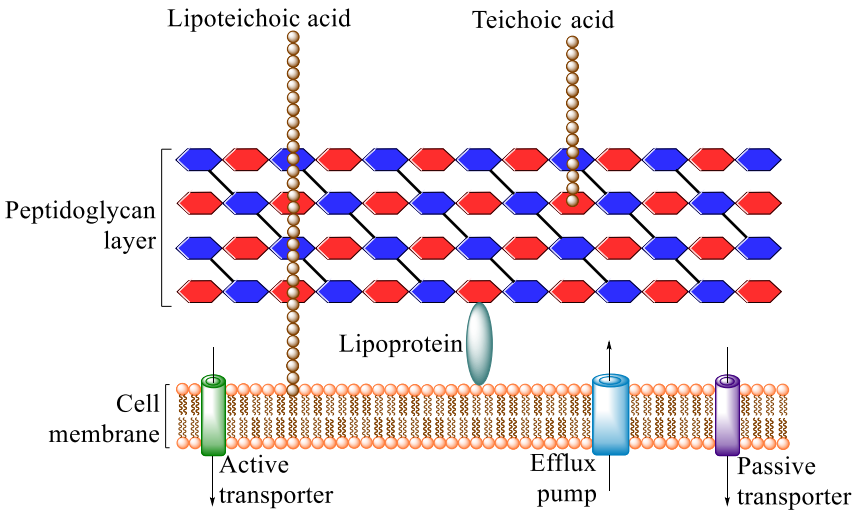

Figure 8: A schematic representation of GPbac cell wall

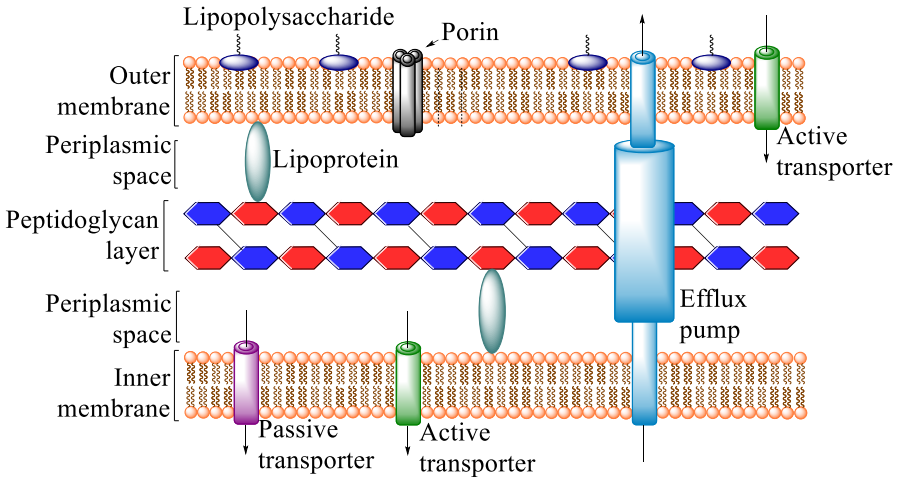

Figure 9: A schematic representation of GNbac cell wall

On the other hand, when foreign substances do gain access to the cytoplasm or periplasmic space of GNbac, they are efficiently and rapidly removed by efflux pumps.[29,30] These multi-component efflux pumps remove not only foreign substances from the cytoplasm, but also from within the inner membrane and periplasm environments. This multi-stage removal of said compounds such as drugs or probes greatly hinders their accumulation within the cytoplasm, and thereby limits their ability to elicit their designed and intended action within GNbac. Furthermore, single component efflux transporters are present within the inner membrane, which rapidly remove compounds to the periplasm. The highly restrictive barrier of entrance to GNbac in combination with its efficient efflux capabilities makes the transport and accumulation of foreign substances arduous. Most antibiotics fail to reach a minimum therapeutic concentration within GNbac due to their rapid efflux. Therefore, there is great need for the development of strategies and platforms that can allow the movement of desired substances via porins to allow for an increase in accumulation of said substances, which have a greater half-life within the GNbac to elicit any biological effect. To accomplish this, understanding how PCPs effect porin-mediated transport is essential in the early stages of solving this complex, and long-lasting problem.

1.5.2 Porin Channels

Porins are transmembrane proteins found in the outer membrane of the GNbac. They are relatively narrow water-filled β-barrel transverse channels where the structures are composed of β-strands and β-sheets in an antiparallel fashion (Figure 10).[33,34] The interior of porins are highly charged and provide a restrictive environment for compound passage governed by PCPs. Porins exist in a trimeric state on the outer membrane of the GNbac. It is suggested that the trimeric structure makes the porin structures more stable, but the monomeric units work independently in their passive transporter function.[35] Though there are some porins that are dedicated to transport specific molecules, the majority of the porins are non-specific transporters or general diffusion porins. While there is a number of structurally different types of these general diffusion porins, OmpF and OmpC porins can be considered as more highly abundant than others.[36]

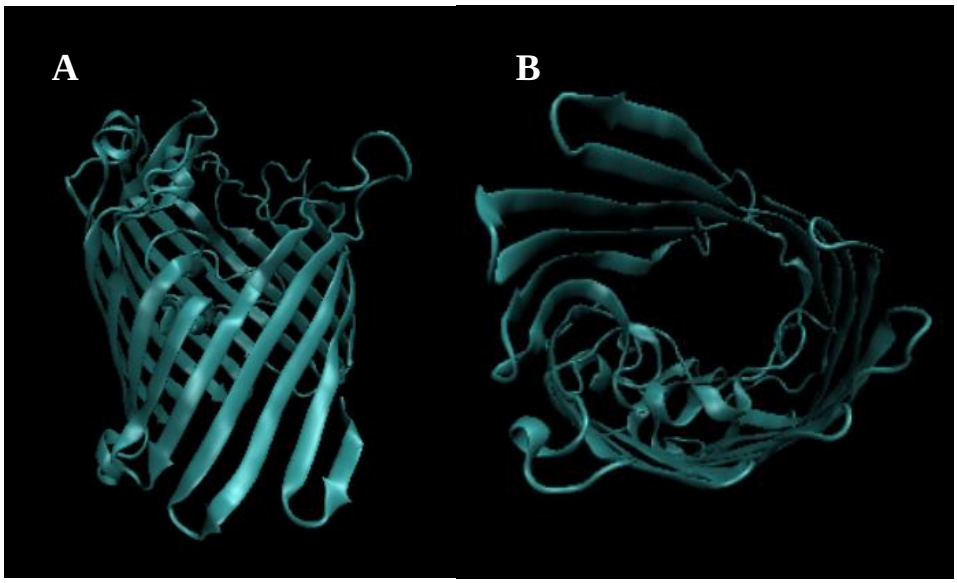

Figure 10: OmpF porin of *Escherichia coli* K-12 crystal structure (2OMF) visualized by VMD software. A: Side view, B: Top view.

Though the exact mechanism of how porins control the molecule entry through in core is unknown, several findings suggest that their interior charges as well as shape highly contribute towards this

controlled permeation. When a porin's structure is considered, its interior can be explained as a somewhat hourglass shape[37] (Figure 11). There is a ~35 amino acid long chain forming a loop inside that forms a constricted area in the inner pore of the porins.[37] It is a negatively charged loop that extends over the top of the barrel and interior walls that are positively charged. This constriction zone brings down the diameter of the porins to around 6.5-7 Å from 15 Å in OmpF. Presence of this constricted region plays a major role in limiting the molecular diffusion through porins. When the interior charge of the porin channel is considered, the residues in the loop creating the constricted region are negatively charged and lie adjacent to the positively charged residues in the non-constricted region.[33, 35] This alternating charge arrangement can be an interesting feature of the porins that needs further attention and understanding so that such knowledge can be used in designing molecules that could interact and are transported through porins.

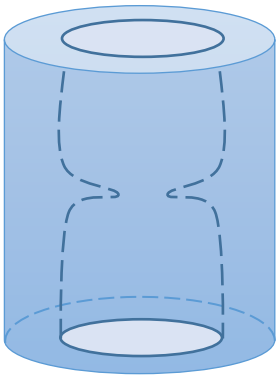

Figure 11: A schematic representation of the porin *β*-barrel being restricted due to interior hourglass shape

1.5.3 PCPs of Molecules Penetrating Porins

Several patterns have been identified regarding the PCPs of molecules that can penetrate GNbac.[38] Researchers have carried out theoretical studies to formulate scoring functions to predict permeability of molecules through porin channels as well.[39,40] However, an ultimate model that

could predict the ability of a molecule to permeate into GNbac is yet to be derived. Systematic studies carried out analyzing different properties associated with the currently available antibiotics show that Lipinski's rules do not simply apply for antibiotics molecules, especially ones against GNbac.[38] Porins tend to be more responsive towards polar molecules owing to the charged interior they have, especially positively charged molecules. It is also reported that when the molecules are more lipophilic, they tend to be easily pumped out by the efflux pumps, further reducing the concentration inside the bacteria. Studies show that size is one of the key criteria that decides a molecule's fate across porins, and molecules have to be less than 600 Da to be able to do that.[41,38] How different researchers are attempting to overcome barriers in porin-mediated transportation by further studying and manipulating PCPs in the molecules will be further discussed in Chapter 2.

Chapter 2 - Previous Work

2.1 Chemistry Related to Synthesis of NPs Related to Balgacyclamides

To date, none of the balgacyclamide family members (A, B, and C) have been synthetically accessed. However, several structurally related macrocyclic NPs, also isolated from cyanobacteria, have been synthetically accessed. These routes provide critical insight and outline synthetic feasibility into the construction of oxazoline, oxazole, and thiazole based NPs. Several examples of this class of NPs are shown in Figure 12. Given the structural similarities of aerucyclamide B, dendroamide A, and bistratamide D to the balgacyclamide family further discussion of these total synthesis's will be presented herein.

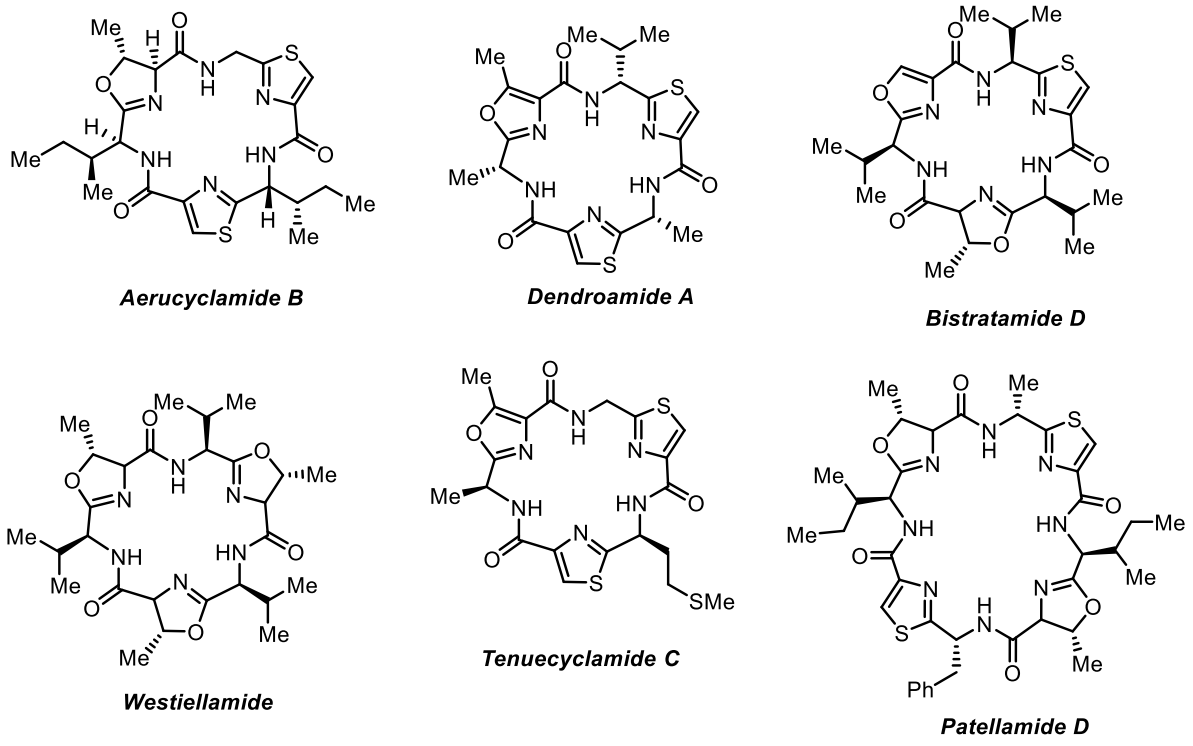

Figure 12: Molecules related to balgacyclamides that have been synthetically accessed.

2.1.1 Total Synthesis of Aerucyclamide B

Aerucyclamide B was synthesized by Serra and co-workers in 2013 with a 9% overall yield over 14-synthetic steps.[42] Their route accessed the NP in a late stage oxazoline cyclization upon **1** with DAST (Figure 13). Construction of **1** was achieved through the coupling of thiazoles **2** and **3** and dipeptide **4**. This route highlights peptide coupling reactions, oxazoline and thiazole ring formation with the aid of DAST, thioester formation from the ring opening of oxazolines with $H_2S_{(g)}$ to access the thiazoline, with subsequent aromatization to the corresponding thiazole.

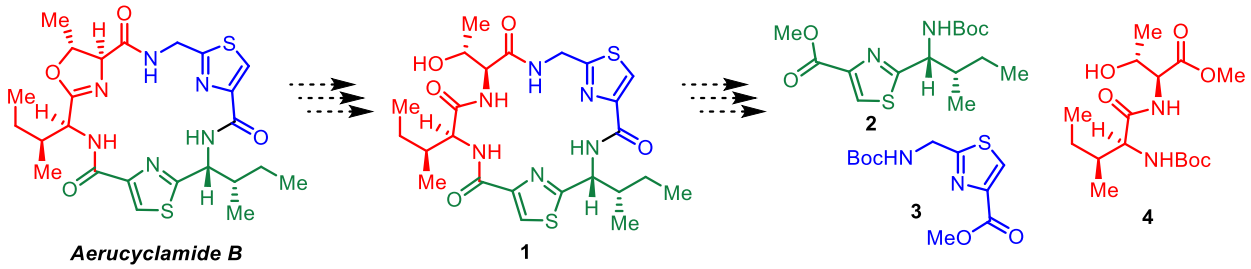

Figure 13: Approach of Serra and co-workers to aerucyclamide B

Assembly of thiazole **2** commenced from the coupling with the free carboxylic acid of Boc-*D-allo*-Ile-OH to the free amine within the methyl ester of *L*-serine to access Boc-*D-allo*-Ile-L-Ser-OMe with HBTU, DIPEA, DMAP in CH_2Cl_2 (Scheme 1). Cyclization of this dipeptide was performed with DAST and K_2CO_3 in CH_2Cl_2 to afford the corresponding oxazoline, which was opened to its thioamide counterpart with $H_2S_{(g)}$ in methanol/Et_3N (1:1). The thioamide was cyclized under the same DAST conditions to gain access to the thiazoline, which was treated with $BrCCl_3$ and DBU to promote aromatization to the desired thiazole **2** in an overall yield of 80% over five steps.

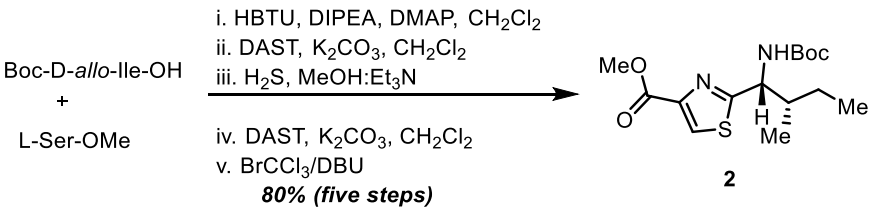

Scheme 1: Synthesis of thiazole 2

Accessing thiazole **6** commenced with the formation of the mix anhydride from *N*-Boc-glycine methyl ester (**5**) and 2,2,2-trichloroethyl chloroformiate with the subsequent treatment with ammonia to form the corresponding amide (Scheme 2). Treatment with Lawesson's reagent transformed the internal amide to a thioamide, and treatment with 3-bromo ethyl pyruvate under refluxing conditions gave access to thiazole **6** in 40% over three-steps. Subjecting **6** to saponification conditions with KOH in H_2O/THF (1:1, v/v) afforded the free carboxylic acid **7** in quantitative yields. Boc deprotection upon **2** was performed with HCl in dioxane to give access to **9**, which was subsequently coupled to **7** using HBTU as the coupling reagent with DIPEA and DMAP in CH_2Cl_2 to give **10** in 94% yield. Employing standard saponification conditions upon **10** afforded **11**. Dipeptide **8** which was formed by deprotecting **4** with HCl in dioxane was coupled to **11** under standard coupling conditions with HBTU to access **12** in 40% yield. Macrocyclization of **12** to access **1** was accomplished by Boc deprotection under saponification conditions, methyl ester hydrolysis, and cyclization via amidation with HBTU in 12% yield.

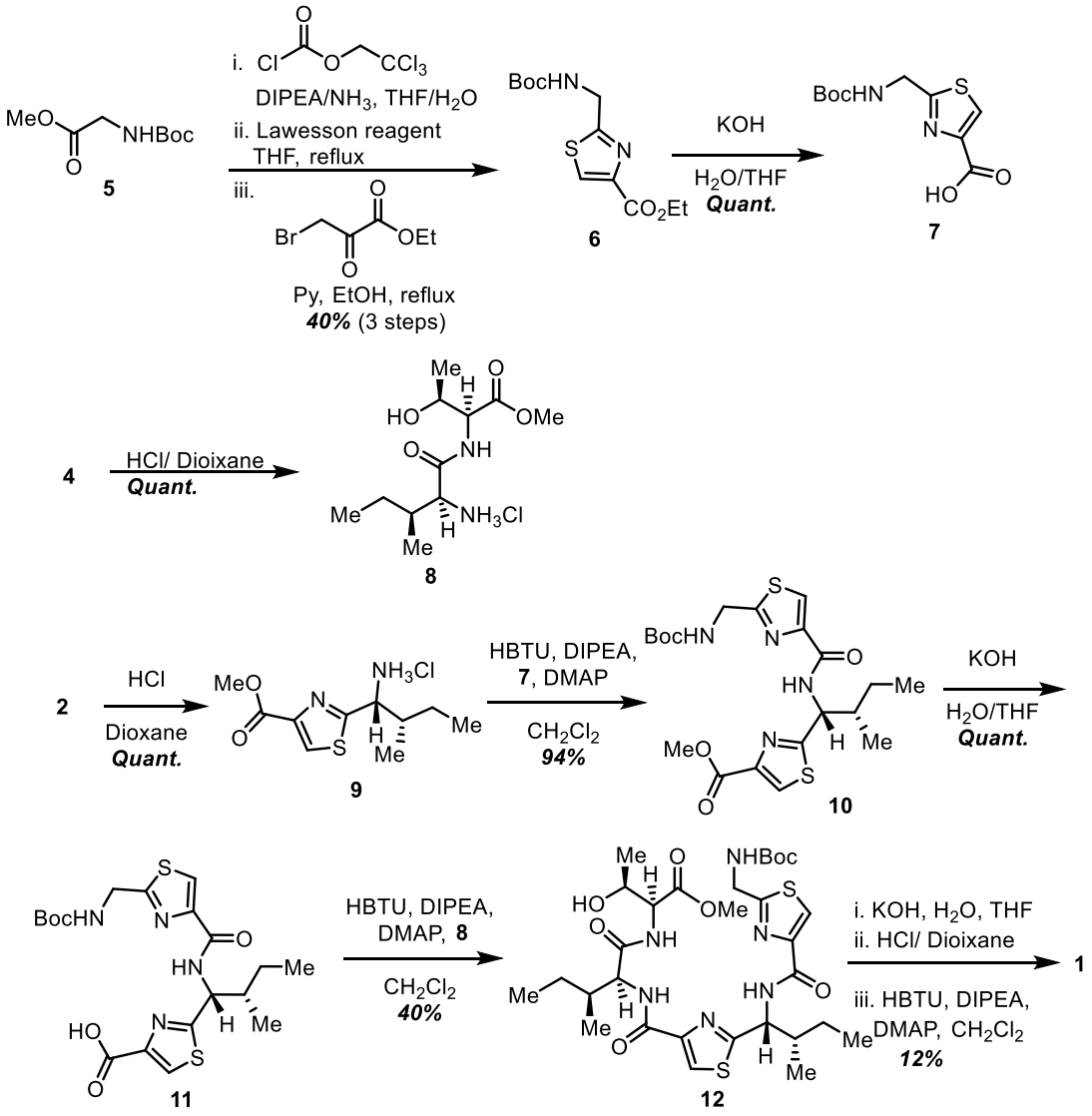

Scheme 2: Synthesis of intermediate 1

With macrocycle **12** in hand, accessing aerucyclamide B was accessed through the treatment of DAST in CH_2Cl_2 at -20 ºC in 67% yield (Scheme 3). It is of interest to note that dipeptide **8** is used rather than the desired oxazoline. It is assumed that the extra degree of flexibility of the dipeptide allowed for greater ease of the macrocyclization. If the oxazoline was employed rather than the dipeptide, the rigid nature of the system could result in the failed cyclization. This synthesis of sets up the hypothesis for synthesis balgacyclamides discussed in this thesis.

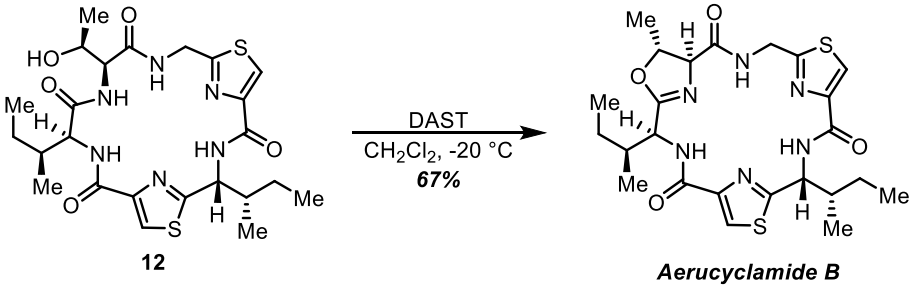

Scheme 3: Accessing aerucyclamide B

2.1.2 Total Synthesis of Dendroamide A

Total synthesis of dendroamide A was reported by Kelly and co-workers in 2003 with a 19% overall yield over 15-synthetic steps (Scheme 24).[43] Their route accessed the NP in a late stage macrocyclization of the dithiazole mono-oxazaoline aliphatic fragment **13**. Construction of **13** was achieved through the coupling of **14** and **15** followed by the incorporation of **16**. This synthesis also follows a modular approach as in aerucyclamide B synthesis.

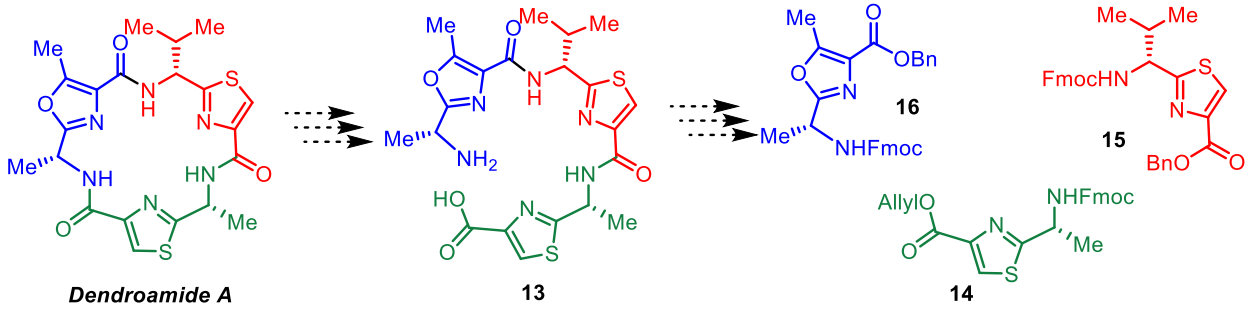

Scheme 4: Approach for the total synthesis of dendroamide A by Kelly and co-workers

Accessing thiazoles **14** and **15** commenced with the esterification of allyl alcohol to *N*-Fmoc-*L*-S-tritylcysteine (**17**) with HOBt and HBTU to furnish **18** in 90% yield (Scheme 5). Elaboration of **18** onto dipeptides **19** and **20** began with Fmoc deprotection by diethyl amine (DEA) in MeCN, which was then added to HOBT/HBTU preactivated solutions of the appropriate single amino acid to access **19** and **20** in 89% and 91% yield, respectively. Trityl deprotection with subsequent thiazoline ring formation was accomplished with triphenyl phosphene and triflic anhydride to

furnish **21** and **22** in 91% and 90% yield, respectively. Aromatization to the required thiazoles **14** and **15** was accomplished with activated manganese (II) oxide in 89% and 91% yield, respectively.

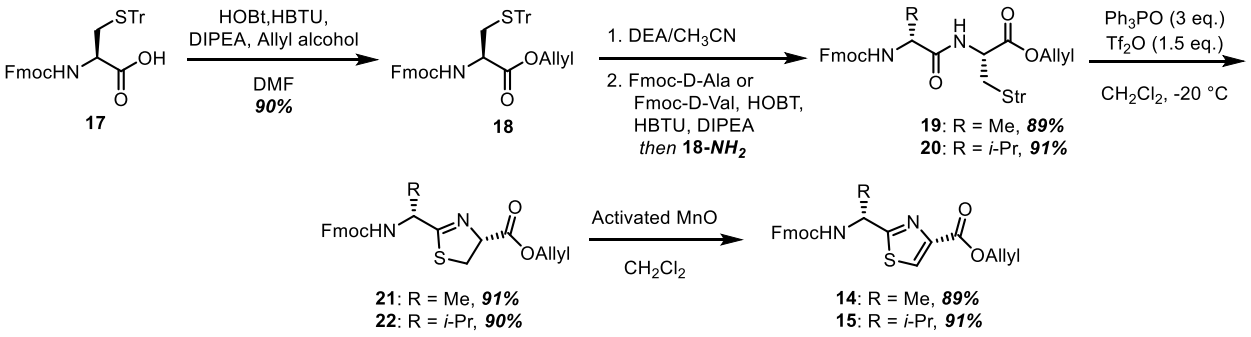

Scheme 5: Synthesis of thiazole 14 and 15

Assembly of oxazole **16** started with the coupling of Fmoc-*D*-alanine to *L*-threonine benzyl ester with HOBT, HBTU, DIPEA in acetonitrile in 85% yield followed by alcohol oxidation to the corresponding ketone **24** with Dess-Martin Periodinane in 80% yield (Scheme 6). In an analogous fashion for the construction of thiazoles **14** and **15**, disclosed above, oxazole **16** was accessed with the treatment of bis(triphenyl)oxodiphosphonium trifluormethanesulfonate in CH_2Cl_2 in 84% yield.

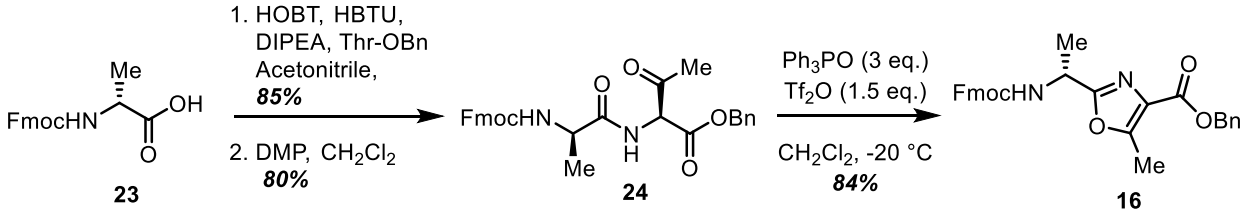

Scheme 6: Synthesis of oxazole 16

Fmoc deprotection upon **14** was facilitated with DEA in MeCN while concurrent allyl deprotection upon **15** was accomplished via a polymer supported triphenyl phosphine reaction with $Pd(OAc)_2$ and phenylsilane. The coupling of the free amine of **14** and carboxylic acid of **15** was accomplished with HOBT, HBTU, and DIPEA in CH_2Cl_2 to access **25** in 92% yield, over three-steps (Scheme

7). Deprotection of the Fmoc group was achieved under standard conditions. The benzyl group in **16** was removed with Pd/C-mediated hydrogenation to afford **26**, which was then coupled to the free amine of **25** to afford **27** in 92% yield over three-steps. Employing conditions used previously, removal of the Fmoc and allyl groups was undertaken. Cyclization to dendroamide A was successfully accomplished by PyBOP and DMAP in DMF/CH_2Cl_2 in 81% yield over three-steps.

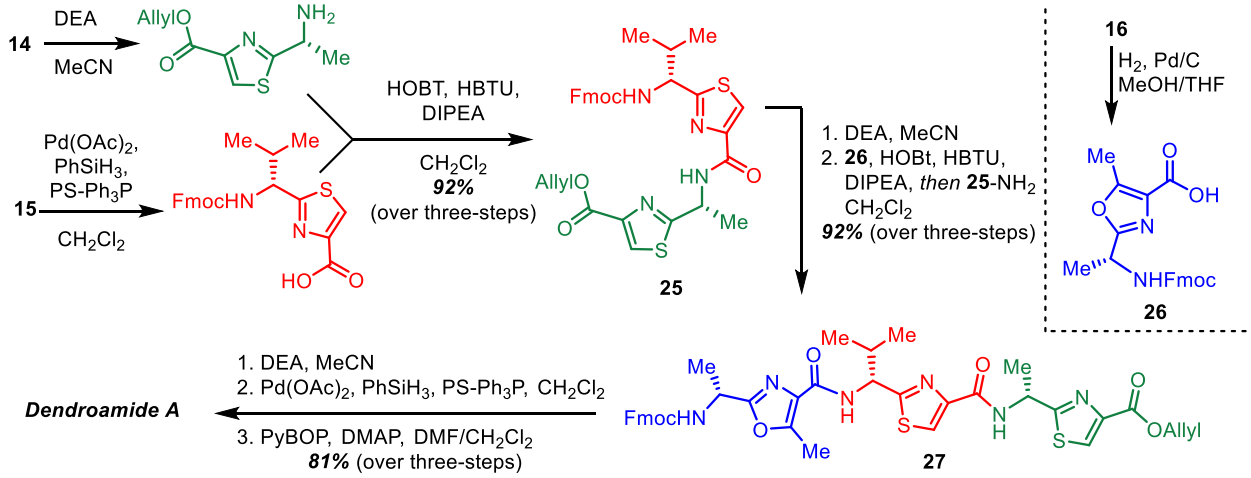

Scheme 7: Synthesis of dendroamide A

2.1.3 Total Synthesis of Bistratamide D

Total synthesis of bistratamide was reported by Albert Meyers and co-workers in 1999 in a 19% overall yield over 11-synthetic steps from oxazole **29**, oxazoline **30**, and thiazole **31** (Scheme 8).[11] In the construction of aerucyclamide B (discussed previously) the NP was accessed through macrocyclization of post dipeptide installation, followed by oxazoline formation from the dipeptide. Unlike this approach, Meyers decided to construct the oxazoline fragment of interest and directly incorporate it into the linear system before cyclization was performed. In doing so, key critical stability insight was obtained regarding Boc deprotections in the presence of oxazoline units, resulting in the ring opening and epimerization. Meyers proved that the use of Cbz rather than Boc groups prevented this ring opening, and successfully used this strategy in their total

synthesis of bistratamide D. This route also highlights the construction of the thiazole fragment using Holzapfel's modified Hantzsch methology.

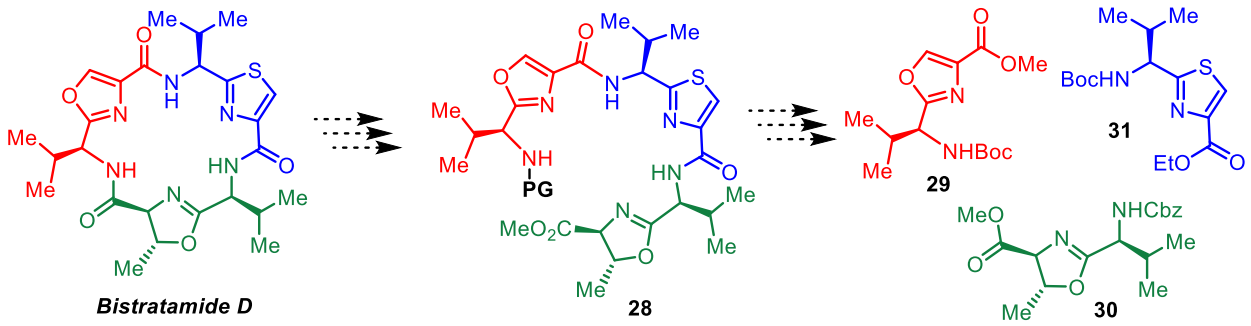

Scheme 8: Retrosynthetic analysis for the construction of bistratamide D

Assembly of thiazole **31** commenced from thioamide **21**, which was accessed from Boc-*L*-valine, by employing Holzapfel's modified Hantzsch methodology. In this method, **32** displaces the bromine upon ethyl bromopyruvate, which upon treatment with trifluoroacetic acid and 2,6-lutidine promoted cyclization and aromatization to access **31** in 71% yield (Scheme 9). Removal of the Boc group was accomplished employing conditions outlined by North,[11] with the in-situ formation of HCl by the treatment of acetyl chloride with ethanol, to give the free amine **33** in quantitative yields. Oxazoline **29** was assembly from the coupling of Boc-*L*-valine to *L*-serine methyl ester followed by cyclization with Burgess reagent via standard protocols. Aromatization of oxazoline **29** to its corresponding oxazole was accomplished with $BrCl_3C$ and DBU in CH_2Cl_2 in quantitative yield, followed by saponification with lithium hydroxide in $MeOH/H_2O$ to furnish the free acid oxazole **34** in 99% yield. Activation of oxazole **34** with EDCI in the presence of HOBt afford the activated ester which was treated with **33** to access **35** in 94% yield. With the Boc-oxazole-thiazole-OMe **35** in hand, efforts were placed in assuring that deprotection of the Boc and methyl ester were achievable. Similar to the condition employed for the Boc removal upon **31**, HCl was generated via acetyl chloride in ethanol to afford the free amine **36** in quantitative yields.

Similarity, saponification of **35** with lithium hydroxide in EtOH/H_2O furnished the free acid **37** in 96% yield.

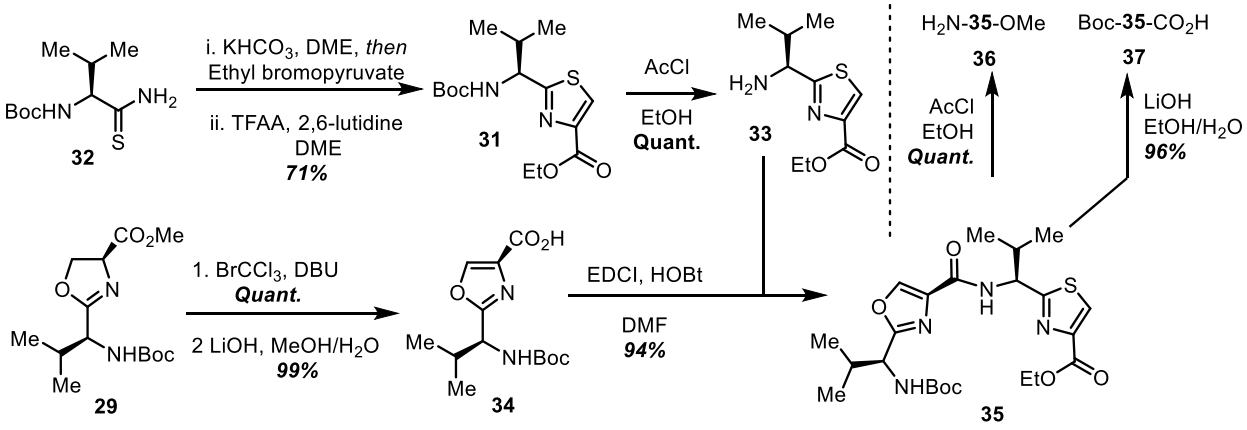

Scheme 9: Accessing intermediate 35 and it deprotections

Oxazoline **38** was constructed from the peptide coupling of Boc-*L*-valine to *L*-threonine methyl ester followed by cyclization with Burgess Reagent (Scheme 10). Subjecting oxazoline **38** to aqueous HCl in THF resulted in the ring opening of the oxazoline, and treatment with potassium carbonate and activated basic alumina in MeOH promoted epimerization about the alcohol within threonine to the *allo*-*L*-threonine configuration. Treating the epimerized compound with Burgess reagent in THF under reflux furnished **30** in 70% yield. Removal of the Cbz group was accomplished under hydrogenation conditions to access **39** in 97% yield. Coupling of **37** to **39** was performed with EDCI, DMAP in CH_2Cl_2 to afford **40** in 53% yield. Unfortunately treating **40** with acetyl chloride in ethanol failed to provide the desired free amine **41**, but rather furnished the ring opened oxazoline. Other attempts at removing the Boc group gave similar undersirable results.

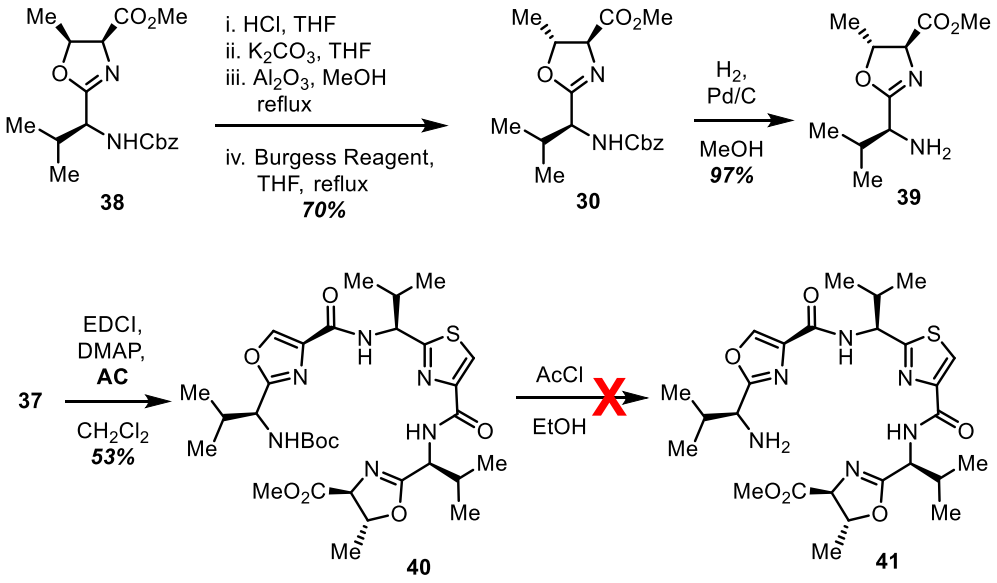

Scheme 10: Attempt to access 41

Noting the instability issue with employing a Boc protecting group in the presence of an oxazoline moiety, Meyer decided to switch the coupling route to allow for a Cbz deprotection rather than Boc. Subjecting oxazoline **30** to saponification conditions to afford **42** in 94% yield, which was coupled to the free amine of the oxazole-thiazole-OMe **36** with EDCI, HOBt in DMF in 79% yield (Scheme 11). Removal of the Cbz group was accomplished under hydrogenation conditions to afford **43** in 83% yield. With the free amine in place, saponifcation was undertaken to furnish the free amine/free acid, which was treated with HATU, DIPEA in DMF to promote macrocyclization to afford bistratamide D in 48% yield over two-synthetic steps.

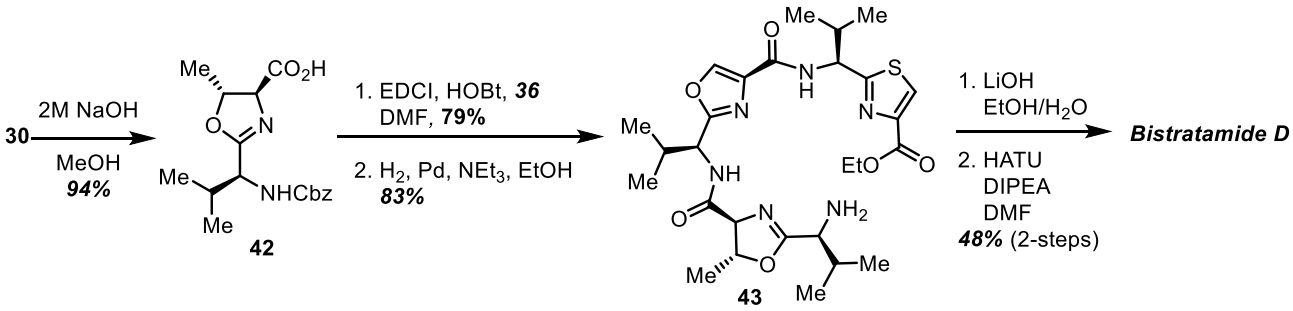

Scheme 11: Accessing bistratamide D

Building up the literature precedence outlined in this chapter, the construction of the balgacyclamide family has not only great promise but expansive precedence. In the total synthesis of aerucyclamide B, the dipeptide fragment, to be elaborated onto the oxazoline unit later on, onto the oxazole-thiazole helped promote cyclization onto the macrocycle. A strategy that can be employed in the pursuit of balgacyclamide A and B; accessing B in a similar dipeptide incorporation as with aerucyclamide and upon cyclization accessing balgacyclamide A. Thiazole assembly was effectively demonstrated via the Hantzsch methodology in both aerucyclamide B and bistratamide D, and via a trityl sulfide approach in dendroamide A. All together, they build a strong fragment for the construction of various substituted thiazole moieties. Efforts in the total synthesis of bistratamide D show the limitation of Boc groups in the protection of amines in the presence of oxazoline units, resulting in decyclization and partial epimeration. While the deprotection of Boc groups upon oxazoline units have been demonstrated in the literature, they are well documented to the "finky" and various in success in the hands of different synthetic chemists.

2.2 Small Molecule Libraries based on NPs and their Applications in Understanding Transport of Small Molecules Across Porins

2.2.1. Complexity to Diversity (CtD): New Method for CSL Construction.

The ChemBridge libraries remains one of the most utilized CSL s for the discovery of new drug lead scaffolds, therapeutics, and in the investigations into other biological inquires. Noting the limitations of the PCPs of this CSLs set outlined in chapter 1 section 1.4, multiple other academic research laboratories have undertaken programs in the development of new methods to construct their own CSLs, and many with targeted PCPs.[44,45,46,47] Prof. Paul Hergenrother at the University of Illinois is one example. His lab employs NPs as starting materials for the construction of screening libraries via ring distortions, termed complexity to diversity, in 2013.[48] In this approach,

the methodology subjects a NP to precedence synthetic transformations that give access to new core scaffolds that differ from the parent NP. These scaffolds are then further functionalized to provide new CSLs for screening purposes that possess complexity imparted from the parent NP. Accessing the core scaffolds was envisioned to arise from the diversification of the NP through known synthetic transformations. Scheme 12 highlights the overview of the core scaffold construction. Starting from a polycyclic NP (**44**), ring cleavage could be performed to give access to scaffold **45**. In a similar way, ring expansion can be performed to give access to **46**, ring fusion accessing **47**, and ring contraction to afford **48**. Further diversification can be performed through combining each of these ring distortion techniques to give rise to compounds such as ring cleavage-expansion **49** and ring contraction-fusion **50**, for example.

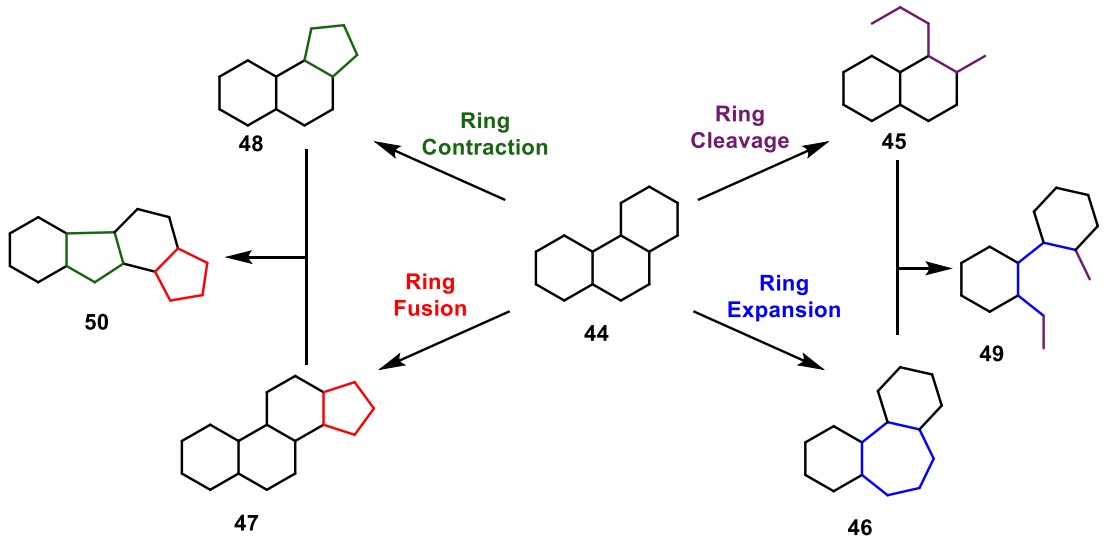

Scheme 12: General concept of the derivatization of small molecules via complexity to diversity

In the CtD methodology, the number of diversification steps could be unlimited, as such, Hergenrother decided to place a five synthetic steps or less as a criterion for accessing the new core scaffolds.[48, 14] Numerous collection of libraries were constructed from various NPs, each possessing high Fsp^3 character, high percentage of stereocenters, and synthetically amendable to

allow for construction of targeted clogP properties. Unfortunately, screening of these collections of compounds revealed activity highly comparable to the parent NP. While undesirable for the construction of variable CSLs, further thought on this matter led to the same conclusion. Each NP employed in this route was synthesized and refined by nature to perform a particular function, and therefore, synthetic manipulations to the final NP is less likely to produce molecules with different biological activities. Therefore, synthesis of libraries via a non-bio-inspired synthetic routes could give rise to small molecule libraries, which have a higher probability of finding molecules with different activities and potential applications into various biological based transport investigations.

2.2.2 Efforts in Overcoming Porin-Mediated Small Molecule Transportation: Identification of Optimal Combinations of PCPs for Enhanced Transport Characteristics towards GNbac

CSLs are one of the most utilized tools in the identification of new drug leads and new drug targets as well as starting points for the identification of compound classes for protein-protein interaction investigations.[14,49] They are also employed in investigations into how PCPs affect biological systems. While commercially available libraries are expansive, the ChemBridge CSLs being the most utilized, they are limited in their PCP profiles. Figure 14-A illustrates the poor overlap between current Gram-negative antibacterial agents and the ChemBridge CSLs with regards to $clogD_{7.4}$, a critical PCP for porin-mediated transport. Comparison of other PCPs, such as hydrogen bonding donors and acceptors[50, 51] (Figure 14) further demonstrate the incompatibility of current CSLs to be employed in GNbac transport studies. In addition to the poor PCP compatibility, specific additive effects of PCPs cannot be explored with commercially available CSLs due to quantity of library material and the lack of synthetic versatility of the library compounds for the introduction and modifications of PCPs upon the library members. To evaluate the additive effects

of PCPs upon complex barrier transport, not only are new CSLs required, but new guidelines are also required for their construction. We propose the following guidelines in the construction of new CSLs for evaluation of additive PCPs: 1) library compounds must be rapidly available on mg scales (to allow synthetic modifications), 2) possess multiple synthetic handles (to allow new PCP introduction, transposition, and alteration), and 3) have core structure transformability (rigidity, planarity). To accomplish this, we propose that CSLs be constructed from the complex intermediates of total synthesis campaigns as each of the proposed guidelines can be met.

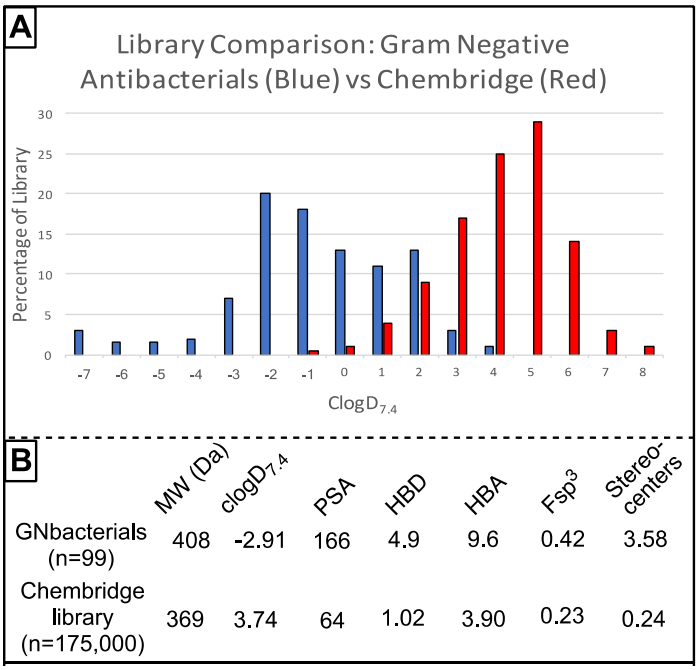

	MW (Da)	clogD$_{7.4}$	PSA	HBD	HBA	Fsp^3	Stereo-centers
GNbacterials (n=99)	408	-2.91	166	4.9	9.6	0.42	3.58
Chembridge library (n=175,000)	369	3.74	64	1.02	3.90	0.23	0.24

Figure 14:. Highlighting the unique PCPs s possessed by Gram-negative antibacterial agents

A systematic statistical analysis done in 2008 by O'Shea and Moser analyzing approved antibiotics reveal a great deal of information about the molecules that can have activity against GNbac.[38] Figure 15 extracted from their work illustrates the clogD$_{7.4}$ value vs molecular weight distribution of different approved drugs. Grey spots indicate data of oral and parenteral drugs obtained from the commercially available CMC data set, red spots represent the Gram-positive only antibacterials, and blue spots represent the Gram-negative active antibacterials. It clearly shows

that the PCPs of antibiotics that are active against GNbac deviate from the generally accepted Lipinski's rule of five. It was observed that molecular weights of these molecules were strictly below 600 Da and the parameters pertaining to lipophilicity such as clogD, relative polar surface, and the number of hydrogen bond donors and acceptors demonstrated that these molecules had to be relatively polar than the other drugs. A major reason for the failures of high-throughput screening campaigns hunting for Gram-negative-antibiotics could be that most of the screening libraries do not have a good concentration of molecules that have the required PCPs. This is hard core evidence to demonstrate that utilizing small molecule libraries that are way too generalized is not the best option in attempting to discover small molecules that can penetrate GNbac and execute antibacterial properties. Therefore, investigating into PCPs of molecules that can penetrate GNbac, as well as populating small molecule libraries that have molecules with suitable physicochemical libraries that facilitate GNbac penetration are equally important.

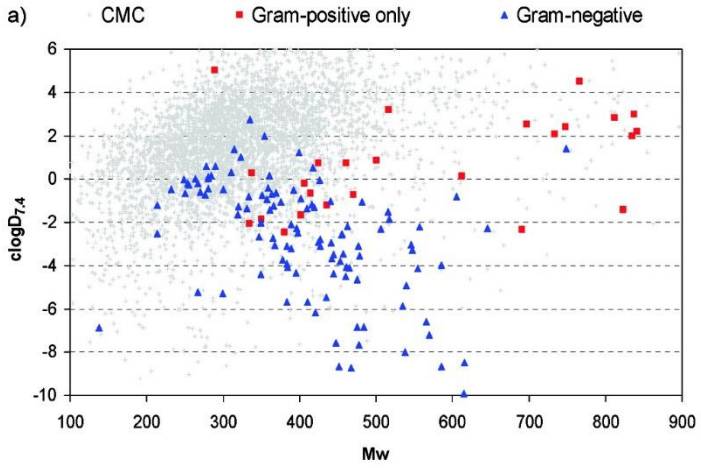

Figure 15: PCPs of general (grey), Gram-positive only (red), and Gram-negative active (blue) drugs. (Graphic extracted from *Journal of Medicinal Chemistry*, 2008, Vol. 51, No. 10, 2874, without permission for educational purposes.)**)**

The concept of structural modification of substances to impart penetration (such as substrate tagging,[52, 53] amino acid appendage,[54,55] and peripheral modification of the substance to impart specific PCPs[41]) has been widely explored by numerous research programs. Each of these

strategies relies upon single agent modification, which has no guarantee of providing transport. However, such studies have discovered key PCPs (e.g. cationic character, lipophilicity, and presence of hydrogen bond donors/acceptors) that could be essential in the transport of foreign substances.

In 2017 the Hergenrother Lab published a study outlining "rules" that a compound must possess for transport into GNbac,[41] based heavily upon previous findings of cationic character.[51, 38] In this work, they took the Gram-Positive antibiotic deoxynybomycin (6DNM) and synthetically modified it to include a primary amine accessing 6DNM-NH_3^+ (Figure 16). The primary amine inclusion not only resulted in GNbac accumulation, but also cytotoxic against GNbac strains. When the GNbac OmpF porin is knocked out the activity is lost, therefore suggesting that this modified antibiotic elicits its action in the interior of the GNbac meaning that transport occurred. While the presence of cationic character upon compounds has been well established to help aid porin-mediated transport, this study revealed a new piece of data, which when analyzed with our pilot study (Chapter 3) further reveals the role of not only charge, but the location of said charge. The Hergenrother study also synthesized other analogs, varying in the carbon tether between the main scaffold and the amine. Interestingly, shorter and longer tethers failed to provide any antibiotic activity, and therefore more and most importantly, did not possess any penetration in GNbac.

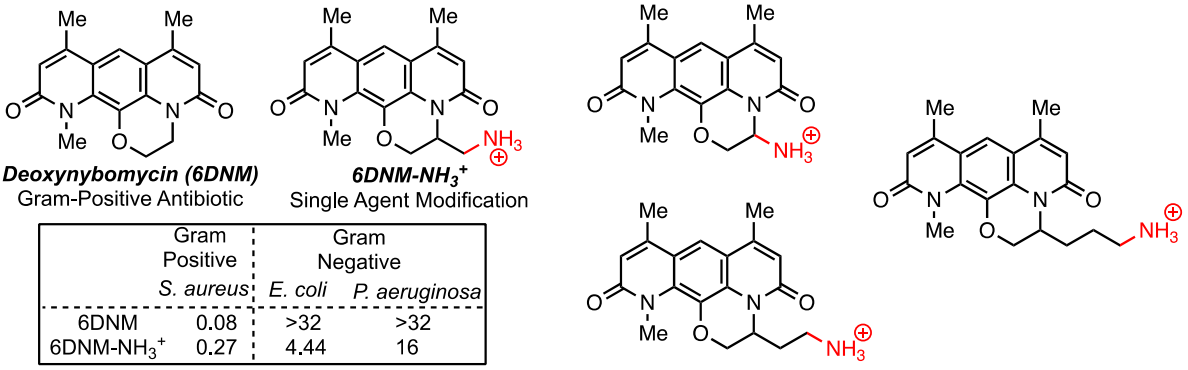

	Gram Positive	Gram Negative	
	S. aureus	*E. coli*	*P. aeruginosa*
6DNM	0.08	>32	>32
6DNM-NH_3^+	0.27	4.44	16

Figure 16: Single agent modification imparting cationic amine PCPs upon 6DNM (Gram-Positive Antibiotic) to 6DNM-NH_3^+ resulting in Gram-negative transport and retention of antibiotic properties

Chapter 3 - Synthetic Efforts Towards Total Synthesis of Balgacyclamide A, and B, and Their Applications

The attention of our research laboratory was drawn towards balgacyclamide A, and B as they possess interesting biological activities[4]; antimalarial activity, moderate cytotoxicity towards rat myoblasts, and implied ability to penetrate into lung and colon cancer cells as mentioned in chapter 1. The structural similarities of balgacyclamide A and B (Scheme 13) also hint towards the similarities in their biological activities. As such, the only difference between balgacyclamide A and B is the open dipeptide in the lower fragment of balgacyclamide B being cyclized to form an oxazoline in balgacyclamide A (both are color-coded in purple in Scheme 13). As previously mentioned, total synthesis of any of the balgacyclamides (balgacyclamide A, B, and C) have not been achieved and reported thus far. Therefore, efforts towards the total synthesis of balgacyclamide A, and B commenced with the aim of utilizing the synthesized balgacyclamides for selective drug delivery and using their intermediates to probe small molecule penetration into GNbac which would be discussed later. It was envisioned to synthesize these two NPs via a convergent synthetic approach.

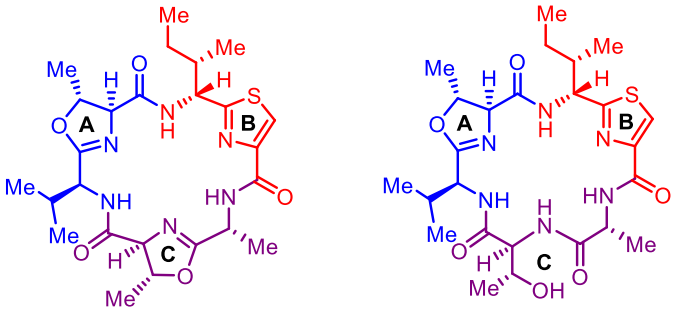

Scheme 13: Structures of balgacyclamide A and B

3.1 Retrosynthetic Analysis of Balgacyclamide A & B

Retrosynthetic analysis for balgacyclamide A and B is given in Scheme 14. It is inspired by the synthesis of similar molecules[42, 11] discussed in chapter 2. As indicated, when an oxazoline is formed in the lower fragment of balgacyclamide B (color-coded in purple), balgacyclamide A can be accessed. That makes this route a convergent synthetic approach that can accesses two NPs in one route. Balgacyclamide B was envisioned to be obtained by coupling the oxazoline-containing ring A (**51**), the thiazole-containing ring B (**52**), and the dipeptide lower fragment C (**53**). Rings A, B, and the lower fragment C were envisioned to be obtained using commercially available amino acids; ring A from *L*-valine and *L*-threonine, ring B from *L*-serine and *D*-alloisoleucine, and the lower fragment C from *L*-threonine and *D*-alanine.

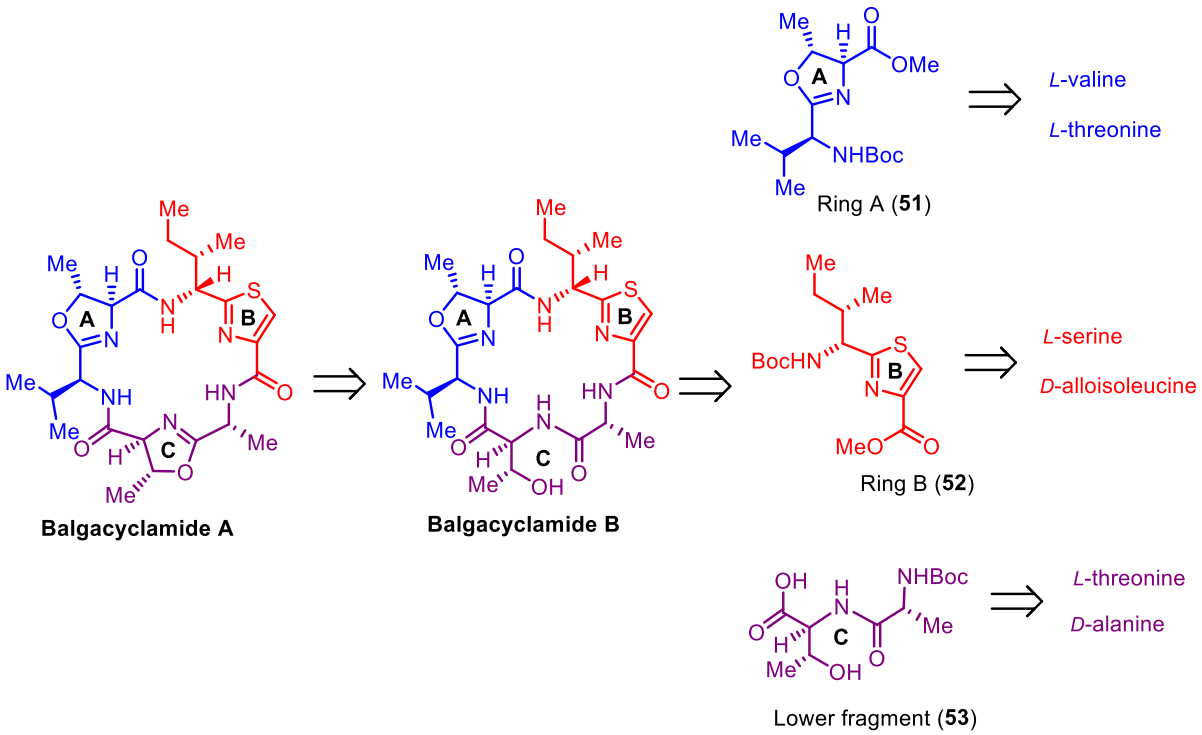

Scheme 14: Retrosynthetic analysis of balgacyclamide A and B

As it was indicated in Scheme 14, synthesis of balgacyclamide A and B requires the use of *D*-alloisoleucine which is an unnatural amino acid. When all the factors concerning the synthesis

of these molecules were considered, it was also envisioned to synthesize two analogs of the balgacyclamides using only naturally occurring amino acids as the starting material. The main reason behind this decision was the high price of *D*-alloisoleucine. Therefore, it was decided to synthesize an *L*-isoleucine-containing analog of balgacyclamides as a model system to establish the synthetic route to access ring B (the thiazole ring) as shown in Scheme 15. When the price of *D*-alloisoleucine was compared with that of Boc-*L*-isoleucine (Sigma-Aldrich prices), *D*-alloisoleucine was about three hundred times the price of Boc-*L*-isoleucine. The benefits of accessing these analogs are not limited to serving as a model system but also, they can be used for SAR analysis, and exploring their biological properties as well.

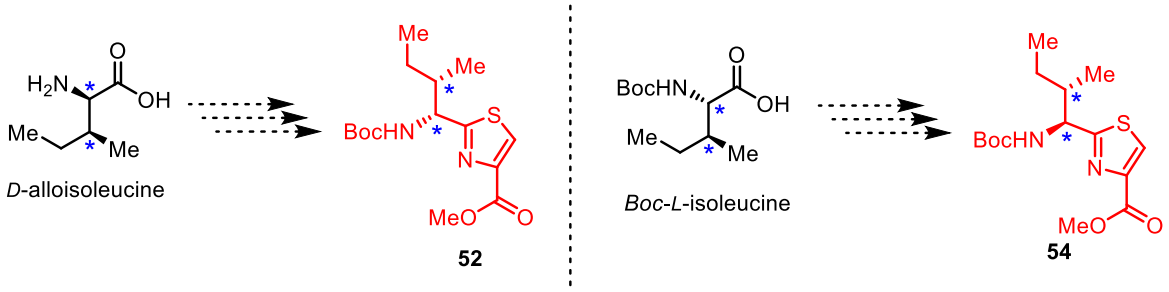

Scheme 15: Isoleucine in balgacyclamides; natural vs unnatural amino acids

Retrosynthetic analysis of the proposed balgacyclamide A and B analogs are shown in Scheme 16. Here, the only difference compared to the retrosynthetic analysis of balgacyclamide A and B is the use of *L*-isoleucine which would introduce a stereocenter with S configuration at the amine containing stereocenter compared to having R configuration in the actual balgacyclamides.

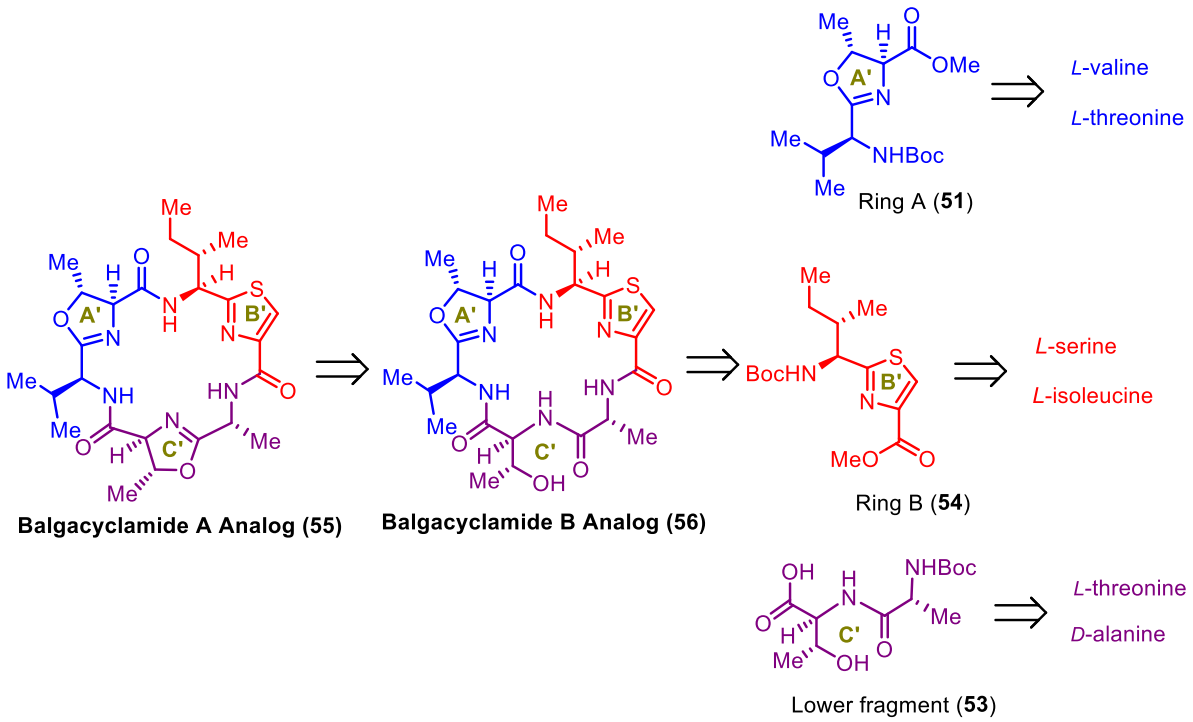

Scheme 16: Retrosynthetic analysis of balgacyclamide A and B analogs

3.2 Synthesis of Ring A: The Valine-Threonine Oxazoline Ring

3.2.1 Oxazoline Formation Utilizing a Molybdenum-Containing Catalyst

The construction of oxazoline **58** commenced with the coupling of Boc-*L*-valine and *L*-threonine methyl ester using PyBOP as the peptide coupling reagent in the presence of DIPEA in methylene chloride to access the dipeptide **57** in 99% yield. It was followed by refluxing **57** with the molybdenum-containing catalyst $(NH_4)_6Mo_7O_{24}$ in toluene to access ring A (**58**).[56] However, the yield of the reaction was 35%. For a reaction in the earlier stage of total synthesis campaign it is a very low yield indicating that this reaction had to be optimized. Despite the several attempts that were made changing the number of equivalents of the catalyst, increasing the reaction time as well as adding *p*-toluenesulfonic acid as an additive to increase the yield of this reaction, the yield of the reaction could not be optimized above 35%. The reason for choosing a molybdenum-

containing catalyst for the oxazoline formation was to retain the stereochemistry at the methyl stereocenter (marked with a red asterisk in Scheme 17).

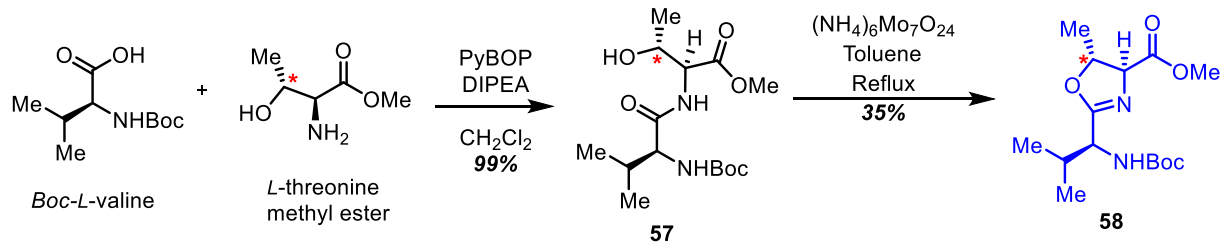

Scheme 17: Formation of ring A using the molybdenum-containing catalyst

As molybdenum coordinates with the carbonyl oxygen and the hydroxyl group (mechanism shown in Scheme 18) and locks them in position, the mechanism for oxazoline formation does not incorporate an S_N2 reaction that causes epimerization. In contrast, most of the other reagents that could be used to form an oxazoline from **57** such as DAST (diethylaminosulfur trifluoride), and Burgess reagent involves an S_N2 reaction that causes epimerization as shown in the example in Scheme 18.

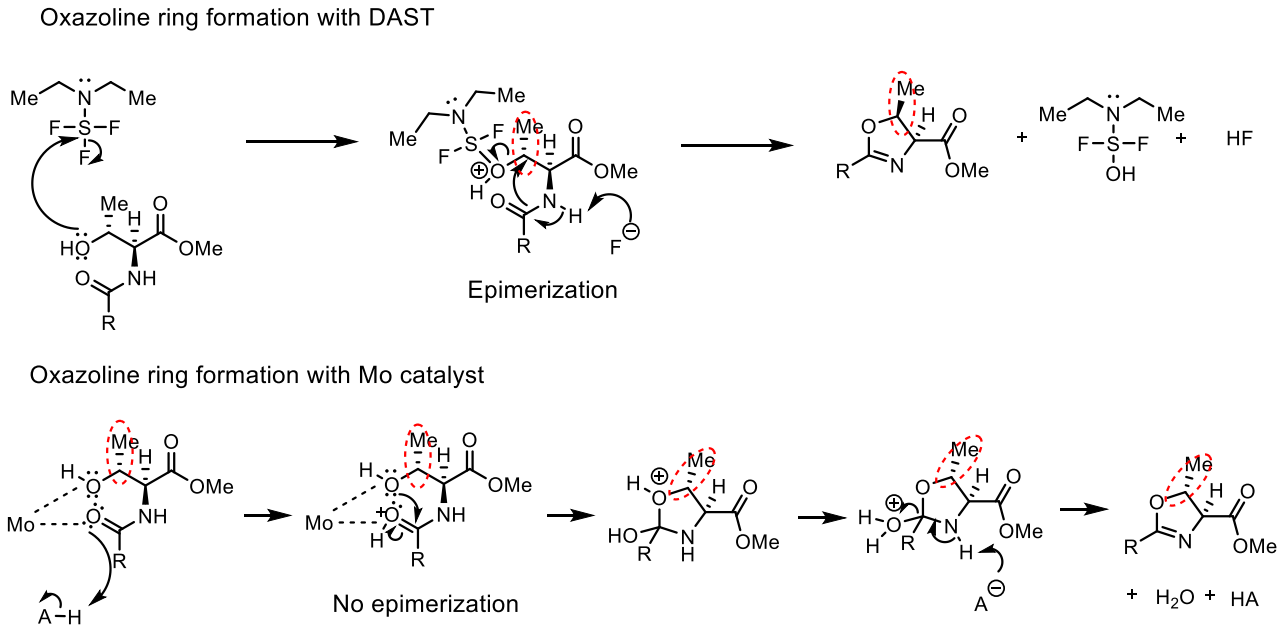

Scheme 18: Oxazoline formation with a molybdenum-containing catalyst vs DAST

To explore the ability to perform the oxazoline formation using DAST[42] in a higher yield, a Mitsunobu inversion was attempted[57] on **57** (scheme 19). There **57** was treated with triphenylphosphine, *p*-nitrobenzoic acid, and diethyl azodicarboxylate (DEAD) in benzene to obtain inverted stereochemistry at the methyl center. And if it was successful, a second epimerization with DAST would give the correct stereochemistry once the oxazoline was formed. However, the Mitsunobu inversion was not successful for this system. Deducing whether the Mitsunobu inversion was successful was not conclusive when the NMRs of **57** (starting dipeptide for the reaction) and the product were compared as the difference in the two molecules were only in one stereocenter and it would not show clearly on NMR as the molecule has so much free rotation around the bonds as well. Therefore, the product of the Mitsunobu inversion reaction was subjected to cyclization using DAST and K_2CO_3 in methylene chloride[42]. Upon the cyclization, changes in NMR chemical shifts were expected as the oxazoline would have restricted rotation around the bonds. Therefore, if **59** was produced during the Mitsunobu inversion reaction, after cyclization with DAST that causes an epimerization at the threonine methyl center, it would produce **58** and the NMRs should match to confirm it. However, when the NMRs were compared (Figure 17) NMR of the cyclized product of **59** did not match with the product that was cyclized using the molybdenum catalyst. It proved that the Mitsunobu inversion was not successful for this system and an alternative way was required to access **58** in higher yields.

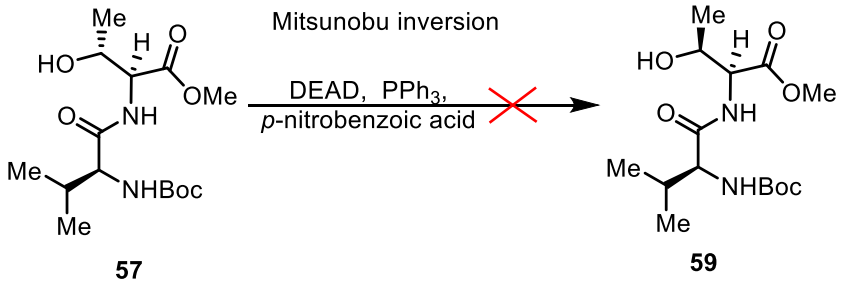

Scheme 19: Attempted Mitsunobu inversion on 57

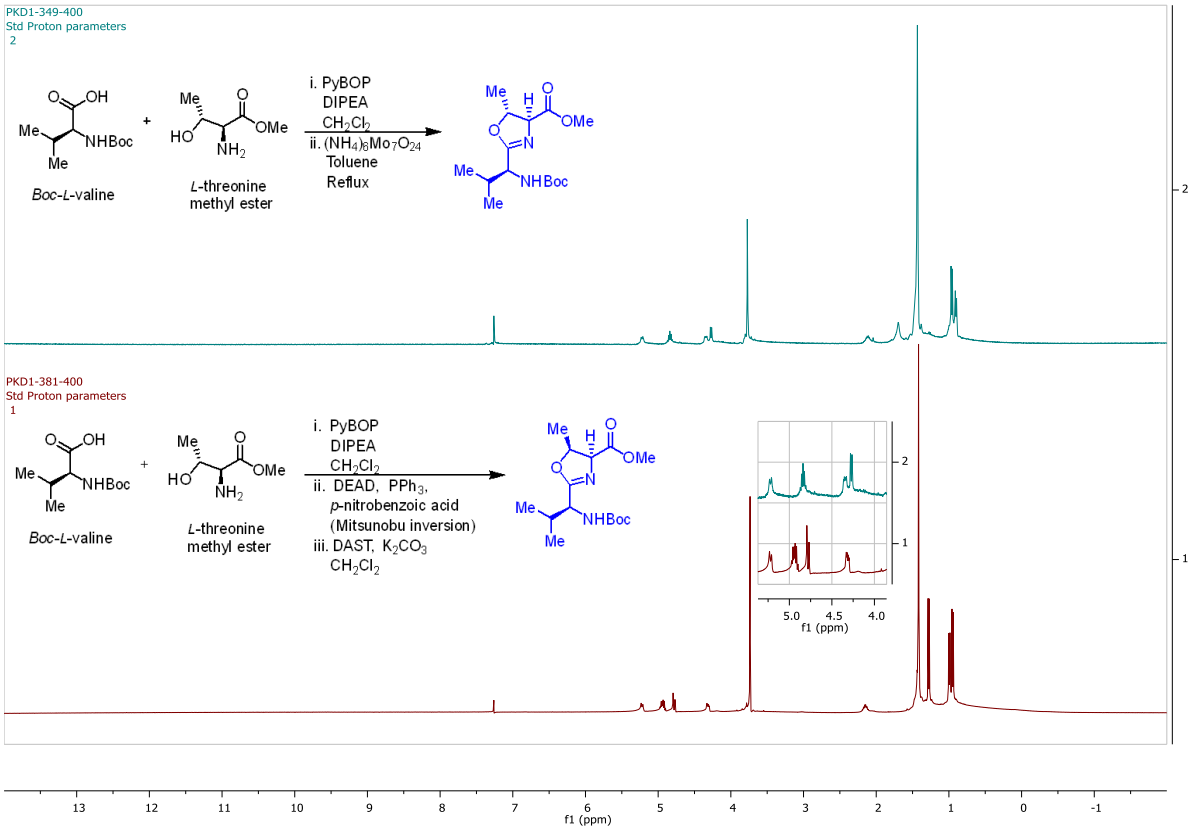

Figure 17: NMR comparison of valine-threonine oxazolines of molybdenum-catalyst- based cyclization vs Mitsunobu inversion followed by DAST-mediated cyclization

3.2.2 Oxazoline Formation Utilizing DAST

Given that the attempts to optimize the formation of oxazoline **58** with the molybdenum-containing catalyst, and the Mitsunobu inversion were unsuccessful, an alternative approach was attempted to access it. This approach (Scheme 20) commenced with coupling Boc-*L*-valine with *L*-allothreonine methyl ester instead of *L*-threonine methyl ester using PyBOP as the coupling reagent in the presence of DIPEA in methylene chloride[58] and the dipeptide **60** was accessed in 99% yield. Having the dipeptide **60** with S configuration at the methyl center (stereocenter marked with the asterisk) DAST could be successfully utilized with K_2CO_3 in methylene chloride[42] to cyclize it with epimerization to access the oxazoline **58** (ring A) that has R configuration at the methyl center with 80% yield. When the NMRs of DAST-mediated cyclization of valine-

allothreonine dipeptide and molybdenum catalyst-mediated cyclization of valine-threonine dipeptide were compared they matched (Figure18), proving that the same molecule was accessed in both approaches but with this novel approach in a much higher yield.

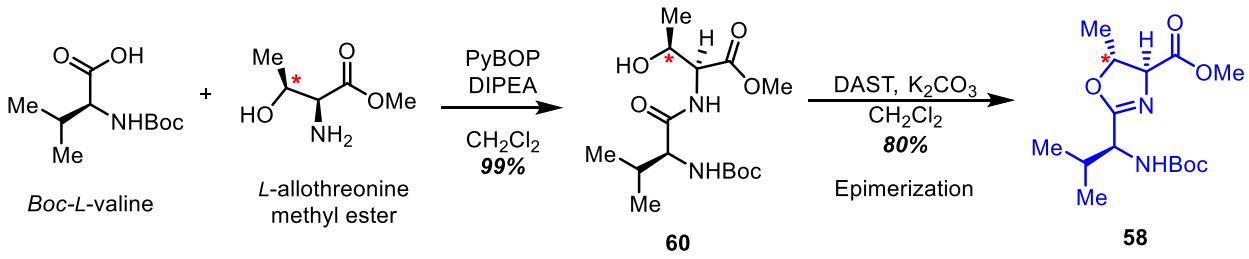

Scheme 20: Accessing 58 with DAST

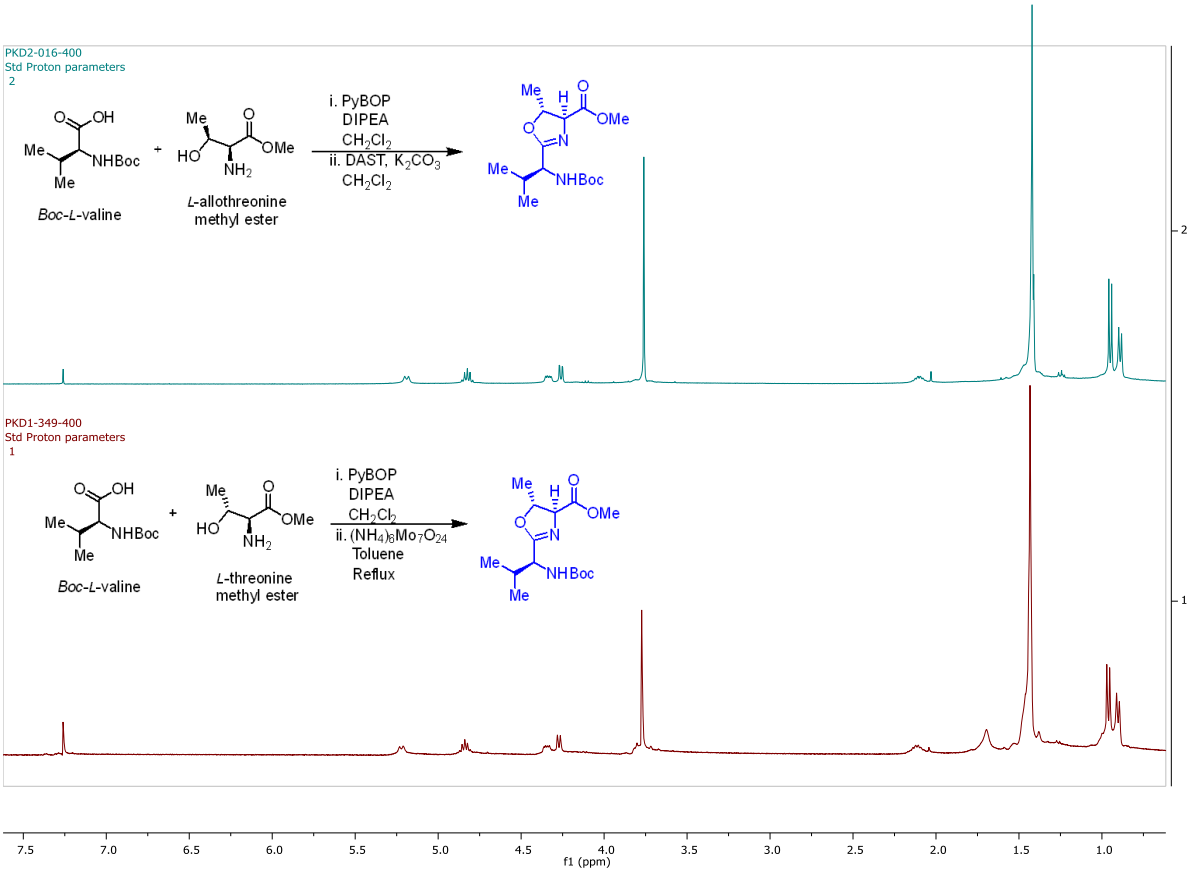

Figure 18: NMR comparison of DAST-mediated cyclization of valine-allothreonine dipeptide vs molybdenum catalyst- mediated cyclization of valine-threonine dipeptide

Given the tendency of oxazolines to ring open and recyclize causing epimerization under strong acidic conditions, and the need to use such conditions (concentrated HCl) to remove the Boc group in **58** raised concerns regarding the use of Boc as the protecting group for the amine group in ring A. Therefore, to avoid such complications in the later stages of the synthesis route, it was decided to incorporate a protecting group that does not require the use of concentrated acids to deprotect, yet stable under other reaction conditions ring A must face. Hence, a Cbz group was introduced to this system as it could be deprotected using hydrogenation with a palladium catalyst (Scheme 21). To execute this approach, Cbz-*L*-valine was coupled to *L*-allothreonine using PyBOP in the presence of DIPEA in methylene chloride to access **61** in 99% yield and the oxazoline formation was performed using DAST, and K_2CO_3 in methylene chloride to obtain **62** with 61% yield. Similarly, the oxazoline **64** which is an analog of ring A with S configuration at the methyl stereocenter was synthesized, so that it could be coupled with ring B analog (thiazole **54**) to act as a model system for establishing the synthesis route to access the A-B dicycle system. This was also performed commencing with a PyBOP-mediated reaction where Cbz-*L*-valine was coupled with *L*-threonine with PyBOP[58], and DIPEA in methylene chloride to access the dipeptide **63** with 99% yield, followed by a DAST-mediated cyclization to access the oxazoline **64** with 80% yield.

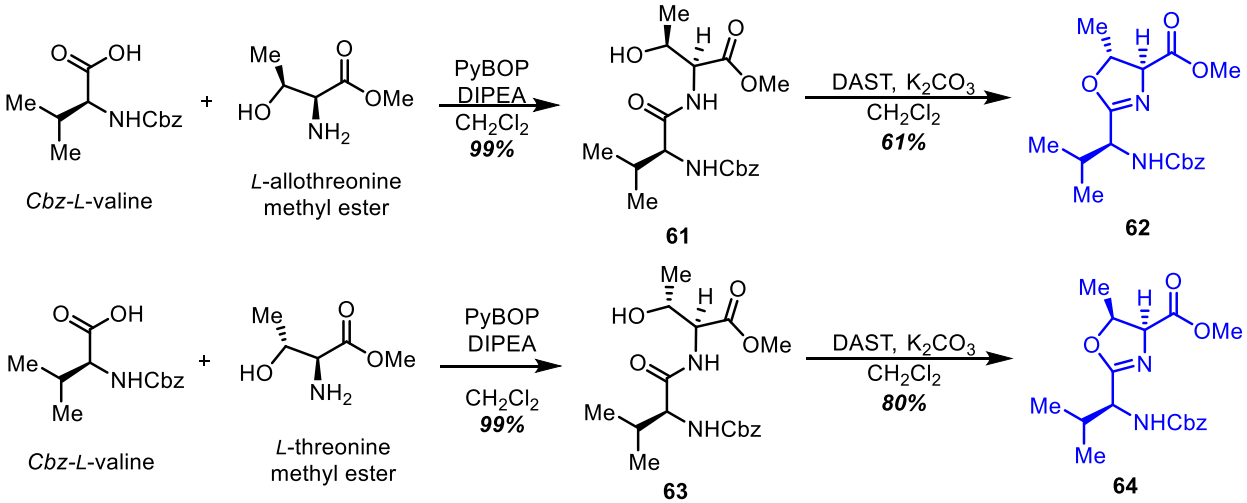

Scheme 21: Changing the protecting group of ring A to Cbz

3.3 Synthesis of Ring B: The Isoleucine-Serine Thiazole Ring

3.3.1 Synthesis of Ring B Analog

To establish the synthetic route (Scheme 22) to the actual balgacyclamide thiazole formation, first ring A (**54**) of the balgacyclamide A and B analogs was synthesized. Efforts towards synthesis of thiazole **54** were based on the work done by Serra and co-workers in the synthesis of aerucyclamide B.[42] As described in section 3.1, this thiazole acted as a model system for accessing the actual thiazole **52**, which also helped establish the synthesis route to access A-B ring system. Synthesis commenced by coupling Boc-*L*-isoleucine to *L*-serine methyl ester using PyBOP as the peptide coupling reagent in the presence of DIPEA in methylene chloride[58] and accessed the dipeptide **65** in quantitative yields. It was then subjected to cyclization to form the oxazoline **66** in 93% yield using DAST, and K_2CO_3 in methylene chloride.[42] It was followed by reacting **66** with gaseous hydrogen sulfide in a 2:1 mixture of methanol/triethylamine to open the oxazoline, forming the thioamide intermediate **67**. The crude material was cyclized by DAST, and K_2CO_3 in methylene chloride and the resultant thiazoline was aromatized using bromotrichloromethane and DBU to form the thiazole **54**.[42]

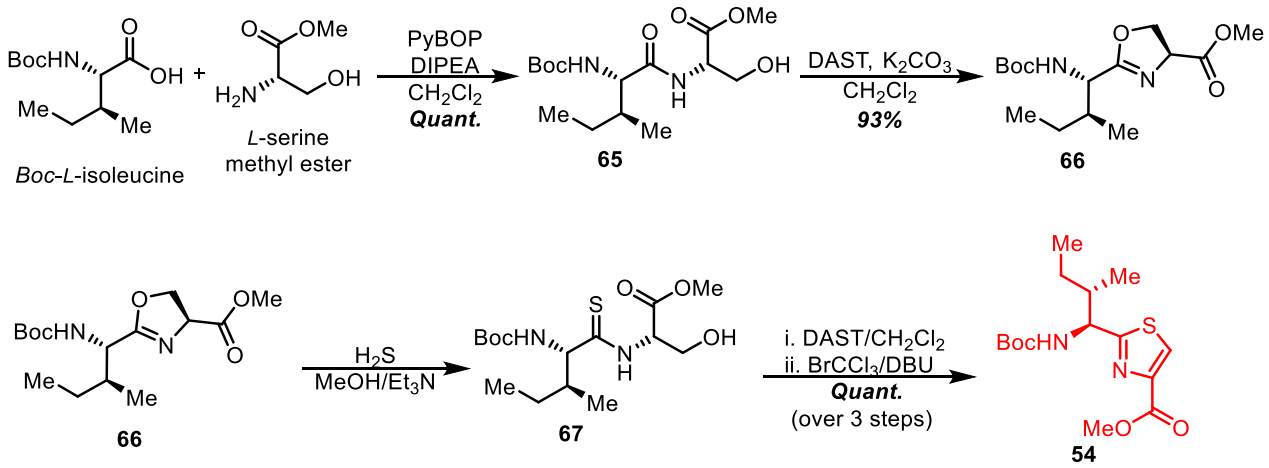

Scheme 22: Synthesis of ring B analog

However, the NMRs of **54** initially showed problems in terms of repeatability of the reaction, where additional peaks were observed in the NMR as shown in Figure 19. Exploring more into this problem it was realized that any residues of unreacted oxazoline starting material **59** being forwarded into the following steps generates the respective oxazole during the aromatization step as shown in Scheme 22, which was the reason behind the additional peaks on the NMR (significant peaks in the NMRs are color-coded and matched with the chemical structures for reference). Optimizing the transformations of **66** to **54** was complicated as **67** could not be purified and isolated from unreacted **66** due to having similar retention times and being overlapped on TLC as well as in chromatography columns. When there is unreacted to **66** in the reaction medium it cannot be detected on TLC. Since the two compounds cannot be separated it is harder to detect on NMR whether unreacted **66** is present or not. If there is unreacted **66** in the medium when the aromatization is done it forms the oxazole **69** as shown in Scheme 23. Again, **54** and **69** have similar retention times and cannot be separated by column chromatography. However, presence of **69** can be detected in NMR. Therefore, as a strategy to solve this problem a very small portion of the reaction mixture of **66** to **67** conversion was used to run a test aromatization to monitor the reaction completion. If there is **69** detected by NMR, more hydrogen sulfide would be bubbled on the **66**/**67** reaction mixture and run it longer. When the conversion of **66** to **67** runs for 2 days, complete conversion could be obtained. After this reaction optimization, **54** could be accessed from **66** with quantitative yields over three steps.

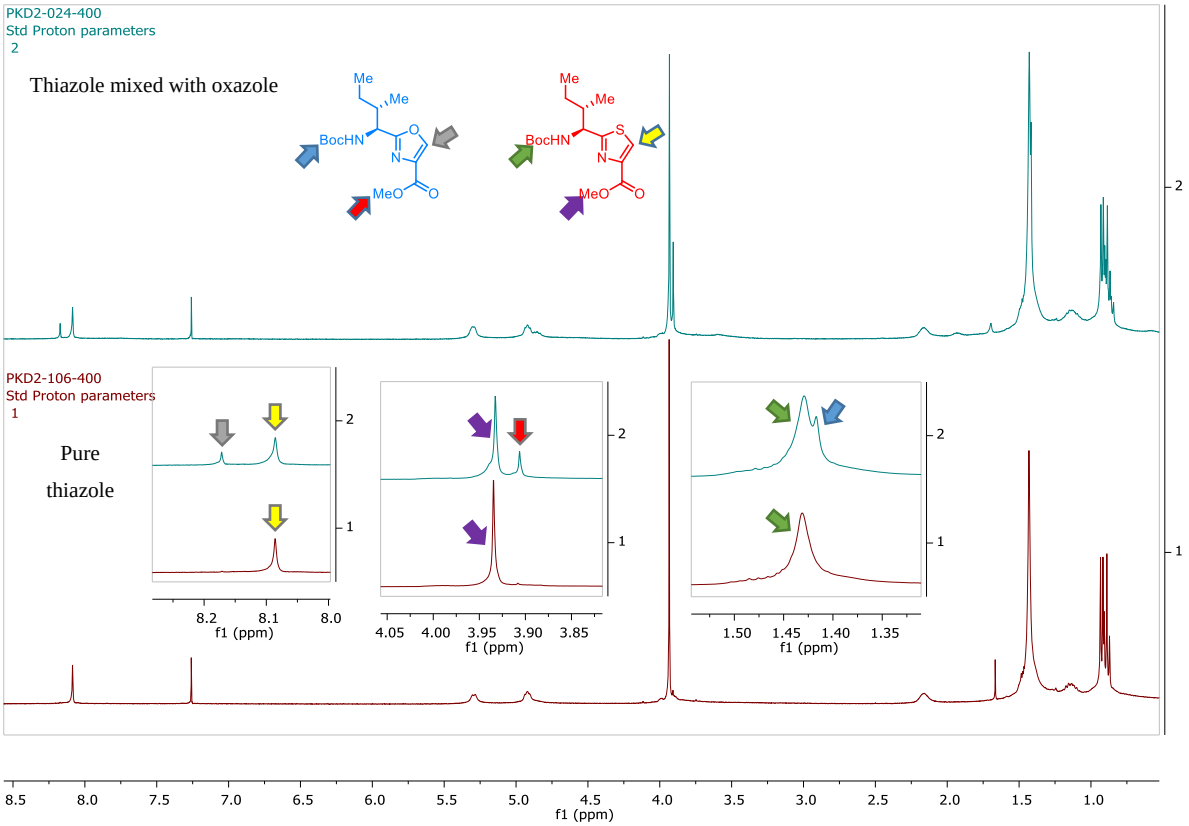

Figure 19: NMR comparison of pure thiazole 54 vs thiazole 54 mixed with oxazole 69

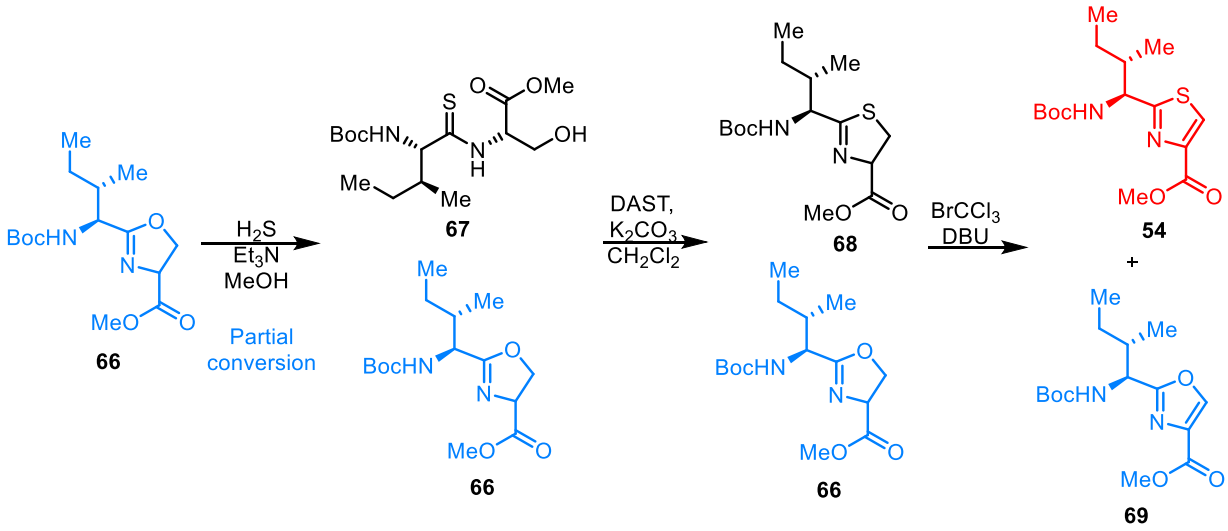

Scheme 23: Unreacted oxazoline complicating the formation of the thiazole

3.3.2 Synthesis of Ring B

Using the improved route to access the thiazole, synthesis of this fragment started by Boc protecting the amine group in commercially available *D*-alloisoleucine using Boc anhydride, and NaOH in a mixture on 2:1 dioxane/water which gave access to Boc-*D*-alloisoleucine (**70**) quantitatively. It was followed by coupling **70** to *L*-serine methyl ester using PyBOP, and DIPEA in methylene chloride[58] in quantitative yields. Cyclization with DAST, and K_2CO_3 in methylene chloride[42] afforded the oxazoline **72** in 96% yield. According to the optimized way explained in the synthesis of ring B analog, the oxazoline intermediate **72** was subjected to ring opening with gaseous hydrogen sulfide in a 2:1 mixture of methanol/triethylamimne followed by thiazoline formation with DAST, and K_2CO_3 in methylene chloride, which was subjected to aromatization with bromotrichloromethane and DBU to form the thiazole **52** in 97% yield over three steps.

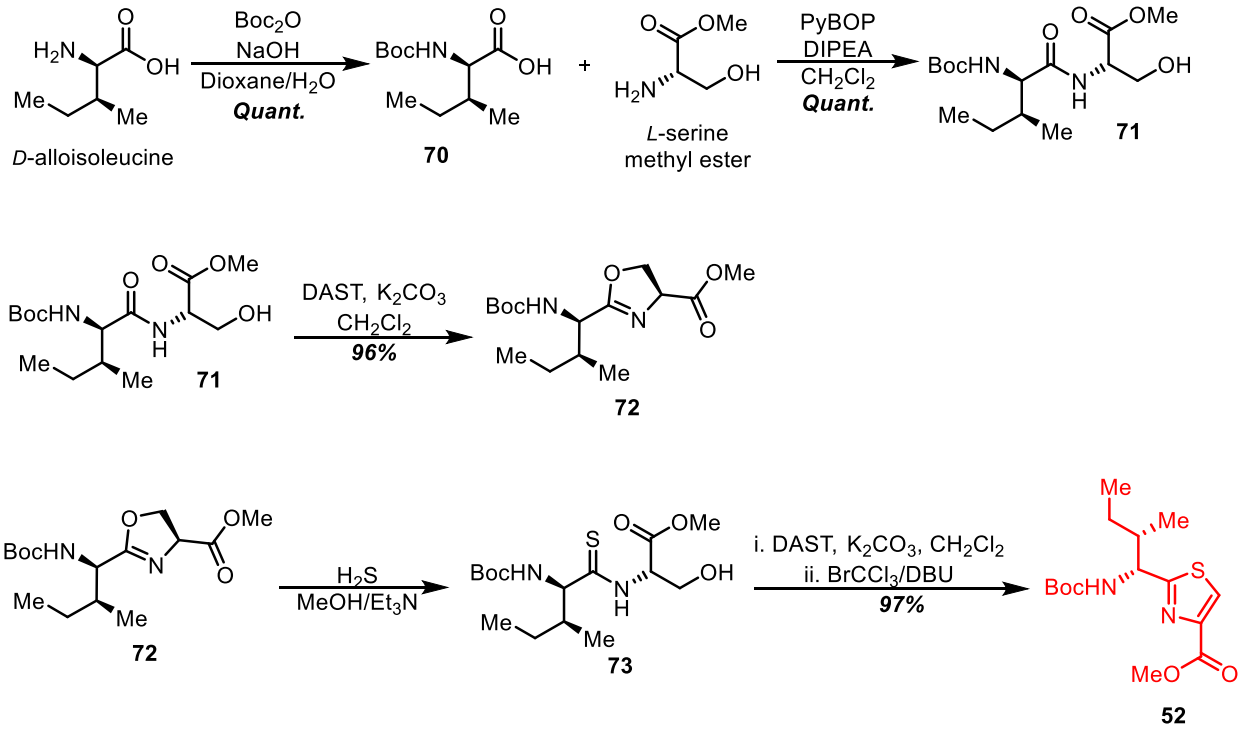

Scheme 24: Synthesis of ring B

3.4 Synthesis of the Lower Fragment C

The dipeptide that forms the lower fragment C was synthesized by coupling *L*-threonine methyl ester and Cbz-*D*-alanine. Several peptide coupling reagent conditions were explored (Table 2) and BOPCl, and DIPEA in methylene chloride gave the highest yield for performing the reaction.

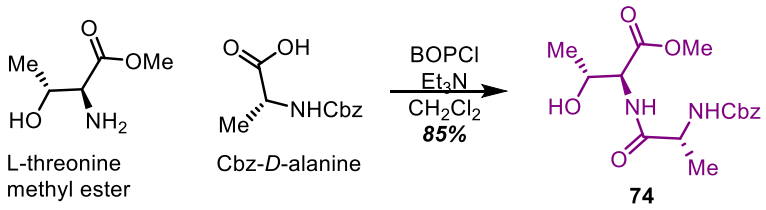

Scheme 25: Synthesis of the lower fragment

Table 2:Peptide coupling reagents for the lower fragment formation

Coupling reagent	Yield
BOPCl, DIPEA, CH_2Cl_2	85%
PyBOP, DIPEA, CH_2Cl_2	79%
EDC•HCl, HOBT, Et_3N, THF	11%

3.5 Synthesis of A-B Ring Dicycle System

Having accessed the actual ring A, and B, the analog of ring A, and B, as well as the lower fragment C, the next step was to couple rings A, and B together in the analog system as well as in the actual system to access A-B dicycle system. Since the analog system acts as the model system for establishing synthesis, coupling ring A and B analogs was attempted first. As shown in Scheme 25, analog of ring A, both Boc protected (**58**) and Cbz protected (**64**) versions were saponified to access the free acids in 47%, and 85% respectively. They were coupled with the Boc deprotected amine **76** using different peptide coupling conditions to obtain A-B ring dicycle system of the analog using. The Boc version was coupled using PyBOP conditions and the Table 3 summarizes

the condition used for the Cbz version. The yields obtained were not that satisfactory to proceed synthesis using this route.

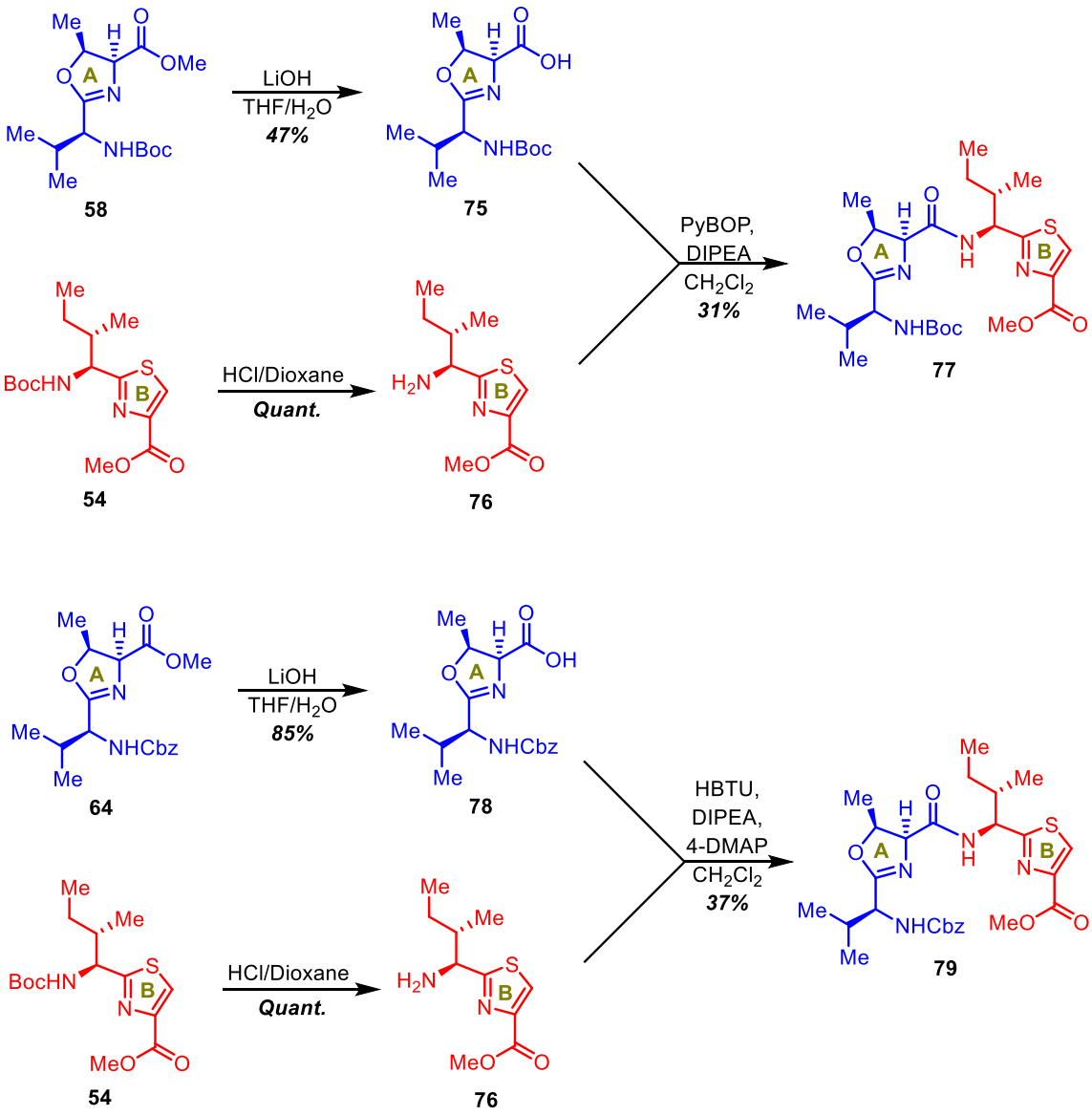

Scheme 26: Synthesis of AB Ring Dicycle System Analog

Table 3: Coupling 76 and 78 to form the AB Ring Dicycle System

Coupling reagent	Yield
HBTU, DIPEA, 4-DMAP, CH_2Cl_2	37%
EDC•HCl, HOBT, Et_3N, THF	No product

The low yields of A-B dicycle formation hinted the need for an alternative approach to access it. Therefore, a reaction was performed as shown in Scheme 27 to test if a single amino acid could be coupled to the deprotected ring B in higher yields to attempt an alternative route to access the A-B ring dicycle system. As such, Cbz-*L*-valine was coupled to **76** using HBTU, DMAP, and DIPEA in methylene chloride.[42] This coupling was accomplished in quantitative yields, hinting that coupling individual amino acids to this system one by one and cyclizing them to construct ring A on ring B could be a possibility rather than coupling the pre-formed ring A and B.

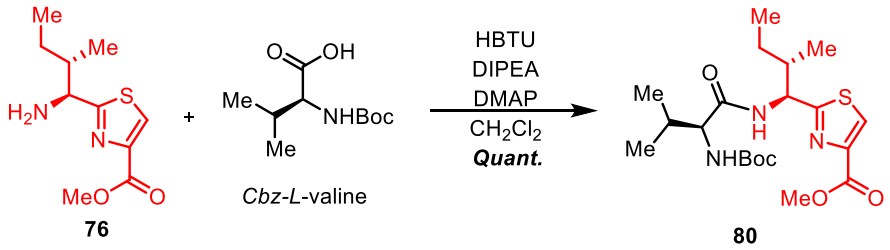

Scheme 27: Single amino acid coupling to ring B analog

With the successful coupling to form **80**, the synthetic strategy was changed to access ring B analog by constructing the ring A on ring B analog. As shown in Scheme 28, Boc-*L*-threonine synthesized from *L*-threonine was coupled to **76** using HBTU as the coupling agent in the presence of DMAP, and DIPEA in methylene chloride in quantitative yields. It was then Boc deprotected with HCl in dioxane and coupled to Cbz-*L*-valine with HBTU, DMAP, and DIPEA in methylene chloride in 88% yield. Cyclization using DAST, and K_2CO_3 in methylene chloride gave access to the oxazoline in ring A in 52% yield.

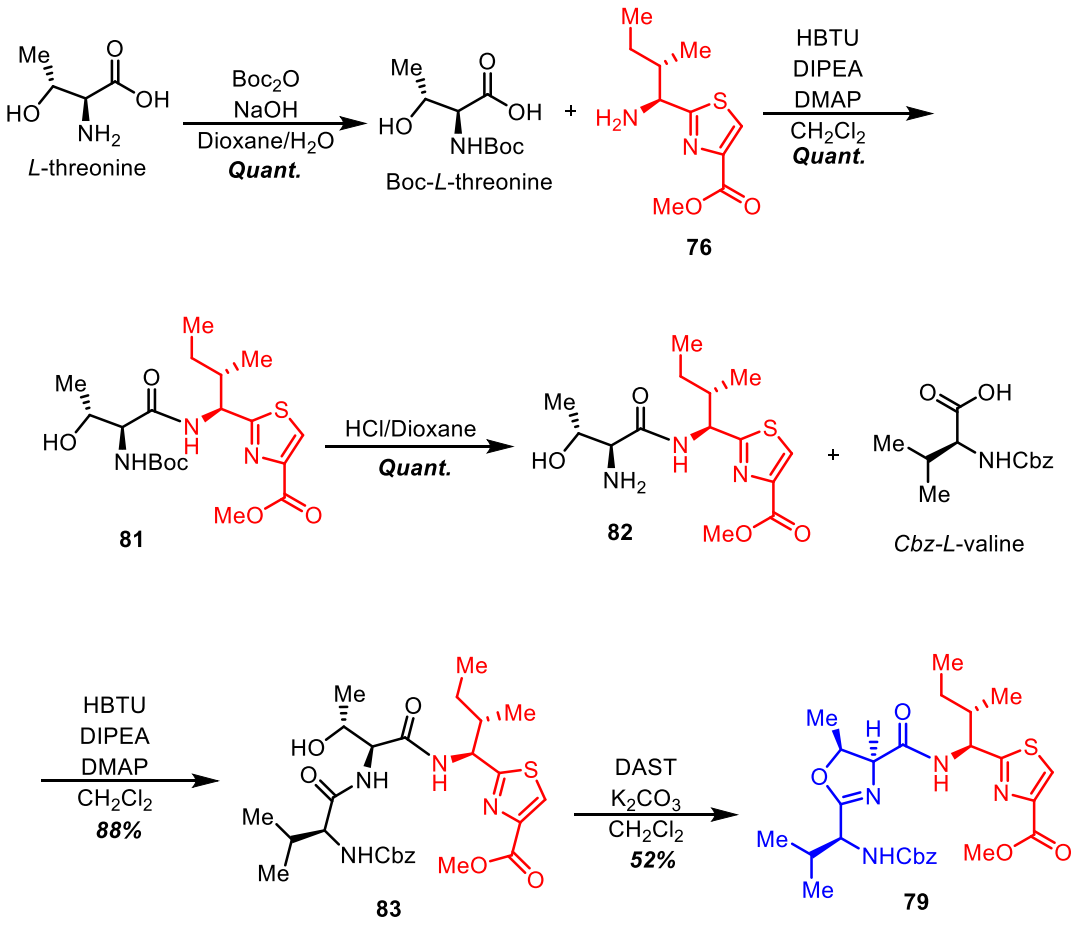

Scheme 28: Constructing ring A analog on ring B analog

Once the route for A-B ring analog dicycle system was established, the actual A-B ring dicycle system was synthesized similarly as shown in Scheme 29. Its synthesis commenced by protecting the amine group in commercially available *L*-allothreonine using Boc anhydride, and NaOH in a mixture on 2:1 dioxane/water which gave access to Boc-allothreonine quantitatively. It was then coupled with the ring B in free amine form with HBTU, DIPEA, and DMAP in methylene chloride to access **85** quantitatively. Deprotection of the Boc group in 3.38 with HCl/dioxane gave access to the free amine **86** quantitatively, which was then coupled with Cbz-*L*-valine with HBTU, DIPEA, and DMAP in methylene chloride to access **87** in 63% yield. Cyclization of **87** with DAST, and K_2CO_3 in methylene chloride gave access to the A-B ring dicycle system in 72% yield.

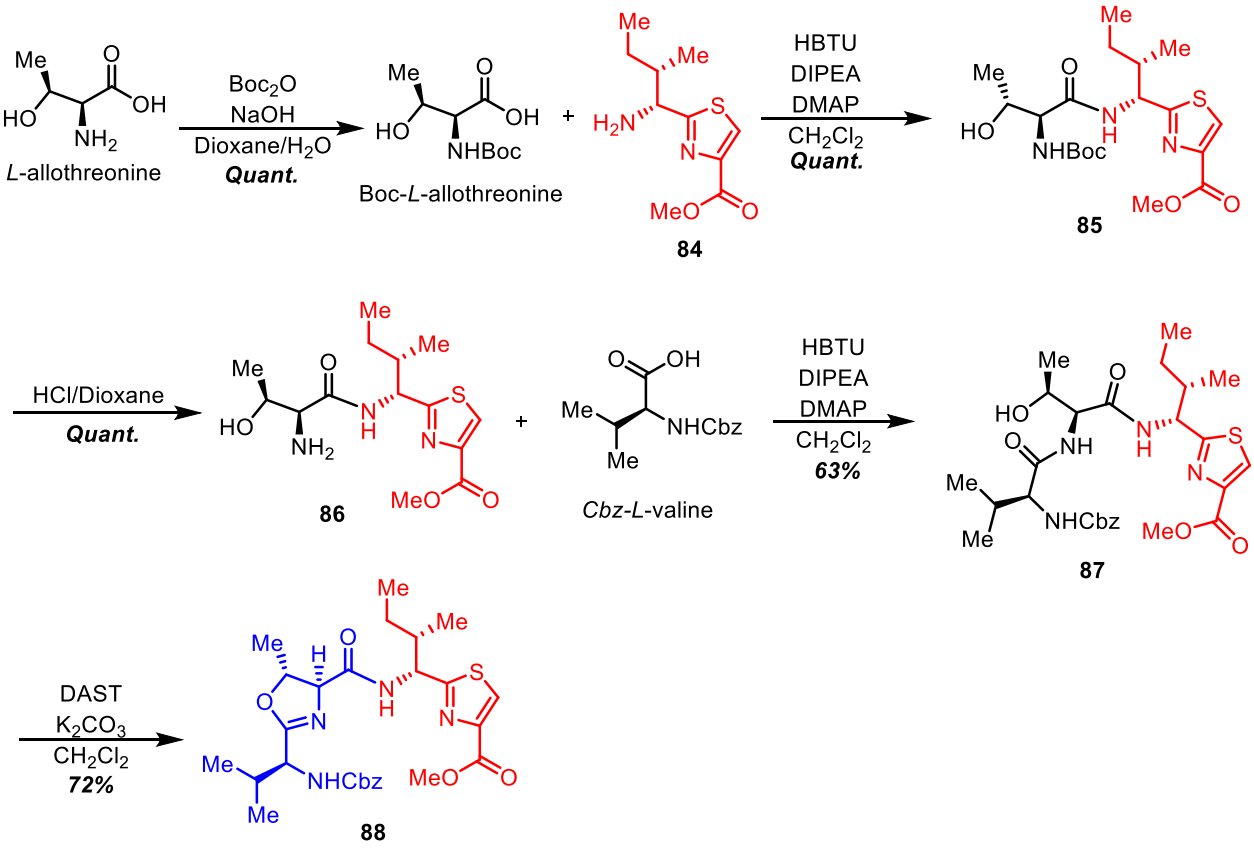

Scheme 29: Constructing ring A on ring B

3.6 Attempts to Couple the Lower Fragment to the A-B Ring Dicycle System and Macrocyclization

3.6.1 Cbz Deprotection on Ring A

In order to couple the lower fragment to the AB ring dicycle system the Cbz on the ring A should be deprotected. As there is a possibility of the oxazoline ring also being reduced with the conditions used for Cbz deprotection, different conditions were used to test for conditions that mediated the Cbz deprotection without causing reductions in the oxazoline ring. The ring A fragment **64** was used as a model system to test this Cbz deprotection step before trying it on the A-B ring dicycle system. Several known protocols for Cbz deprotections (Scheme 30) were applied (Table 4) to determine which conditions would successfully deprotect the Cbz group on **64** retaining the rest

of the molecule intact without reducing the oxazoline double bond. When $Pd(OAc)_2$, Et_3N, and Et_3SiH were used to generate hydrogen in-situ,[59] at room temperature the Cbz did not get deprotected while at 45 °C it caused degradation in the molecule. Hydrogen with palladium on carbon (10% w/w) in ethyl acetate did not deprotect the Cbz group while the same in methanol yielded deprotected **89** quantitatively. Integrity of the oxazoline was confirmed by re-Cbz protecting **89** and matching the NMR with that of the starting material (**64**).

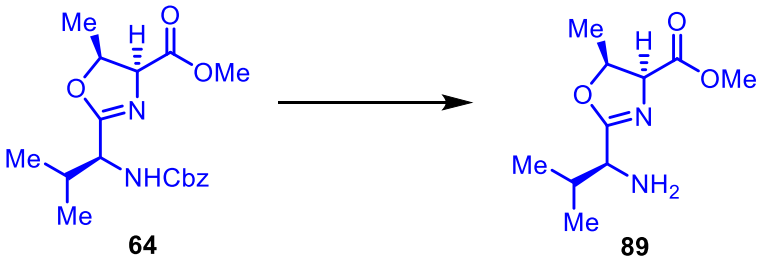

Scheme 30: Cbz deprotection on ring A

Table 4: Cbz deprotection conditions for ring A

Conditions	Yield
$Pd(OAc)_2$, Et_3N, Et_3SiH, CH_2Cl_2, 45 °C	Degradation
$Pd(OAc)_2$, Et_3N, Et_3SiH, CH_2Cl_2, RT	Cbz does not get deprotected
H_2, Pd/C (10% w/w), EtOAc	Cbz does not get deprotected
H_2, Pd/C (10% w/w), MeOH	Quant.

Since using hydrogen with palladium on carbon (10% w/w) in methanol successfully deprotected the Cbz group in **64**, the same conditions were applied on the A-B ring dicycle system to perform the deprotection (Scheme 31). However, Cbz group remained intact under these conditions. Palladium on carbon content was increased then changed to using palladium black instead.[11] It was not surprising that the reaction was harder to perform with palladium as the sulfur in the thiazole

ring poisons the palladium. The deprotection could be made successful upon increasing the palladium content in the reaction up to 10 equivalents as shown in table 3D with a 98% yield.

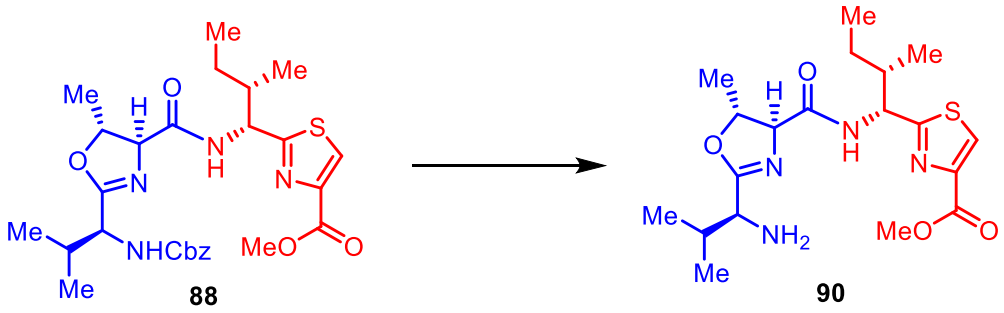

Scheme 31: Cbz deprotection on the AB ring dicycle system

Table 5: Cbz deprotection on the AB ring dicycle system

Conditions	Yield
H_2, Pd/C (10% w/w), MeOH	No conversion
H_2, Pd/C (50% w/w), MeOH	No conversion
H_2, Pd-black (0.5 eq.), MeOH	No conversion
H_2, Pd-black (1.8 eq.), MeOH	Negligible conversion
H_2, Pd-black (5 eq.), MeOH	Incomplete conversion
High pressure H_2 (using a hydrogenator), Pd-black (5 eq.), EtOH/treiethylamine (2:1)	Incomplete conversion
H_2, Pd-black (10 eq.), EtOH/treiethylamine (2:1)	98%

3.6.2 Coupling the Lower Fragment to the AB Ring Dicycle System from the Left Side

After successfully accomplishing the Cbz deprotection on **88**, coupling the lower fragment and macrocyclization after deprotections of the amino and carboxyl ends was undertaken as shown in Scheme 32. The lower fragment **74** was saponified with LiOH in a 1:1 methanol/water system, and Cbz deprotection of **88** was performed with Pd-black in an ethanol/triethylamine system. The

resultant deprotected carboxylic acid **91** was coupled to the free amine of deprotected A-B ring dicycle system analog (**90**) using HBTU, DMAP, and DIPEA in methylene chloride in 63% yield.

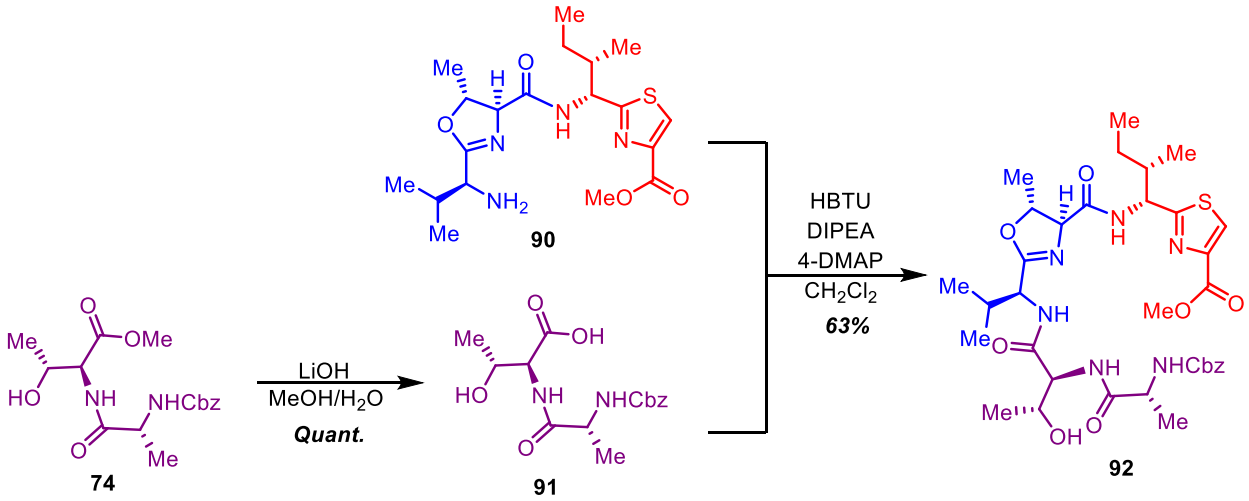

Scheme 32: Coupling the lower fragment to the AB ring dicycle system from the left side

The resultant system was subjected to a saponification with LiOH in a 1:1 THF/water and a Cbz deprotection was carried using Pd-black in a 2:1 ethanol/triethylamine system, both in quantitative yields to access **94** (Scheme 33). Macrocyclization was attempted on **94** using HBTU, DMAP, and DIPEA in methylene chloride to access balgacyclamide B. Unfortunately, macrocyclization was not successful for this system with HBTU. This step should be further tested using different coupling reagents if macrocyclization is to be achieved via this route.

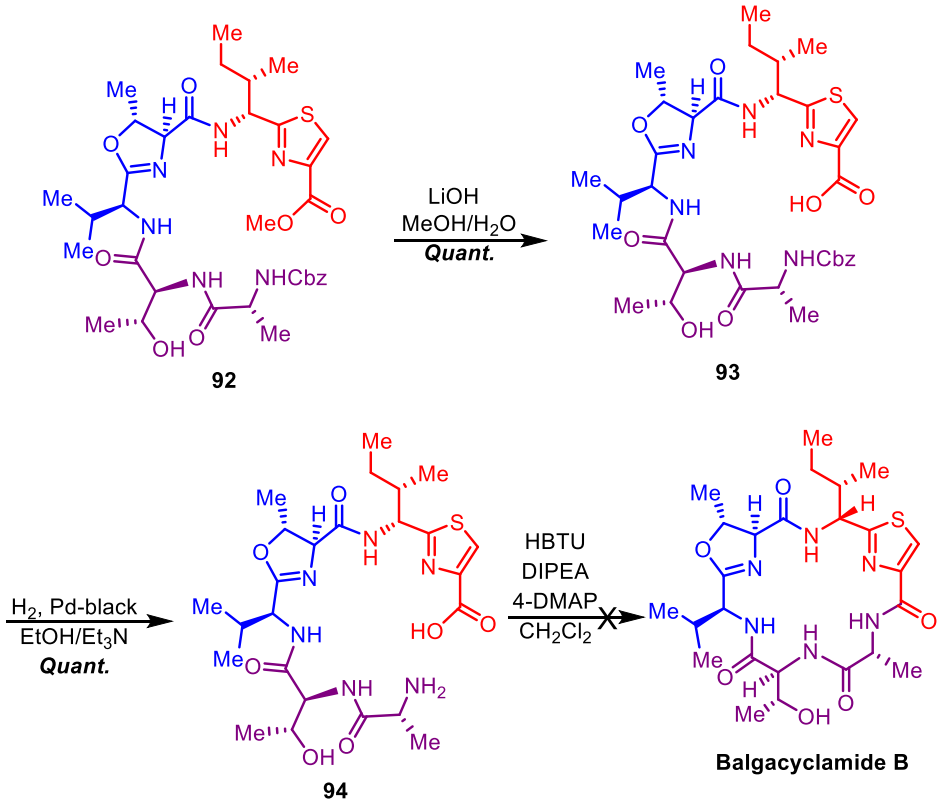

Scheme 33: Attempt to form balgacyclamide B analog via coupling the lower fragment to the AB ring dicycle system from the left side

3.6.3 Coupling the Lower Fragment to the A-B Ring Dicycle System from the Right Side

Macrocyclization to access balgacyclamide B analog was attempted in different ways at the same time. Because, steric factors, electronics, and three-dimensional orientation of the molecule can hinder or facilitate the two open ends; the carboxyl end and the amino end of the linear molecule coming together to form a peptide bond, even with the same peptide coupling reagent. While attempting the macrocyclization as described in section 3.4.2, efforts also went on to couple the lower fragment to the A-B ring dicycle system analog from the right side to explore the possibility of performing macrocyclization from the other side of the molecule. A saponification was performed on **88** with lithium hydroxide to access **95** free carboxylic acid which was reacted with

the Cbz deprotected lower fragment using HBTU as the coupling reagent. However, this reaction was not successful.

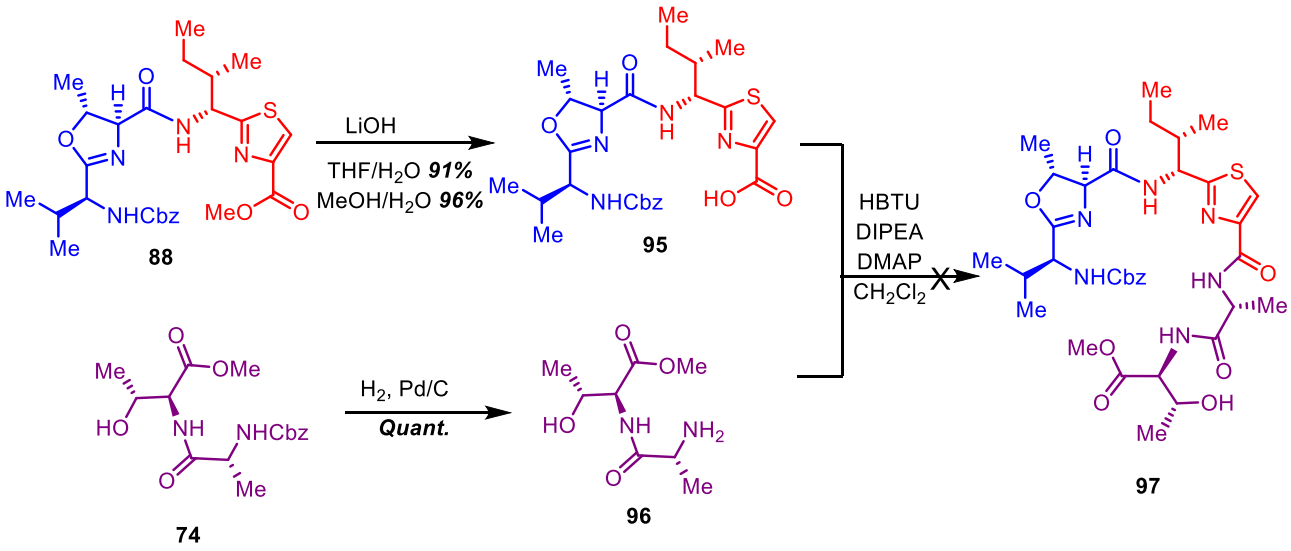

Scheme 34: Attempt to couple the lower fragment to the A-B ring dicycle system from the right side

3.6.4 Coupling Individual Components of the Lower Fragment

As previous attempts to form the macrocycle did not give the expected success at once, a third strategy was attempted to perform the macrocyclization. That is, without attaching the entire lower fragment to either ring A or B, separately coupling the *L*-threonine and *D*-alanine fragments to ring A and ring B respectively. It was hypothesized that having less steric hindrance to both the amine end and the carboxyl end compared to the other macrocyclization attempts in section 3.4.2.and 3.4.3, amide formation here could be more feasible. Hence, as shown in Scheme 35, after saponifying **88** in quantitative yields *D*-alanine methyl ester was coupled with the resultant free acid to form **98** in 51% yield. Then the Cbz deprotection was carried out using hydrogen and palladium black with 98% yield followed by coupling the resultant amine **99** with Cbz-*L*-threonine using HBTU in 74% yield. After performing a saponification and a Cbz deprotection,

macrocyclization was attempted to form balgacyclamide B. However, the final product was not isolated or formed.

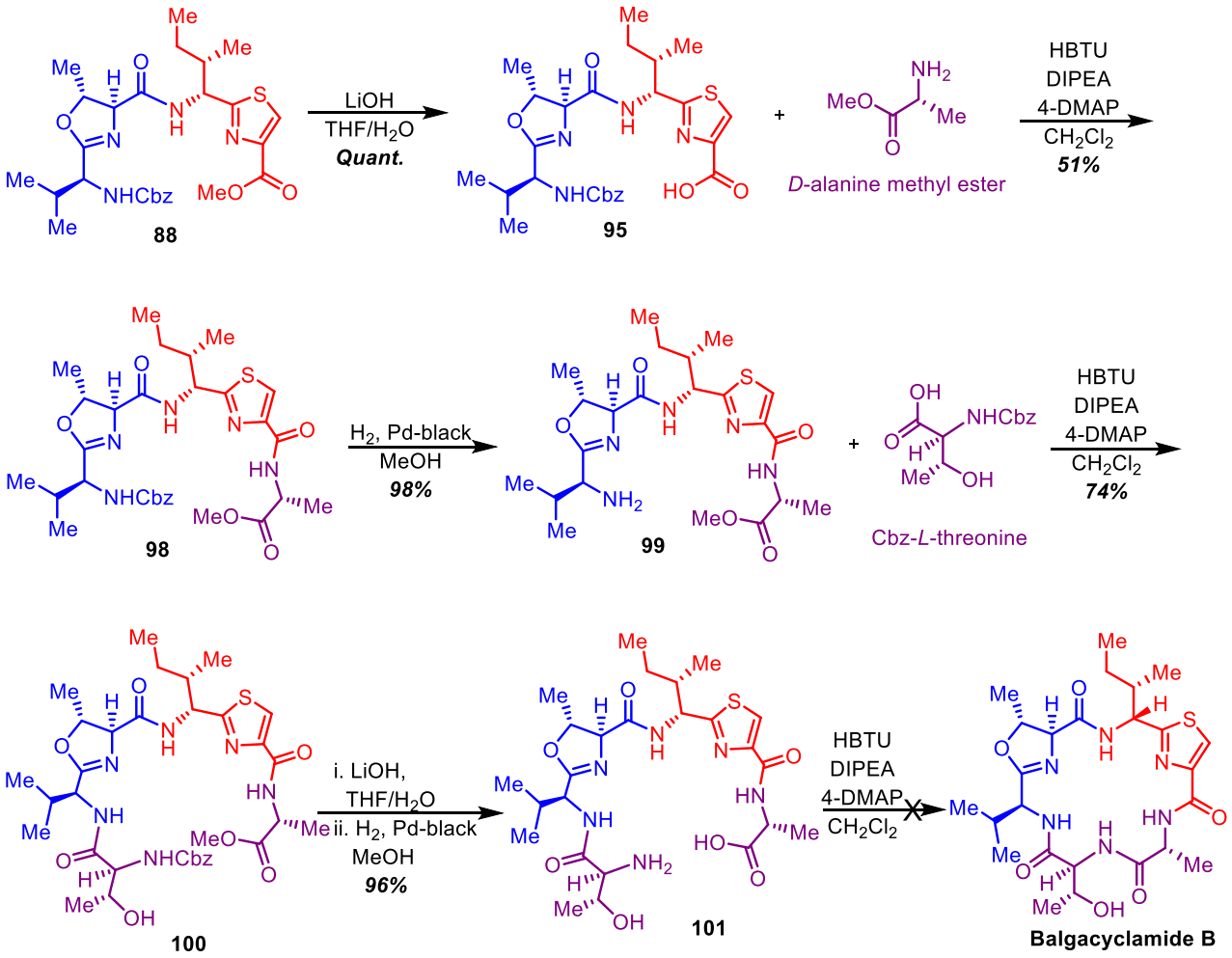

Scheme 35: Coupling the single amino acids that make up the lower fragment separately to ring A and B

3.6.5 Accessing Balgacyclamides

To complete the formation of balgacyclamide B, the final macrocyclization step need to be explored and optimized. For this purpose, all three routes explored so far can be further analyzed. However, with the success of accessing **94**, and **101** it would be efficient to focus on the routes explained in section 3.4.2, 3.4.4. One way these macrocyclization steps can be optimized is by purifying the saponified products rather than using the crude material to proceed to

macrocyclization. Also, exploring different peptide coupling reagents as well as changing the order of addition and slowly adding the compound to be cyclized to a solution of peptide coupling reagent, the macrocyclization could be attempted.

3.6.6 Accessing Final Balgacyclamide A

Once balgacyclamide B is accessed, the lower fragment could be cyclized to form an oxazoline using a molybdenum catalyst to obtain balgacyclamide A. With our laboratory's experience of using $(NH_4)_6Mo_7O_{24}$ as the catalyst for oxazoline formation, low yields could be expected for this reaction. However, unreacted starting material was always recoverable in high yields. Therefore, at this late stage of synthesis, this would be a reasonable reagent to be used for oxazoline formation, retaining the stereochemistry of the methyl center marked with an asterisk in Scheme 37.

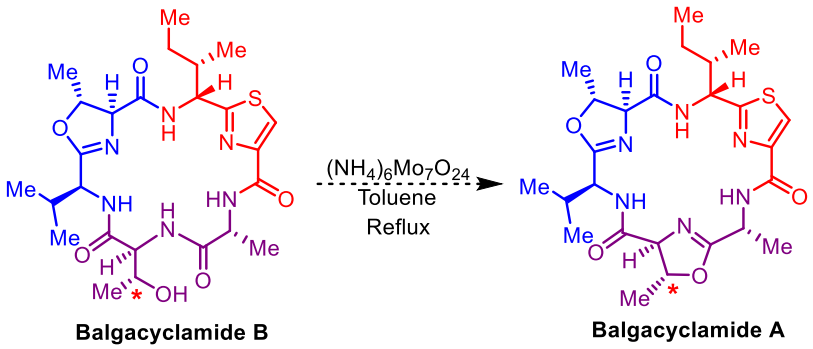

Scheme 36: Accessing Balgacyclamide A from Balgacyclamide B

Once balgacyclamide A and B is accessed, using the same synthetic route balgacyclamide analogs also will be accessed (Scheme 37). Finally, cytotoxicity of balgacyclamide A and B, their analogs as well as all the intermediates will be assessed.

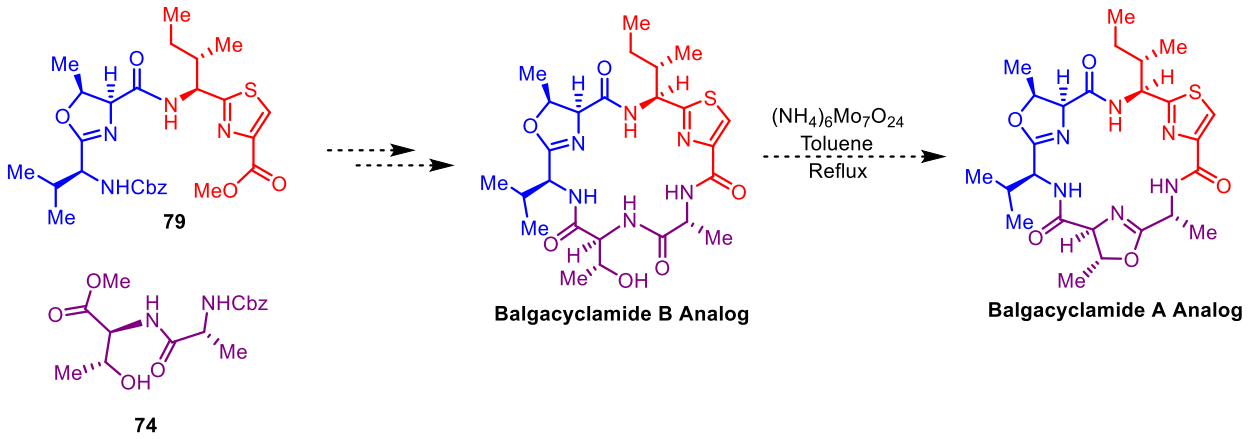

Scheme 37: Accessing Balgacyclamide A from Balgacyclamide B Analogs

3.7 Other Applications of Balgacyclamides and Their Intermediates

3.7.1 Balgacyclamides as an Anticancer Drug Delivery System

Among the many anticancer agents available, a common dark side most of the approved anticancer drugs or molecules that are potential anticancer drug suffer is their non-specific distribution in the body causing off-target side effects. A major proportion of cancer-related research is dedicated to exploring ways to combat this non-specific drug delivery utilizing targeted drug delivery methods.[60] Drug targeting strategies for cancer cells could be passive targeting or active targeting[61,62]: passive targeting takes advantage of the leaky vasculature in tumors to penetrate once they accumulate around the tumor and active targeting uses specific ligand-receptor interactions to enter cancer cells.[62] While a large number of nano-carrier based ways of targeting cancer for drug delivery are in research,[63] others use ways such as conjugating an anticancer drug with a molecule that has the inherent ability to penetrate cancer cells. For example, several anticancer molecules such as chlorambucil, and paclitaxel have shown less toxicity when they are conjugated to glucose as cancer cells have an increased rate of glucose uptake compared to normal cells with their overexpressed GLUT receptors.[64,65]

Using a similar concept, given that balgacyclamides penetrate to lung and colon cancer cells our lab has hypothesized that conjugating balgacyclamide with an anticancer drug (Figure 20) could potentially deliver anticancer drug to cancer cells minimizing off-target effects. As lung and colon cancers are among the highly reported types of cancer,[66] our approach will help explore more into this problem and potentially help develop a good drug carrier to these cell lines. For this purpose, once the total synthesis of balgacyclamides is accomplished, SAR analysis needs to be performed to identify a site in the NP to conjugate the anticancer agent without losing its ability to penetrate to cancer cells. If the free hydroxyl group in balgacyclamide B is not essential for its penetration abilities, it could be a readily available group that can be used to easily conjugate a drug.

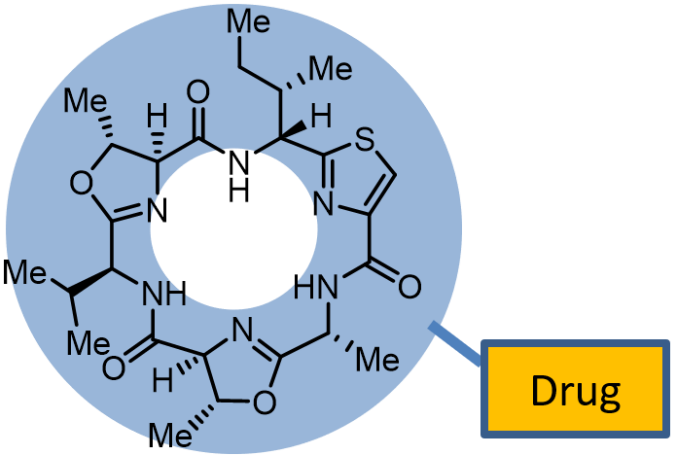

Figure 20: Conjugating an anticancer drug to balgacyclamides for selective drug delivery

3.7.2 Using the Intermediates of Balgacyclamides to Explore Porin-Mediated Small Molecule Transport

As explained in Chapter 1 and 2, developing molecules with antibacterial properties for GNbac is challenging mainly due to the limitations caused by porin-mediated small molecule transportation. Our lab embarked on a journey to explore PCPs that govern PCPs of small molecules affecting porin-mediated transportation. To initialize a systematic study on this based on a small molecule library, an intermediate of balgacyclamide was used. The A-B ring dicycle system was used as the

core scaffold to construct a small molecule library to explore these aspects by our laboratory. The reason behind choosing this scaffold is that due to the presence of the amino end and the carboxylic acid ends, it can be derivatized altering different tethers.

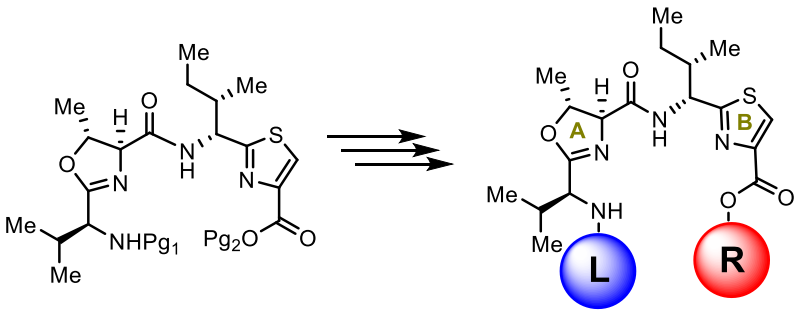

Scheme 38: Derivatizing the main scaffold

To assess GNbac transport/accumulation capabilities our lab has developed a whole cell assay as the bases of evaluation. All compounds will be assessed for transport with these methods, in triplicate against control compounds in parallel for statistical analysis. The screening of transport for GNbac will be accomplished through the use of *Escherichia coli* (*E. coli*) MG1655, as this strain had minimal alterations from its K-12 progenitor. The method we have developed grows cultures to an optical density of 0.55 and the number of colony-forming units (CFUs) are assessed (Figure 21, Step 1). Test compounds (50 μM) were added and allowed to incubate at 37 °C (Step 2). After 10 min, the sample were layered onto silicone oil, centrifuged for 2 min, the supernatant discarded, and pellets were lysed by freeze thaw cycles in liquid nitrogen. Lysates were pelleted and the supernatant collected (Step 3). Samples, injection volume 15 μL, was analyzed via a Ion-trap LC/MS-MS (Thermo-Finnigan) with a HP 1100 high performance liquid chromatograph system in both positive and negative electrospray ionization (Step 4). Controls employed are based upon their known accumulation properties within *E. coli*: ciprofloxacin (high), tetracycline (moderate), and novobiocin (low-negative).

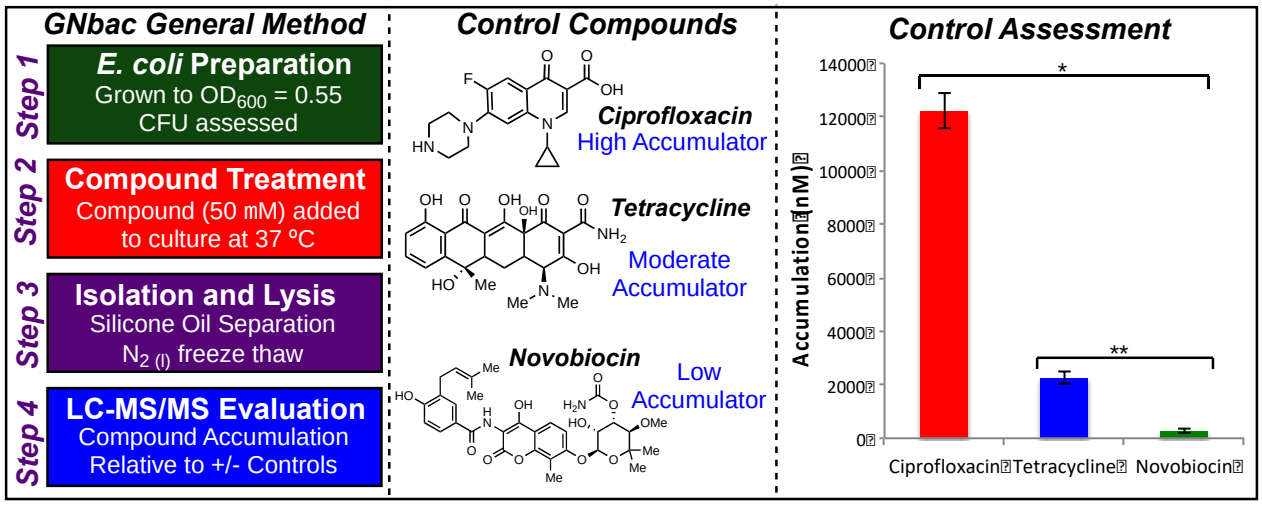

Figure 21: Left: GNbac method for compound assessment of penetration. Middle: Control compounds for assay. Right: Control compound assessment in developed assay. Performed in triplicate. Statistical significance was determined by using a two-sample Student's *t*-test (two-tailed, equal variance). *P<0.01, **P<0.001.

The small molecule library consisted molecules that had carboxylic acids coupled to the left side via amide bonds, and different alcohols forming esters with the carboxylic group in the right side as shown in Figure 22. The right-side substituents R1, R3, and R5 were tested in protected (RCO_2Me) as well as the deprotected free acid form (RCO_2H). The molecular accumulation inside *E. coli* was assessed for all the molecules by treating the bacteria with the compounds and analyzing the isolated cell lysates by LC-MS/MS. Several trends were observed in terms of the properties of the small molecules that penetrated *E. coli*.

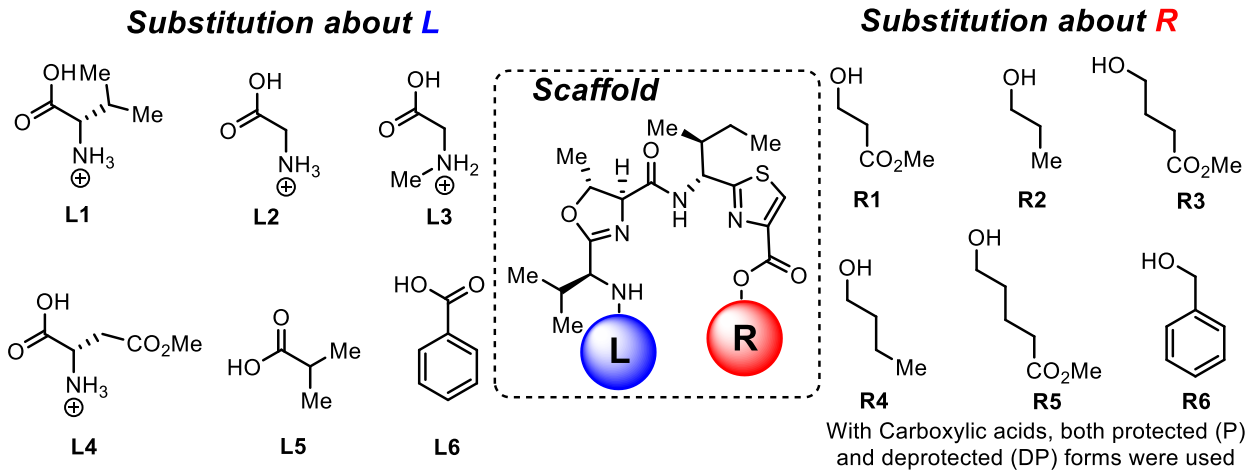

Figure 22: Different tethers used to derivatize the main scaffold

First the bacterial accumulation of A-B ring dicycle system was tested with the two termini protected and deprotected (Table 6). It was observed that the parent scaffold in the protected state did not have bacterial penetration. It confirms that this scaffold is an acceptable inactive scaffold which would allow exploring how the chemical nature of the appended tethers affect penetration into bacteria. Also, interestingly the zwitterionic form of the scaffold showed considerably higher bacterial penetration. Though it has been known in literature that the presence of an ionizable primary amine increases the porin-mediated penetration, in this experiment it was not observed so, instead the very high penetration shown by the zwitterionic form suggests that more consideration should be given to exploring how zwitterionic forms behave or can be used to increase the bacterial penetration of small molecule.

Table 6: Bacterial penetration of protected and deprotected parent scaffold

R1	R2	% Penetration Relative to Control
Boc	Me	2.4
Boc	H	2.9
H	Me	1.8
H	H	33.8

Then to explore how the chain length of the tethers affect penetration of the small molecules into bacteria, a series of molecules were synthesized changing the length of the tether in the right (attached to the carboxylic acid end). When the values are compared it can be seen that with increasing chain length the penetration has increased.

Another series of molecules were synthesized in our lab as shown in Table 7. Exploring the bacterial accumulation of these molecules it was identified that **102** had the highest penetration ability. When **103** is compared with **102** (Figure 23) they have similar tethers attached where the tethers have flipped the side to which they are attached. Therefore, they have approximately the same physicochemical parameters (e.g. charge, polarity/ clogD, size, and molecular weight). From what is reported in the literature, we would expect both these molecules to have similar abilities to penetrate through porins as they have similar PCPs. However, surprisingly, despite sharing approximately the same PCPs, was non-penetrant compared the most penetrant **102**. This observation leads us to think that not only the PCPs, but also the charge distribution and the spatial orientation of charge has a major effect on the porin-mediated small molecule transportation.

Table 7: Bacterial penetration of AB ring dicycle analogs with changing chain lengths

R1	R2	% Penetration Relative to Control
Boc	R1	16.7
H	R1	40.8
Boc	R2	Not observed
H	R2	2.3
Boc	R3	17
H	R3	45.2
Boc	R4	Not observed
H	R4	Not observed
Boc	R5	Not observed
H	R5	49.7
Boc	R6	Not observed
H	R6	Not observed

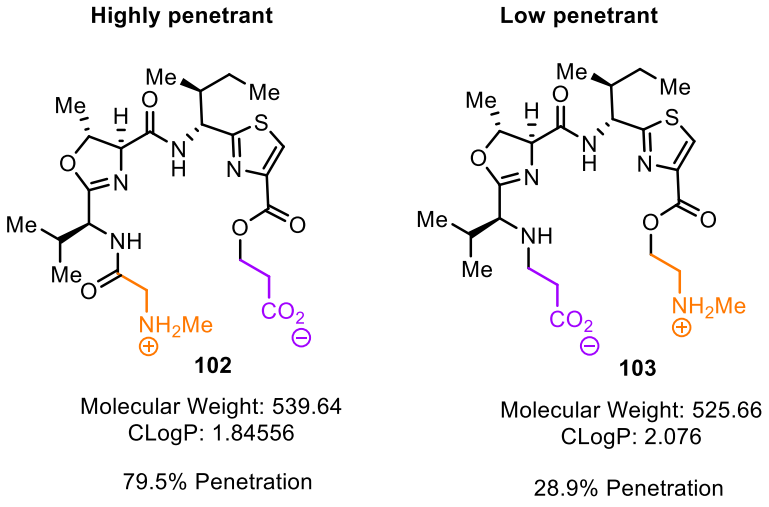

Figure 23: Molecules with approximately the same PCPs showing drastically different GNbac penetration values

Further exploring the patterns of PCPs that enhance porin-mediated small molecule transportation will greatly help designing and repurposing antibiotics that would be active against GNBac. Also, understanding how spatial orientation of charge in a molecule affect its porin-mediated transportation is a novel area of research that has not been explored. Exploring this aspect using different scaffolds, most importantly a rigid scaffold will be the next step in our research to more systematically study charge to 3D structure

Chapter 4 - Conclusion & Future Work

The efforts towards the total synthesis of balgacyclamide A and B, and their analogs (Figure 24) are underway with promising results. The synthetic route established for this purpose has a convergent synthetic approach to access two NPs (both balgacyclamide A and B) in one route. In the efforts to synthesize balgacyclamide NPs, as a model system and analogs for SAR analysis, two analogs of balgacyclamides are being synthesized.

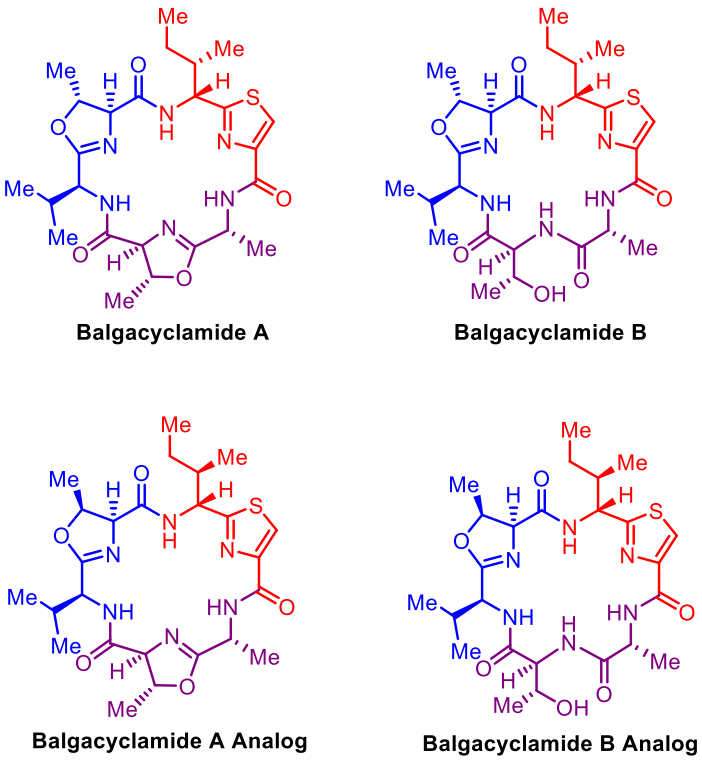

Figure 24: Balgacyclamide A and B and their analogs being synthesized

All the fragments of balgacyclamide A and B as well as the analogs have been successfully accessed (Scheme 39). As such, the thiazole rings of actual balgacyclamides, and balgacyclamide analogs were accessed with an overall yield of 93%. The lower fragment was accessed in 85% yield. As established in chapter 3, the best way to access the A-B dicycle system is constructing ring A (oxazoline ring) on ring B (thiazole ring) rather than coupling the individual rings. As such,

the A-B dicycle system was constructed on the thiazole of both the analog system (**79**) and actual balgacyclamides (**88**) with overall yields 43% and 42% respectively.

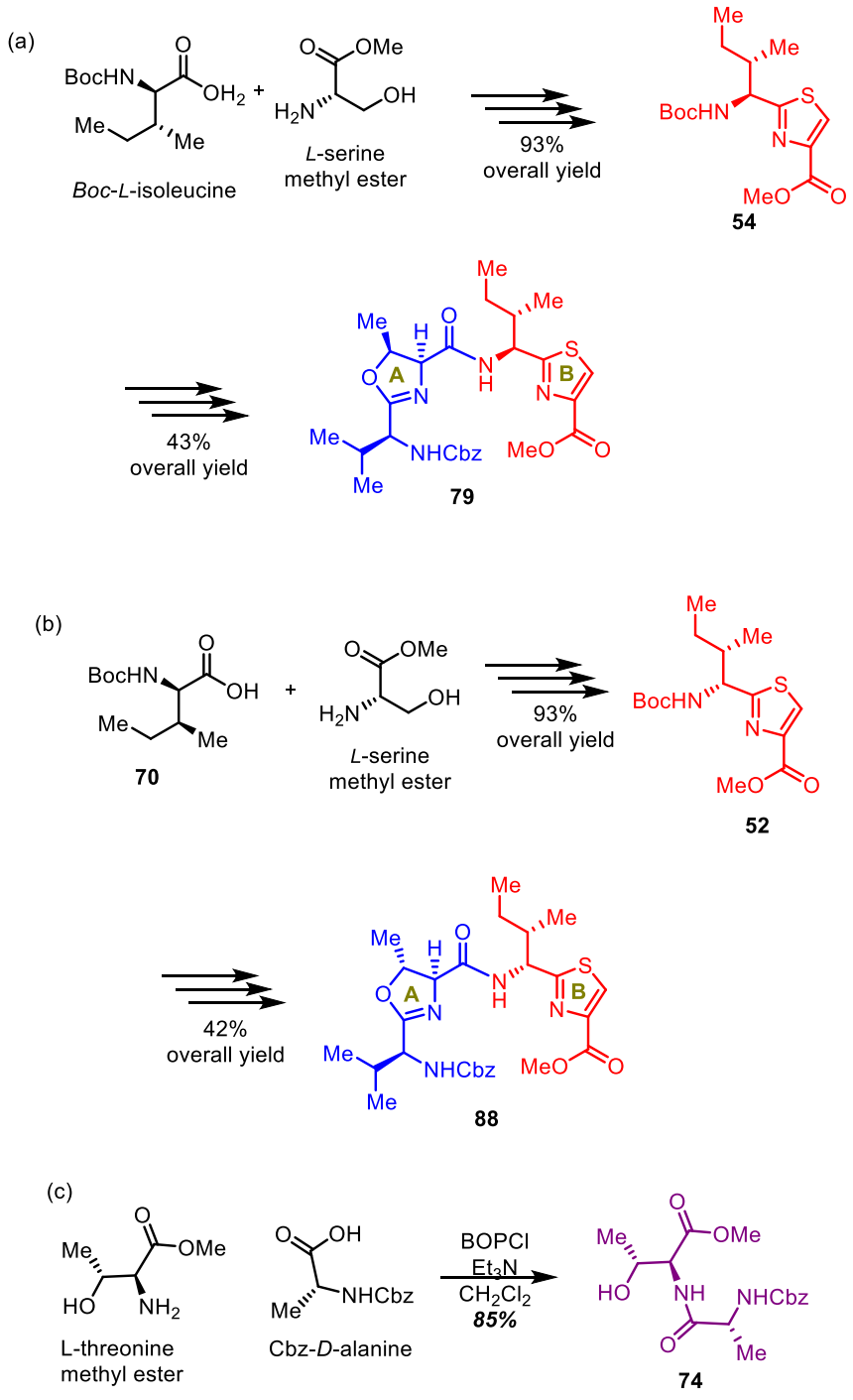

Scheme 39: (a) Accessing A-B dicycle system analog, (b) accessing the actual A-B dicycle system, (c) accessing the lower fragment

The lower fragment was successfully coupled on to ring A to access intermediate **92** in 36% overall yield, while the other approach of coupling the components of the lower fragment separately to the A-B dicycle system gave access to **100** in 15% overall yield (Scheme 40). Macrocyclization was attempted on both the systems with unsuccessful results. The macrocyclization was attempted. The macrocyclization should be investigated to successfully access balgacyclamide B. Due to the less steric hindrance in intermediate **100** compared to intermediate **92**, there is a higher possibility of successfully accessing balgacyclamide B via **100**. Aminolysis conditions, as well as other different peptide coupling conditions would be attempted to access balgacyclamide B.

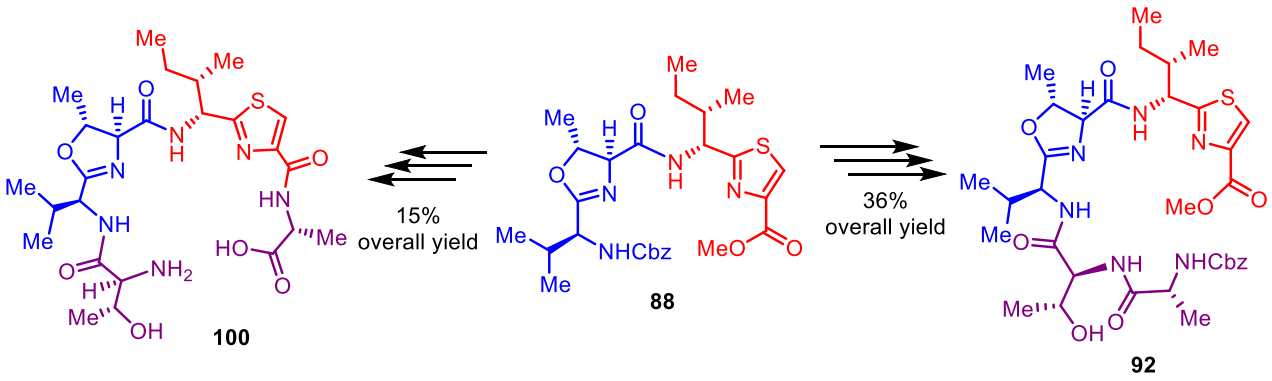

100 **88** **92**

Scheme 40: Accessing intermediates 92 and 100

Once balgacyclamide B is accessed, the lower fragment would be cyclized to form an oxazoline while retaining the stereochemistry at the methyl stereocenter (Scheme 41). Therefore, a molybdenum-containing catalyst would be employed for this reaction. Using the same established route, the two analogs also would be accessed. Biological activity of both NPs as well as the analogs will be tested. SAR analysis would be done on these molecules to elucidate the best point of conjugation for attaching an anticancer drug to selectively deliver anticancer drugs to cancer cells.

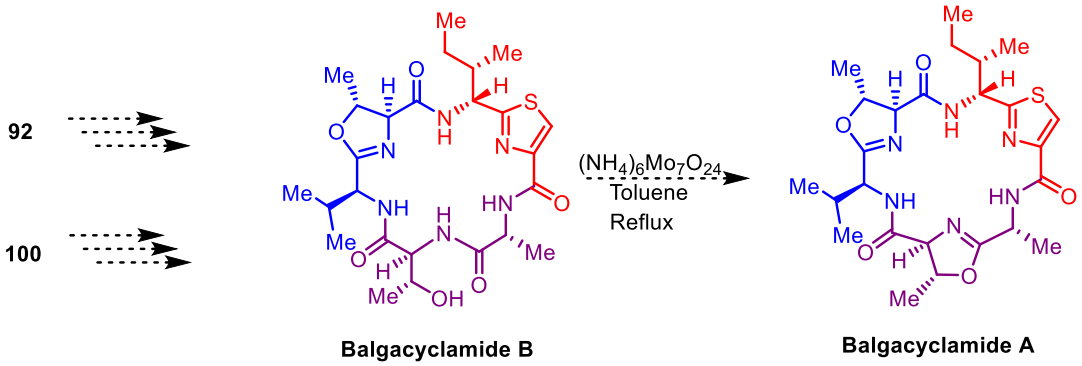

Scheme 41: Accessing balgacyclamide A and B

The pilot study done using the small molecule library constructed based on AB-dicycle system to investigate the effect of PCPs on small molecular penetration to GNbac, many intriguing findings were observed. The main highlight of the study was observing how the three-dimensional orientation of the molecules greatly affected the GNbac penetrating ability of the molecules despite having the same PCPs. However, as these molecules have a significant amount of free rotation, it is difficult to systematically study how the charge distribution of a molecule affect their GNbac penetration ability. Therefore, using an intermediate of another total synthesis in our lab that has a rigid core structure scheme (brocazine family of NPs), another small molecule library will be constructed to systematically study how charge distribution of a molecule and their three-dimensional orientation affects their porin-mediated transport into GNbac cells Scheme 42.

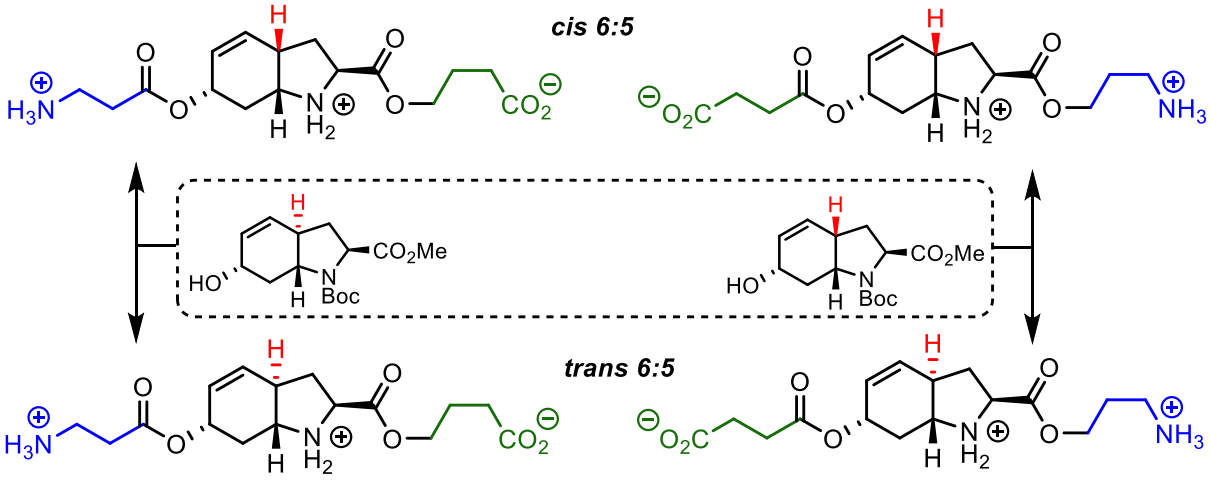

Scheme 42: Studies into the effects of cis/trans bicycles with imparted PCPs for GNbac penetration

Chapter 5 - References

(1) Martín, J. F.; Casqueiro, J.; Liras, P. Secretion Systems for Secondary Metabolites: How Producer Cells Send out Messages of Intercellular Communication. *Current Opinion in Microbiology*. Elsevier Current Trends June 1, 2005, pp 282–293. https://doi.org/10.1016/j.mib.2005.04.009.

(2) Isah, T. Stress and Defense Responses in Plant Secondary Metabolites Production. *Biological research*. NLM (Medline) July 29, 2019, p 39. https://doi.org/10.1186/s40659-019-0246-3.

(3) Newman, D. J.; Cragg, G. M. Natural Products as Sources of New Drugs over the Nearly Four Decades from 01/1981 to 09/2019. *Journal of Natural Products*. American Chemical Society March 27, 2020, pp 770–803. https://doi.org/10.1021/acs.jnatprod.9b01285.

(4) Portmann, C.; Sieber, S.; Wirthensohn, S.; Blom, J. F.; Da Silva, L.; Baudat, E.; Kaiser, M.; Brun, R.; Gademann, K. Balgacyclamides, Antiplasmodial Heterocyclic Peptides from *Microcystis Aeruguinosa* EAWAG 251. *J. Nat. Prod.* **2014**, *77* (3), 557–562. https://doi.org/10.1021/np400814w.

(5) Sivonen, K.; Leikoski, N.; Fewer, D. P.; Jokela, J. Cyanobactins-Ribosomal Cyclic Peptides Produced by Cyanobacteria. https://doi.org/10.1007/s00253-010-2482-x.

(6) Martins, J.; Vasconcelos, V. Cyanobactins from Cyanobacteria: Current Genetic and Chemical State of Knowledge. *Marine Drugs*. MDPI AG November 1, 2015, pp 6910–6946. https://doi.org/10.3390/md13116910.

(7) Salvatella, X.; Caba, J. M.; Albericio, F.; Giralt, E. Solution Structure of the Antitumor Candidate Trunkamide A by 2D NMR and Restrained Simulated Annealing Methods. *J. Org. Chem.* **2003**, *68* (2), 211–215. https://doi.org/10.1021/jo026464s.

(8) Prinsep, M. R.; Moore, R. E.; Levine, I. A.; Patterson, G. M. L. Westiellamide, a

Bistratamide-Related Cyclic Peptide from the Blue-Green Alga Westiellopsis Prolifica. *J. Nat. Prod.* **1992**, *55* (1), 140–142. https://doi.org/10.1021/np50079a022.

(9) Patellamide A - an overview | ScienceDirect Topics https://www.sciencedirect.com/topics/agricultural-and-biological-sciences/patellamide-a (accessed Jul 6, 2020).

(10) Portmann, C.; Blom, J. F.; Gademann, K.; Jüttner, F. Aerucyclamides A and B: Isolation and Synthesis of Toxic Ribosomal Heterocyclic Peptides from the Cyanobacterium Microcystis Aeruginosa PCC 7806. *J. Nat. Prod.* **2008**, *71* (7), 1193–1196. https://doi.org/10.1021/np800118g.

(11) Downing, S. V.; Aguilar, E.; Meyers, A. I. Total Synthesis of Bistratamide D. *J. Org. Chem.* **1999**, *64* (3), 826–831. https://doi.org/10.1021/jo981664i.

(12) Gu, W.; Dong, S.-H.; Sarkar, S.; Nair, S. K.; Schmidt, E. W. The Biochemistry and Structural Biology of Cyanobactin Biosynthetic Enzymes. https://doi.org/10.1016/bs.mie.2018.03.002.

(13) McIntosh, J. A.; Schmidt, E. W. Marine Molecular Machines: Heterocyclization in Cyanobactin Biosynthesis. *ChemBioChem* **2010**, *11* (10), 1413–1421. https://doi.org/10.1002/cbic.201000196.

(14) Rafferty, R. J.; Hicklin, R. W.; Maloof, K. A.; Hergenrother, P. J. Synthesis of Complex and Diverse Compounds through Ring Distortion of Abietic Acid. *Angew. Chemie Int. Ed.* **2014**, *53* (1), 220–224. https://doi.org/10.1002/anie.201308743.

(15) Scior, T.; Bender, A.; Tresadern, G.; Medina-Franco, J. L.; Martínez-Mayorga, K.; Langer, T.; Cuanalo-Contreras, K.; Agrafiotis, D. K. Recognizing Pitfalls in Virtual Screening: A Critical Review. *Journal of Chemical Information and Modeling*. UTC 2012, pp 867–881. https://doi.org/10.1021/ci200528d.

(16) Yun, H.; Chou, T. C.; Dong, H.; Tian, Y.; Li, Y. M.; Danishefsky, S. J. Total Synthesis as a Resource in Drug Discovery: The First in Vivo Evaluation of Panaxytriol and Its Derivatives. *J. Org. Chem.* **2005**, *70* (25), 10375–10380. https://doi.org/10.1021/jo0515475.

(17) Kawano, S.; Ito, K.; Yahata, K.; Kira, K.; Abe, T.; Akagi, T.; Asano, M.; Iso, K.; Sato, Y.; Matsuura, F.; et al. A Landmark in Drug Discovery Based on Complex Natural Product Synthesis. *Sci. Rep.* **2019**, *9* (1), 1–9. https://doi.org/10.1038/s41598-019-45001-9.

(18) Shipps, G. W.; Pryor, K. E.; Xian, J.; Skyler, D. A.; Davidson, E. H.; Rebek, J. Synthesis and Screening of Small Molecule Libraries Active in Binding to DNA. *Proc. Natl. Acad. Sci. U. S. A.* **1997**, *94* (22), 11833–11838. https://doi.org/10.1073/pnas.94.22.11833.

(19) Kingwell, K. Medicinal Chemistry: Exploring the Third Dimension. *Nat. Rev. Drug Discov.* **2009**, *8* (12), 931. https://doi.org/10.1038/nrd3058.

(20) Ghose, A. K.; Viswanadhan, V. N.; Wendoloski, J. J. Prediction of Hydrophobic (Lipophilic) Properties of Small Organic Molecules Using Fragmental Methods: An Analysis of ALOGP and CLOGP Methods. *J. Phys. Chem. A* **1998**, *102* (21), 3762–3772. https://doi.org/10.1021/jp980230o.

(21) Huigens, R. W.; Morrison, K. C.; Hicklin, R. W.; Timothy, T. A.; Richter, M. F.; Hergenrother, P. J. A Ring-Distortion Strategy to Construct Stereochemically Complex and Structurally Diverse Compounds from Natural Products. *Nat. Chem.* **2013**, *5* (3), 195–202. https://doi.org/10.1038/nchem.1549.

(22) Ventola, C. L. The Antibiotic Resistance Crisis: Causes and Threats. *P T J.* **2015**, *40* (4), 277–283. https://doi.org/Article.

(23) Ventola, C. L. The Antibiotic Resistance Crisis: Part 1: Causes and Threats. *P T* **2015**, *40* (4), 277–283.

(24) Munita, J. M.; Arias, C. A. Mechanisms of Antibiotic Resistance. *Microbiol. Spectr.* **2016**, *4* (2). https://doi.org/10.1128/microbiolspec.VMBF-0016-2015.

(25) Kapoor, G.; Saigal, S.; Elongavan, A. Action and Resistance Mechanisms of Antibiotics: A Guide for Clinicians. *J. Anaesthesiol. Clin. Pharmacol.* **2017**, *33* (3), 300–305. https://doi.org/10.4103/joacp.JOACP_349_15.

(26) Vouga, M.; Greub, G. Emerging Bacterial Pathogens: The Past and Beyond. *Clinical Microbiology and Infection*. Elsevier B.V. January 1, 2016, pp 12–21. https://doi.org/10.1016/j.cmi.2015.10.010.

(27) Spellberg, B.; Guidos, R.; Gilbert, D.; Bradley, J.; Boucher, H. W.; Scheld, W. M.; Bartlett, J. G.; Edwards, J. The Epidemic of Antibiotic-Resistant Infections: A Call to Action for the Medical Community from the Infectious Diseases Society of America. *Clin. Infect. Dis.* **2008**, *46* (2), 155–164. https://doi.org/10.1086/524891.

(28) Beveridge, T. J. Structures of Gram-Negative Cell Walls and Their Derived Membrane Vesicles. *Journal of Bacteriology*. American Society for Microbiology 1999, pp 4725–4733. https://doi.org/10.1128/jb.181.16.4725-4733.1999.

(29) Delcour, A. H. Outer Membrane Permeability and Antibiotic Resistance. *Biochimica et Biophysica Acta - Proteins and Proteomics*. Biochim Biophys Acta May 2009, pp 808–816. https://doi.org/10.1016/j.bbapap.2008.11.005.

(30) Plésiat, P.; Nikaido, H. Outer Membranes of Gram-negative Bacteria Are Permeable to Steroid Probes. *Mol. Microbiol.* **1992**, *6* (10), 1323–1333. https://doi.org/10.1111/j.1365-2958.1992.tb00853.x.

(31) Coughlin, R. T.; Tonsager, S.; McGroarty, E. J. Quantitation of Metal Cations Bound to Membranes and Extracted Lipopolysaccharide of Escherichia Coli. *Biochemistry* **1983**, *22* (8), 2002–2007. https://doi.org/10.1021/bi00277a041.

(32) Seydel, U.; Labischinski, H.; Kastowsky, M.; Brandenburg, K. Phase Behavior, Supramolecular Structure, and Molecular Conformation of Lipopolysaccharide. *Immunobiology* **1993**, *187* (3–5), 191–211. https://doi.org/10.1016/S0171-2985(11)80339-6.

(33) Cowan, S. W.; Schirmer, T.; Rummel, G.; Steiert, M.; Ghosh, R.; Pauptit, R. A.; Jansonius, J. N.; Rosenbusch, J. P. Crystal Structures Explain Functional Properties of Two E. Coli Porins. *Nature* **1992**, *358* (6389), 727–733. https://doi.org/10.1038/358727a0.

(34) Benz, R. Structure and Function of Porins from Gram-Negative Bacteria. *Annu. Rev. Microbiol.* **1988**, *42* (1), 359–393. https://doi.org/10.1146/annurev.mi.42.100188.002043.

(35) Cowan, S. W.; Garavito, R. M.; Jansonius, J. N.; Jenkins, J. A.; Karlsson, R.; König, N.; Pai, E. F.; Pauptit, R. A.; Rizkallah, P. J.; Rosenbusch, J. P.; et al. The Structure of OmpF Porin in a Tetragonal Crystal Form. *Structure* **1995**, *3* (10), 1041–1050. https://doi.org/10.1016/S0969-2126(01)00240-4.

(36) Choi, U.; Lee, C.-R. Distinct Roles of Outer Membrane Porins in Antibiotic Resistance and Membrane Integrity in Escherichia Coli. *Front. Microbiol.* **2019**, *10* (APR), 953. https://doi.org/10.3389/fmicb.2019.00953.

(37) Vergalli, J.; Bodrenko, I. V.; Masi, M.; Moynié, L.; Acosta-Gutiérrez, S.; Naismith, J. H.; Davin-Regli, A.; Ceccarelli, M.; van den Berg, B.; Winterhalter, M.; et al. Porins and Small-Molecule Translocation across the Outer Membrane of Gram-Negative Bacteria. *Nature Reviews Microbiology*. Nature Research March 1, 2020, pp 164–176. https://doi.org/10.1038/s41579-019-0294-2.

(38) O'Shea, R.; Moser, H. E. Physicochemical Properties of Antibacterial Compounds: Implications for Drug Discovery. *J. Med. Chem.* **2008**, *51* (10), 2871–2878. https://doi.org/10.1021/jm700967e.

(39) Bodrenko, I. V.; Salis, S.; Acosta-Gutierrez, S.; Ceccarelli, M. Diffusion of Large Particles through Small Pores: From Entropic to Enthalpic Transport. *J. Chem. Phys.* **2019**, *150* (21). https://doi.org/10.1063/1.5098868.

(40) Acosta-Gutierrez, S.; Scorciapino, M. A.; Bodrenko, I.; Ceccarelli, M. Filtering with Electric Field: The Case of E. Coli Porins. *J. Phys. Chem. Lett.* **2015**, *6* (10), 1807–1812. https://doi.org/10.1021/acs.jpclett.5b00612.

(41) Richter, M. F.; Drown, B. S.; Riley, A. P.; Garcia, A.; Shirai, T.; Svec, R. L.; Hergenrother, P. J. Predictive Compound Accumulation Rules Yield a Broad-Spectrum Antibiotic. *Nature* **2017**, *545* (7654), 299–304. https://doi.org/10.1038/nature22308.

(42) Peña, S.; Scarone, L.; Manta, E.; Serra, G. First Total Synthesis of Aerucyclamide B. *Tetrahedron Lett.* **2013**, *54* (22), 2806–2808. https://doi.org/10.1016/j.tetlet.2013.03.060.

(43) You, S. L.; Kelly, J. W. Total Synthesis of Dendroamide A: Oxazole and Thiazole Construction Using an Oxodiphosphonium Salt. *J. Org. Chem.* **2003**, *68* (24), 9506–9509. https://doi.org/10.1021/jo0302657.

(44) Rogers, S. A.; Melander, C. Construction and Screening of a 2-Aminoimidazole Library Identifies a Small Molecule Capable of Inhibiting and Dispersing Bacterial Biofilms across Order, Class, and Phylum. *Angew. Chemie Int. Ed.* **2008**, *47* (28), 5229–5231. https://doi.org/10.1002/anie.200800862.

(45) Liu, S.; Scotti, J. S.; Kozmin, S. A. Emulating the Logic of Monoterpenoid Alkaloid Biogenesis to Access a Skeletally Diverse Chemical Library. *J. Org. Chem.* **2013**, *78* (17), 8645–8654. https://doi.org/10.1021/jo401262v.

(46) Lee, H.; Suzuki, M.; Cui, J.; Kozmin, S. A. Synthesis of an Azide-Tagged Library of 2,3-Dihydro-4-Quinolones. *J. Org. Chem.* **2010**, *75* (5), 1756–1759. https://doi.org/10.1021/jo9025447.

(47) Jones, L. H.; Bunnage, M. E. Applications of Chemogenomic Library Screening in Drug Discovery. *Nature Reviews Drug Discovery*. Nature Publishing Group April 1, 2017, pp 285–296. https://doi.org/10.1038/nrd.2016.244.

(48) Huigens, R. W.; Morrison, K. C.; Hicklin, R. W.; Timothy, T. A.; Richter, M. F.; Hergenrother, P. J. A Ring-Distortion Strategy to Construct Stereochemically Complex and Structurally Diverse Compounds from Natural Products. *Nat. Chem.* **2013**, *5* (3), 195–202. https://doi.org/10.1038/nchem.1549.

(49) Garcia, A.; Drown, B. S.; Hergenrother, P. J. Access to a Structurally Complex Compound Collection via Ring Distortion of the Alkaloid Sinomenine. *Org. Lett.* **2016**, *18* (19), 4852–4855. https://doi.org/10.1021/acs.orglett.6b02333.

(50) Lovering, F.; Bikker, J.; Humblet, C. Escape from Flatland: Increasing Saturation as an Approach to Improving Clinical Success. *J. Med. Chem.* **2009**, *52* (21), 6752–6756. https://doi.org/10.1021/jm901241e.

(51) Walters, W. P.; Green, J.; Weiss, J. R.; Murcko, M. A. What Do Medicinal Chemists Actually Make? A 50-Year Retrospective. *Journal of Medicinal Chemistry*. American Chemical Society October 13, 2011, pp 6405–6416. https://doi.org/10.1021/jm200504p.

(52) Deeken, J. F.; Löscher, W. The Blood-Brain Barrier and Cancer: Transporters, Treatment, and Trojan Horses. *Clinical Cancer Research*. American Association for Cancer Research March 15, 2007, pp 1663–1674. https://doi.org/10.1158/1078-0432.CCR-06-2854.

(53) Nawashiro, H.; Otani, N.; Shinomiya, N.; Fukui, S.; Ooigawa, H.; Shima, K.; Matsuo, H.; Kanai, Y.; Endou, H. L-Type Amino Acid Transporter 1 as a Potential Molecular Target in Human Astrocytic Tumors. *Int. J. Cancer* **2006**, *119* (3), 484–492. https://doi.org/10.1002/ijc.21866.

(54) Graef, F.; Gordon, S.; Lehr, C.-M. Anti-Infectives in Drug Delivery—Overcoming the

Gram-Negative Bacterial Cell Envelope. In *Current topics in microbiology and immunology*; 2016; Vol. 398, pp 475–496. https://doi.org/10.1007/82_2016_491.

(55) Nasrollahi, S. A.; Taghibiglou, C.; Azizi, E.; Farboud, E. S. Cell-Penetrating Peptides as a Novel Transdermal Drug Delivery System. *Chem. Biol. Drug Des.* **2012**, *80* (5), 639–646. https://doi.org/10.1111/cbdd.12008.

(56) Sakakura, A.; Kondo, R.; Ishihara, K. Molybdenum Oxides as Highly Effective Dehydrative Cyclization Catalysts for the Synthesis of Oxazolines and Thiazolines. *Org. Lett.* **2005**, *7* (10), 1971–1974. https://doi.org/10.1021/ol050543j.

(57) Mitsunobu, O.; Yamada, M.; Mukaiyama, T. Preparation of Esters of Phosphoric Acid by the Reaction of Trivalent Phosphorus Compounds with Diethyl Azodicarboxylate in the Presence of Alcohols. *Bull. Chem. Soc. Jpn.* **1967**, *40* (4), 935–939. https://doi.org/10.1246/bcsj.40.935.

(58) Hoang, V. L.; Zhang, Y.; Rafferty, R. J. In Pursuit of Balgacyclamide A – Discovery of an Oxazoline Macrocycle with Multiple Myeloma Cytotoxicity and Penetration. *Tetrahedron Lett.* **2017**, *58* (47), 4432–4435. https://doi.org/10.1016/j.tetlet.2017.09.071.

(59) Mandal, P. K.; McMurray, J. S. Pd-C-Induced Catalytic Transfer Hydrogenation with Triethylsilane. *J. Org. Chem.* **2007**, *72* (17), 6599–6601. https://doi.org/10.1021/jo0706123.

(60) Kutova, O. M.; Guryev, E. L.; Sokolova, E. A.; Alzeibak, R.; Balalaeva, I. V. Targeted Delivery to Tumors: Multidirectional Strategies to Improve Treatment Efficiency. *Cancers*. MDPI AG January 1, 2019. https://doi.org/10.3390/cancers11010068.

(61) De Kraker, M.; Stewardson, A. J.; Harbarth, S. Will 10 Million People Die a Year Due to Antimicrobial Resistance by 2050? *PLoS Med* **2016**, *13* (11), 1002184. https://doi.org/10.1371/journal.pmed.1002184.

(62) Bae, Y. H.; Park, K. Targeted Drug Delivery to Tumors: Myths, Reality and Possibility. *Journal of Controlled Release*. Elsevier B.V. August 10, 2011, pp 198–205. https://doi.org/10.1016/j.jconrel.2011.06.001.

(63) Yoo, J.; Park, C.; Yi, G.; Lee, D.; Koo, H. Active Targeting Strategies Using Biological Ligands for Nanoparticle Drug Delivery Systems. *Cancers (Basel).* **2019**, *11* (5). https://doi.org/10.3390/cancers11050640.

(64) Calvaresi, E. C.; Hergenrother, P. J. Glucose Conjugation for the Specific Targeting and Treatment of Cancer. *Chem. Sci.* **2013**, *4* (6), 2319–2333. https://doi.org/10.1039/c3sc22205e.

(65) Dyshlovoy, S. A.; Pelageev, D. N.; Hauschild, J.; Borisova, K. L.; Kaune, M.; Krisp, C.; Venz, S.; Sabutskii, Y. E.; Khmelevskaya, E. A.; Busenbender, T.; et al. Successful Targeting of Thewarburg Effect in Prostate Cancer by Glucose-Conjugated 1,4-Naphthoquinones. *Cancers (Basel).* **2019**, *11* (11), 1690. https://doi.org/10.3390/cancers11111690.

(66) Home | American Cancer Society - Cancer Facts & Statistics https://cancerstatisticscenter.cancer.org/?_ga=2.257577419.199772378.1594122566-1216379243.1594122566&_gac=1.15079748.1594122566.Cj0KCQjwupD4BRD4ARIsABJMmZ_ld4CXyTNxbX14uUr3EUYKuQ3lX_ue0AQ39qPEyvkVG7Dy-UscgH0aAiivEALw_wcB#!/ (accessed Jul 7, 2020).

Chapter 6 - Procedures and NMRs

General Methods

Reactions were performed under inert conditions as well as open atmosphere, unless otherwise stated and performed under an inert Argon atmosphere with flamed-dried glassware and stir bars with anhydrous solvents. Reactions were monitored by thin-layer chromatography (TLC) carried out on 0.25 mm E. Merck silica gel plates (60F-254) and the visualization was done using UV light and PMA/heat or $KMnO_4$/heat. Sorbtech silica gel (60, particle size 40-63 μm) was used for silica gel chromatography. Nuclear magnetic resonance (NMR) spectra were recorded on a Bruker spectrometers for ^{1}H (400 MHz or 600 MHz) and ^{13}C (101 MHz or 151 MHz) in deuterated chloroform ($CDCl_3$), unless otherwise indicated. Anhydrous diethyl ether (Et_2O), toluene (PhMe), *N*,*N*-dimethylsulforamide (DMF), tetrahydrofuran (THF), dichloromethane (DCM), and acetonitrile (MeCN) were obtained via a dual column solvent purification system (J.C Mayer of Glass Contour). All other solvents and reagents were obtained from commercial sources without further purification unless noted. Organic extracts were dried with $NaSO_4$ (unless otherwise noted) before filtration and concentration under reduced pressure.

Standard protocol for peptide coupling reactions using PyBOP

Unless otherwise specified, in a flask 1 eq. of free carboxylic acid version of the amino acid (amine protected) and 1.05 eq. of PyBOP were dissolved in methylene chloride (0.1 M) and 1.5 eq. of diisopropylethylamine was added and stirred for ~30 minutes at room temperature to activate the acid. In a separate 2 eq. free amine hydrochloride version of the amino acid (carboxylic acid protected) was dissolved in methylene chloride (1 M), which was activated by adding 4.5 eq. of diisopropylethylamine (DIPEA) and stirring until the solid material was solubilized. Then activated free amine was transferred to the flask containing the activated acid and reaction was stirred overnight at room temperature. It was quenched with 1 M HCl or saturated ammonium chloride, extracted with methylene chloride 3 times and dried with sodium sulfate. Then the extract was concentrated under reduced pressure (using rotary evaporator) and purified using flash column chromatography.

Standard protocol for peptide coupling reactions using HBTU

Unless otherwise specified, 1 eq. of the free acid and 1.1 eq. of the free amine were mixed with DCM (1M to the free acid) followed by addition of diisopropylethylamine and stirring for ~5 minutes. HBTU (1.2 eq.) and and 4-DMAP (0.2 eq.) were added to the reaction and the reaction mixture was allowed to stir at room temperature overnight. It was quenched with 1 M HCl or saturated ammonium chloride, extracted with methylene chloride 3 times and dried with sodium sulfate. Then the extract was concentrated under reduced pressure (using rotary evaporator) and purified using flash column chromatography.

Standard protocol for DAST (diethylaminosulfur trifluoride)-mediated cyclizations (oxazoline formations)

Under inert conditions in a dry flask starting material (1 eq.) was mixed with dry DCM and cooled to -78 °C. Then the reaction mixture was treated with DAST an stirred at -78 °C with constant monitoring until the reaction was completed (general reaction time: 2-4 hours). Then 1.5 eq. of potassium carbonate is added to the reaction mixture and stirred for ~30 minutes at room temperature. Reaction was quenched with saturated sodium bicarbonate (~1 volume), the organic layer was separated, and the aqueous layer was extracted three times with methylene chloride. Combined organic layers were dried with anhydrous sodium sulfate and concentrated. Product was purified by flash column chromatography.

Standard protocol for Boc protections of amine groups

The amino acid (1 eq.) was dissolved in a 2:1 dioxane/water system (0.15 M) followed by treating it with 1M NaOH (2.27 eq.) and stirring it for ~5 minutes (or until the amino acid is completely dissolved). Boc-anhydride (1.1 eq.) was then added and the reaction was allowed to stir at room temperature overnight. The reaction was quenched with 5 M NaOH, adding the base slowly while checking the pH of the reaction to mixture to bring its pH to ~2. Then the reaction mixture was extracted with ethyl acetate (three times), dried with sodium sulfate and concentrated under reduced pressure.

Standard protocol for Boc deprotections

Boc protected starting material was mixed with 4 M HCl in dioxane solution (starting material was 0.25 M in solution). Reaction mixture was allowed to stir at room temperature with constant monitoring until the starting material disappeared on TLC. Then solvents were removed under reduced pressure (rotary evaporator/hi-vac).

Standard protocol for saponifications (base-mediated ester hydrolysis)

Unless otherwise specified, the starting material reacted with 3.3 eq. of LiOH. Starting material was dissolved in THF (volume that would make the required amount of LiOH 1M), followed by addition of an equal volume of water then crushed LiOH (not pellets). Reaction was allowed to stir at room temperature with constant monitoring until the starting material disappeared on TLC. Reaction was quenched carefully to allow the reaction pH to come to ~2 using 1M HCl. Then the reaction was extracted with ethyl acetate (three times). Combined organic layers were dried with anhydrous sodium sulfate and concentrated under reduced pressure.

Methyl (*tert*-butoxycarbonyl)-*L*-valyl-*L*-threoninate

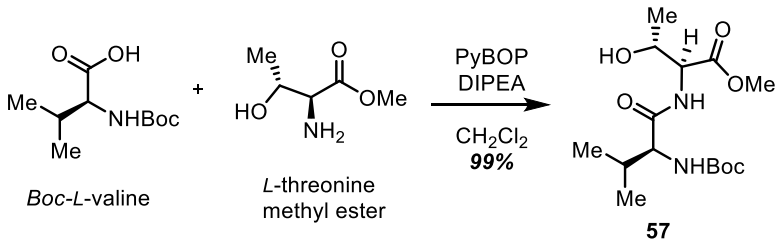

Reaction was performed using standard PyBOP peptide coupling conditions. The product was afforded in 99% yield with purification by flash column chromatography with 4:1 ethyl acetate/hexanes. R_f = 0.6 (4:1 ethyl acetate/hexanes)

^{1}H NMR (400 MHz, Chloroform-*d*) δ 6.92 – 6.86 (m, 2H), 5.20 (s, 1H), 4.62 (dd, *J* = 9.0, 2.6 Hz, 0H), 4.35 (qd, *J* = 6.5, 2.7 Hz, 1H), 3.98 – 3.90 (m, 1H), 3.78 (s, 4H), 3.76 (s, 1H), 2.08 (s, 2H), 1.47 (s, 1H), 1.28 – 1.13 (m, 4H), 1.00 (s, 8H), 0.97 (dd, *J* = 11.1, 6.7 Hz, 3H).

^{13}C NMR (101 MHz, Chloroform-*d*) δ 172.85, 171.53, 156.38, 80.18, 68.24, 60.33, 57.56, 52.66, 31.02, 28.45, 19.96, 19.34, 18.37.

Notebook Entries

Procedure: PKD1-345

^{1}H: PKD1-345-400, ^{13}C: AXT-006-A-carbon

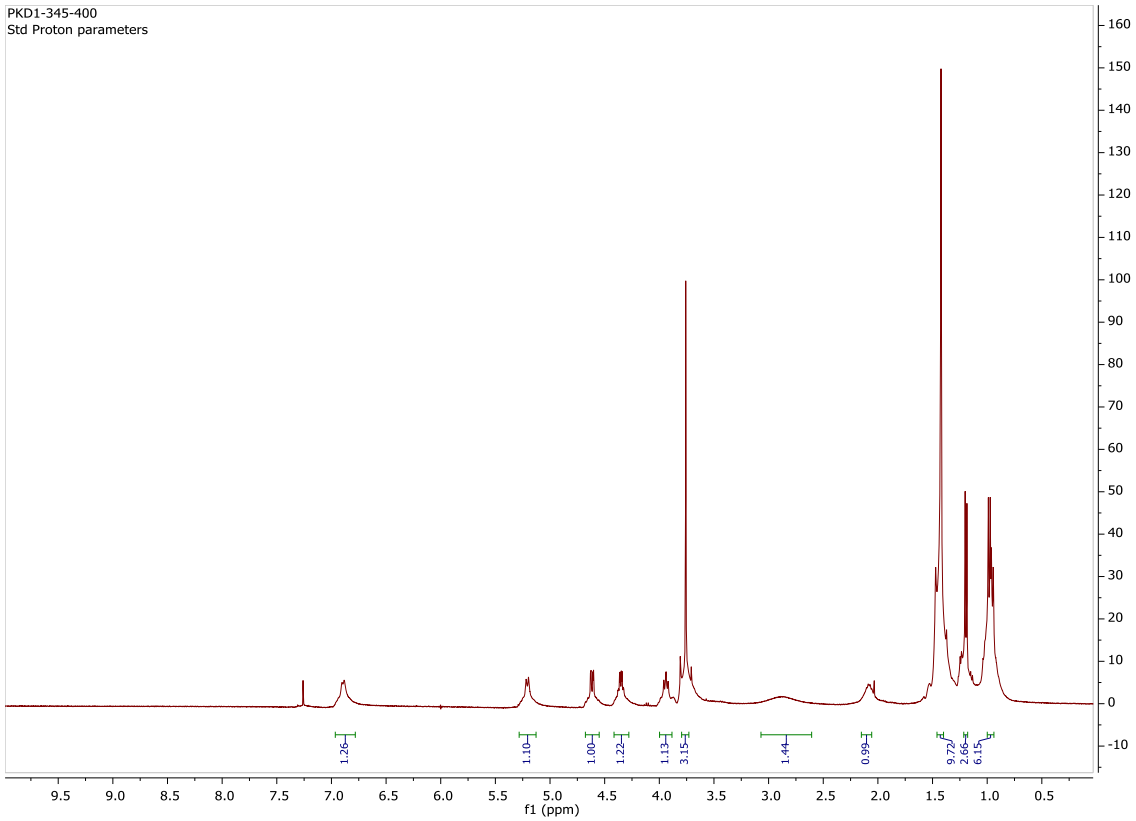
PKD1-345-400
Std Proton parameters
1.26
1.10
1.00
1.22
1.13
3.15
1.44
0.99
9.72
2.66
6.15
f1 (ppm)

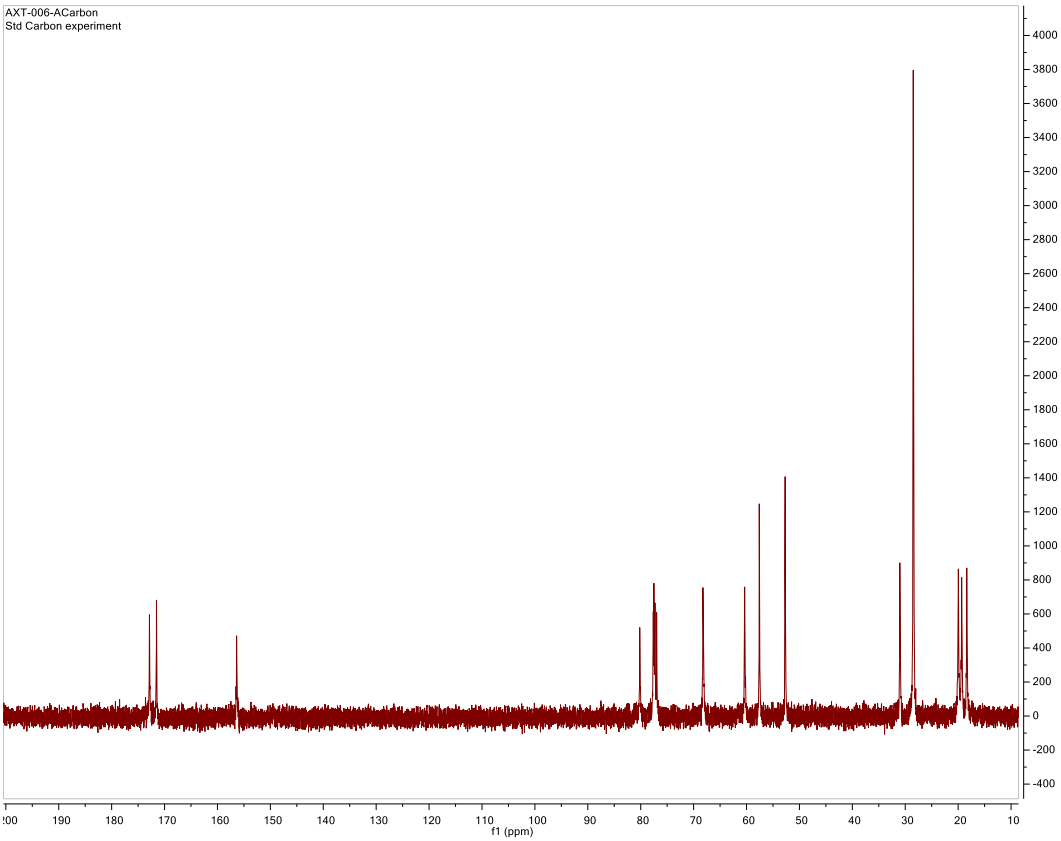
AXT-006-ACarbon
Std Carbon experiment
f1 (ppm)

Methyl (4S,5R)-2-((S)-1-((*tert*-butoxycarbonyl)amino)-2-methylpropyl)-5-methyl-4,5-dihydrooxazole-4-carboxylate

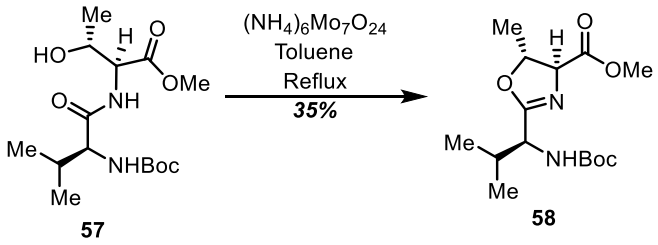

A dry flask was charged with **57** (1 eq.) and dry toluene (0.5 M) followed by addition of $(NH_4)_6Mo_7O_{24}$ (0.1 eq.), and anhydrous sodium sulfate (a little, to absorb moisture being generated). The mixture was brought to refluxed, heat plate set at 115 °C, overnight under an inert atmosphere. Reaction was then quenched with saturated sodium bicarbonate (1 volume eq.), followed by extraction with ethyl acetate (x3) and dried with sodium sulfate. Upon concentration under reduced pressure, product was afforded in 35% yield with purification by flash column chromatography with 3:1 ethyl acetate/hexanes. Rf = 0.75 (3:1 ethyl acetate/hexanes). Unreacted starting material was recovered at Rf = 0.55 (3:1 ethyl acetate/hexanes)

^{1}H NMR (400 MHz, Chloroform-*d*) δ 5.22 (d, *J* = 9.5 Hz, 1H), 4.84 (p, *J* = 6.5 Hz, 1H), 4.35 (dd, *J* = 9.2, 4.7 Hz, 1H), 4.27 (dd, *J* = 7.1, 1.5 Hz, 1H), 3.77 (s, 3H), 2.18 – 2.08 (m, 1H), 1.43 (d, *J* = 2.8 Hz, 9H), 1.00 – 0.94 (m, 6H), 0.90 (d, *J* = 6.9 Hz, 3H).

Notebook Entries

Procedure: PKD1-349

^{1}H: PKD1-349-400

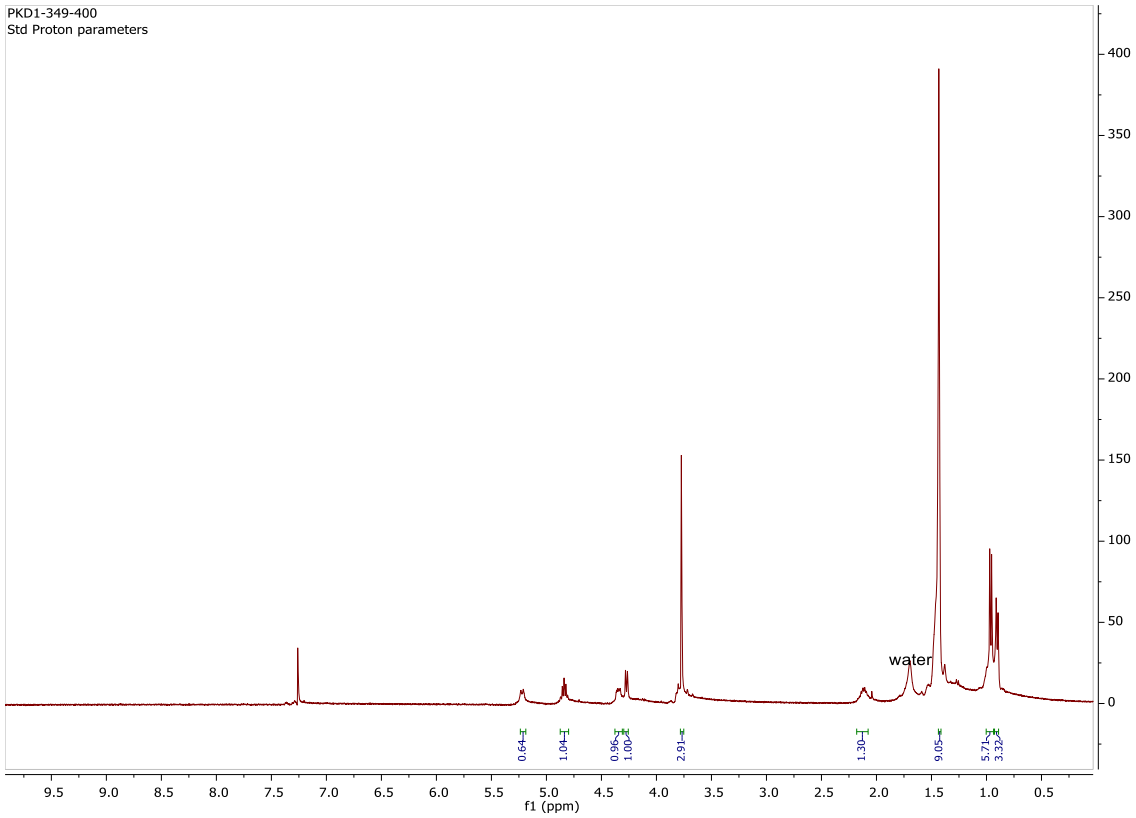
PKD1-349-400
Std Proton parameters
water
0.64
1.04
0.96
1.00
2.91
1.30
9.05
5.71
3.32
f1 (ppm)

Methyl (*tert*-butoxycarbonyl)-*L*-valyl-*L*-allothreoninate

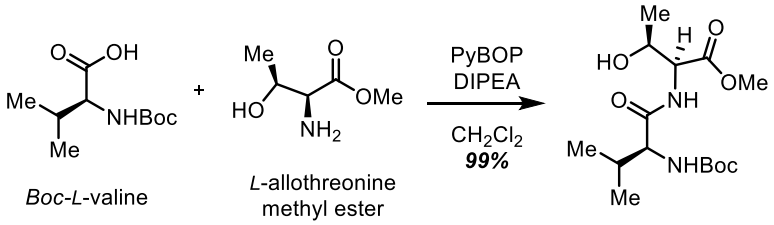

Reaction was performed using standard PyBOP peptide coupling conditions. The product was afforded in in 99% yield with purification by flash column chromatography with 3:1 ethyl acetate/hexanes. R_f = 0.5 (3:1 ethyl acetate/hexanes).

^{1}H NMR (400 MHz, Chloroform-*d*) δ 7.35 (d, *J* = 8.0 Hz, 1H), 5.40 (d, *J* = 8.8 Hz, 1H), 4.62 (dd, *J* = 7.9, 3.5 Hz, 1H), 4.09 (m, 1H), 3.99 (m, 2H), 3.73 (s, 3H), 2.04 (dt, *J* = 13.5, 6.6 Hz, 1H), 1.38 (s, 9H), 1.18 (d, *J* = 6.4 Hz, 3H), 0.91 (dd, *J* = 12.2, 6.7 Hz, 6H).

Notebook Entries

Procedure: HH1-29 (Performed by Hannah Henderson)

^{1}H: HH1-29-400

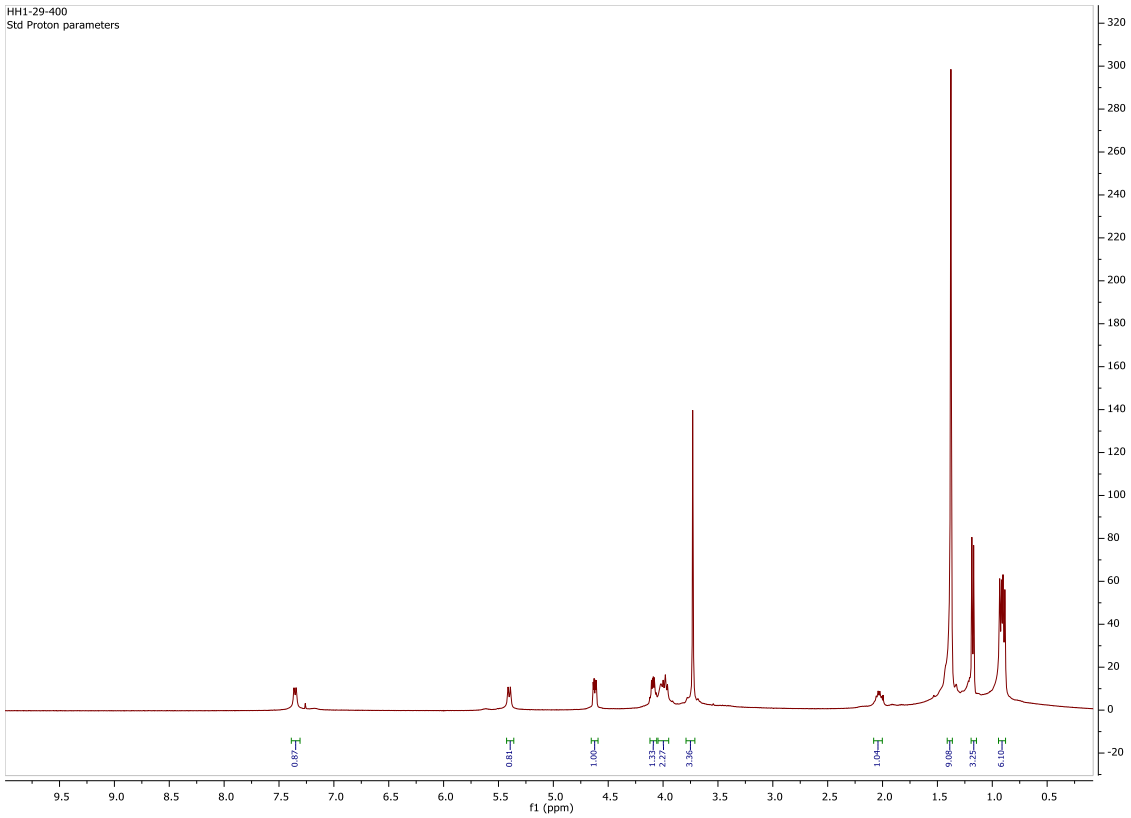
HH1-29-400
Std Proton parameters
0.87
0.81
1.00
1.33
2.27
3.36
1.04
9.08
3.25
6.10
f1 (ppm)

Methyl (4S,5R)-2-((S)-1-((*tert*-butoxycarbonyl)amino)-2-methylpropyl)-5-methyl-4,5-dihydrooxazole-4-carboxylate

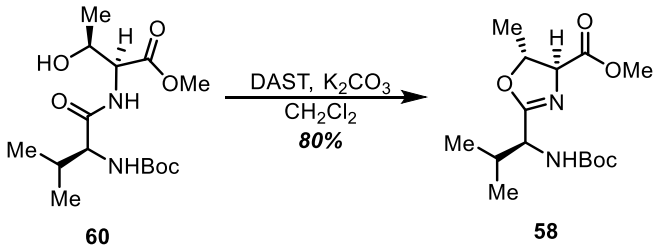

60 **58**

Reaction was performed using standard DAST conditions. The product was afforded in 80% yield with purification by flash column chromatography with 3:1 ethyl acetate/hexanes. R_f = 0.75 (3:1 ethyl acetate/hexanes)

^{1}H NMR (400 MHz, Chloroform-*d*) δ 5.19 (d, *J* = 9.3 Hz, 1H), 4.82 (p, *J* = 6.5 Hz, 1H), 4.37 – 4.31 (m, 1H), 4.26 (dd, *J* = 7.0, 1.5 Hz, 1H), 3.76 (s, 3H), 2.10 (td, *J* = 6.9, 4.7 Hz, 1H), 1.42 (d, *J* = 2.4 Hz, 9H), 0.95 (d, *J* = 6.8 Hz, 3H), 0.89 (d, *J* = 6.9 Hz, 3H).

Notebook Entries

Procedure: PKD2-016

^{1}H: PKD2-016-400

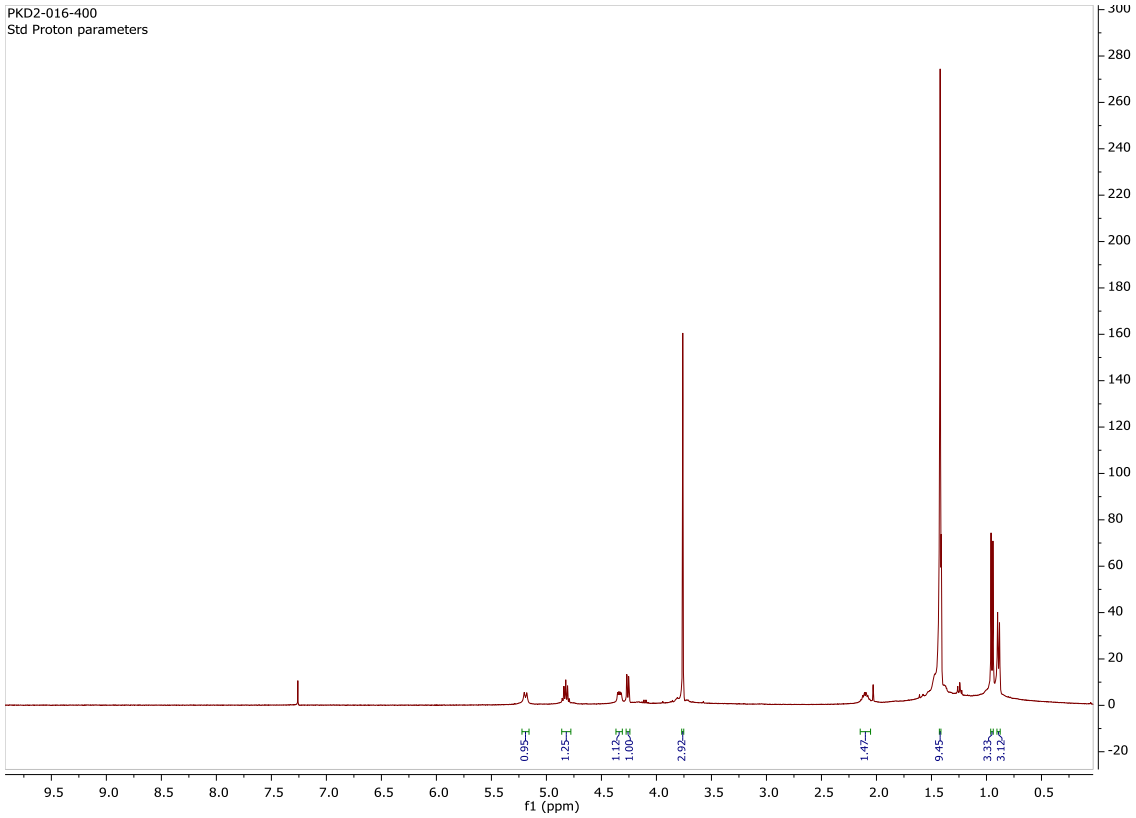
PKD2-016-400
Std Proton parameters
0.95
1.25
1.12
1.00
2.92
1.47
9.45
3.33
3.12
f1 (ppm)

Methyl ((benzyloxy)carbonyl)-*L*-valyl-*L*-allothreoninate

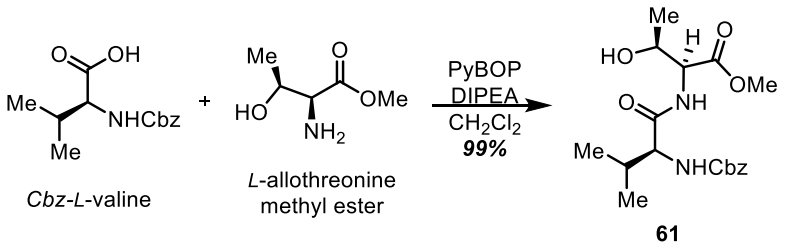

Cbz-L-valine

L-allothreonine methyl ester

61

Reaction was performed using standard PyBOP peptide coupling conditions. The product was afforded in 99% yield with purification by flash column chromatography with 3:1 ethyl acetate/hexanes. R_f = 0.5 (3:1 ethyl acetate/hexanes).

^{1}H NMR (400 MHz, Chloroform-*d*) δ 7.41 – 7.30 (m, 5H), 7.03 (d, *J* = 7.5 Hz, 1H), 5.48 (d, *J* = 8.6 Hz, 1H), 5.09 (q, *J* = 12.4, 10.1 Hz, 2H), 4.68 – 4.61 (m, 1H), 4.14 (s, 1H), 4.07 (t, *J* = 7.7 Hz, 1H), 3.77 (s, 3H), 3.49 (d, *J* = 11.7 Hz, 1H), 2.20 – 2.06 (m, 1H), 1.18 (d, *J* = 6.5 Hz, 3H), 1.00 – 0.92 (m, 6H).

^{13}C NMR (400 MHz, Chloroform-*d*) δ 172.35, 170.60, 136.33, 128.78, 128.46, 128.29, 68.91, 67.44, 60.78, 58.39, 52.82, 31.22, 19.39, 19.09, 18.17.

Notebook Entries

Procedure: PKD2-080

^{1}H: PKD2-080-400, ^{13}C: PKD2-080-C13-400

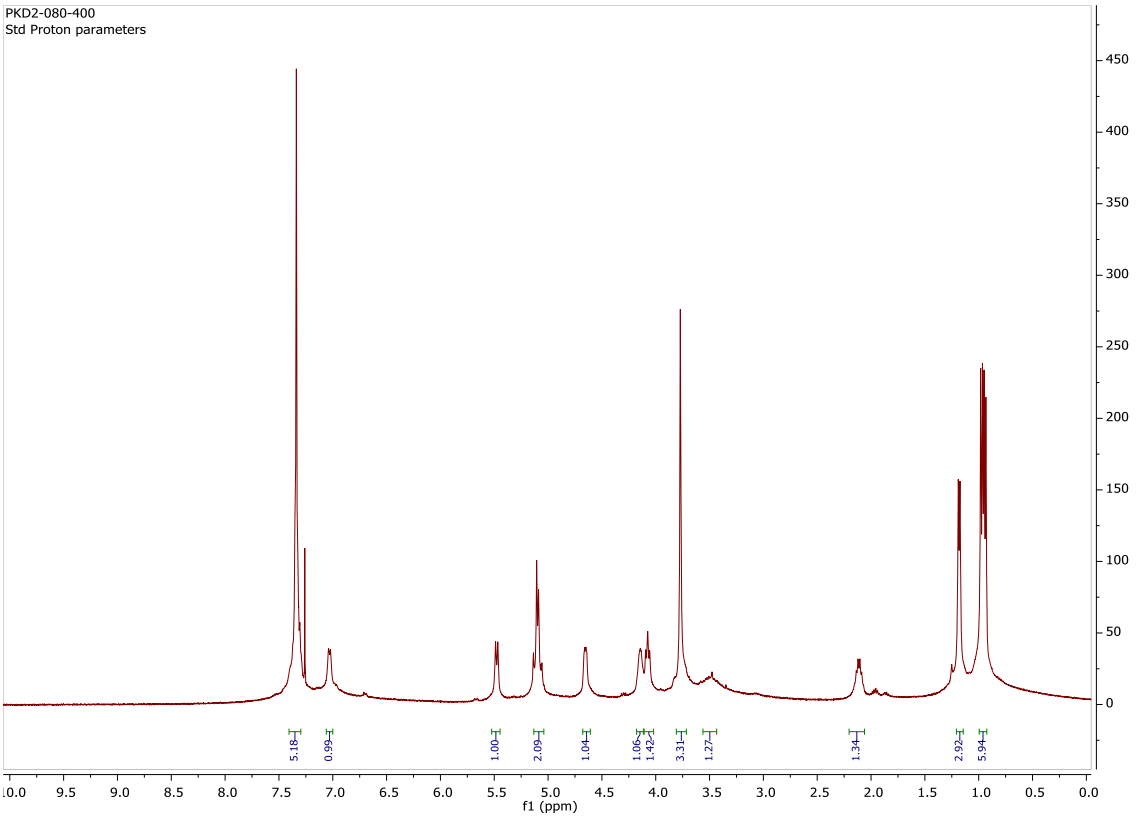
PKD2-080-400
Std Proton parameters
f1 (ppm)

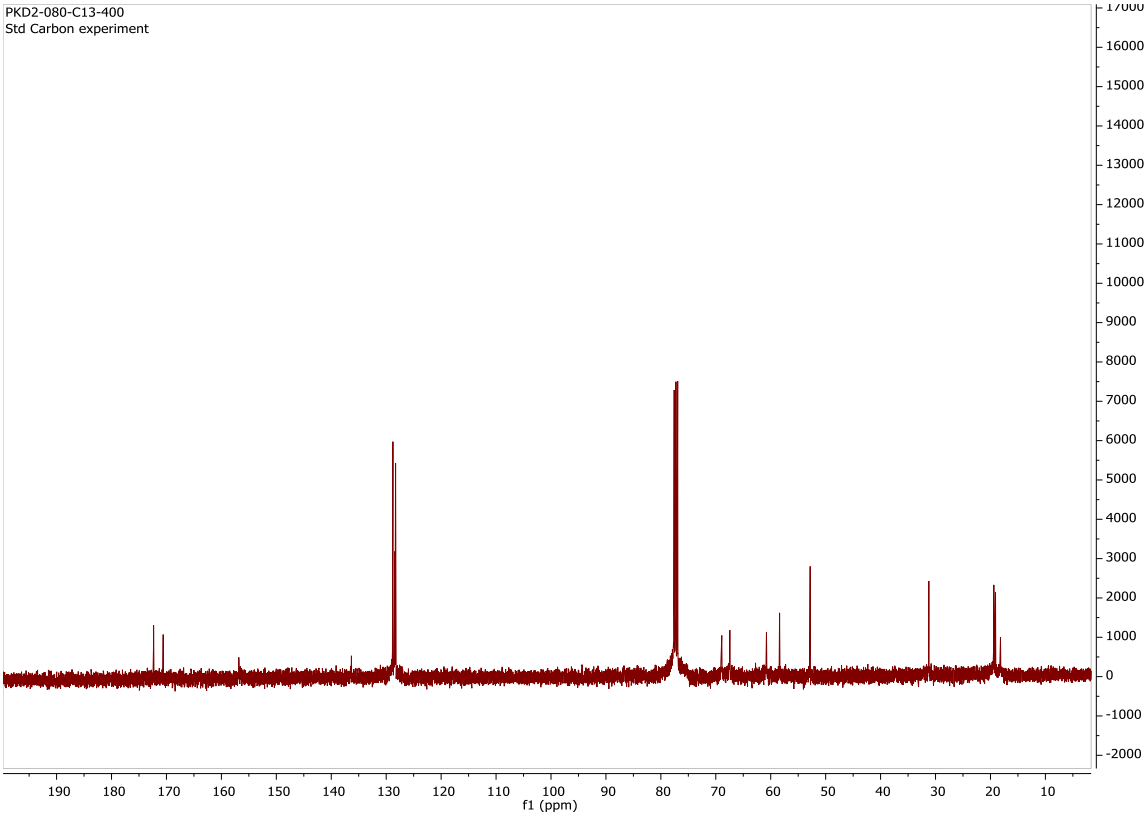
PKD2-080-C13-400
Std Carbon experiment
f1 (ppm)

Methyl (4S,5R)-2-((S)-1-(((benzyloxy)carbonyl)amino)-2-methylpropyl)-5-methyl-4,5-dihydrooxazole-4-carboxylate

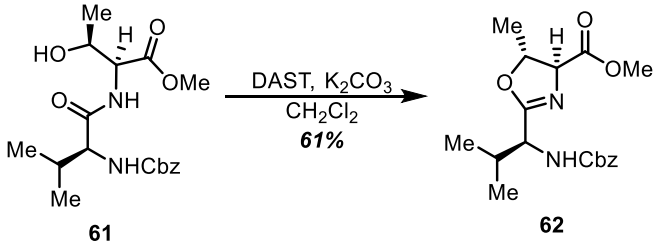

61 **62**

Reaction was performed using standard DAST conditions. The product was afforded in 61% yield with purification by flash column chromatography with 1:1 ethyl acetate/hexanes. R_f = 0.5 (1:1 ethyl acetate/hexanes)

^{1}H NMR (400 MHz, Chloroform-*d*) δ 7.37 – 7.28 (m, 5H), 5.48 (d, *J* = 9.3 Hz, 1H), 5.09 (d, *J* = 8.3 Hz, 2H), 4.83 (p, *J* = 6.4 Hz, 1H), 4.41 (ddd, *J* = 9.2, 4.7, 1.4 Hz, 1H), 4.25 (dd, *J* = 7.0, 1.4 Hz, 1H), 3.75 (s, 3H), 2.13 (pd, *J* = 6.8, 4.7 Hz, 1H), 1.41 (d, *J* = 6.3 Hz, 3H), 0.97 (d, *J* = 6.8 Hz, 3H), 0.91 (d, *J* = 6.9 Hz, 3H).

^{13}C NMR (101 MHz, Chloroform-*d*) δ 171.54, 169.05, 156.38, 136.58, 128.70, 128.31, 128.28, 79.92, 74.34, 67.15, 54.62, 52.80, 31.96, 21.10, 19.00, 17.40.

Notebook Entries

Procedure: PKD2-086

^{1}H: PKD2-086-400, ^{13}C: PKD2-086-C13-1st-400

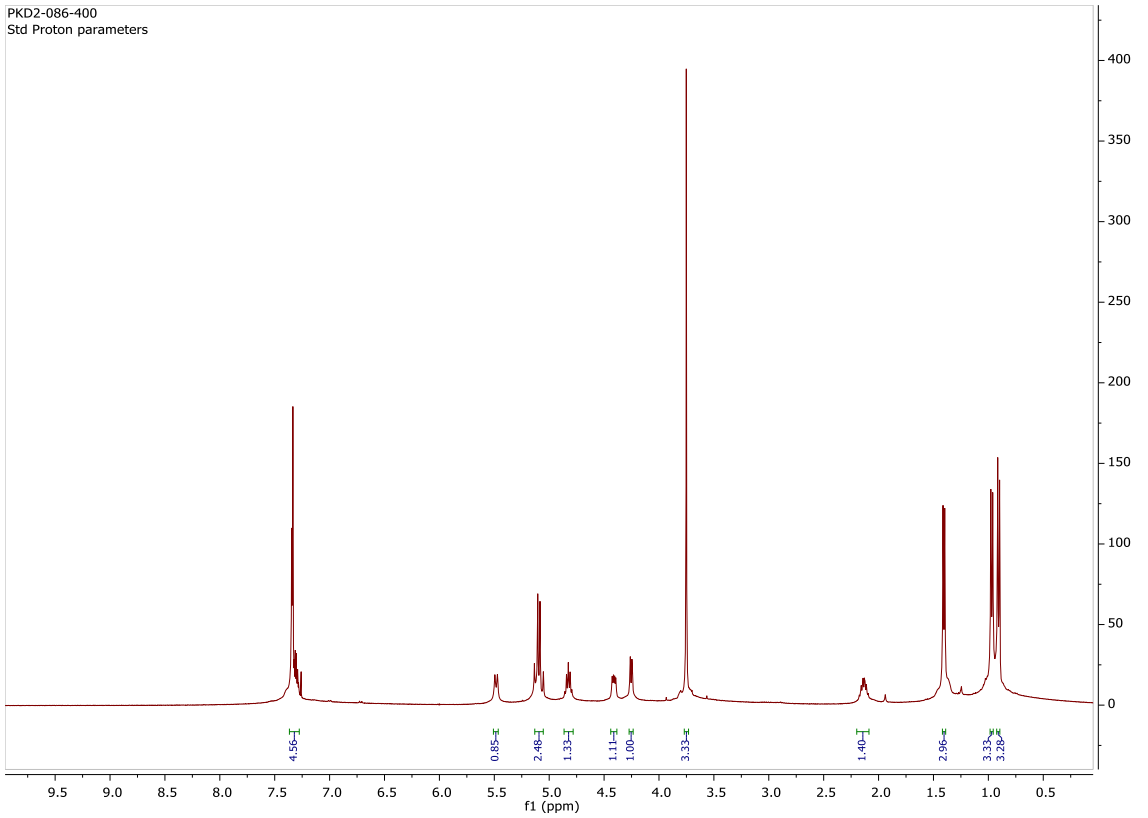
PKD2-086-400
Std Proton parameters
4.56
0.85
2.48
1.33
1.11
1.00
3.33
1.40
2.96
3.33
3.28
f1 (ppm)

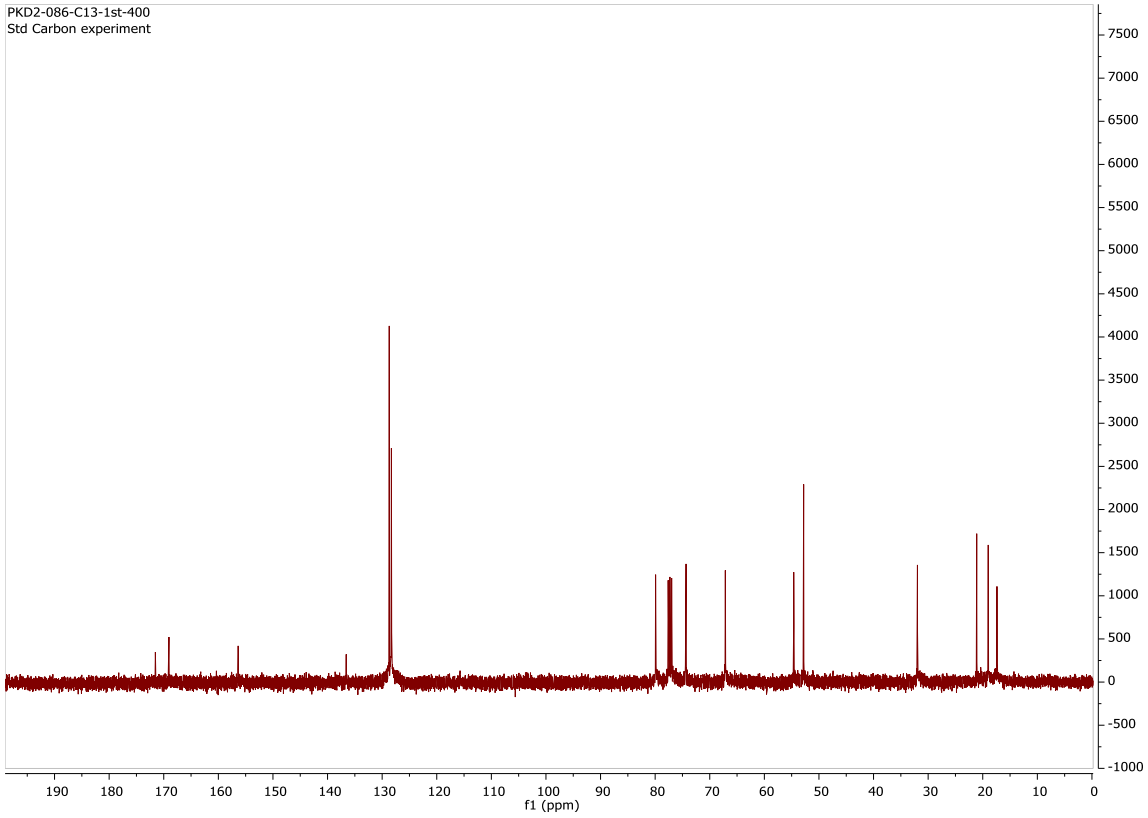
PKD2-086-C13-1st-400
Std Carbon experiment
f1 (ppm)

Methyl ((benzyloxy)carbonyl)-*L*-valyl-*L*-threoninate

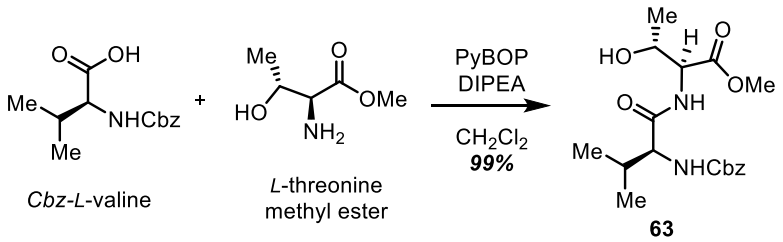

Cbz-L-valine + *L*-threonine methyl ester

63

Reaction was performed using standard PyBOP peptide coupling conditions. The product was afforded in quantitative yield with purification by flash column chromatography with 3:1 ethyl acetate/hexanes. Rf = 0.65 (3:1 ethyl acetate/ hexanes).

^{1}H NMR (400 MHz, Chloroform-*d*) δ 7.32 (d, *J* = 3.9 Hz, 5H), 6.92 (d, *J* = 9.0 Hz, 1H), 5.55 (d, *J* = 9.0 Hz, 1H), 5.13 – 5.04 (m, 2H), 4.61 (dd, *J* = 9.0, 2.6 Hz, 1H), 4.34 (s, 1H), 4.08 (dd, *J* = 8.9, 6.7 Hz, 1H), 3.75 (s, 3H), 3.04 (s, 1H), 2.10 (p, *J* = 6.7 Hz, 1H), 1.96 (s, 1H), 1.17 (d, *J* = 6.4 Hz, 3H), 0.97 (dd, *J* = 14.1, 6.8 Hz, 6H).

^{13}C NMR (101 MHz, Chloroform-*d*) δ 172.27, 171.51, 156.86, 136.42, 128.75, 128.39, 128.22, 68.31, 67.33, 60.71, 57.57, 52.78, 31.36, 20.12, 19.33, 18.22.

Notebook Entries

Procedure: PKD2-128

^{1}H: PKD2-128-1A-2nd-400, ^{13}C: PKD2-085-RC-C13-400

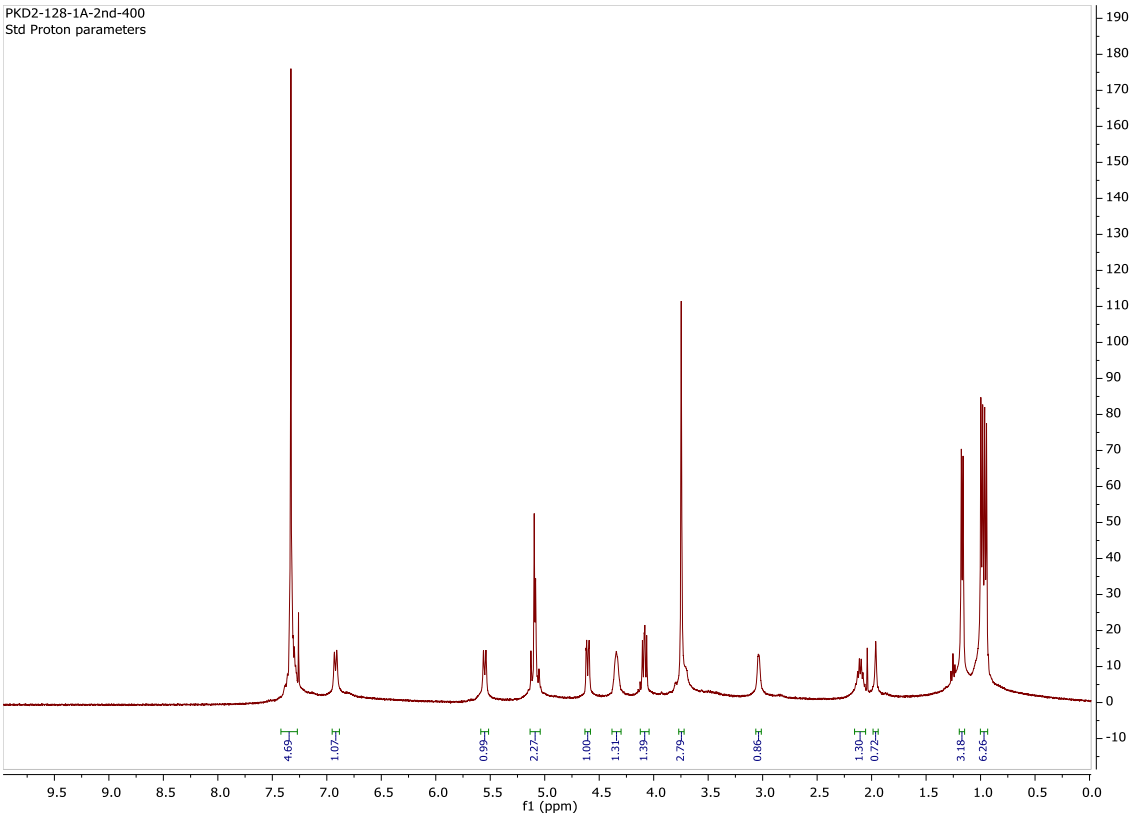
PKD2-128-1A-2nd-400
Std Proton parameters
4.69
1.07
0.99
2.27
1.00
1.31
1.39
2.79
0.86
1.30
0.72
3.18
6.26
f1 (ppm)

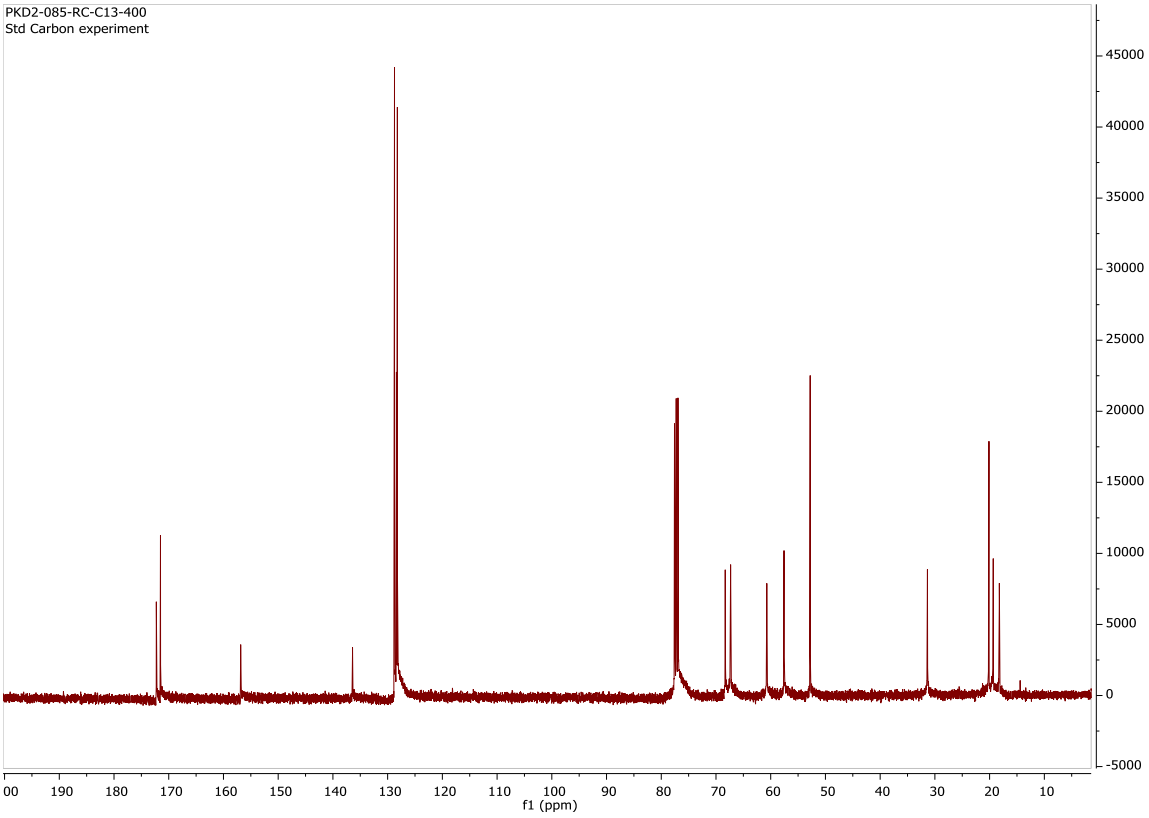
PKD2-085-RC-C13-400
Std Carbon experiment
f1 (ppm)

Methyl (4S,5S)-2-((S)-1-(((benzyloxy)carbonyl)amino)-2-methylpropyl)-5-methyl-4,5-dihydrooxazole-4-carboxylate

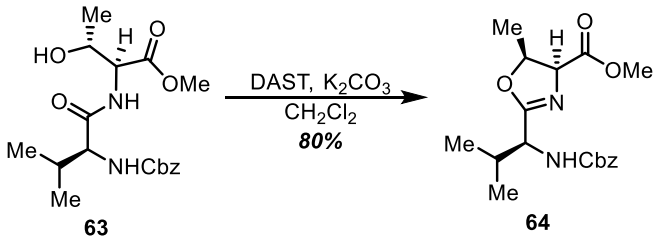

63 64

Reaction was performed using standard DAST peptide coupling conditions. The product was afforded in quantitative yield with purification by flash column chromatography with 1:1 ethyl acetate/hexanes. Rf = 0. 5 (1:1 ethyl acetate/ hexanes).

^{1}H NMR (400 MHz, Chloroform-*d*) δ 7.38 – 7.30 (m, 5H), 5.51 (d, *J* = 9.2 Hz, 1H), 5.17 – 5.08 (m, 2H), 4.96 (dq, *J* = 10.1, 6.5 Hz, 1H), 4.80 (dd, *J* = 10.1, 1.5 Hz, 1H), 4.42 (ddd, *J* = 9.3, 4.4, 1.5 Hz, 1H), 3.76 (s, 3H), 2.21 (pd, *J* = 6.8, 4.4 Hz, 1H), 1.31 (d, *J* = 6.5 Hz, 3H), 1.04 (d, *J* = 6.8 Hz, 3H), 0.99 (d, *J* = 6.9 Hz, 3H).

^{13}C NMR (101 MHz, Chloroform-*d*) δ 170.11, 169.65, 156.23, 136.38, 128.49, 128.09, 128.04, 78.52, 70.78, 66.93, 54.28, 52.07, 31.41, 18.81, 17.02, 16.13.

Notebook Entries

Procedure: PKD2-088

^{1}H: PKD2-269-pure-400N, ^{13}C: PKD2-269-pure-C13-400N

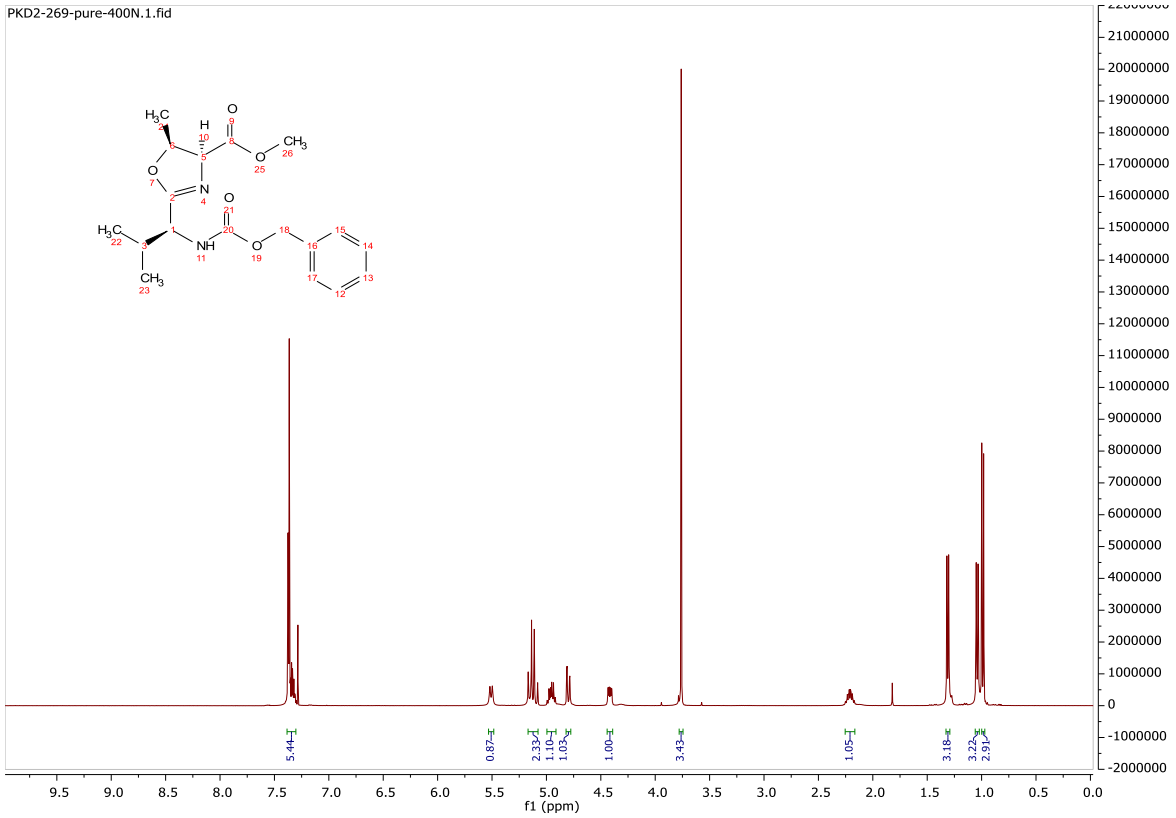
PKD2-269-pure-400N.1.fid
f1 (ppm)

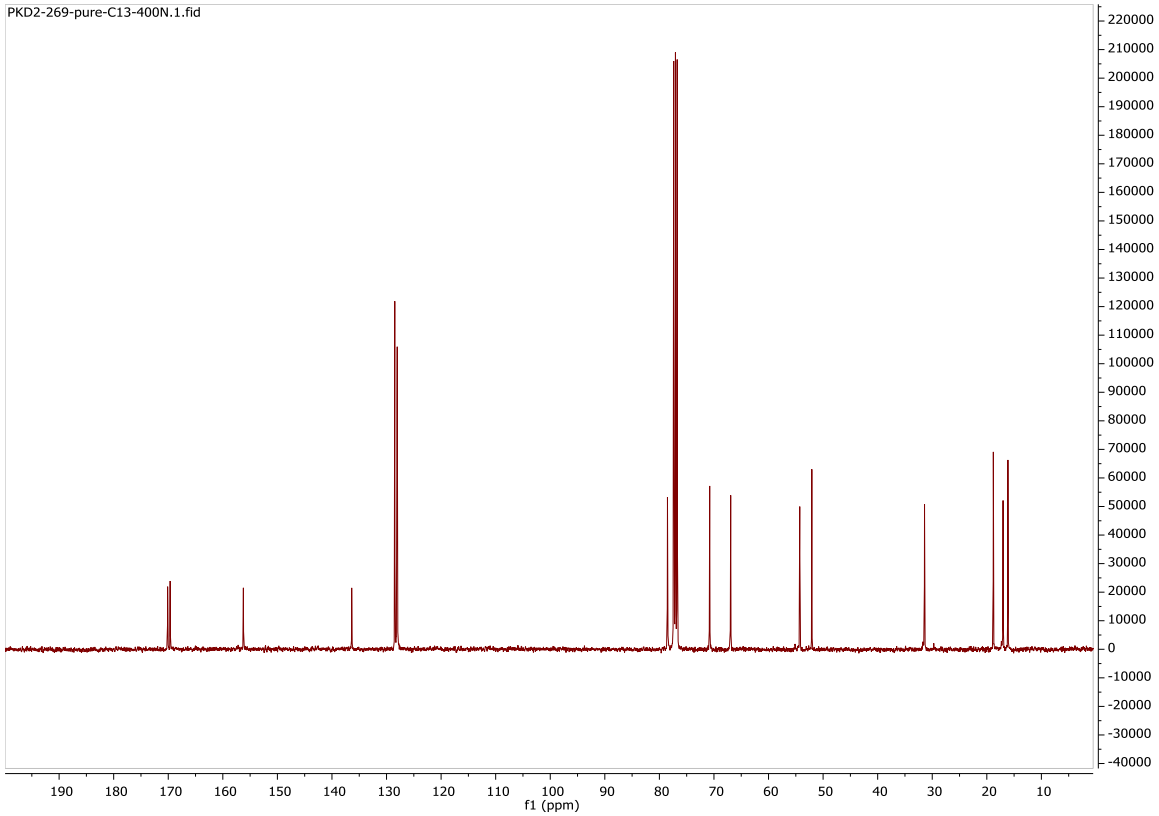
PKD2-269-pure-C13-400N.1.fid
f1 (ppm)

Methyl (*tert*-butoxycarbonyl)-*L*-isoleucyl-*L*-serinate

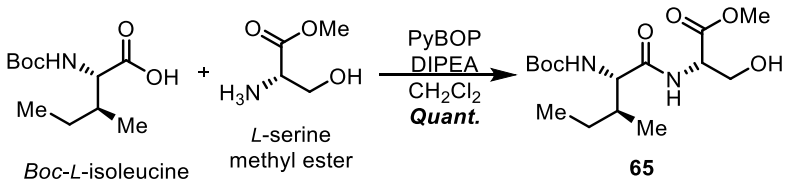

Reaction was performed using standard PyBOP peptide coupling conditions. The product was afforded in quantitative yield with purification by flash column chromatography with 3:1 ethyl acetate/hexanes. R_f = 0.5 (3:1 ethyl acetate/ hexanes).

^{1}H NMR (600 MHz, Chloroform-*d*) δ 7.08 (d, *J* = 7.8 Hz, 1H), 5.29 (d, *J* = 8.2 Hz, 1H), 4.69 (dt, *J* = 7.6, 3.6 Hz, 1H), 4.00 – 3.91 (m, 3H), 3.79 (s, 3H), 3.58 (t, *J* = 6.1 Hz, 1H), 1.89 – 1.81 (m, 1H), 1.61 – 1.54 (m, 1H), 1.46 (s, 1H), 1.44 (s, 9H), 1.18 (ddq, *J* = 14.4, 9.6, 7.3 Hz, 1H), 0.98 (d, *J* = 6.8 Hz, 3H), 0.93 (t, *J* = 7.4 Hz, 3H).

^{13}C NMR (101 MHz, Chloroform-*d*) δ 172.50, 171.00, 156.50, 80.41, 62.88, 59.67, 54.88, 52.84, 37.41, 28.51, 25.03, 15.59, 11.46.

Notebook Entries

Procedure: PKD1-405

^{1}H: PKD2-219-600, ^{13}C: PKD2-034-C13-400

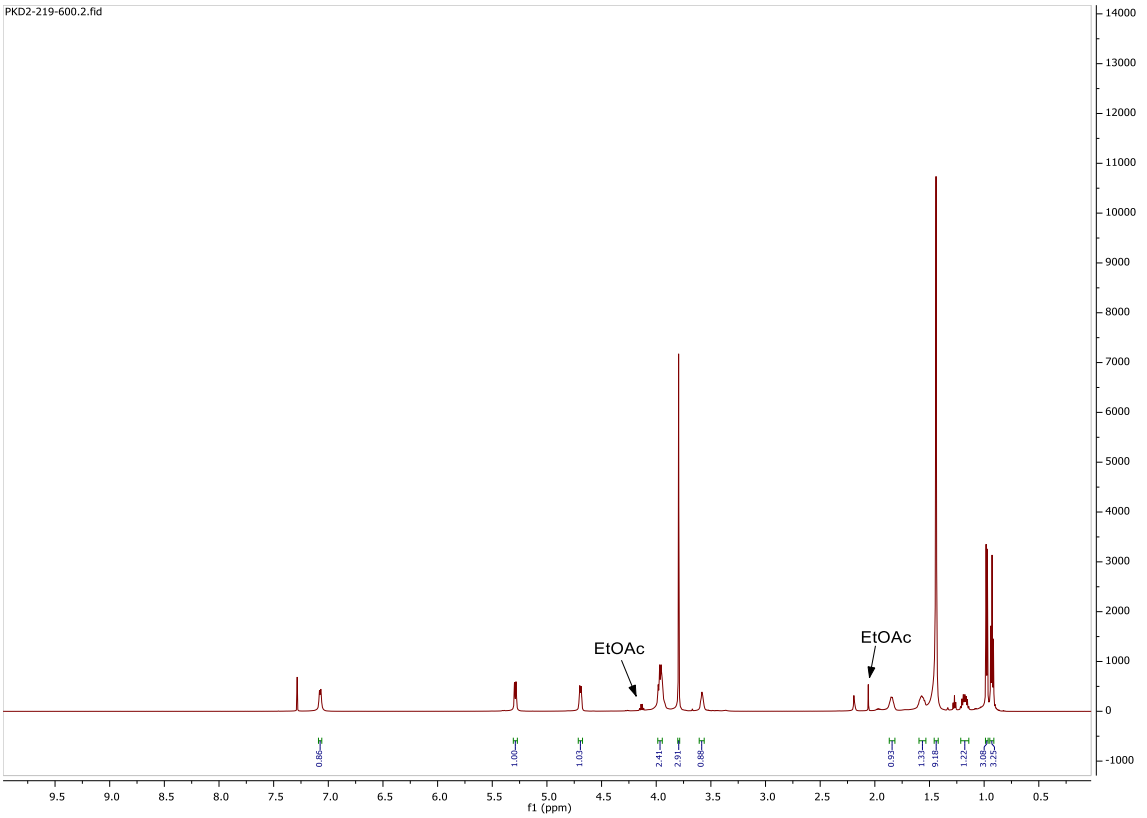
PKD2-219-600.2.fid
EtOAc
EtOAc
f1 (ppm)

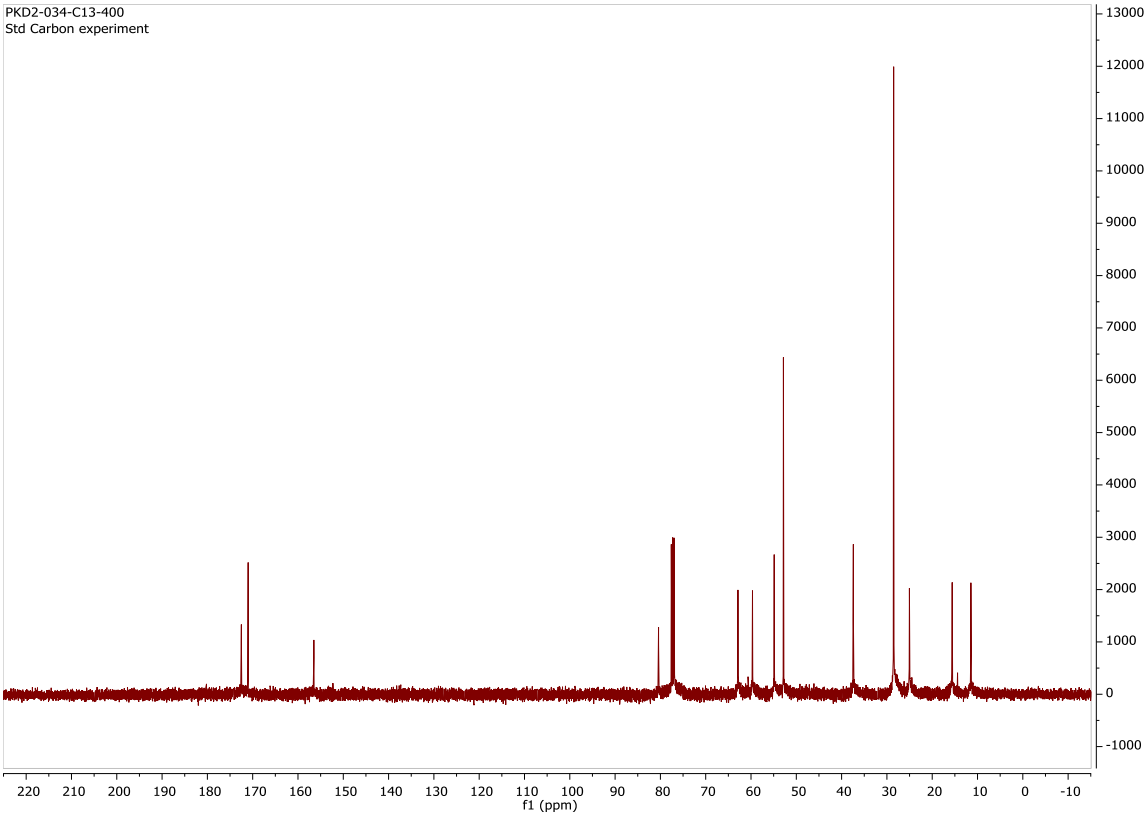
PKD2-034-C13-400
Std Carbon experiment
f1 (ppm)

Methyl (S)-2-((1S,2S)-1-((tert-butoxycarbonyl)amino)-2-methylbutyl)-4,5-dihydrooxazole-4-carboxylate

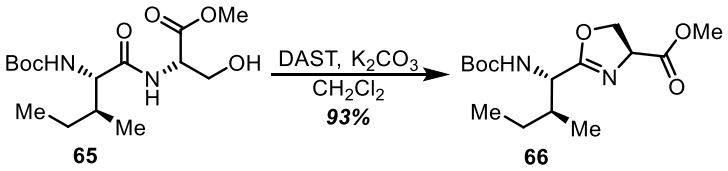

65 66

Reaction was performed using standard DAST conditions. The product was afforded in 93% yield with purification by flash column chromatography with 1:1 ethyl acetate/hexanes. R_f = 0. 5 (1:1 ethyl acetate/ hexanes).

^{1}H NMR (600 MHz, Chloroform-*d*) δ 5.22 (d, *J* = 9.2 Hz, 1H), 4.80 – 4.76 (m, 1H), 4.55 (t, *J* = 8.2 Hz, 1H), 4.48 (t, *J* = 9.6 Hz, 1H), 4.41 (dd, *J* = 9.2, 4.8 Hz, 1H), 3.81 (d, *J* = 1.2 Hz, 3H), 1.86 (h, *J* = 5.3 Hz, 1H), 1.54 – 1.49 (m, 1H), 1.45 (s, 9H), 1.21 – 1.14 (m, 1H), 0.94 (t, *J* = 7.6 Hz, 6H).

^{13}C NMR (101 MHz, Chloroform-*d*) δ 171.43, 170.05, 155.36, 79.67, 70.02, 67.67, 53.08, 52.70, 38.60, 28.33, 24.78, 15.08, 11.69.

Notebook Entries

Procedure: PKD2-221

^{1}H: PKD2-221-600, ^{13}C: PKD2-081-C13-400N

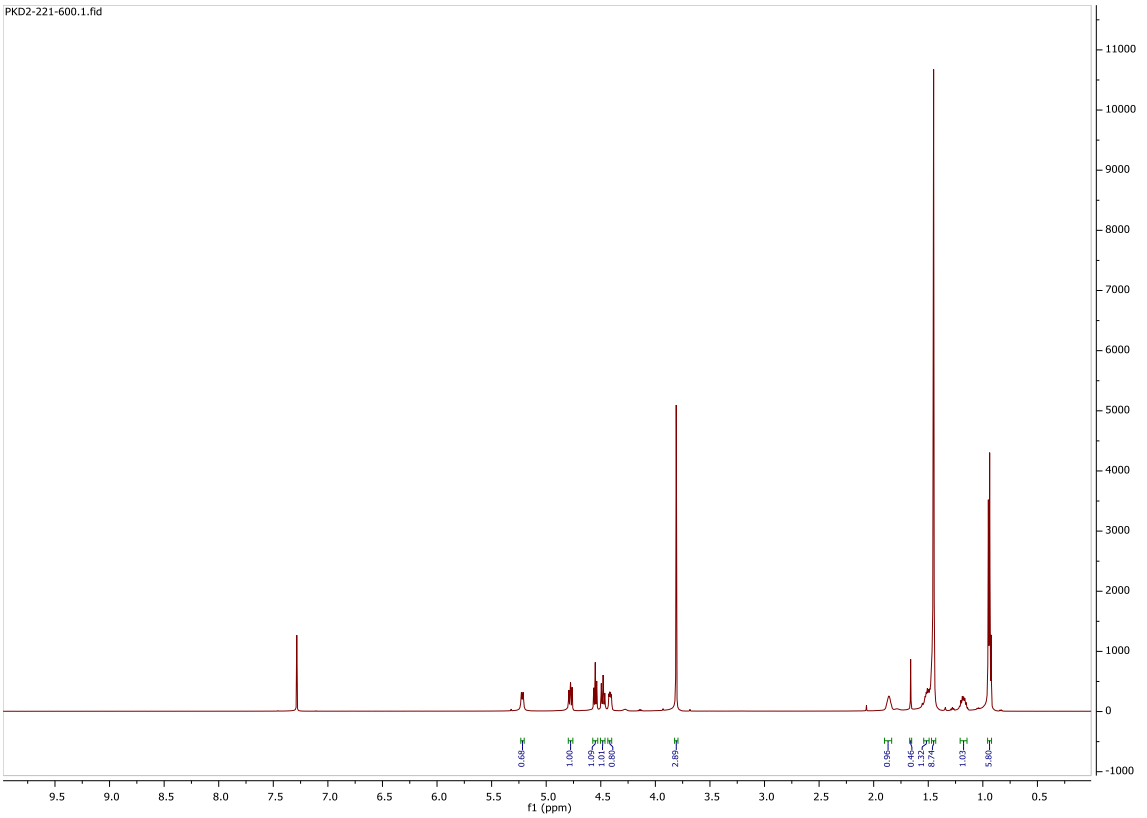
PKD2-221-600.1.fid
f1 (ppm)

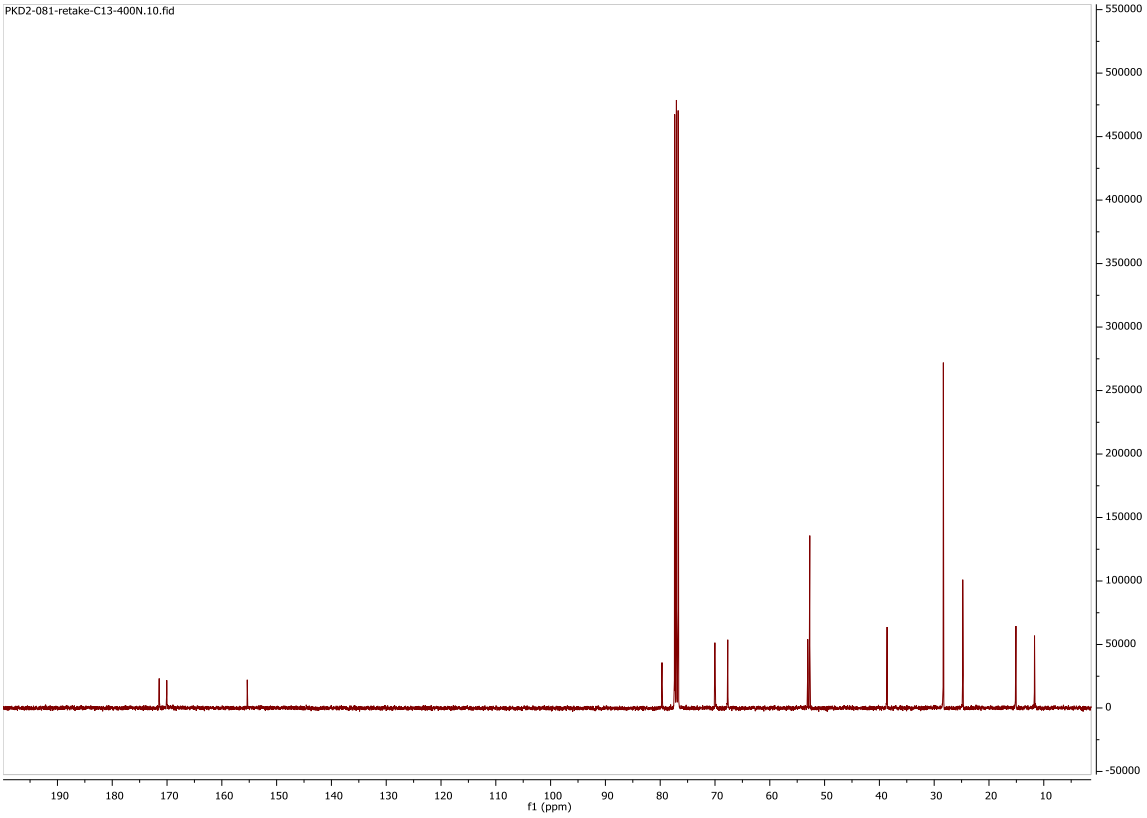
PKD2-081-retake-C13-400N.10.fid
f1 (ppm)

Methyl ((2S,3S)-2-((*tert*-butoxycarbonyl)amino)-3-methylpentanethioyl)-*L*-serinate

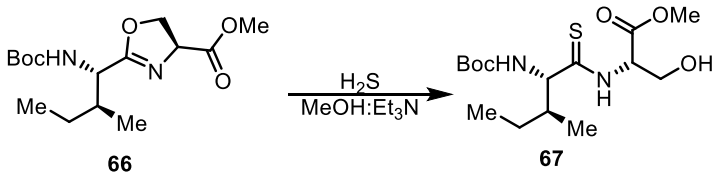

66 **67**

In a flask, **66** was dissolved in methanol/triethylamine (2:1), a volume enough to dissolve the material and H_2S was bubbled for 10 mins. The flask was sealed and stirred overnight. Then solvents and H_2S were removed under reduced pressure to obtain yellow colored crude material. Note: when reaction is stirred for 2 days, the reaction is highly likely to convert all the starting material to product. (to avoid complications explained in chapter 3)

Notebook Entries

Procedure: PKD2-105

^{1}H: PKD-105-1st-400 (crude NMR: Therefore, no peaks integrated)

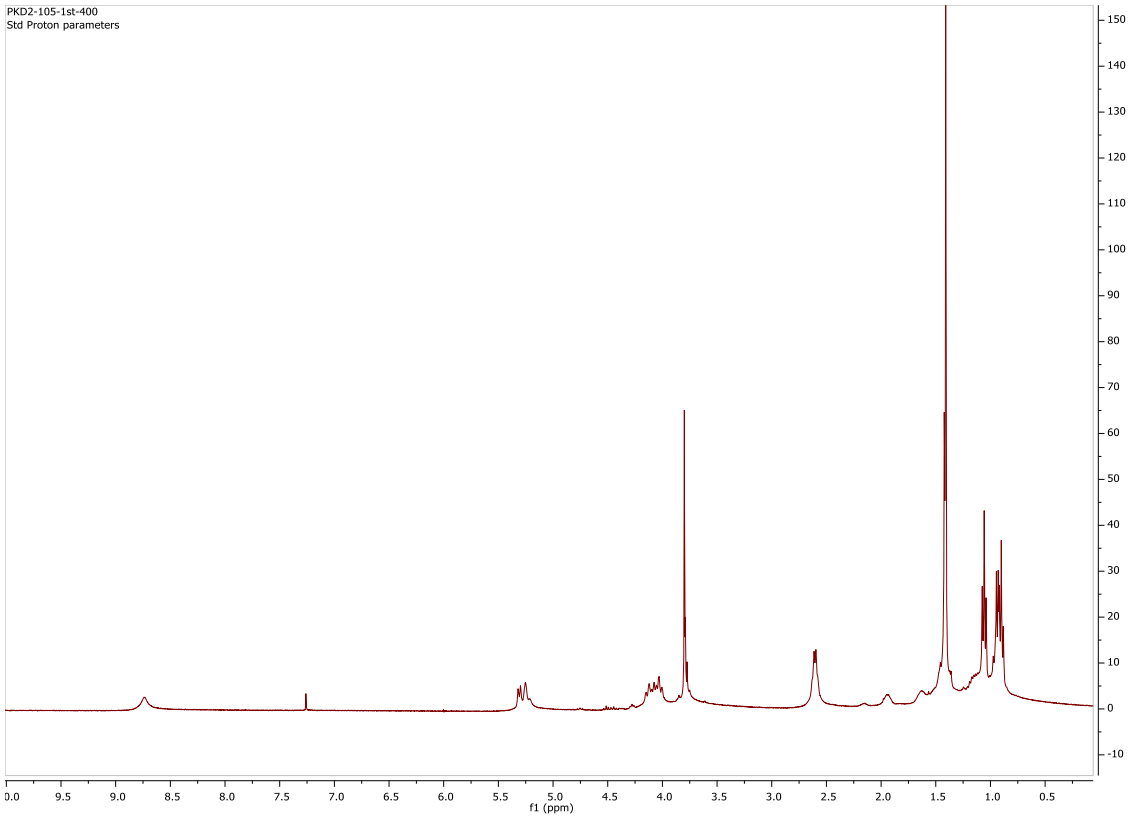
PKD2-105-1st-400
Std Proton parameters
150
140
130
120
110
100
90
80
70
60
50
40
30
20
10
0
-10
0.0
9.5
9.0
8.5
8.0
7.5
7.0
6.5
6.0
5.5
5.0
4.5
4.0
3.5
3.0
2.5
2.0
1.5
1.0
0.5
f1 (ppm)

Methyl 2-((1S,2S)-1-((*tert*-butoxycarbonyl)amino)-2-methylbutyl)thiazole-4-carboxylate

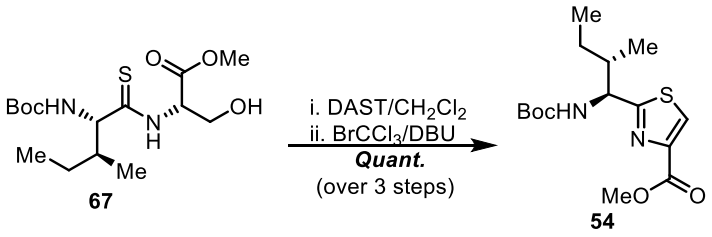

The crude material **67** was dissolved in methylene chloride (0.14 M), cooled to -78 °C, treated with diethylaminosulfur trifluoride (1.1 eq) and stirred for 2 hours at -78 °C, followed by addition of potassium carbonate (1.5 eq) and stirring for 30 mins at room temperature. $BrCCl_3$ (4 eq) was added to the reaction mixture followed by addition of DBU (4 eq). The reaction was quenched with saturated sodium bicarbonate (1 volume), the organic layer was separated, and the aqueous layer was extracted three times with methylene chloride. Combined organic layers were dried with anhydrous sodium sulfate and concentrated. Product was purified by flash column chromatography with 2:1 hexanes/ ethyl acetate to afford the yellow solid product in quantitative yield. R_f = 0.5 (2:1 hexanes/ ethyl acetate)

^{1}H NMR (600 MHz, Chloroform-*d*) δ 8.11 (s, 1H), 5.32 (d, *J* = 9.1 Hz, 1H), 4.94 (dd, *J* = 8.9, 5.8 Hz, 1H), 3.95 (s, 3H), 2.22 – 2.16 (m, 1H), 1.45 (s, 9H), 1.41 – 1.37 (m, 1H), 1.18 – 1.12 (m, 1H), 0.94 (d, *J* = 6.8 Hz, 3H), 0.91 (t, *J* = 7.4 Hz, 3H).

^{13}C NMR (151 MHz, Chloroform-*d*) δ 173.29, 161.90, 155.36, 146.99, 127.13, 80.11, 57.52, 52.47, 39.73, 28.33, 24.44, 15.83, 11.58.

Notebook Entries

Procedure: PKD2-072

^{1}H: PKD2-247-600, ^{13}C: PKD2-072-C13-600

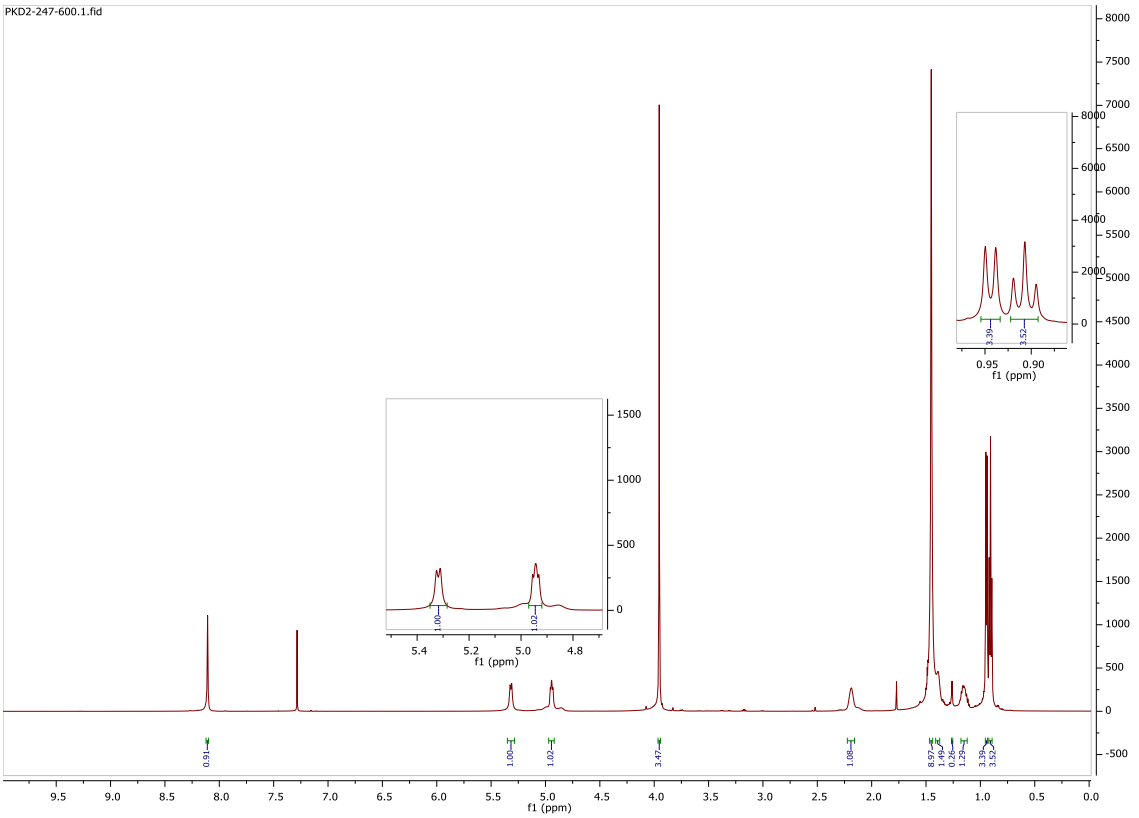
PKD2-247-600.1.fid
f1 (ppm)

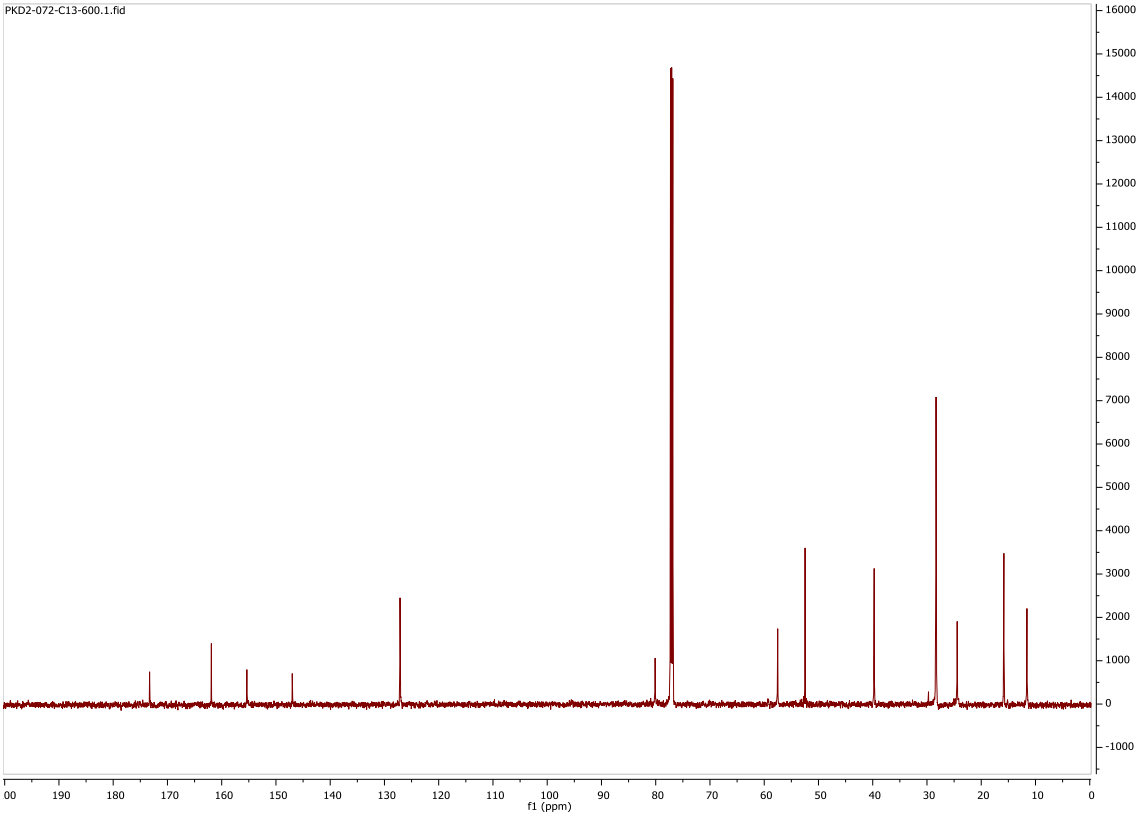
PKD2-072-C13-600.1.fid
f1 (ppm)

(*tert*-butoxycarbonyl)-*D*-alloisoleucine

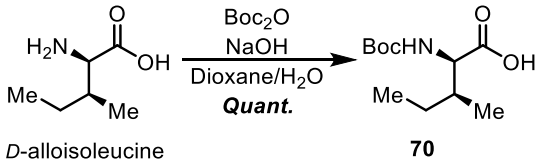

D-alloisoleucine **70**

Reaction was performed under standard Boc protection conditions. The product was afforded in quantitative yield. R_f = 0.0 (3:1 ethyl acetate/hexanes): (Product retains on the baseline due to free carboxylic acid)

Notebook Entries

Procedure: PKD2-077

^{1}H: PKD2-077-crude-1st-MeOH-400 (crude NMR: Therefore, no peaks integrated)

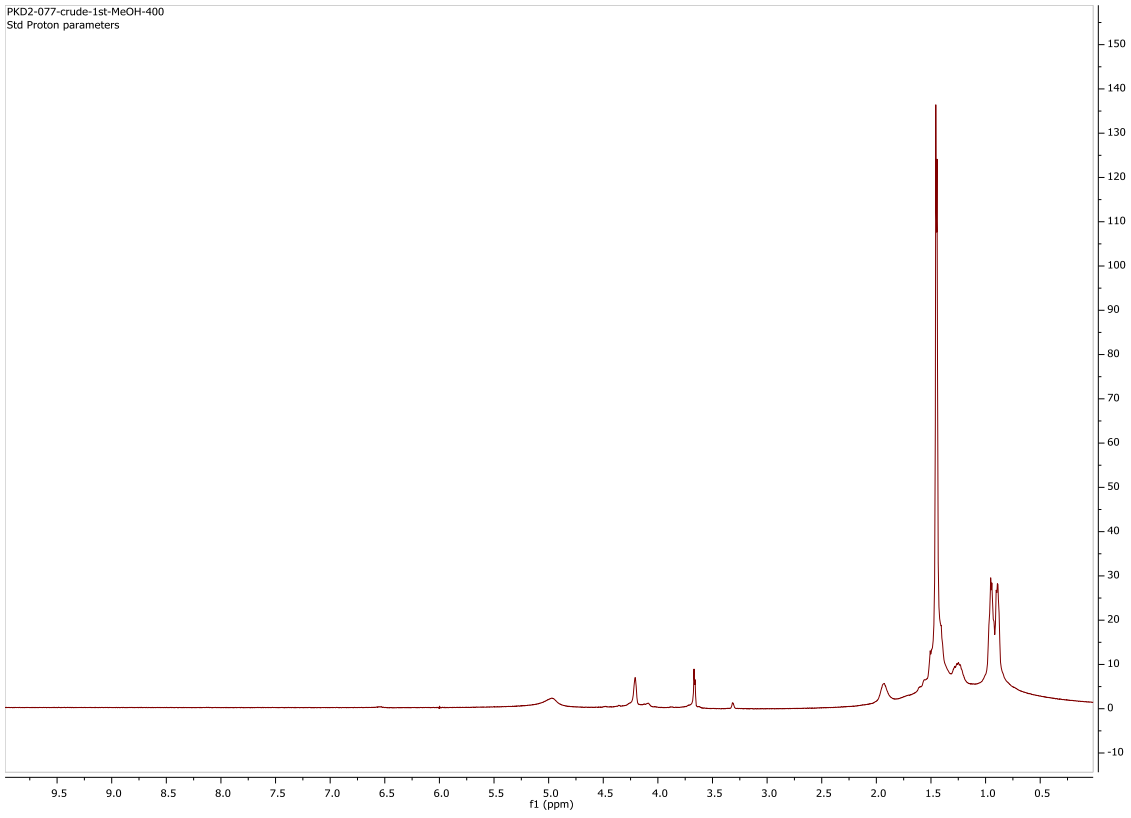

Methyl (*tert*-butoxycarbonyl)-*D*-alloisoleucyl-*L*-serinate

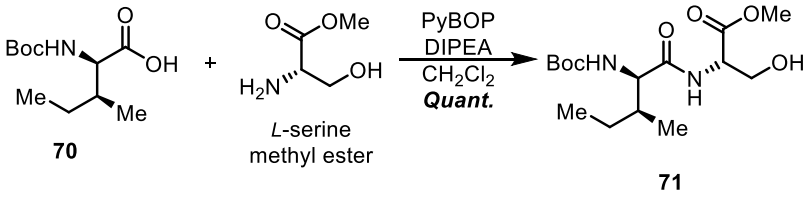

Reaction was performed using standard PyBOP peptide coupling conditions. The product was afforded in quantitative yield with purification by flash column chromatography with 3:1 ethyl acetate/hexanes.

^{1}H NMR (400 MHz, Chloroform-d) δ 7.11 (s, 1H), 5.09 (s, 1H), 4.63 (d, J = 8.0 Hz, 1H), 4.15 – 4.11 (m, 1H), 3.94 (s, 1H), 3.75 (s, 3H), 2.00 (t, J = 6.1 Hz, 1H), 1.42 (s, 9H), 1.40 – 1.37 (m, 1H), 1.26 – 1.21 (m, 1H), 0.95 – 0.91 (m, 3H), 0.90 – 0.86 (m, 3H).

^{13}C NMR (101 MHz, Chloroform-*d*) δ 171.31, 156.57, 80.78, 62.80, 58.73, 54.85, 52.96, 37.10, 28.47, 26.56, 14.42, 11.92.

Notebook Entries

Procedure: PKD1-129

^{1}H: PKD2-103-400, ^{13}C: AXT-024-ACarbon

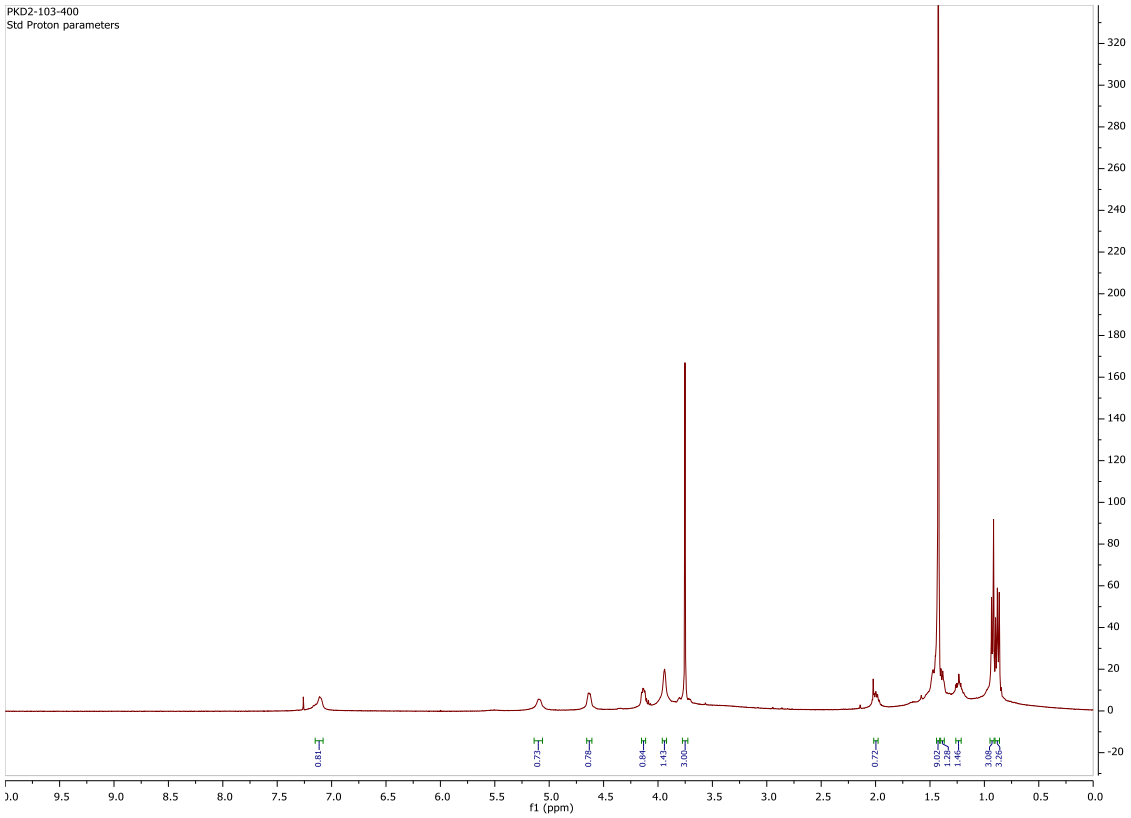
PKD2-103-400
Std Proton parameters
f1 (ppm)

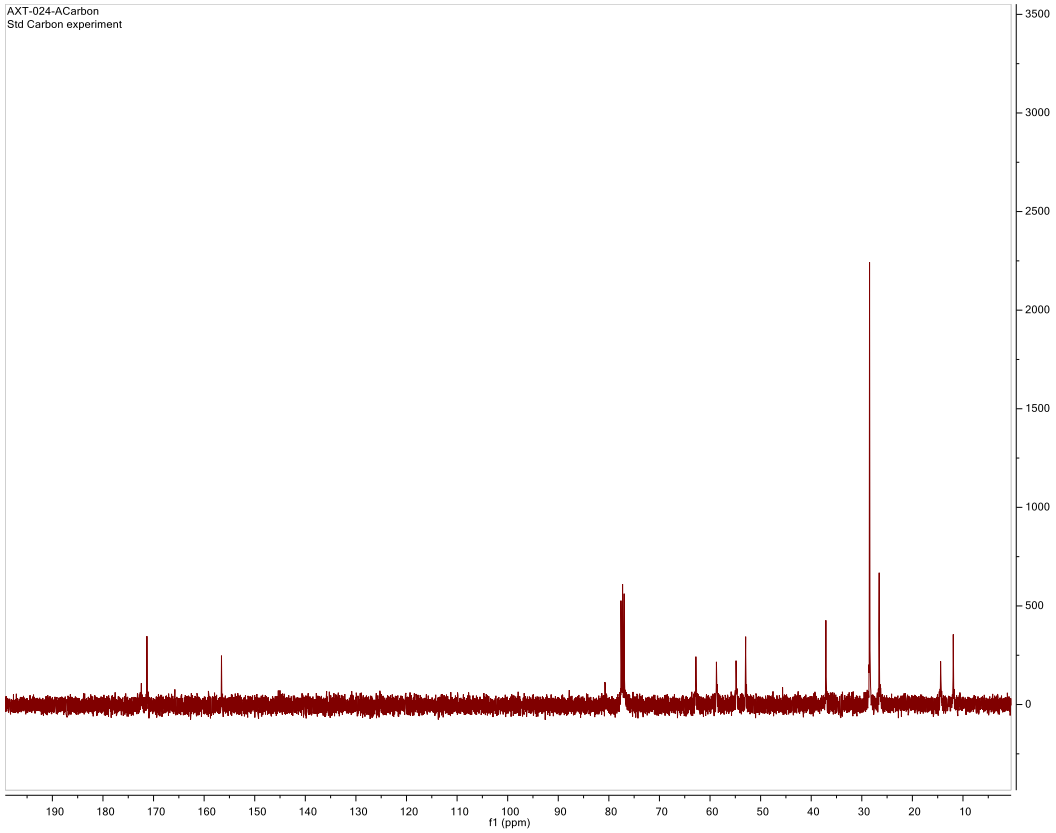
AXT-024-ACarbon
Std Carbon experiment
f1 (ppm)

Methyl (S)-2-((1R,2S)-1-((*tert*-butoxycarbonyl)amino)-2-methylbutyl)-4,5-dihydrooxazole-4-carboxylate

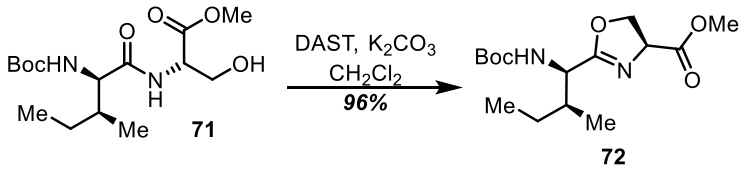

Reaction was performed using standard DAST protocol. Product was purified by flash column chromatography with 2:1 hexanes/ethyl acetate to afford the white solid product in quantitative yield. R_f = 0.4 (2:1 hexanes/ethyl acetate)

^{1}H NMR (400 MHz, Chloroform-*d*) δ 4.98 (d, *J* = 9.5 Hz, 1H), 4.69 (ddd, *J* = 10.5, 7.8, 0.8 Hz, 1H), 4.51 (dd, *J* = 8.8, 7.9 Hz, 1H), 4.43 – 4.34 (m, 2H), 3.72 (s, 3H), 1.79 (dq, *J* = 12.9, 6.5 Hz, 1H), 1.45 – 1.39 (m, 1H), 1.37 (s, 9H), 1.19 – 1.05 (m, 1H), 0.87 (t, *J* = 7.4 Hz, 3H), 0.81 (d, *J* = 6.9 Hz, 3H).

^{13}C NMR (101 MHz, Chloroform-*d*) δ 171.25, 170.01, 155.57, 79.71, 69.83, 67.82, 52.69, 52.44, 38.19, 28.30, 25.96, 14.30, 11.73.

Notebook Entries

Procedure: PKD2-218

^{1}H: PKD2-137-retake-400N, ^{13}C: PKD2-137-retake-C13-400N

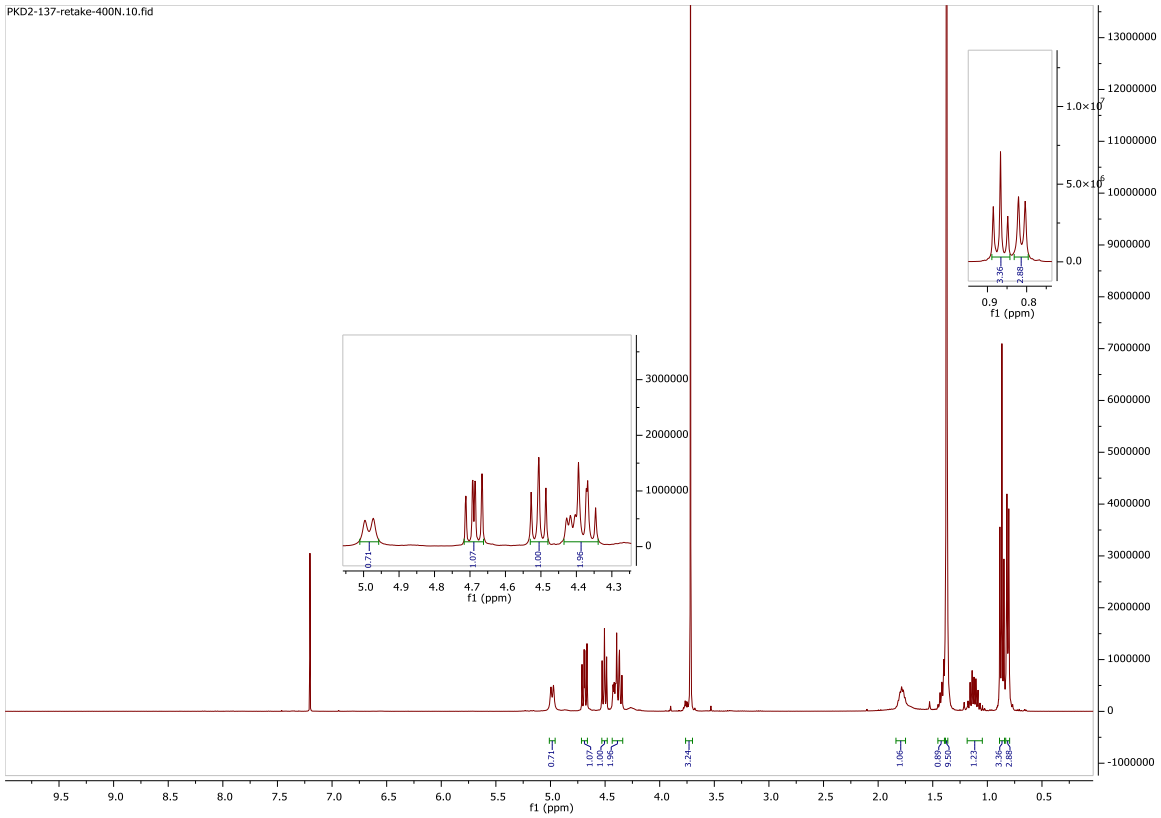
PKD2-137-retake-400N.10.fid
f1 (ppm)

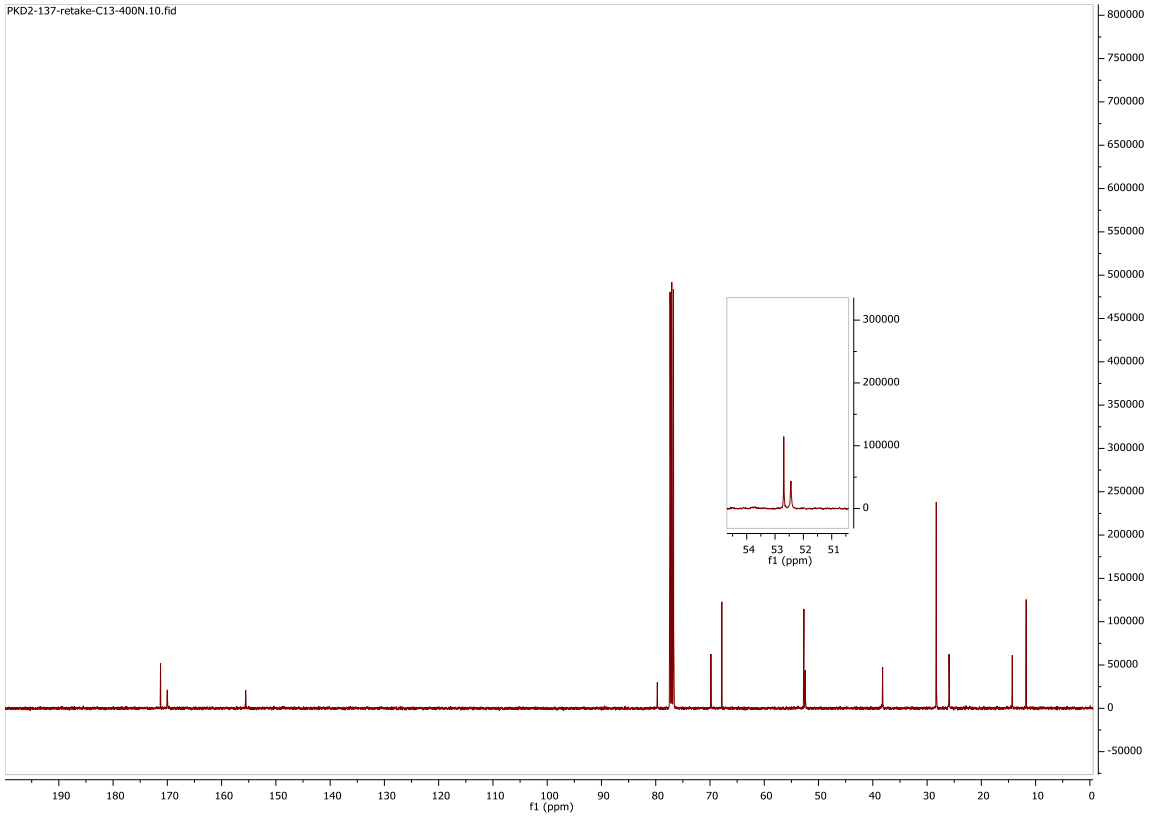
PKD2-137-retake-C13-400N.10.fid
f1 (ppm)

Methyl ((2R,3S)-2-((*tert*-butoxycarbonyl)amino)-3-methylpentanethioyl)-*L*-serinate

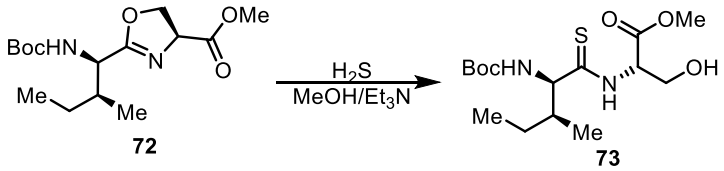

In a flask, **72** was dissolved in methanol/triethylamine (2:1), a volume enough to dissolve the material and H_2S was bubbled for 10 mins. The flask was sealed and stirred overnight. Then solvents and H_2S were removed under reduced pressure to obtain yellow colored crude material. Note: when reaction is stirred for 2 days, the reaction is highly likely to convert all the starting material to product. (to avoid complications explained in chapter 3)

Notebook Entries

Procedure: PKD2-218

^{1}H: PKD2-143-crude-400 (Crude NMR – Therefore, not integrated)

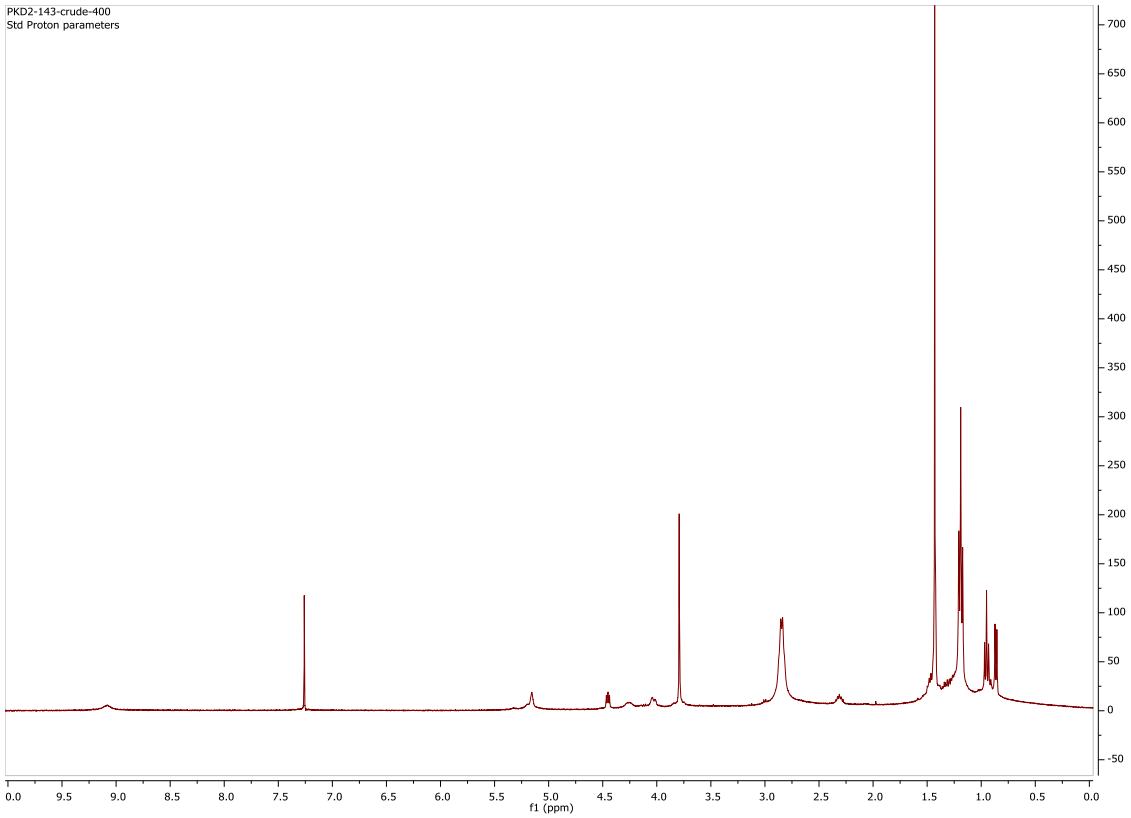
PKD2-143-crude-400
Std Proton parameters
700
650
600
550
500
450
400
350
300
250
200
150
100
50
0
-50
0.0
9.5
9.0
8.5
8.0
7.5
7.0
6.5
6.0
5.5
5.0
4.5
4.0
3.5
3.0
2.5
2.0
1.5
1.0
0.5
0.0
f1 (ppm)

Methyl 2-((1R,2S)-1-((*tert*-butoxycarbonyl)amino)-2-methylbutyl)thiazole-4-carboxylate

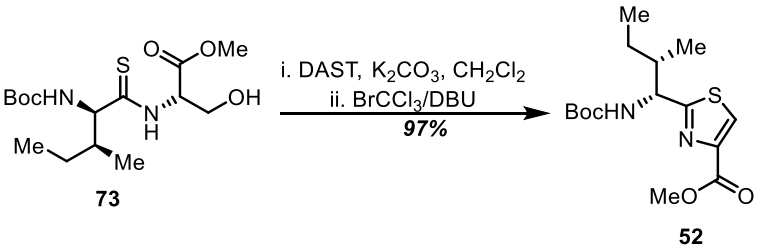

73 52

The crude material **73** was then dissolved in methylene chloride (0.14 M), cooled to -78 °C, treated with diethylaminosulfur trifluoride (1.1 eq) and stirred for 2 hours at -78 °C, followed by addition of potassium carbonate (1.5 eq) and stirring for 30 mins at room temperature. $BrCCl_3$ (4 eq) was added to the reaction mixture followed by addition of DBU (4 eq). The reaction was quenched with saturated sodium bicarbonate, the organic layer was separated, and the aqueous layer was extracted three times with methylene chloride. Combined organic layers were dried with anhydrous sodium sulfate and concentrated. Product was purified by flash column chromatography with 2:1 hexanes/ethyl acetate to afford the yellow solid product in 97% yield. R_f = 0.5 (2:1 hexanes/ethyl acetate)

^{1}H NMR (400 MHz, Chloroform-*d*) δ 8.10 (s, 1H), 5.24 (d, *J* = 9.0 Hz, 1H), 5.07 (dd, *J* = 9.2, 4.7 Hz, 1H), 3.95 (s, 3H), 2.29 (tq, *J* = 13.3, 7.2 Hz, 1H), 1.52 – 1.39 (m, 10H), 1.31 – 1.23 (m, 1H), 0.96 (t, *J* = 7.4 Hz, 3H), 0.84 (d, *J* = 6.9 Hz, 3H).

^{13}C NMR (101 MHz, Chloroform-*d*) δ 174.70, 161.89, 155.57, 147.13, 127.23, 80.06, 77.66, 56.69, 52.41, 39.64, 28.37, 26.63, 13.93, 11.67.

Notebook Entries

Procedure: PKD2-254/256

^{1}H: PKD2-399-400N, ^{13}C: AXT-039-ACarbon

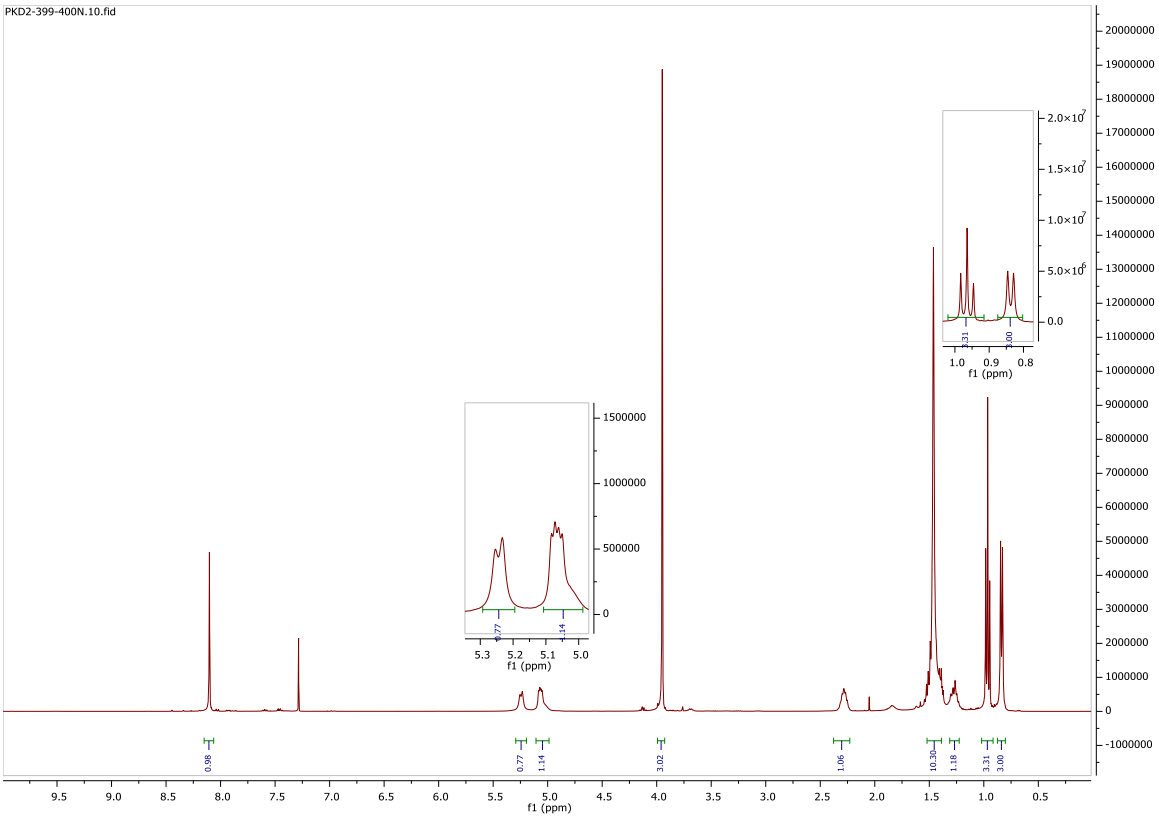
PKD2-399-400N.10.fid
f1 (ppm)
0.98
0.77
1.14
3.02
1.06
10.36
1.18
3.31
3.00

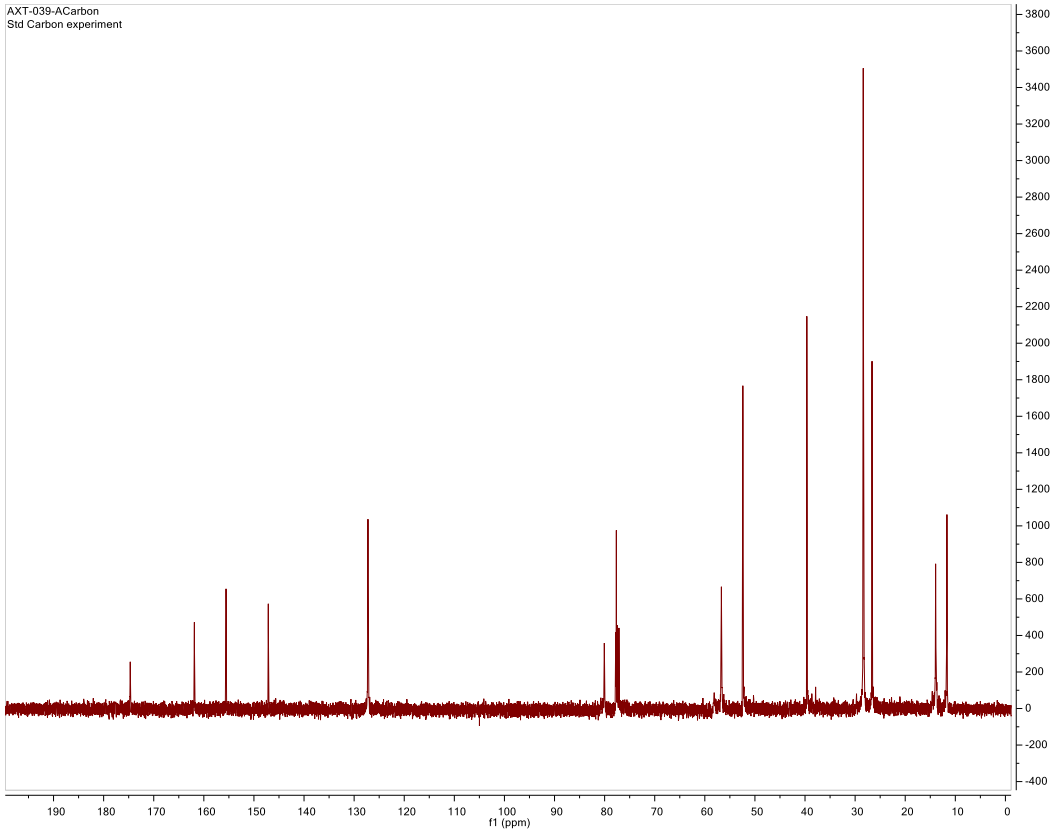
AXT-039-ACarbon
Std Carbon experiment
f1 (ppm)

Methyl ((benzyloxy)carbonyl)-*D*-alanyl-*L*-threoninate

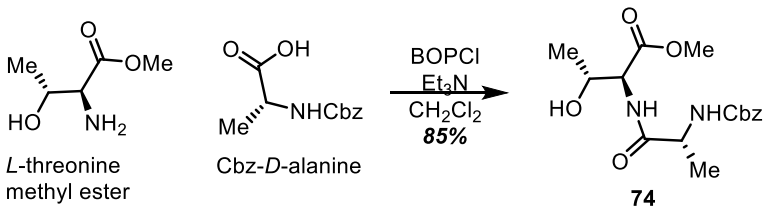

In a dry flask, Cbz-D-alanine (1 eq.) and L-threonine (1.2 eq.) methyl ester were mixed and dissolved in methylene chloride (0.1 M) and cooled to 0 °C. Then triethylamine (3 eq.) was added to the reaction mixture and stirred for 5 mins followed by the addition of BOP-chloride (1.1 eq.). Reaction mixture was allowed to come to room temperature and stirred overnight under argon atmosphere. Solvents were removed under reduced pressure and the concentrated syrupy mixture was purified by flash column chromatography using 3:1 ethyl acetate/hexanes to afford the product in 79% yield. R_f = 0.3 (3:1 ethyl acetate/hexanes)

^{1}H NMR (400 MHz, Chloroform-*d*) δ 7.41 – 7.29 (m, 5H), 6.98 (d, *J* = 9.0 Hz, 1H), 5.56 (s, 1H), 5.11 (s, 2H), 4.57 (dd, *J* = 9.0, 2.5 Hz, 1H), 4.33 (s, 2H), 3.73 (s, 3H), 2.58 (s, 1H), 1.42 (d, *J* = 7.1 Hz, 3H), 1.18 (d, *J* = 6.3 Hz, 3H).

^{13}C NMR (101 MHz, Chloroform-*d*) δ 173.26, 171.67, 156.23, 128.79, 128.47, 128.38, 68.13, 67.34, 57.44, 52.88, 50.99, 20.10, 19.11.

Notebook Entries

Procedure: PKD2-082

^{1}H: PKD2-082-400, ^{13}C: PKD2-082-C13-400

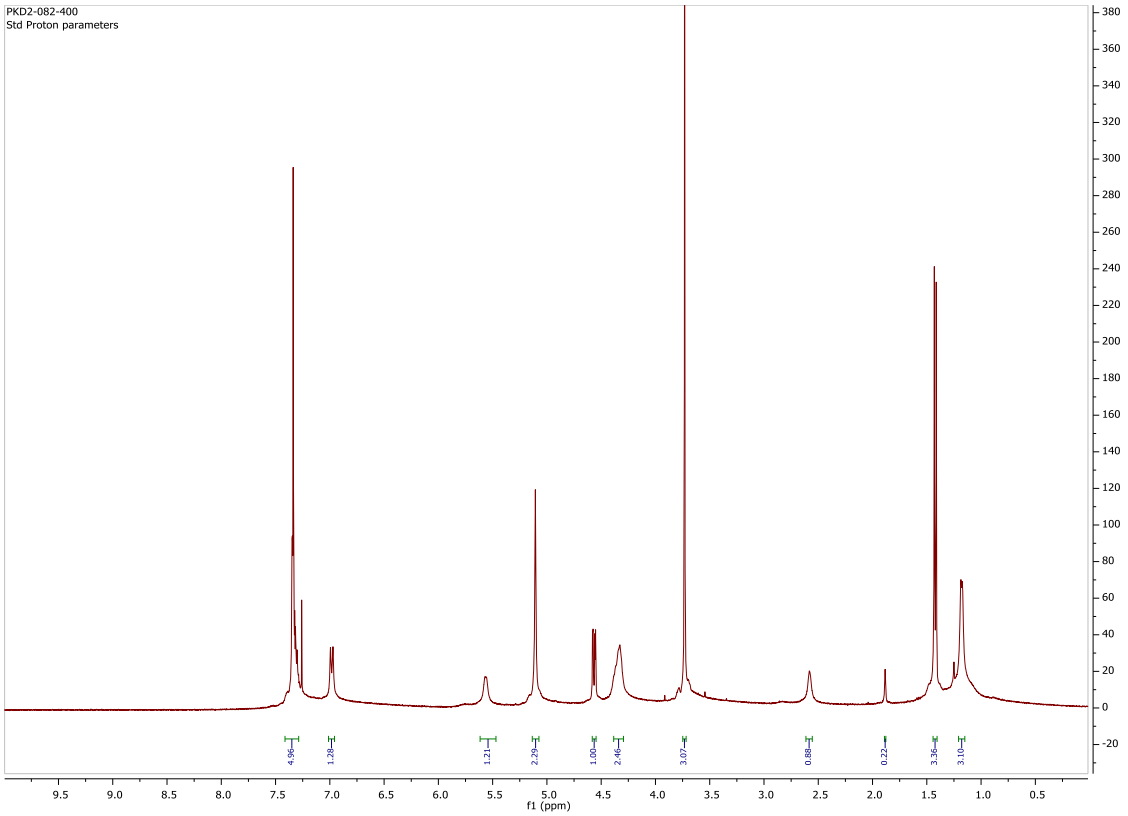
PKD2-082-400
Std Proton parameters
f1 (ppm)

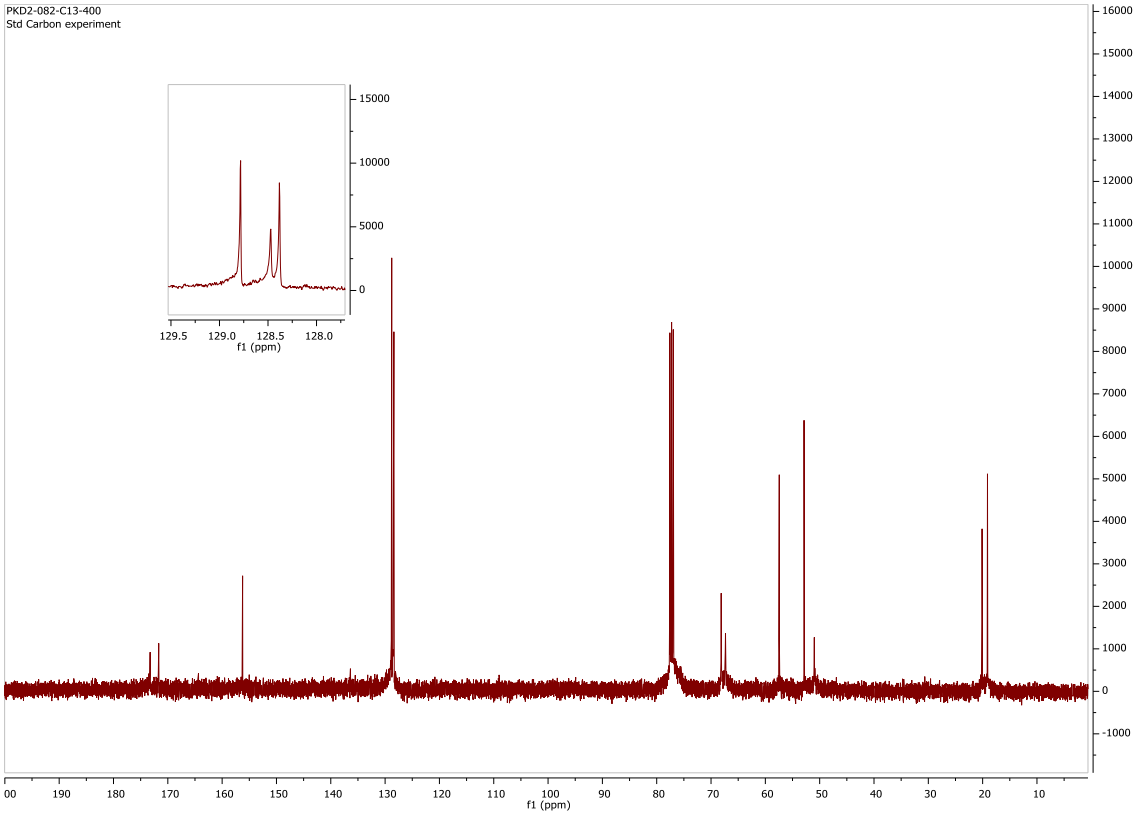
PKD2-082-C13-400
Std Carbon experiment
f1 (ppm)
f1 (ppm)

(4S,5S)-2-((S)-1-(((benzyloxy)carbonyl)amino)-2-methylpropyl)-5-methyl-4,5-dihydrooxazole-4-carboxylic acid

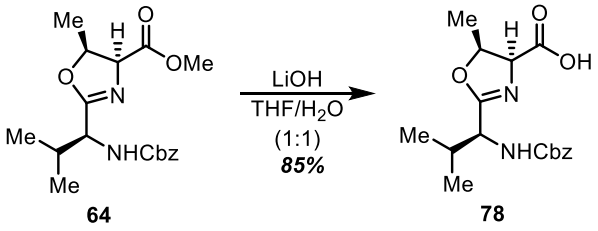

64 **78**

The reaction was performed under standard saponification conditions and yielded the product in 91% yield. Rf = 0.0 (3:1 ethyl acetate/hexanes): (Deprotected material retains on the baseline)

^{1}H NMR (400 MHz, Methanol-d_4) δ 7.38 – 7.27 (m, 5H), 5.45 (s, 1H), 5.19 – 5.04 (m, 2H), 4.06 (s, 1H), 3.92 (dd, *J* = 10.0, 3.1 Hz, 1H), 2.15 (dt, *J* = 13.2, 6.7 Hz, 1H), 1.40 (d, *J* = 6.6 Hz, 1H), 1.34 (d, *J* = 6.6 Hz, 1H), 1.01 – 0.87 (m, 4H).

Notebook Entries

Procedure: PKD2-089

^{1}H: PKD2-089-crude-MeOH-400 (Crude NMR)

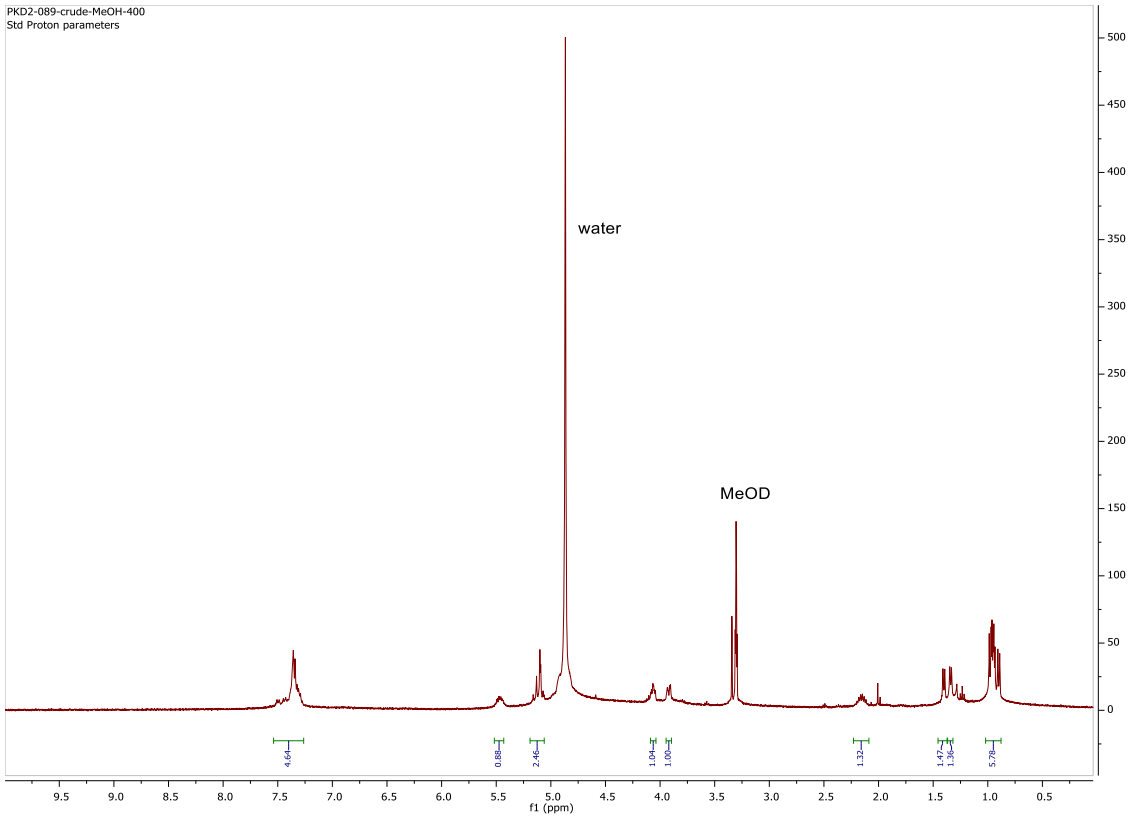
PKD2-089-crude-MeOH-400
Std Proton parameters
water
MeOD
4.64
0.88
2.46
1.04
1.00
1.32
1.47
1.36
5.78
f1 (ppm)

Methyl 2-((1S,2S)-1-amino-2-methylbutyl)thiazole-4-carboxylate

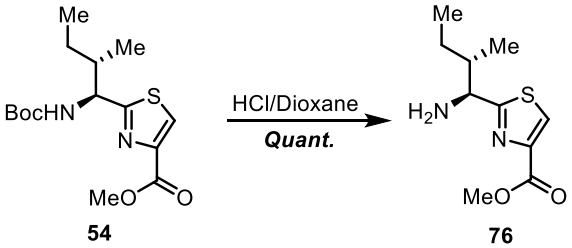

54 76

The reaction was performed under standard Boc deprotection conditions and gave access to **76** in quantitative yield. R_f = 0.0 (3:1 ethyl acetate/hexanes): (Deprotected material retains on the baseline)

^{1}H NMR (400 MHz, Methanol-d_4) δ 4.76 (d, *J* = 5.8 Hz, 1H), 3.93 (s, 3H), 2.18 – 2.09 (m, 1H), 1.60 (ddd, *J* = 13.7, 7.5, 4.5 Hz, 1H), 1.35 – 1.23 (m, 2H), 1.02 (t, *J* = 7.4 Hz, 3H), 0.96 (d, *J* = 6.9 Hz, 3H).

Notebook Entries

Procedure: PKD2-090

^{1}H: PKD2-090-crude-MeOH-400 (Crude NMR. Impurities present)

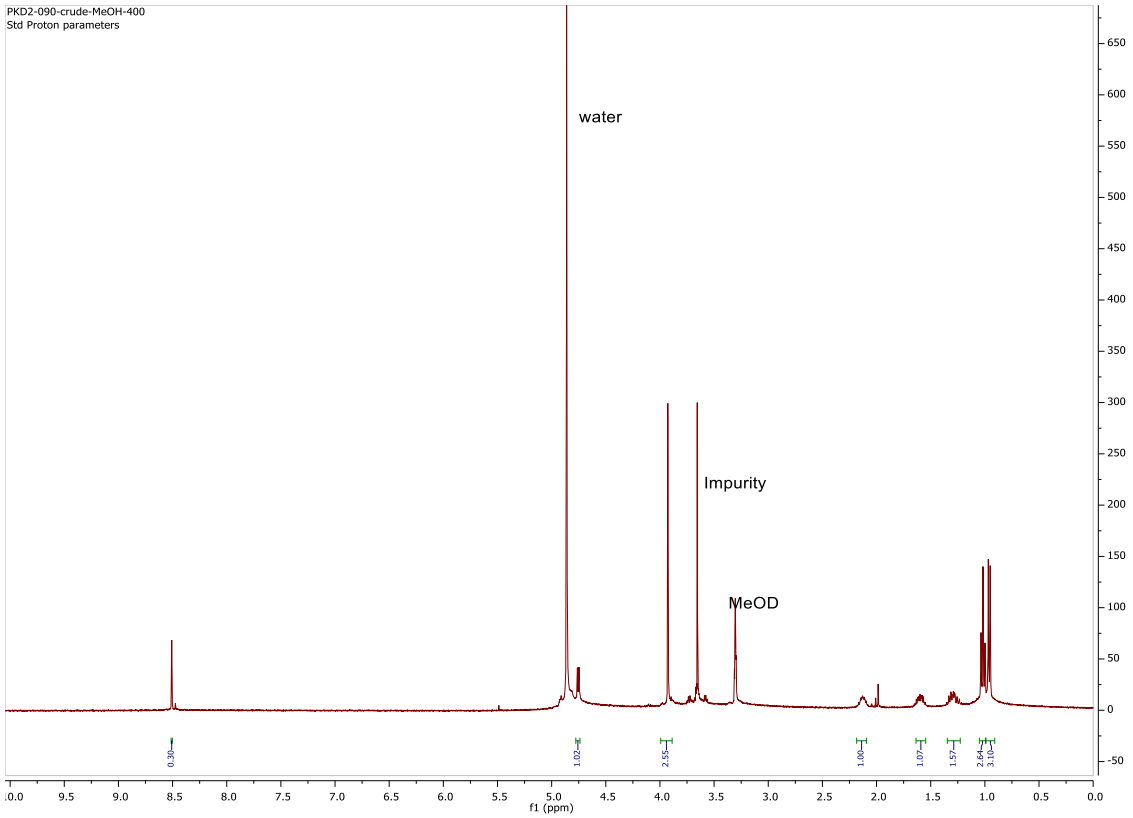
PKD2-090-crude-MeOH-400
Std Proton parameters
water
Impurity
MeOD
f1 (ppm)

Methyl 2-((1S,2S)-1-((S)-2-(((benzyloxy)carbonyl)amino)-3-methylbutanamido)-2-methylbutyl)thiazole-4-carboxylate

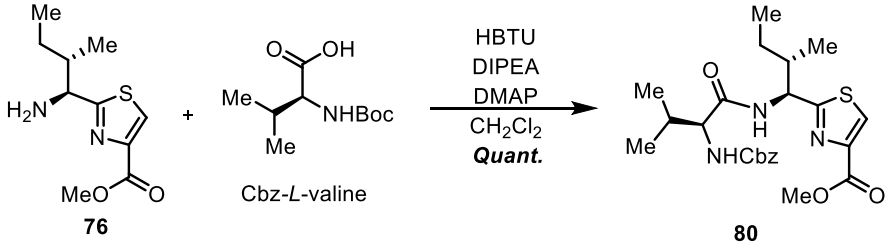

Reaction was performed using standard HBTU peptide coupling conditions. The product was afforded in quantitative yields with purification by flash column chromatography with 100% hexane. R_f = 0.5 (100% hexane)

^{1}H NMR (400 MHz, Chloroform-*d*) δ 8.07 (s, 1H), 7.44 – 7.28 (m, 5H), 6.77 (d, *J* = 8.8 Hz, 1H), 5.36 (d, *J* = 8.8 Hz, 1H), 5.23 (dd, *J* = 8.8, 6.4 Hz, 1H), 5.11 (s, 1H), 4.06 – 3.99 (m, 1H), 3.92 (s, 3H), 2.24 – 2.14 (m, 2H), 1.46 (ddd, *J* = 13.5, 7.6, 3.7 Hz, 1H), 1.15 (d, *J* = 10.2 Hz, 1H), 0.94 – 0.85 (m, 12H).

Notebook Entries

Procedure: PKD2-119

^{1}H: PKD2-119-400

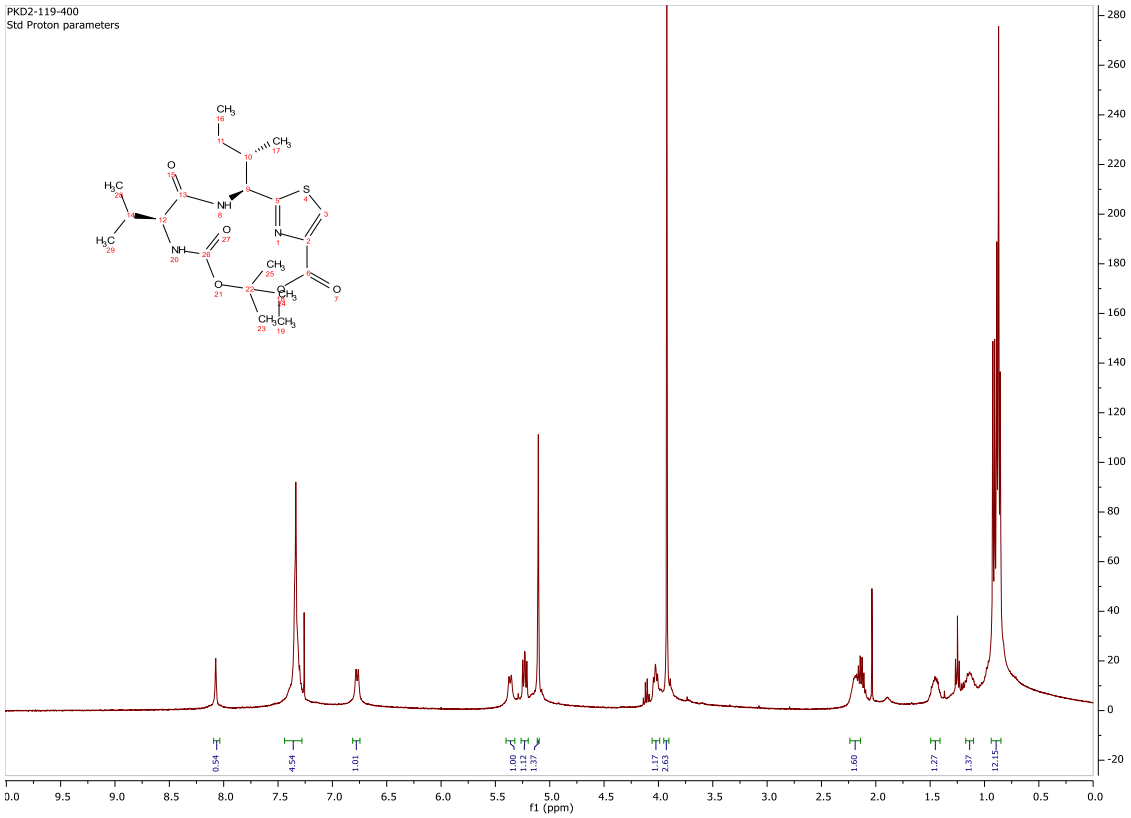
PKD2-119-400
Std Proton parameters
f1 (ppm)
0.54
4.54
1.01
1.00
1.12
1.37
1.17
2.63
1.60
1.27
1.37
12.15

(*tert*-butoxycarbonyl)-*L*-threonine

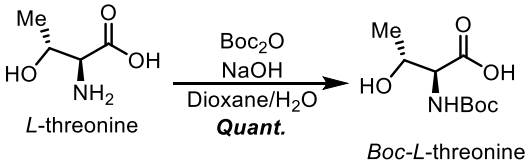

The reaction was carried out under standard Boc protection conditions and yielded Boc-L-threonine quantitatively. R_f = 0.0 (3:1 ethyl acetate/hexanes): (Product retains on the baseline due to free carboxylic acid.

^{1}H NMR (400 MHz, Methanol-d_4) δ 4.28 (qd, *J* = 6.2, 2.8 Hz, 1H), 4.10 (d, *J* = 3.1 Hz, 1H), 1.48 (d, *J* = 4.9 Hz, 9H), 1.23 (t, *J* = 5.7 Hz, 3H).

Notebook Entries

Procedure: PKD2-148

^{1}H: PKD2-148-MeOH-400N (Crude NMR)

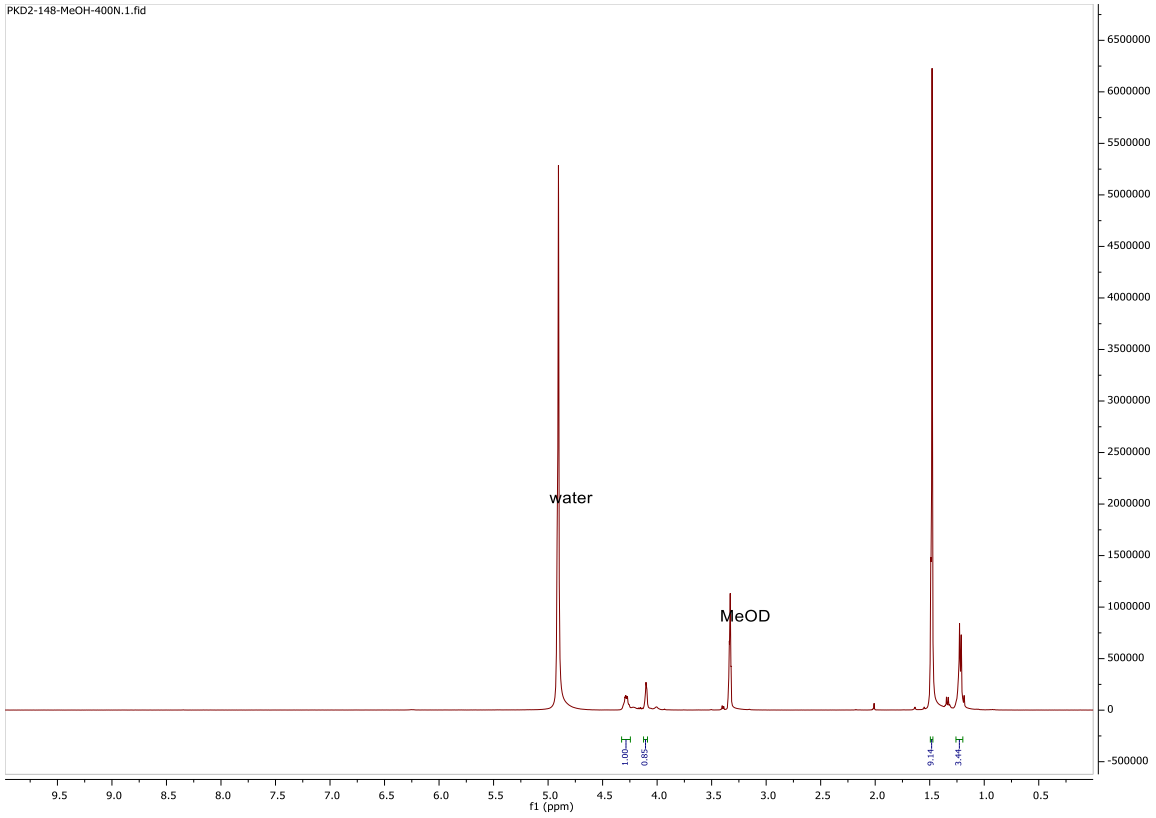

Methyl 2-((1S,2S)-1-((2S,3R)-2-((*tert*-butoxycarbonyl)amino)-3-hydroxybutanamido)-2-methylbutyl)thiazole-4-carboxylate

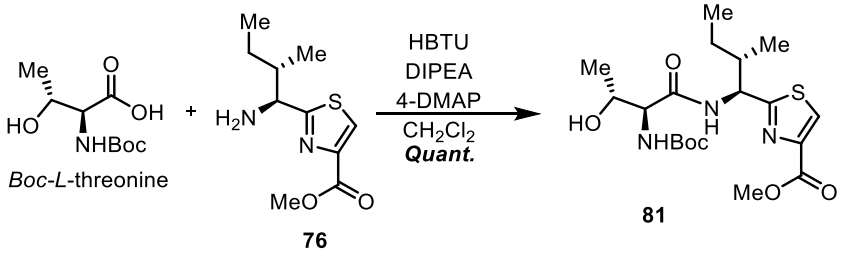

Reaction was performed using standard HBTU peptide coupling conditions. The product was afforded in quantitative yields with purification by flash column chromatography with 3:1 ethyl acetate/hexane. R_f = 0.75 (3:1 ethyl acetate/hexane).

Note: In small scale reactions (<100 mg) reaction was not quenched and extracted. Instead the reactions were concentrated and directly purified through column chromatography. In large scale reactions, standard protocol was followed.

^{1}H NMR (400 MHz, Chloroform-*d*) δ 8.12 (s, 1H), 7.32 (d, *J* = 9.0 Hz, 1H), 5.59 (d, *J* = 8.0 Hz, 1H), 5.29 (dd, *J* = 8.9, 5.7 Hz, 1H), 4.34 (tt, *J* = 6.7, 4.0 Hz, 1H), 4.15 (dd, *J* = 7.9, 2.6 Hz, 1H), 3.95 (s, 4H), 2.20 (q, *J* = 7.8 Hz, 1H), 1.46 (s, 10H), 1.41 (d, *J* = 3.5 Hz, 1H), 1.18 (d, *J* = 6.5 Hz, 3H), 0.95 (d, *J* = 6.8 Hz, 3H), 0.89 (t, *J* = 7.4 Hz, 3H).

^{13}C NMR (101 MHz, Chloroform-*d*) δ 172.25, 171.87, 161.67, 156.48, 146.68, 127.38, 80.43, 77.26, 66.71, 57.73, 56.18, 52.45, 39.58, 28.31, 24.12, 18.10, 15.90, 11.46.

Notebook Entries

Procedure: PKD2-289

^{1}H: PKD2-289-pure-400N, ^{13}C: PKD2-289-C13-400N

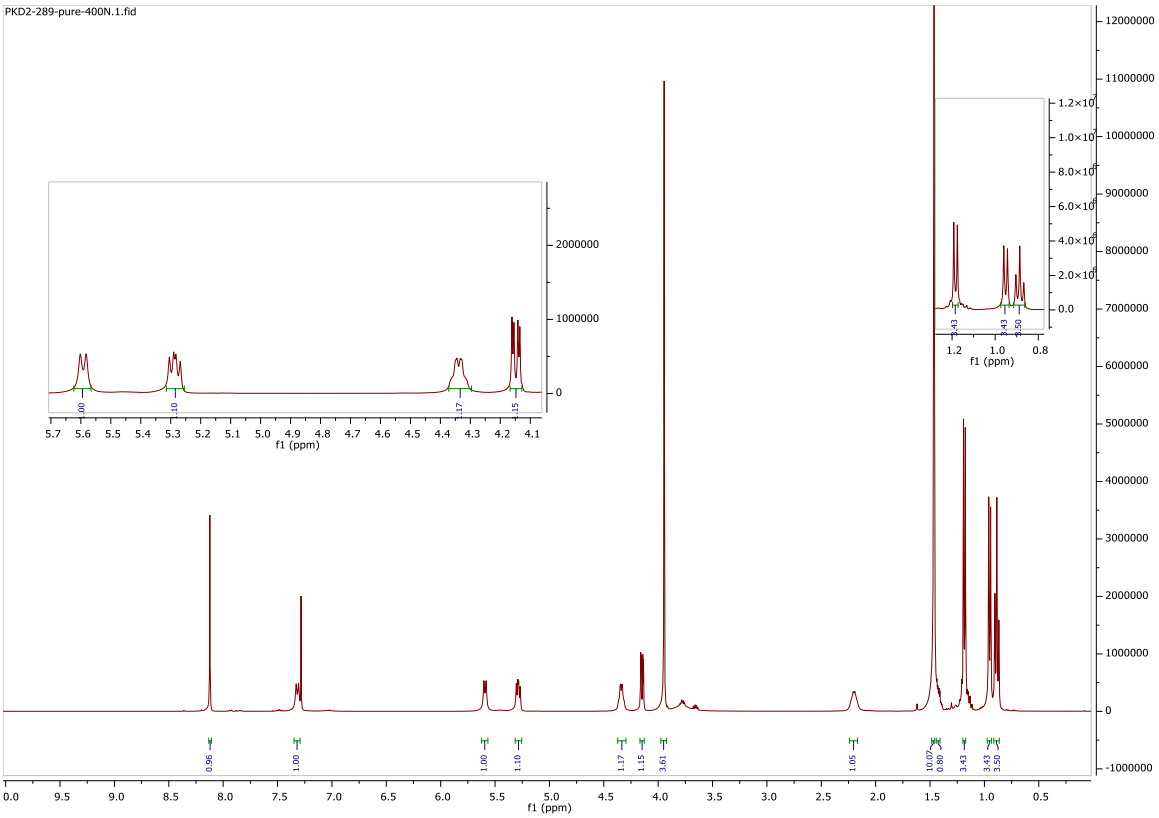
PKD2-289-pure-400N.1.fid
f1 (ppm)

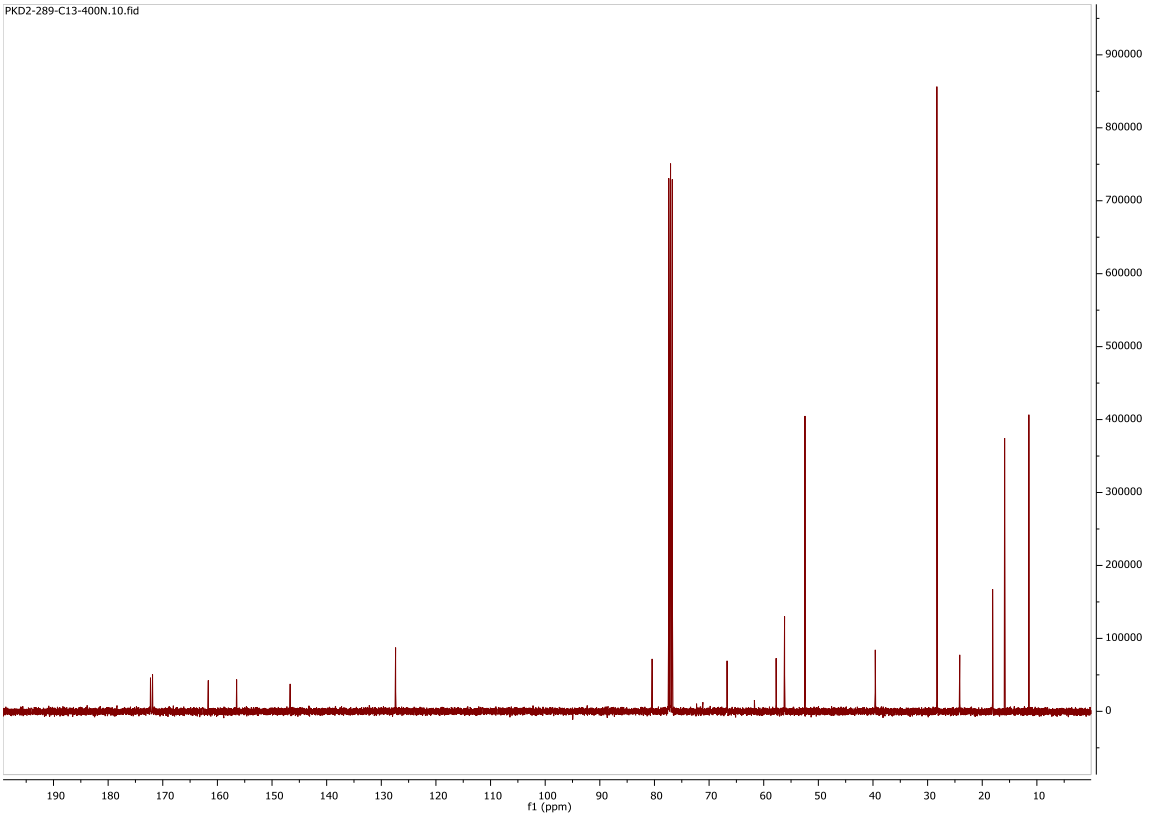
PKD2-289-C13-400N.10.fid
f1 (ppm)

Methyl 2-((1S,2S)-1-((2S,3R)-2-amino-3-hydroxybutanamido)-2-methylbutyl)thiazole-4-carboxylate

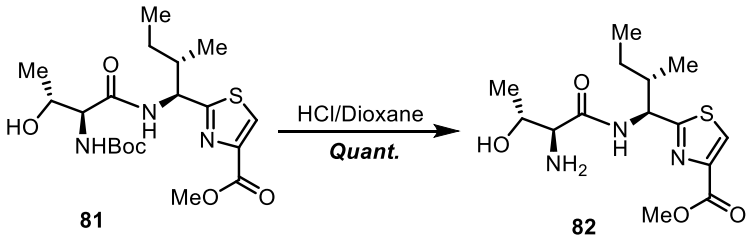

81 82

The reaction was performed using the standard Boc deprotection protocol and yielded the free amine **82** quantitatively. Rf = 0.0 (3:1 ethyl acetate/hexanes): (Deprotected material retains on the baseline)

^{1}H NMR (400 MHz, Methanol-d_4) δ 8.41 (s, 1H), 5.21 (d, J = 7.5 Hz, 1H), 4.09 (p, J = 6.3 Hz, 1H), 3.96 (d, J = 6.1 Hz, 1H), 3.93 (s, 3H), 2.15 (td, J = 10.1, 5.2 Hz, 1H), 1.63 (ddp, J = 14.8, 7.3, 3.5 Hz, 1H), 1.40 – 1.30 (m, 1H), 1.27 (d, J = 6.4 Hz, 3H), 0.98 – 0.90 (m, 6H).

Notebook Entries

Procedure: PKD2-159/301

^{1}H: PKD-301-crude-MeOH-400N

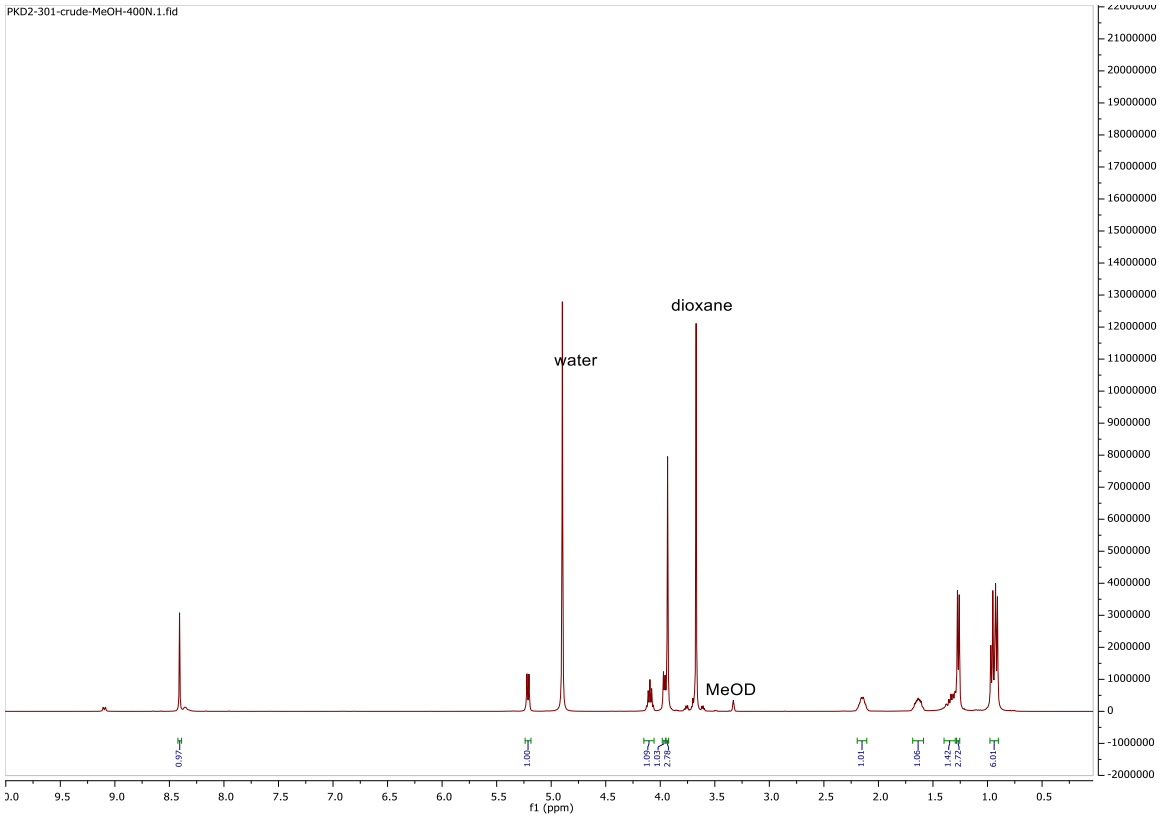
PKD2-301-crude-MeOH-400N.1.fid
water
dioxane
MeOD
f1 (ppm)

Methyl 2-((5S,8S,11S,12S)-8-((R)-1-hydroxyethyl)-5-isopropyl-12-methyl-3,6,9-trioxo-1-phenyl-2-oxa-4,7,10-triazatetradecan-11-yl)thiazole-4-carboxylate

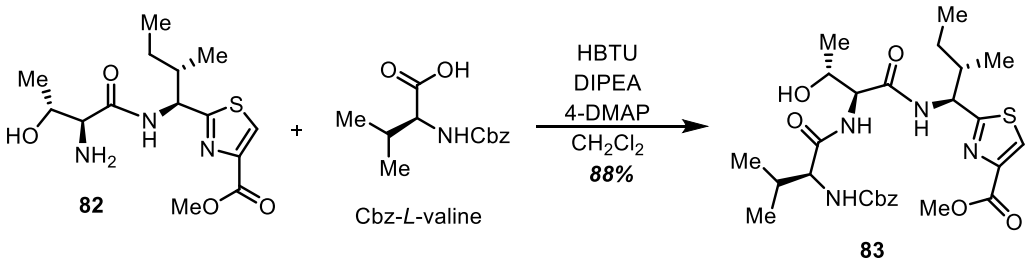

Reaction was performed using standard HBTU peptide coupling conditions. The product was afforded in 88% yield with purification by flash column chromatography with 3:1 ethyl acetate/hexane. R_f = 0. 5 (3:1 ethyl acetate/hexane).

Note: In large scale reactions (>100 mg or depending on solubility) reaction had to be adsorbed to silica to dry load into columns for chromatography.

^{1}H NMR (400 MHz, Chloroform-*d*) δ 8.12 (s, 1H), 7.36 (p, *J* = 2.8, 2.2 Hz, 5H), 7.03 (d, *J* = 7.7 Hz, 1H), 5.53 (d, *J* = 8.2 Hz, 1H), 5.28 (dd, *J* = 8.8, 5.9 Hz, 1H), 5.13 (t, *J* = 9.2 Hz, 2H), 4.54 (dd, *J* = 7.6, 3.1 Hz, 1H), 4.35 (d, *J* = 8.4 Hz, 1H), 4.16 – 4.10 (m, 1H), 3.94 (s, 3H), 2.18 (dq, *J* = 13.4, 5.9 Hz, 2H), 1.48 (d, *J* = 14.0 Hz, 2H), 1.28 (s, 2H), 1.20 (d, *J* = 7.9 Hz, 1H), 1.14 – 1.10 (m, 3H), 0.99 (d, *J* = 6.8 Hz, 3H), 0.95 (dd, *J* = 6.8, 1.7 Hz, 6H), 0.91 (d, *J* = 7.3 Hz, 3H).

^{13}C NMR (101 MHz, Chloroform-*d*) δ 172.14, 172.06, 170.71, 161.69, 136.06, 128.58, 128.27, 128.11, 127.53, 77.24, 67.23, 66.70, 60.61, 57.11, 56.40, 52.50, 39.57, 30.86, 24.42, 19.31, 18.05, 17.72, 15.87, 11.48.

Notebook Entries

Procedure: PKD2-276

^{1}H: PKD2-276-400, ^{13}C: PKD2-276-C13-400

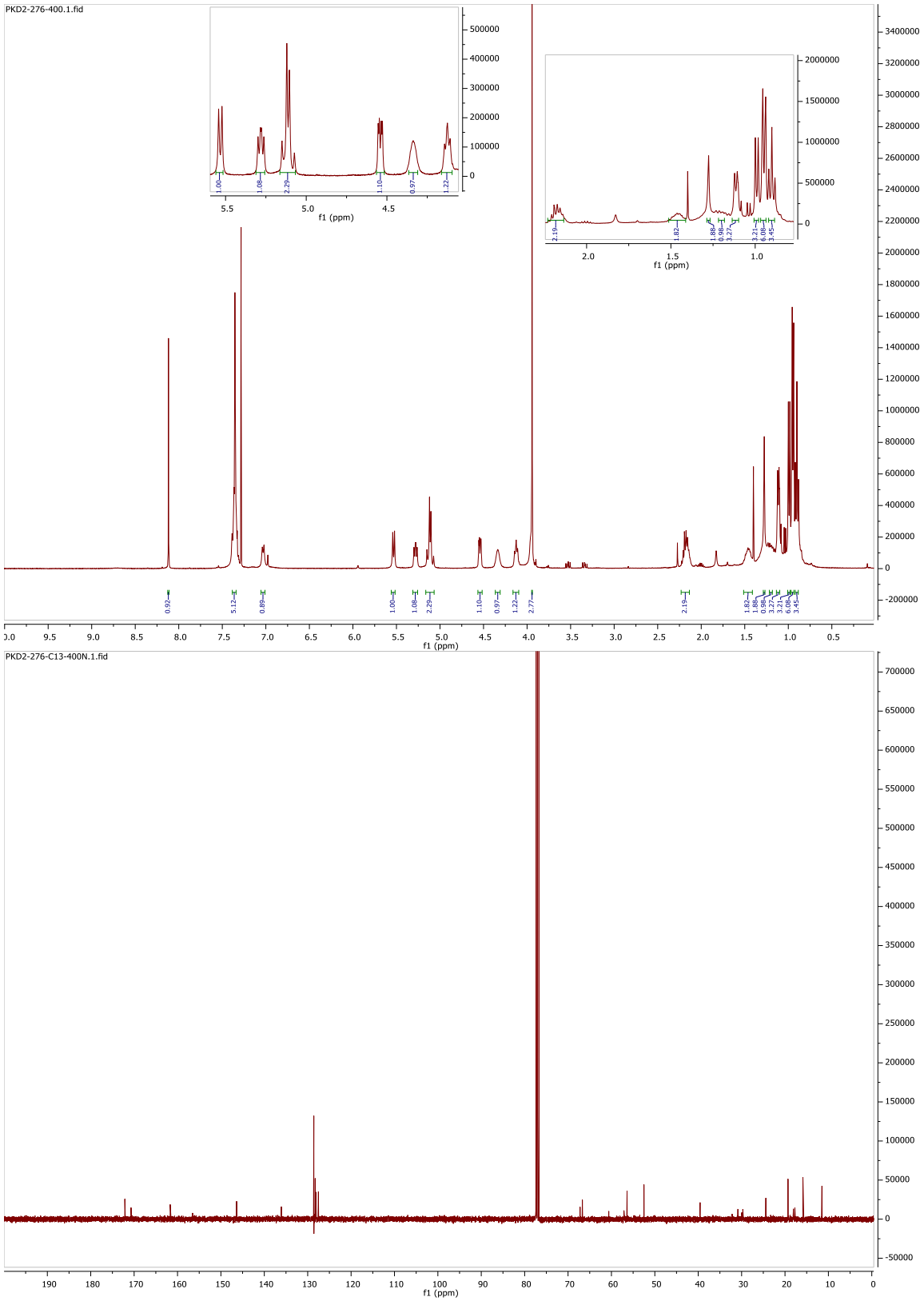
PKD2-276-400.1.fid
f1 (ppm)
PKD2-276-C13-400N.1.fid
f1 (ppm)

Methyl 2-((1S,2S)-1-((4S,5S)-2-((S)-1-(((benzyloxy)carbonyl)amino)-2-methylpropyl)-5-methyl-4,5-dihydrooxazole-4-carboxamido)-2-methylbutyl)thiazole-4-carboxylate

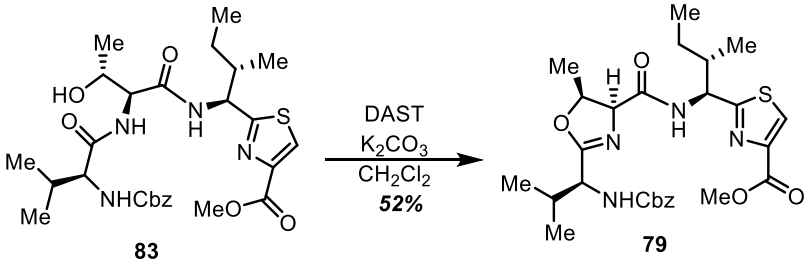

83 79

The reaction was performed using the standard DAST conditions. The product was purified by flash column chromatography with 1:3 hexanes/ethyl acetate to afford the white solid product in 52% yield. R_f = 0.7 (1:3 hexanes/ ethyl acetate)

^{1}H NMR (400 MHz, Chloroform-*d*) δ 8.12 – 8.09 (m, 1H), 7.51 (d, *J* = 8.8 Hz, 1H), 7.35 (ddt, *J* = 13.3, 4.9, 2.3 Hz, 5H), 5.54 – 5.47 (m, 1H), 5.24 – 5.17 (m, 1H), 5.16 – 5.04 (m, 3H), 4.71 (d, *J* = 10.3 Hz, 1H), 4.40 (dd, *J* = 9.3, 5.3 Hz, 1H), 3.94 – 3.88 (s, 3H), 2.30 (dtt, *J* = 10.1, 6.6, 3.3 Hz, 1H), 2.20 (q, *J* = 7.8, 7.1 Hz, 1H), 1.50 (qt, *J* = 9.2, 4.1 Hz, 1H), 1.32 – 1.28 (m, 3H), 1.18 (dt, *J* = 14.5, 7.6 Hz, 1H), 1.06 – 0.98 (m, 6H), 0.93 – 0.87 (m, 6H).

^{13}C NMR (101 MHz, Chloroform-*d*) δ 171.07, 169.52, 169.10, 156.19, 136.25, 128.51, 128.18, 128.13, 127.36, 79.36, 77.45, 77.13, 76.81, 71.23, 67.04, 55.47, 54.66, 52.42, 38.75, 38.73, 31.19, 24.75, 18.82, 17.59, 16.48, 15.75, 11.12.

Notebook Entries

Procedure: PKD-277

^{1}H: PKD-277-400, ^{13}C: PKD-277-C13-400N

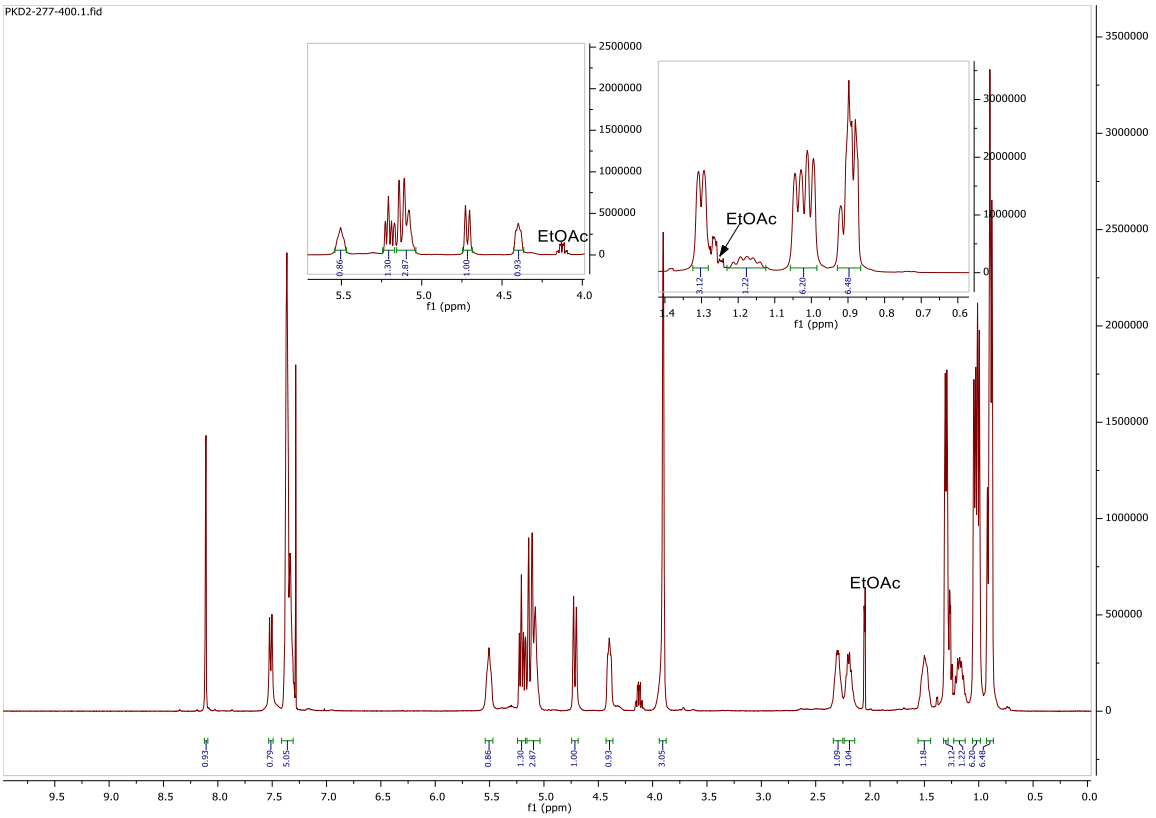
PKD2-277-400.1.fid
EtOAc
EtOAc
EtOAc
f1 (ppm)

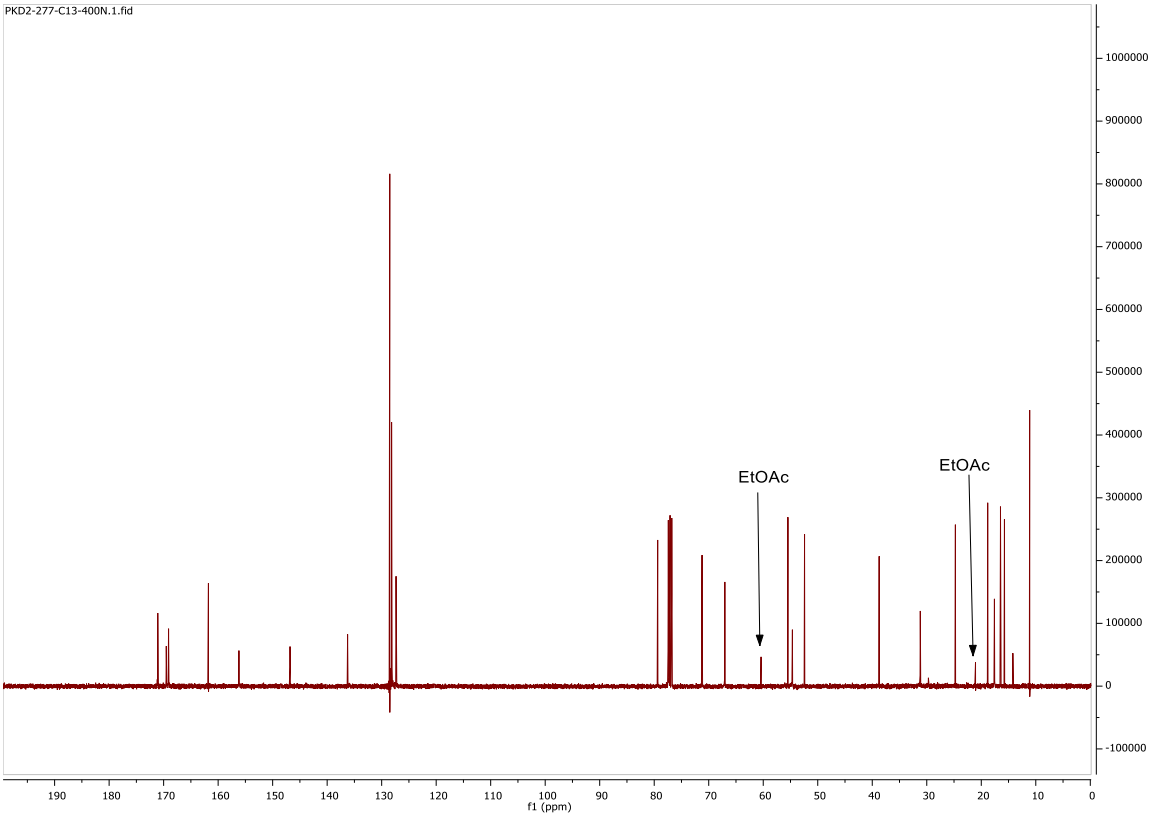
PKD2-277-C13-400N.1.fid
EtOAc
EtOAc
f1 (ppm)

(*tert*-butoxycarbonyl)-*L*-allothreonine

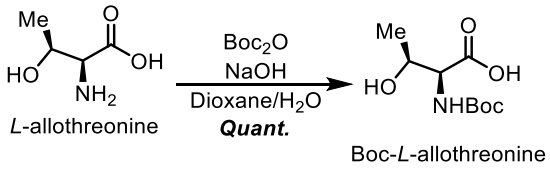

The reaction was performed using standard Boc protection protocol to access Boc-L-threonine as colorless oily product quantitatively. R_f = 0.0 (3:1 ethyl acetate/hexanes): (Product retains on the baseline due to free carboxylic acid)

^{1}H NMR (400 MHz, Methanol-d_4) δ 4.13 (d, *J* = 5.3 Hz, 1H), 4.06 (p, *J* = 7.1, 6.7 Hz, 1H), 1.47 (d, *J* = 2.7 Hz, 10H), 1.22 (d, *J* = 6.4 Hz, 3H).

Notebook Entries

Procedure: PKD2-281

^{1}H: PKD2-281-1-MeOH-400N

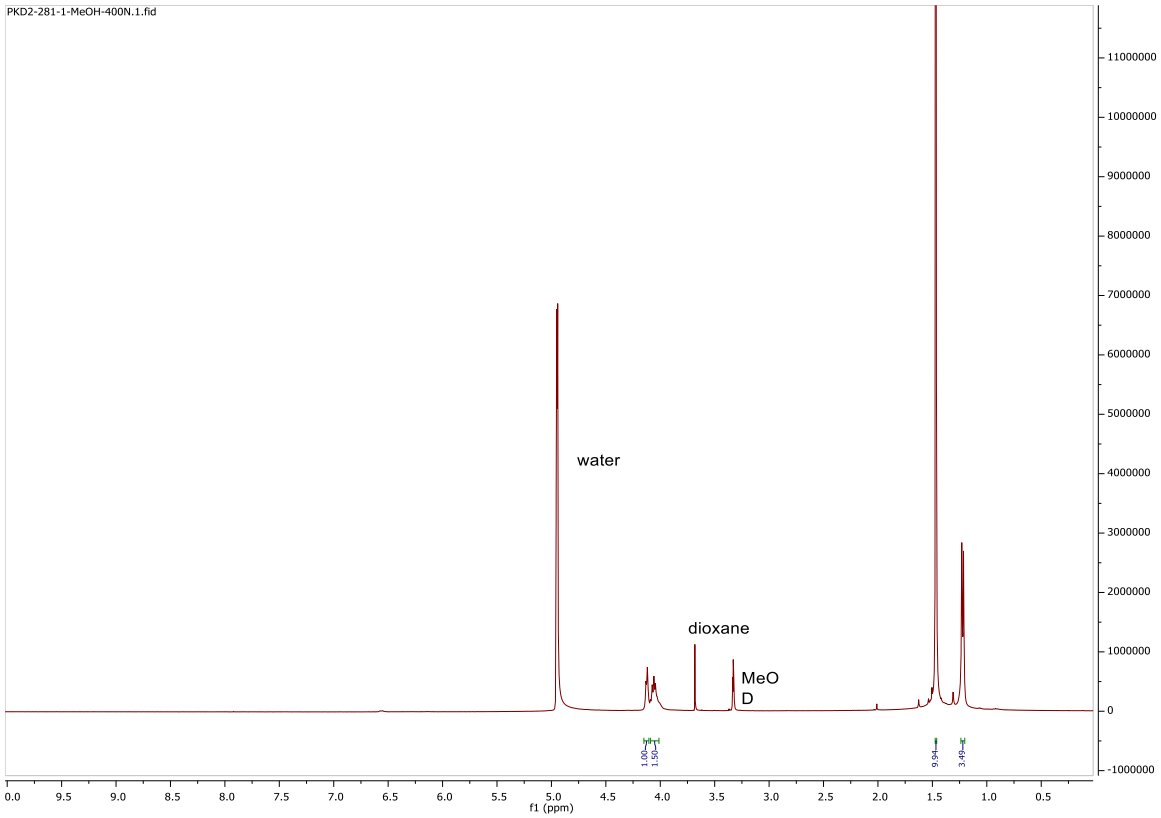

Methyl 2-((1R,2S)-1-((2S,3S)-2-((*tert*-butoxycarbonyl)amino)-3-hydroxybutanamido)-2-methylbutyl)thiazole-4-carboxylate

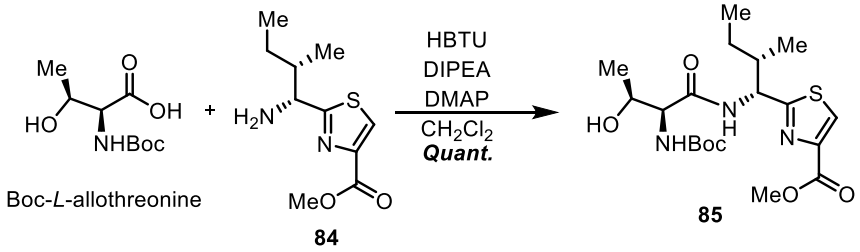

Reaction was performed using standard HBTU peptide coupling conditions. The product was afforded in quantitative yields with purification by flash column chromatography with 3:1 ethyl acetate/hexane. R_f = 0.75 (3:1 ethyl acetate/ hexane).

Note: In small scale reactions (<100 mg) reaction was not quenched and extracted. Instead the reactions were concentrated and directly purified through column chromatography. In large scale reactions, standard protocol was followed.

^{1}H NMR (400 MHz, Chloroform-*d*) δ 8.11 (s, 1H), 7.21 (d, *J* = 9.0 Hz, 1H), 5.66 (d, *J* = 7.2 Hz, 1H), 5.41 (dd, *J* = 9.3, 4.5 Hz, 1H), 4.15 – 4.07 (m, 1H), 4.06 – 3.96 (m, 2H), 3.93 (s, 3H), 2.28 – 2.21 (m, 1H), 1.51 – 1.47 (m, 1H), 1.44 (s, 9H), 1.31 (d, *J* = 5.9 Hz, 3H), 1.28 – 1.24 (m, 1H), 0.96 (t, *J* = 7.4 Hz, 3H), 0.85 (d, *J* = 6.9 Hz, 3H).

^{13}C NMR (101 MHz, Chloroform-*d*) δ 173.20, 171.27, 161.62, 156.06, 146.61, 127.40, 80.45, 68.76, 59.18, 54.89, 52.43, 39.48, 28.28, 26.69, 19.76, 13.96, 11.58.

Notebook Entries

Procedure: PKD2-294

^{1}H: PKD2-294-pure-400N, ^{13}C: PKD2-294-pure-C13-400N

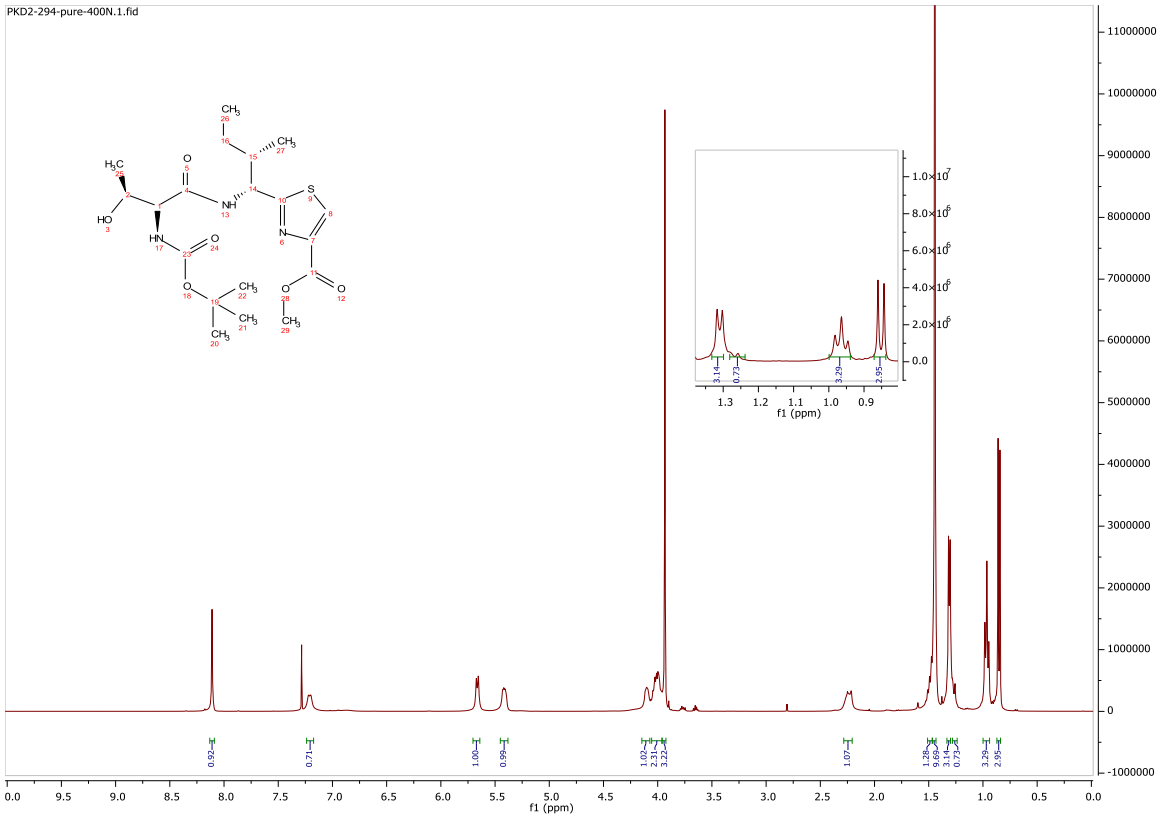
PKD2-294-pure-400N.1.fid
f1 (ppm)

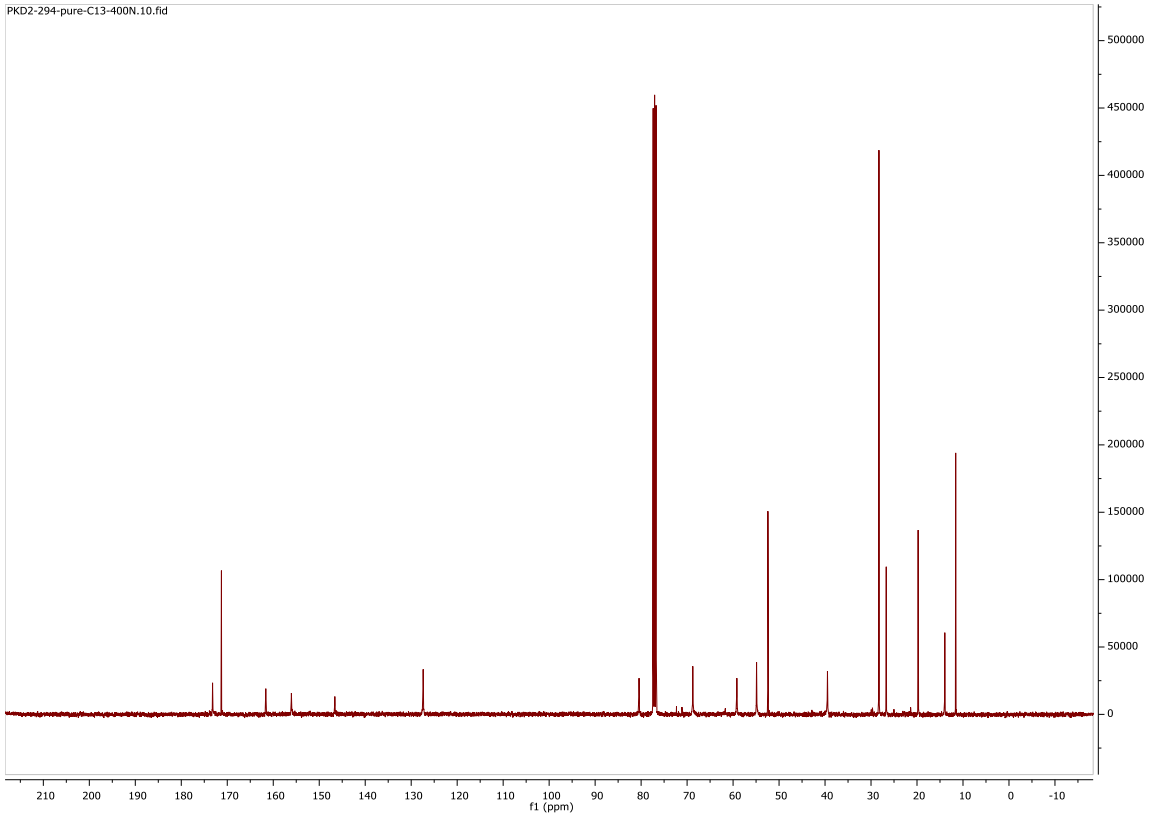
PKD2-294-pure-C13-400N.10.fid
f1 (ppm)

Methyl 2-((1R,2S)-1-((2S,3S)-2-amino-3-hydroxybutanamido)-2-methylbutyl)thiazole-4-carboxylate

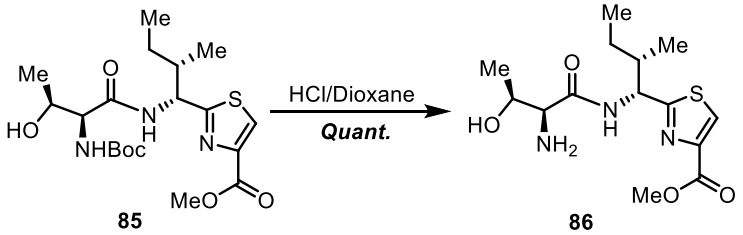

85 86

The reaction was carried out using standard Boc deprotection protocol to obtain **86** in quantitative yields. R_f = 0.0 (3:1 ethyl acetate/hexanes): (Deprotected material retain in the baseline)

^{1}H NMR (400 MHz, Methanol-d_4) δ 5.34 (d, *J* = 4.5 Hz, 1H), 4.28 (s, 1H), 4.09 (s, 1H), 3.92 (s, 3H), 2.20 (d, *J* = 11.9 Hz, 1H), 1.39 (d, *J* = 18.4 Hz, 2H), 1.29 – 1.20 (m, 4H), 0.96 (d, *J* = 5.6 Hz, 6H).

Notebook Entries

Procedure: PKD2-160

^{1}H: PKD2-291-crude-MeOH-400N (Crude NMR)

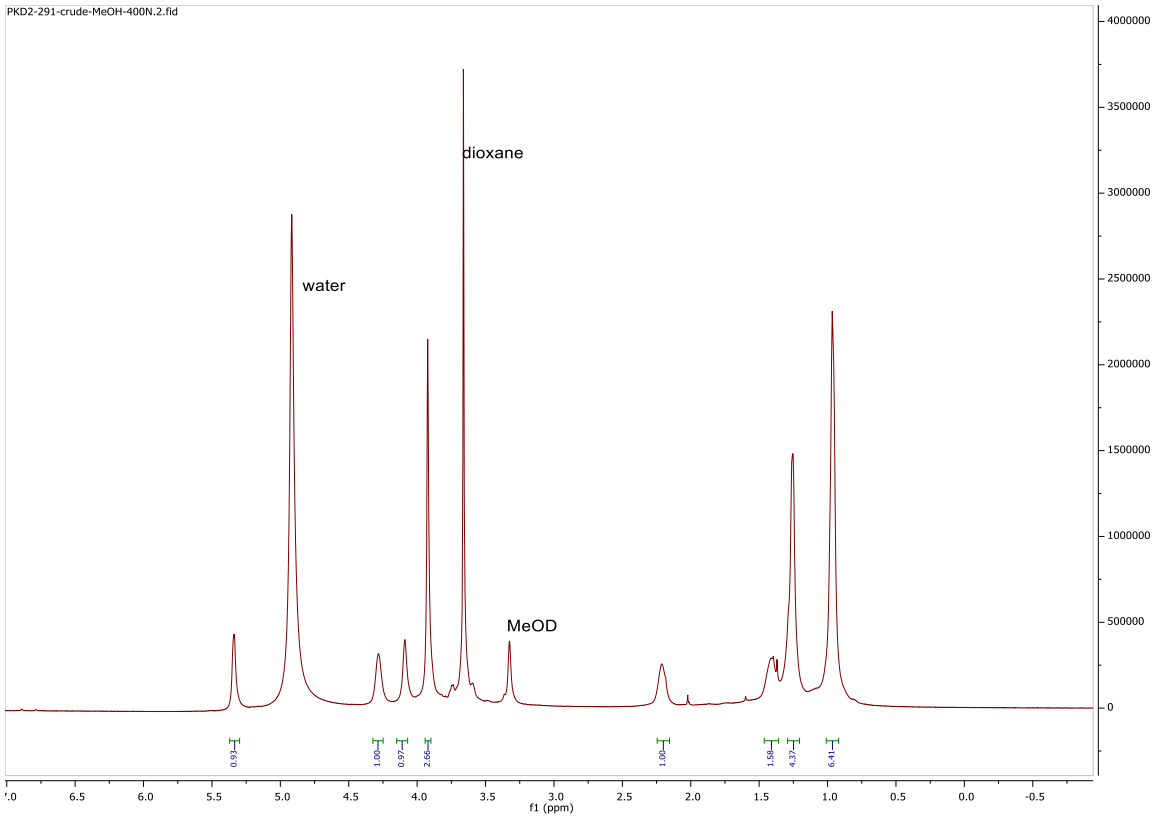
PKD2-291-crude-MeOH-400N.2.fid
dioxane
water
MeOD
4000000
3500000
3000000
2500000
2000000
1500000
1000000
500000
0
0.93
1.00
0.97
2.66
1.00
1.58
4.37
6.41
6.5
6.0
5.5
5.0
4.5
4.0
3.5
3.0
2.5
2.0
1.5
1.0
0.5
0.0
-0.5
f1 (ppm)

Methyl 2-((5S,8S,11R,12S)-8-((S)-1-hydroxyethyl)-5-isopropyl-12-methyl-3,6,9-trioxo-1-phenyl-2-oxa-4,7,10-triazatetradecan-11-yl)thiazole-4-carboxylate

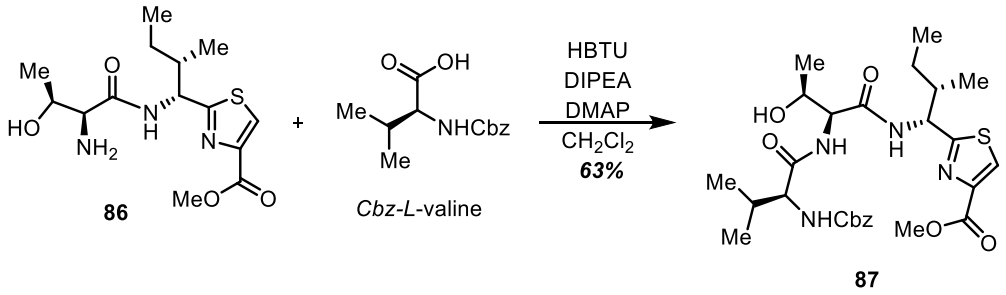

Reaction was performed using standard HBTU peptide coupling conditions. The product was afforded in 63% yield with purification by flash column chromatography with 3:1 ethyl acetate/hexane. R_f = 0. 5 (3:1 ethyl acetate/ hexane).

Note: In large scale reactions (>100 mg or depending on solubility) reaction had to be adsorbed to silica to dry load into columns for chromatography.

^{1}H NMR (400 MHz, Chloroform-*d*) δ 8.10 (s, 1H), 7.40 – 7.32 (m, 5H), 7.24 (d, *J* = 8.5 Hz, 1H), 5.42 (dd, *J* = 8.9, 4.7 Hz, 2H), 5.11 (t, *J* = 10.1 Hz, 2H), 4.44 (dd, *J* = 7.5, 4.5 Hz, 1H), 4.15 – 4.09 (m, 1H), 4.06 – 4.00 (m, 1H), 3.94 (s, 3H), 2.83 (s, 1H), 2.26 – 2.17 (m, 2H), 1.53 – 1.43 (m, 1H), 1.31 – 1.25 (m, 4H), 1.00 – 0.95 (m, 6H), 0.90 (dd, *J* = 12.4, 6.9 Hz, 6H).

^{13}C NMR (101 MHz, Chloroform-*d*) δ 172.50, 170.84, 162.03, 156.85, 146.46, 136.24, 128.79, 128.48, 128.28, 127.82, 68.87, 67.46, 60.76, 58.27, 55.45, 52.72, 39.96, 30.96, 26.80, 19.87, 19.51, 17.82, 14.29, 11.78.

Notebook Entries

Procedure: PKD2-293

^{1}H: PKD2-349-NMR-400N, ^{13}C: PKD2-162-C13-400

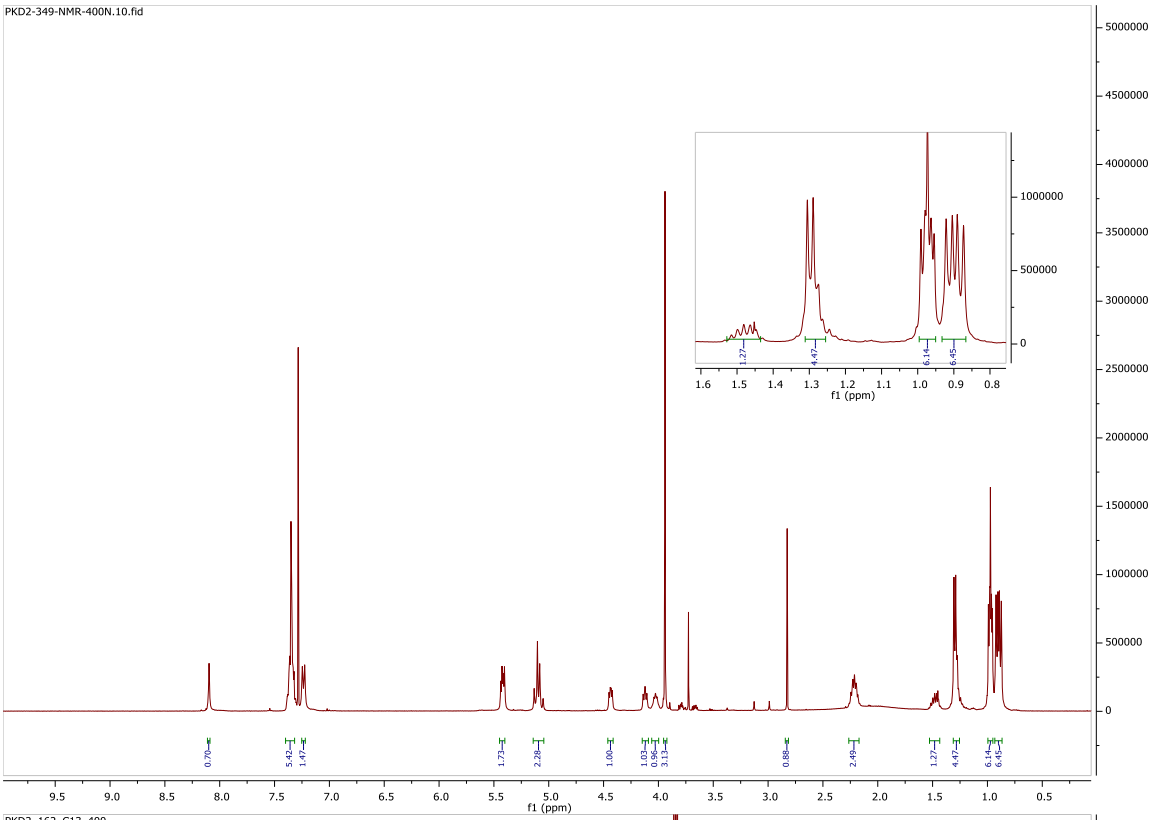
PKD2-349-NMR-400N.10.fid
f1 (ppm)

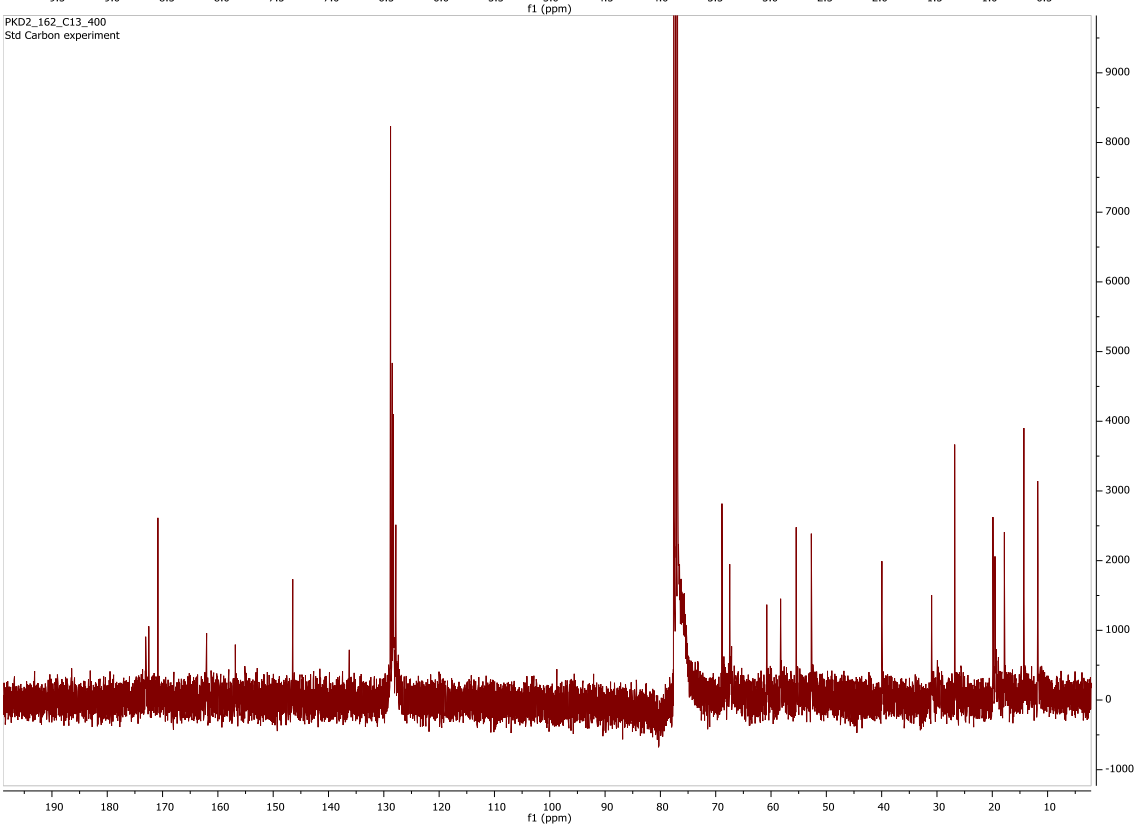
PKD2_162_C13_400
Std Carbon experiment
f1 (ppm)

Methyl 2-((1R,2S)-1-((4S,5R)-2-((S)-1-(((benzyloxy)carbonyl)amino)-2-methylpropyl)-5-methyl-4,5-dihydrooxazole-4-carboxamido)-2-methylbutyl)thiazole-4-carboxylate

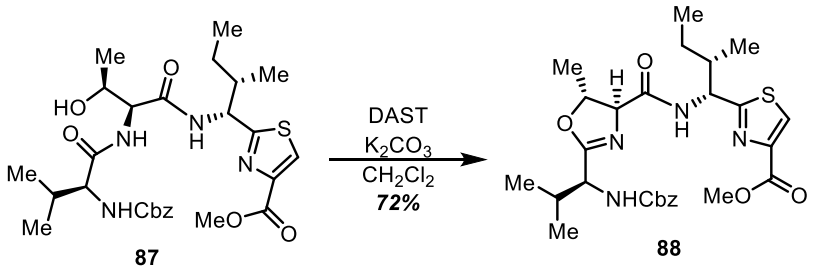

The reaction was performed under standard DAST conditions to access **88**. Product was purified by flash column chromatography with 1:3 hexanes/ ethyl acetate to afford the white solid product in 72% yield. R_f = 0.65 (1:3 hexanes/ethyl acetate)

^{1}H NMR (400 MHz, Chloroform-*d*) δ 8.02 (s, 1H), 7.38 (d, *J* = 4.9 Hz, 5H), 7.26 (s, 1H), 5.43 (d, *J* = 8.9 Hz, 1H), 5.37 (dd, *J* = 9.1, 5.0 Hz, 1H), 5.17 – 5.05 (m, 3H), 4.78 (q, *J* = 6.5 Hz, 1H), 4.42 (dd, *J* = 9.0, 5.4 Hz, 1H), 4.28 – 4.23 (m, 1H), 3.93 (s, 3H), 2.34 (dd, *J* = 9.6, 4.5 Hz, 1H), 2.16 – 2.10 (m, 1H), 1.53 – 1.43 (m, 5H), 1.33 – 1.24 (m, 3H), 0.97 (t, *J* = 3.4 Hz, 6H), 0.90 (d, *J* = 6.8 Hz, 6H).

^{13}C NMR (101 MHz, Chloroform-*d*) δ 172.78, 171.35, 169.07, 161.72, 156.06, 136.22, 128.57, 128.26, 128.12, 127.02, 80.74, 74.40, 67.06, 54.90, 54.83, 52.41, 39.46, 31.34, 29.72, 26.58, 21.82, 18.82, 17.65, 14.09, 11.57.

Notebook Entries

Procedure: PKD2-297

^{1}H: PKD2-297-2nd-400N, ^{13}C: PKD2-297-2nd-C13-400N

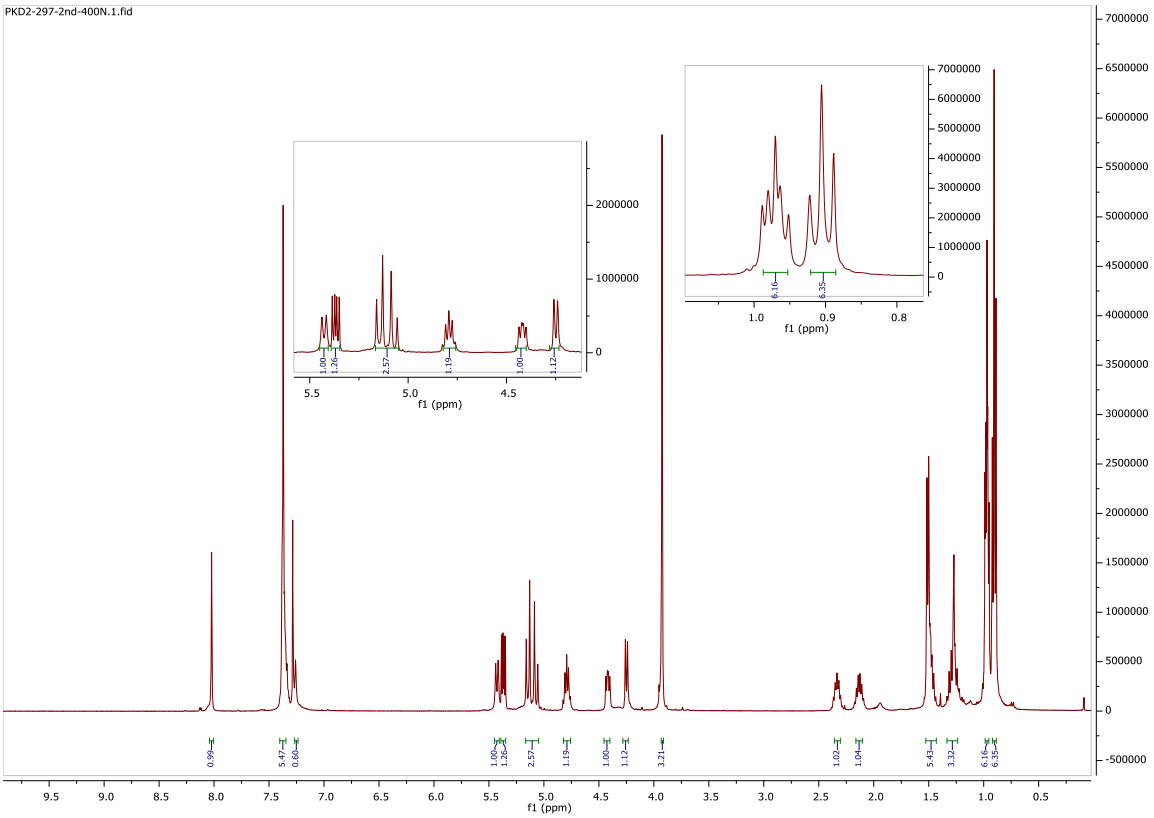
PKD2-297-2nd-400N.1.fid
f1 (ppm)

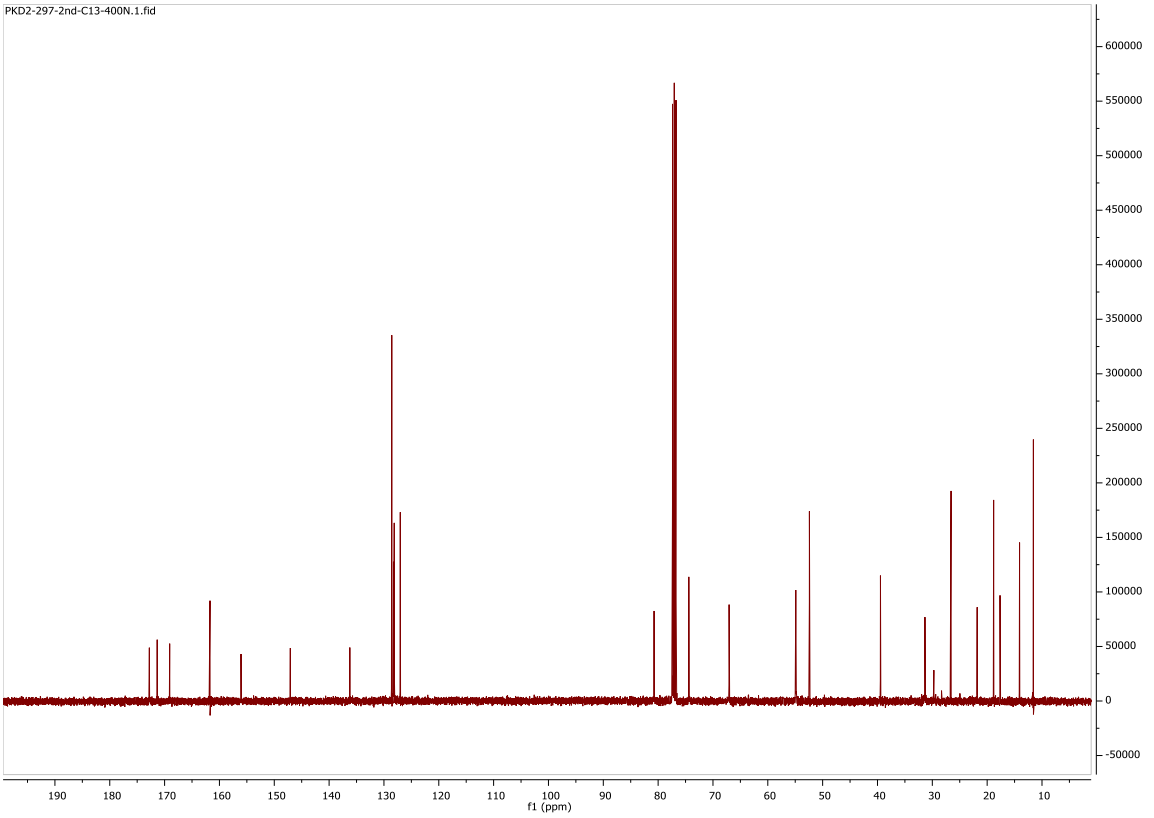
PKD2-297-2nd-C13-400N.1.fid
f1 (ppm)

Methyl (4S,5S)-2-((S)-1-amino-2-methylpropyl)-5-methyl-4,5-dihydrooxazole-4-carboxylate

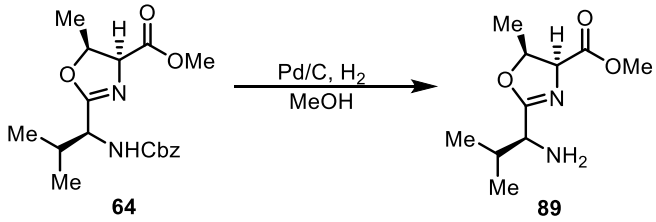

In a flask the dipeptide was dissolved in methanol and 10% w/w of Pd on carbon was added. Hydrogen gas was bubbled into the reaction mixture and was stirred 30 minutes at room temperature. Resultant mixture was filtered with celite and concentrated under reduced pressure to yield free amine in quantitative yield. R_f = 0.0 (3:1 ethyl acetate/hexanes): (Deprotected material retain in the baseline)

^{1}H NMR (400 MHz, Chloroform-*d*) δ 8.26 (d, *J* = 7.1 Hz, 1H), 4.73 (dd, *J* = 7.1, 3.5 Hz, 1H), 4.26 (qd, *J* = 6.4, 3.5 Hz, 1H), 3.81 (s, 3H), 3.38 (d, *J* = 4.1 Hz, 1H), 2.33 (pd, *J* = 6.8, 3.8 Hz, 1H), 1.17 (d, *J* = 6.4 Hz, 3H), 1.11 – 0.98 (m, 3H), 0.96 – 0.83 (m, 3H).

Notebook Entries

Procedure: PKD2-311

^{1}H: PKD2-311-crude-400N (Crude NMR)

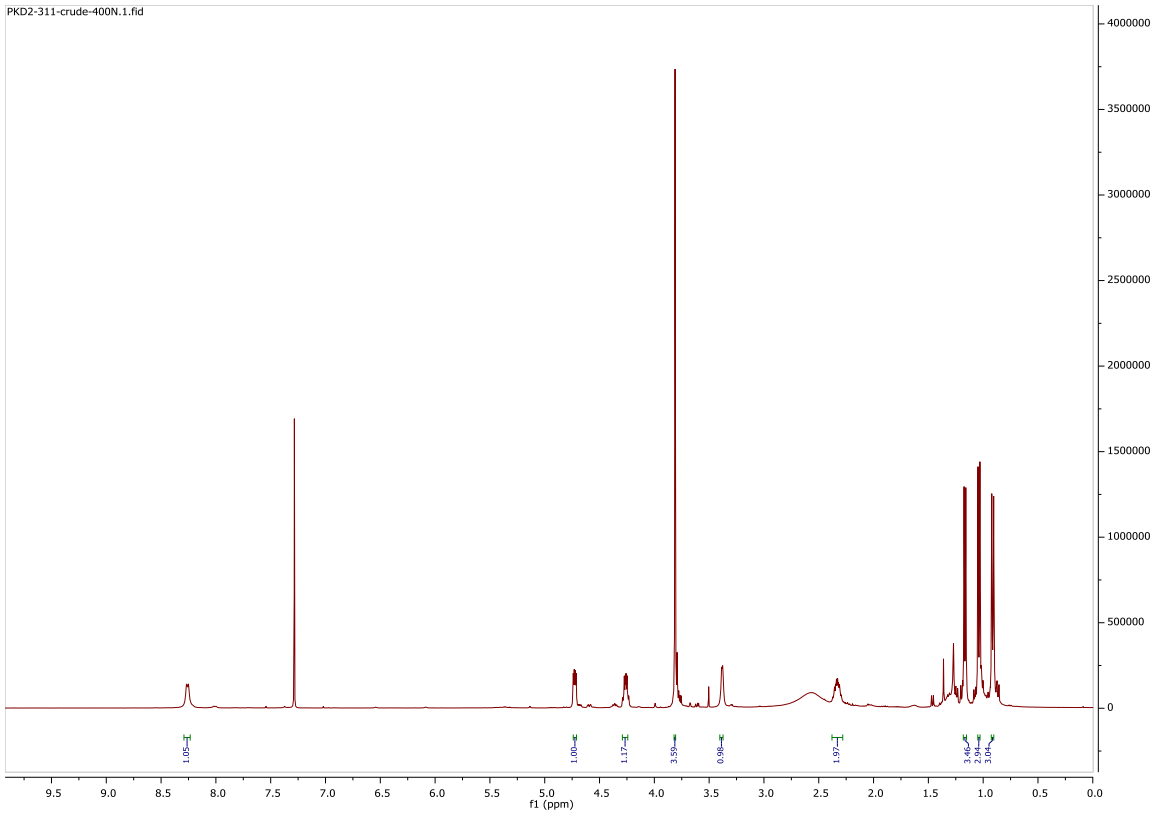
PKD2-311-crude-400N.1.fid
4000000
3500000
3000000
2500000
2000000
1500000
1000000
500000
0
1.05
1.00
1.17
3.59
0.98
1.97
3.46
2.94
2.04
9.5
9.0
8.5
8.0
7.5
7.0
6.5
6.0
5.5
5.0
4.5
4.0
3.5
3.0
2.5
2.0
1.5
1.0
0.5
0.0
f1 (ppm)

Methyl 2-((1R,2S)-1-((4S,5R)-2-((S)-1-amino-2-methylpropyl)-5-methyl-4,5-dihydrooxazole-4-carboxamido)-2-methylbutyl)thiazole-4-carboxylate

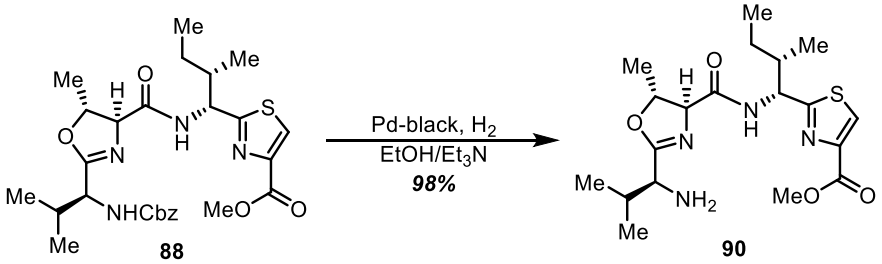

In a flask **88** was dissolved in enough solvent to bubble hydrogen gas. Palladium-black (10 eq.) was added and the system was sealed. Hydrogen gas was bubbled with a venting needle for ~10 minutes. The extra venting needle was removed, and reaction was vigorously stirred for 30 minutes. Palladium was filtered using celite and the filtrate was concentrated under reduced pressure to yield **90** with 98% yield. R_f = 0.0 (3:1 ethyl acetate/hexanes): (Deprotected material retain in the baseline)

^{1}H NMR (400 MHz, Acetone-d_6) δ 8.34 (s, 1H), 7.47 (d, J = 9.1 Hz, 1H), 5.36 – 5.31 (m, 1H), 4.72 – 4.61 (m, 1H), 4.29 – 4.21 (m, 1H), 3.88 (s, 3H), 2.31 – 2.17 (m, 2H), 1.53 – 1.46 (m, 1H), 1.42 (d, J = 6.3 Hz, 3H), 1.33 – 1.27 (m, 2H), 1.00 – 0.87 (m, 16H).

Notebook Entries

Procedure: PKD2-348

^{1}H: PKD2-348acetone-crude-400N

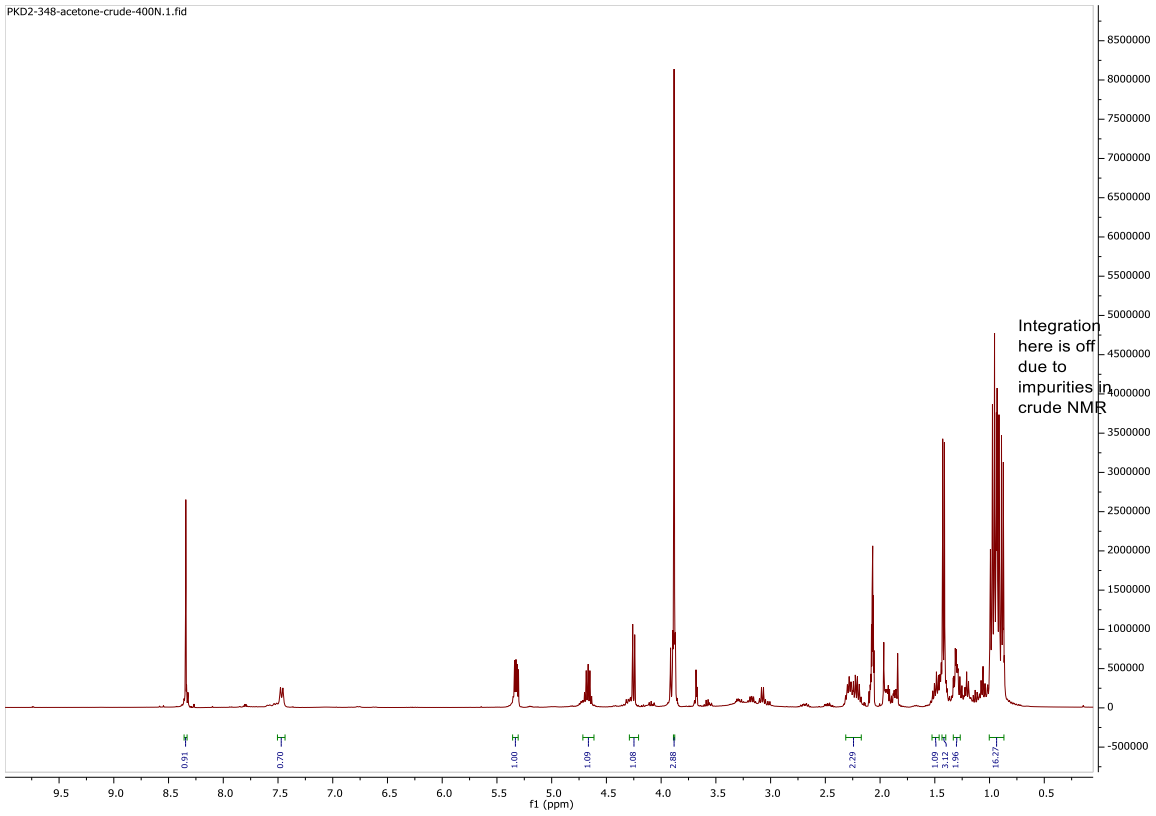
PKD2-348-acetone-crude-400N.1.fid
Integration here is off due to impurities in crude NMR
f1 (ppm)

((Benzyloxy)carbonyl)-*D*-alanyl-*L*-threonine

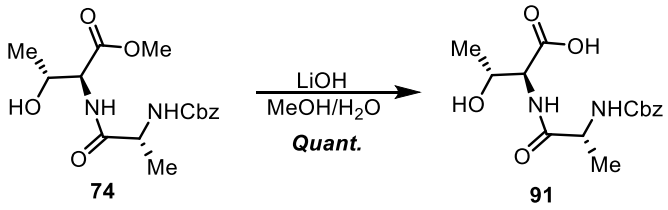

The reaction was performed using saponification conditions. THF was substituted with methanol. The product **91** was obtained quantitatively. R_f = 0.0 (3:1 ethyl acetate/hexanes): (Deprotected material retain in the baseline)

^{1}H NMR (400 MHz, Acetone-d_6) δ 7.41 – 7.30 (m, 5H), 6.69 (d, *J* = 7.5 Hz, 1H), 5.11 (s, 2H), 4.49 (dd, *J* = 8.9, 2.7 Hz, 1H), 4.42 – 4.33 (m, 2H), 1.42 (d, *J* = 7.1 Hz, 3H), 1.31 (s, 1H), 1.20 – 1.15 (m, 3H).

Notebook Entries

Procedure: PKD2-339

^{1}H: PKD2-339-acetone-400N (crude NMR)

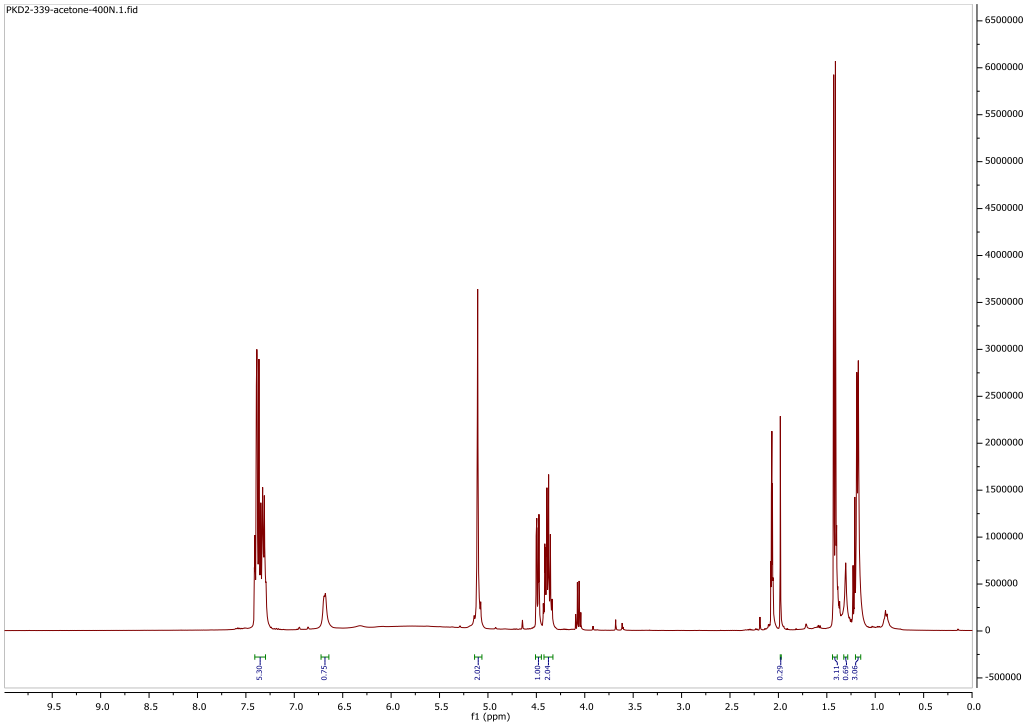

Methyl 2-((1R,2S)-1-((4S,5R)-2-((5R,8S,11S)-8-((R)-1-hydroxyethyl)-5,12-dimethyl-3,6,9-trioxo-1-phenyl-2-oxa-4,7,10-triazatridecan-11-yl)-5-methyl-4,5-dihydrooxazole-4-carboxamido)-2-methylbutyl)thiazole-4-carboxylate

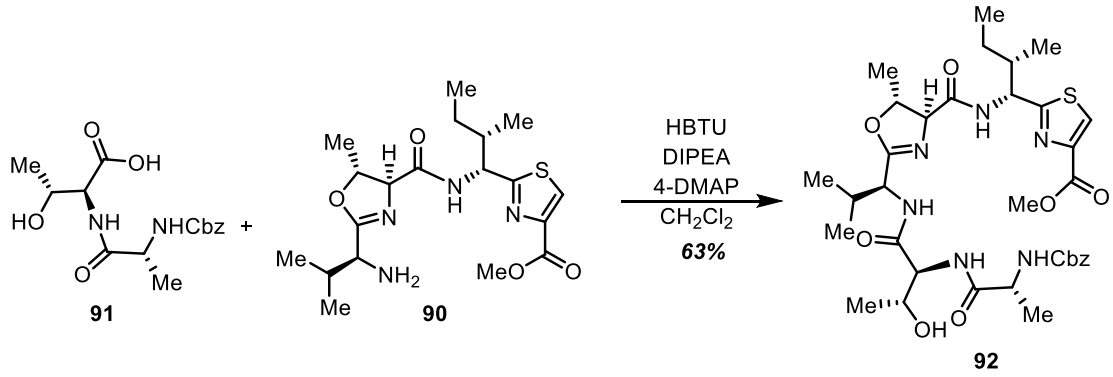

91 90 92

Reaction was performed using standard HBTU peptide coupling conditions. The product was afforded in 63% yield with purification by flash column chromatography with 5% methanol in DCM. R_f = 0. 3 (5% methanol in DCM).

^{13}C NMR (101 MHz, Chloroform-*d*) δ 172.85, 171.00, 161.93, 128.55, 128.15, 127.92, 127.12, 81.16, 73.35, 67.53, 67.05, 57.34, 54.74, 53.12, 52.81, 50.91, 41.72, 38.63, 29.38, 26.35, 21.67, 19.08, 18.01, 16.70, 13.82, 11.77.

Notebook Entries

Procedure: PKD2-380

^{1}H: PKD2-380-400N (Some inseparable impurities in the sample, one spot on TLC: urea biproduct from HBTU reaction and impurities according to integration values. However, all the peaks suggest the presence of the desired product being formed)

^{13}C: PKD2-380-C13-400N

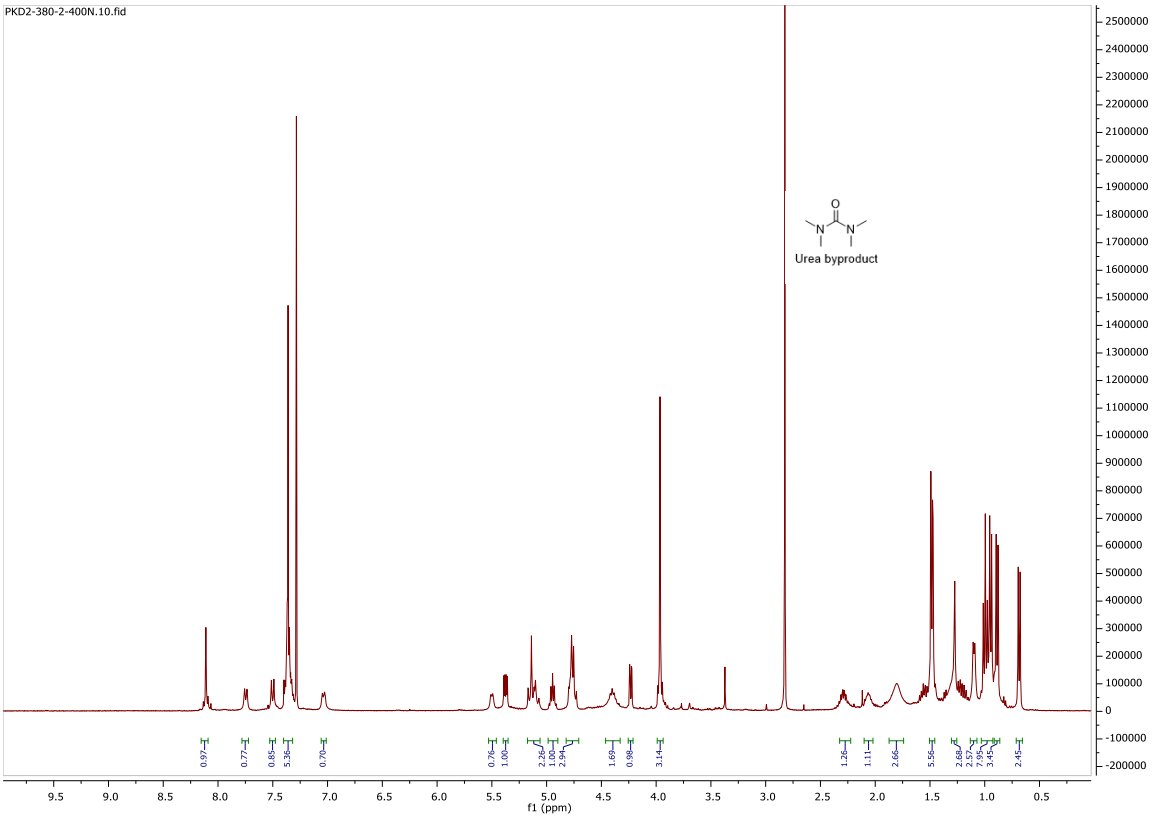
PKD2-380-2-400N.10.fid
Urea byproduct
0.97
0.77
0.85
5.36
0.70
0.76
1.00
2.26
1.06
2.94
1.69
0.98
3.14
1.26
1.11
2.66
5.56
2.68
2.57
7.95
3.45
2.45
f1 (ppm)

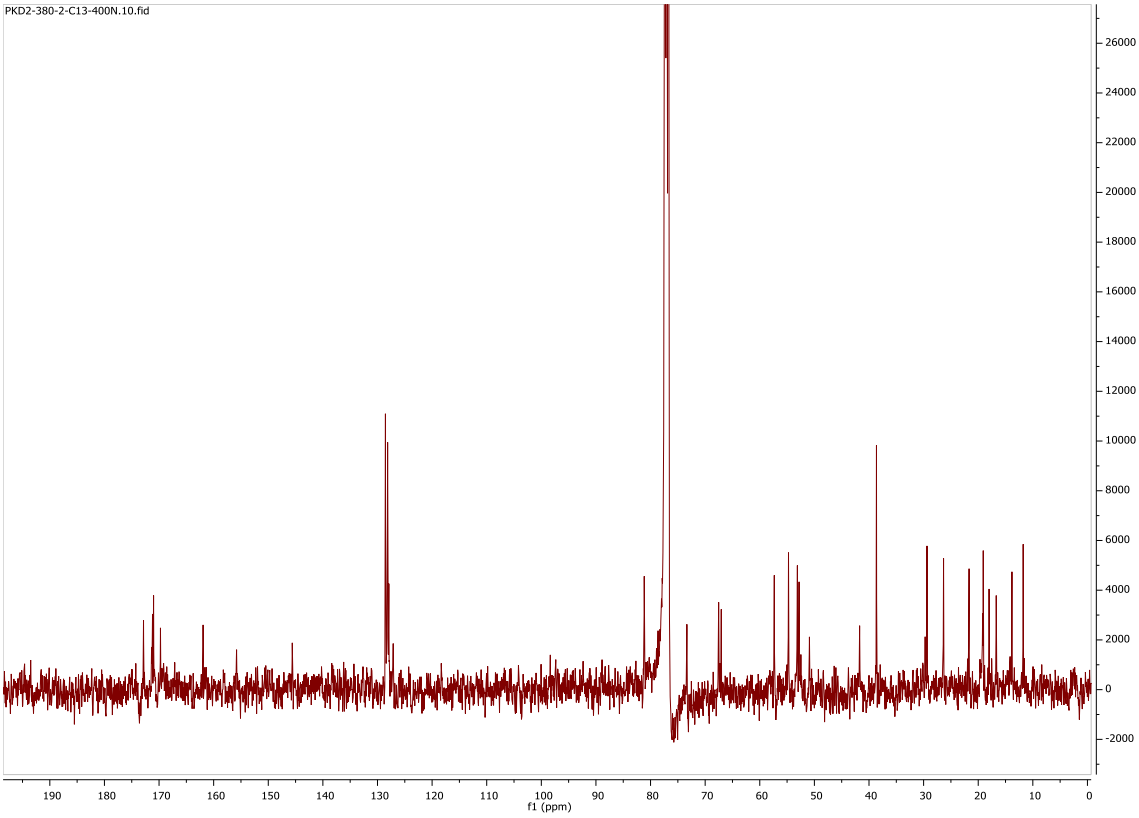
PKD2-380-2-C13-400N.10.fid
f1 (ppm)

2-((1R,2S)-1-((4S,5R)-2-((5R,8S,11S)-8-((R)-1-hydroxyethyl)-5,12-dimethyl-3,6,9-trioxo-1-phenyl-2-oxa-4,7,10-triazatridecan-11-yl)-5-methyl-4,5-dihydrooxazole-4-carboxamido)-2-methylbutyl)thiazole-4-carboxylic acid

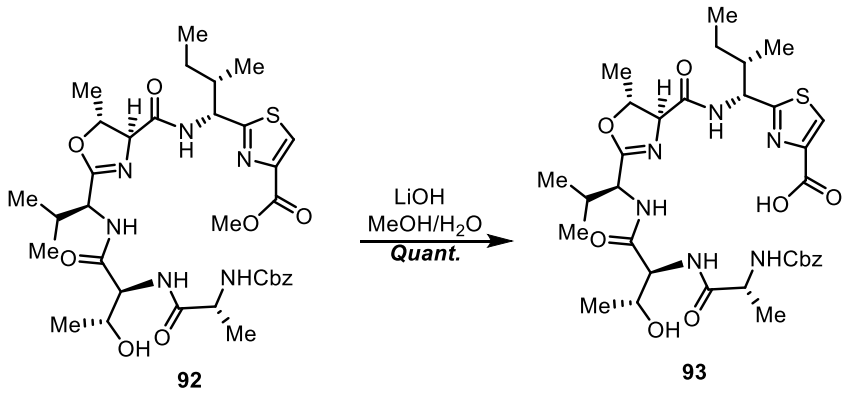

92 93

The reaction was performed using saponification conditions. THF was substituted with methanol. The product **93** was obtained quantitatively. R_f = 0.0 (3:1 ethyl acetate/hexanes): (Deprotected material retain in the baseline)

^{1}H NMR (400 MHz, Methanol-d_4) δ 8.35 (d, J = 2.1 Hz, 1H), 7.41 – 7.24 (m, 5H), 5.39 (t, J = 6.0 Hz, 1H), 5.32 (d, J = 5.8 Hz, 1H), 5.12 (q, J = 8.2, 6.8 Hz, 1H), 4.39 – 4.29 (m, 2H), 4.26 – 4.14 (m, 4H), 2.28 – 2.11 (m, 3H), 1.48 – 1.21 (m, 20H), 1.08 – 0.95 (m, 14H). (As this is a crude NMR integration values are not perfect. However, it can be seen that the reaction was successful and saponification took place as the methyl ester peak is absent in this NMR)

Notebook Entries

Procedure: PKD2-388

^{1}H: PKD2-388-crude-MeOH-400N (crude NMR)

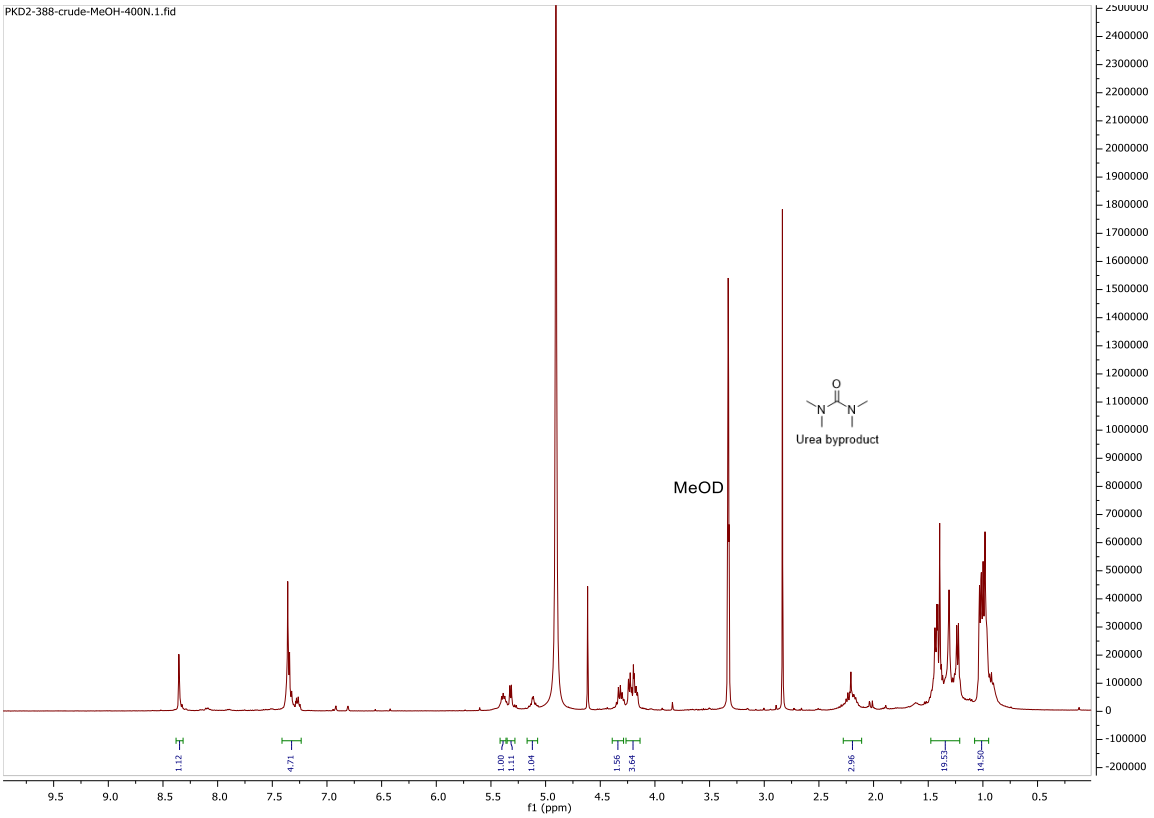
PKD2-388-crude-MeOH-400N.1.fid
MeOD
Urea byproduct
1.12
4.71
1.00
1.11
1.04
1.56
3.64
2.96
19.53
14.50
f1 (ppm)

2-((1R,2S)-1-((4S,5R)-2-((S)-1-((2S,3R)-2-((R)-2-aminopropanamido)-3-hydroxybutanamido)-2-methylpropyl)-5-methyl-4,5-dihydrooxazole-4-carboxamido)-2-methylbutyl)thiazole-4-carboxylic acid

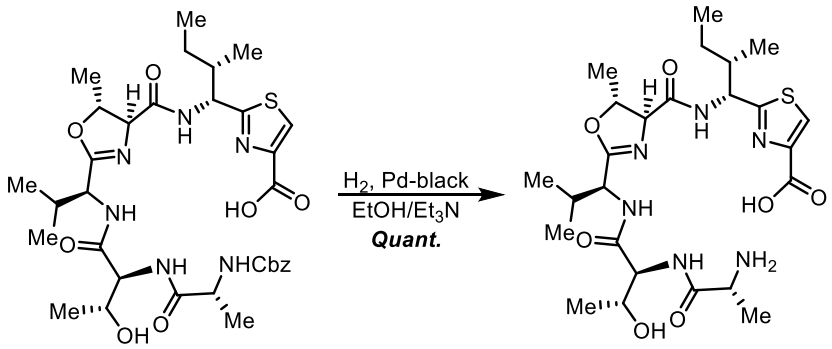

93 **94**

In a flask **93** was dissolved in enough solvent (2:1 EtOH/Et_3N) to bubble hydrogen gas. Palladium-black (10 eq.) was added and the system was sealed. Hydrogen gas was bubbled with a venting needle for ~10 minutes. The extra venting needle was removed, and reaction was vigorously stirred for 30 minutes. Palladium was filtered using celite and the filtrate was concentrated under reduced pressure to yield **94** quantitatively. R_f = 0.0 (3:1 ethyl acetate/hexanes): (Deprotected material retain in the baseline)

Notebook Entries

Procedure: PKD2-352

Crude directly subjected to cyclization

2-((1R,2S)-1-((4S,5R)-2-((S)-1-(((benzyloxy)carbonyl)amino)-2-methylpropyl)-5-methyl-4,5-dihydrooxazole-4-carboxamido)-2-methylbutyl)thiazole-4-carboxylic acid

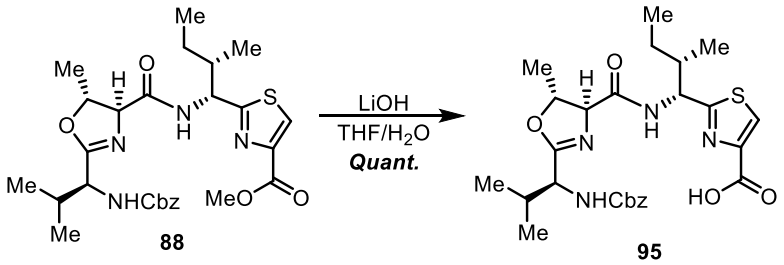

The reaction was performed using standard saponification conditions. The product **95** was obtained quantitatively. R_f = 0.0 (3:1 ethyl acetate/hexanes): (Deprotected material retain in the baseline)

Notebook Entries

Procedure: PKD2-330

^{1}H: PKD2-330-crude1-acetone-400N

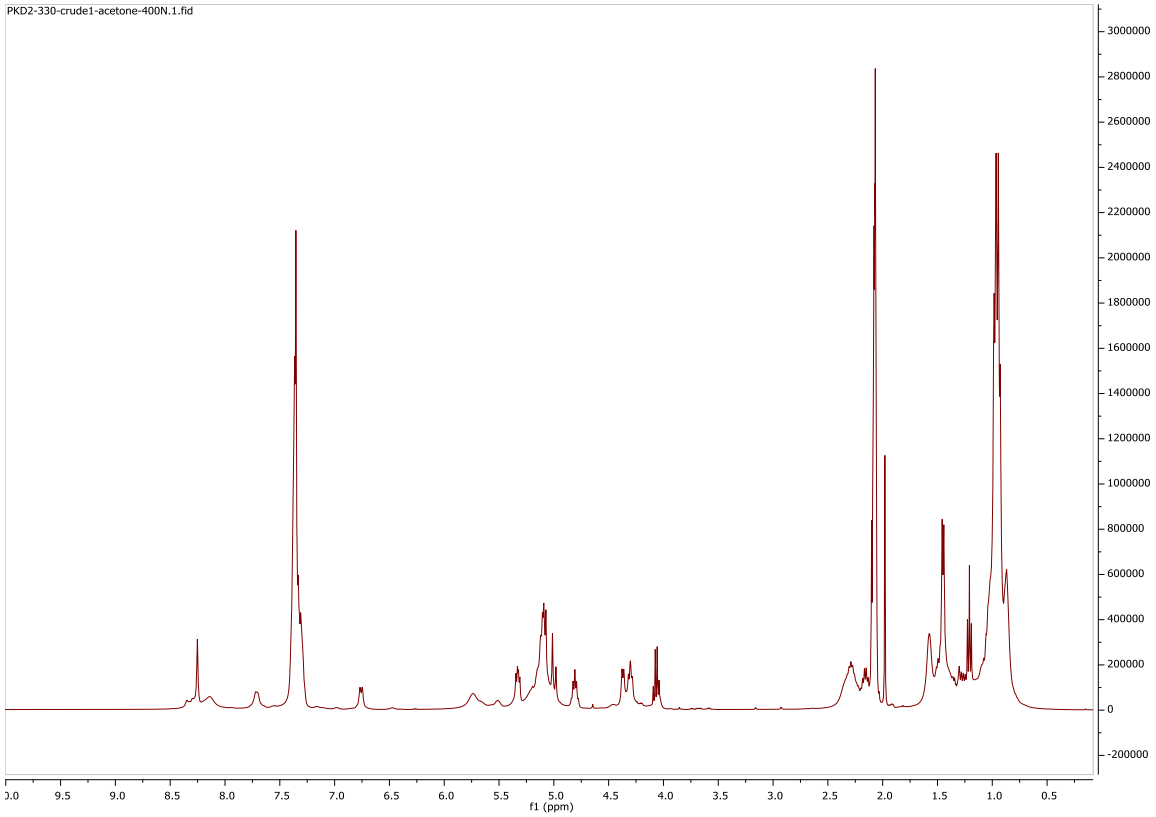

Methyl D-alanyl-L-threoninate

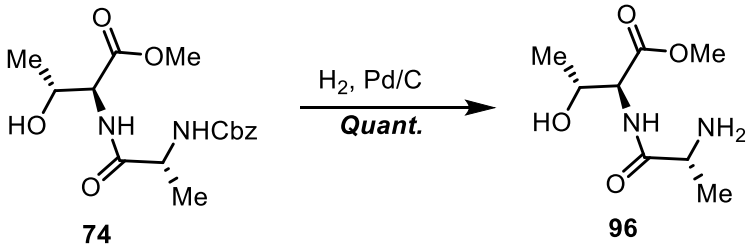

In a flask 100 mg of the dipeptide was dissolved in methanol and 10 mg of Pd on carbon was added. Hydrogen gas was bubbled into the reaction mixture and was stirred overnight at room temperature. Resultant mixture was filtered with celite and concentrated under reduced pressure to yield free amine in quantitative yield. Rf = 0.0 (3:1 ethyl acetate/hexanes): (Deprotected material retain in the baseline)

Notebook Entries

Procedure: PKD2-198

^{1}H: PKD2-198-400 (crude NMR)

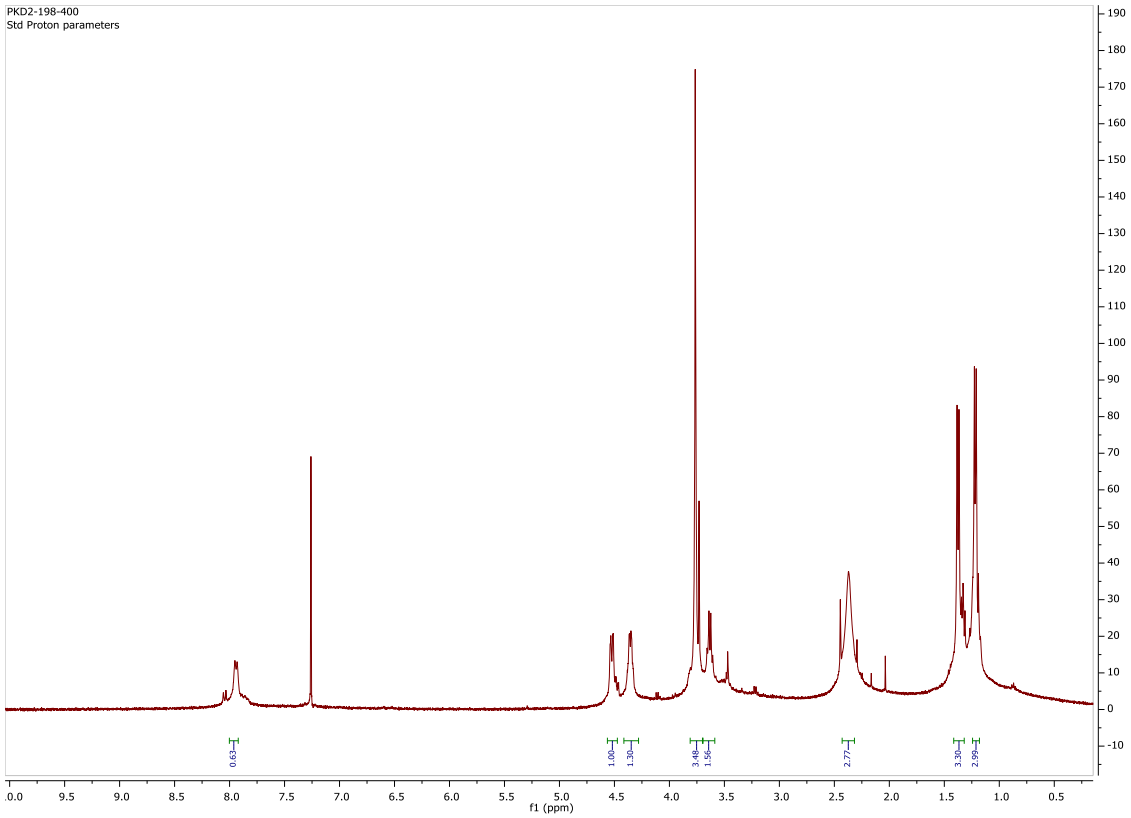
PKD2-198-400
Std Proton parameters
0.63
1.00
1.30
3.48
1.56
2.77
3.30
2.99
f1 (ppm)

Methyl (2-((1R,2S)-1-((4S,5R)-2-((S)-1-(((benzyloxy)carbonyl)amino)-2-methylpropyl)-5-methyl-4,5-dihydrooxazole-4-carboxamido)-2-methylbutyl)thiazole-4-carbonyl)-*D*-alaninate

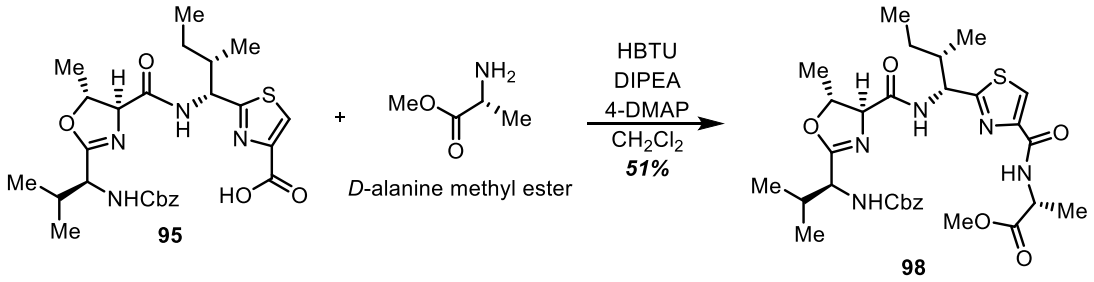

Reaction was performed using standard HBTU peptide coupling conditions. The product was afforded in 51% yield with purification by flash column chromatography with 3:1 ethyl acetate/hexanes. R_f = 0. 7 (3:1 ethyl acetate/hexanes).

^{1}H NMR (400 MHz, Chloroform-*d*) δ 7.97 (s, 1H), 7.36 (d, *J* = 3.2 Hz, 5H), 5.31 (dd, *J* = 9.0, 5.2 Hz, 1H), 5.21 – 4.97 (m, 2H), 4.78 (p, *J* = 7.4 Hz, 2H), 4.41 – 4.36 (m, 1H), 4.33 – 4.25 (m, 1H), 3.86 – 3.74 (m, 1H), 3.71 (s, 2H), 2.23 – 2.15 (m, 1H), 2.10 (h, *J* = 6.7, 6.3 Hz, 1H), 1.80 (s, 1H), 1.52 (t, *J* = 7.0 Hz, 6H), 1.48 – 1.39 (m, 1H), 1.26 (tt, *J* = 14.2, 7.6 Hz, 1H), 1.00 – 0.96 (m, 6H), 0.93 (d, *J* = 6.9 Hz, 3H), 0.86 (d, *J* = 6.9 Hz, 3H).

^{13}C NMR (151 MHz, Chloroform-*d*) δ 173.58, 160.34, 156.24, 149.54, 136.14, 128.57, 128.32, 128.30, 123.04, 67.17, 55.09, 54.80, 52.56, 47.87, 39.89, 31.06, 26.29, 21.74, 18.77, 18.40, 17.65, 14.53, 11.58.

Notebook Entries

Procedure: PKD3-012

^{1}H: PKD3-012-400N, ^{13}C: PKD3-012-C13-400N

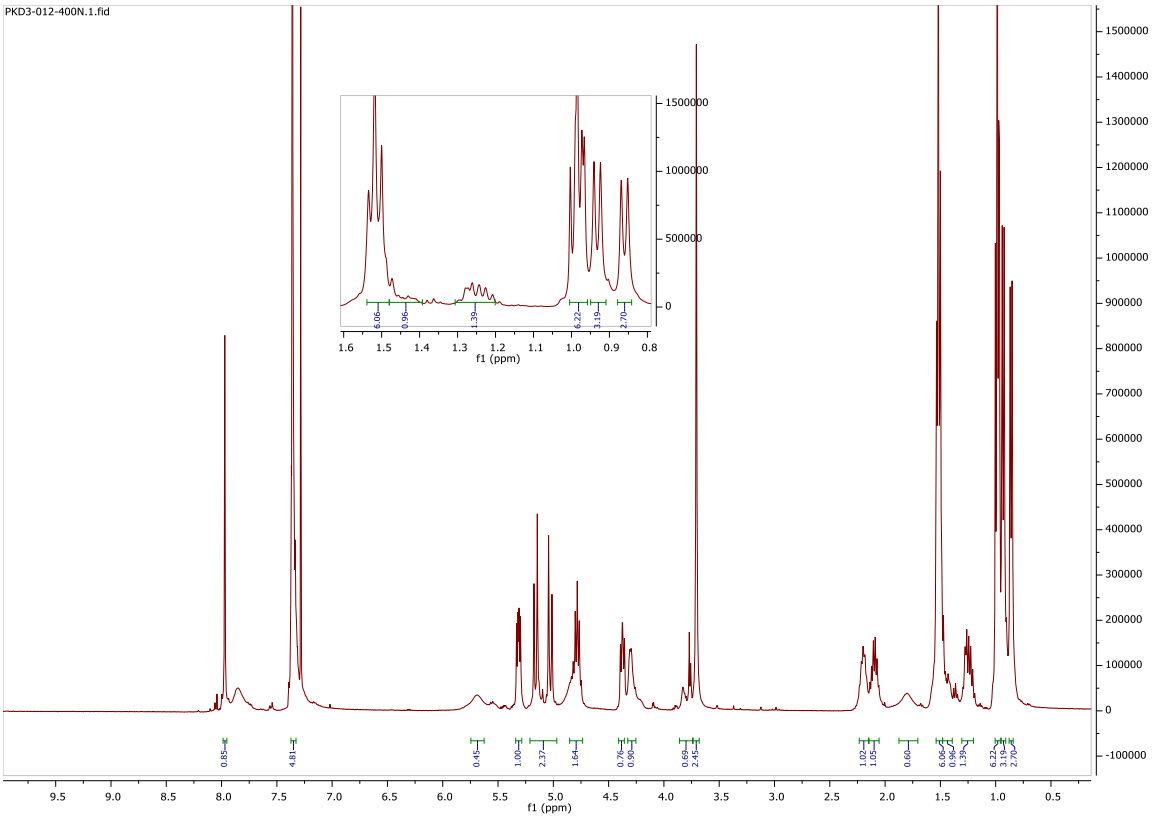
PKD3-012-400N.1.fid
f1 (ppm)

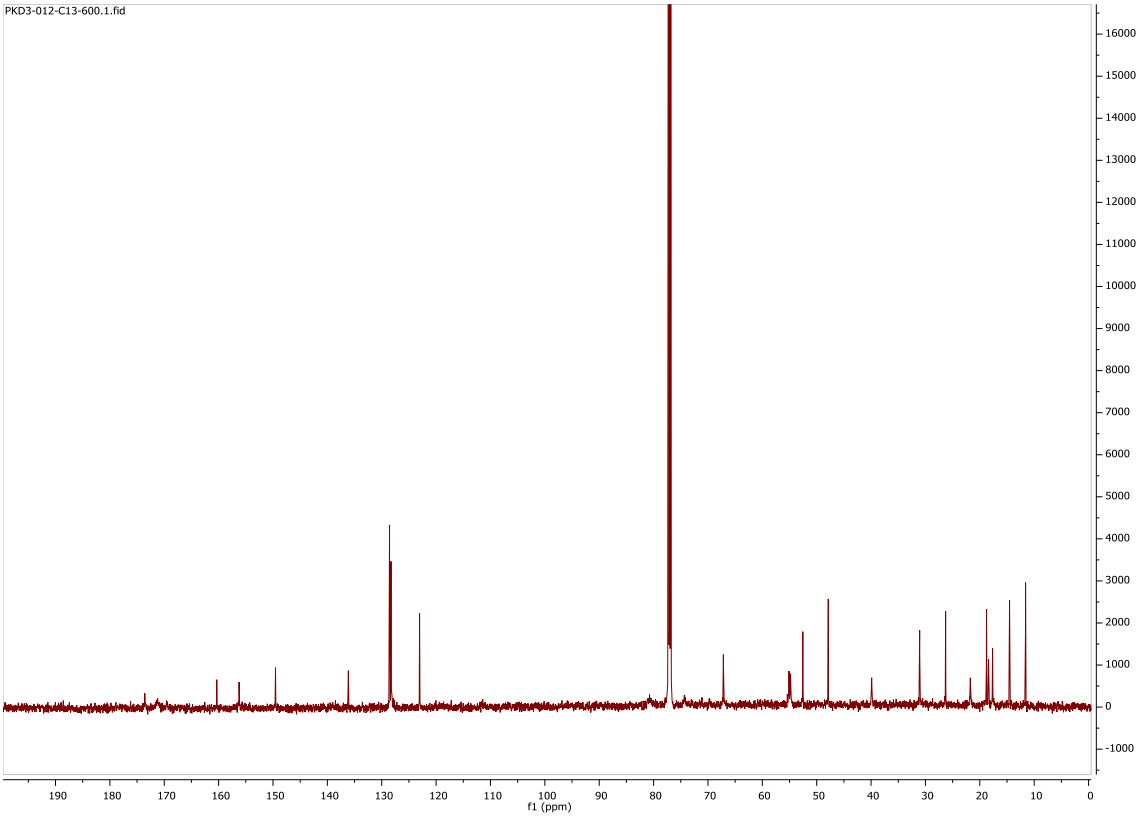
PKD3-012-C13-600.1.fid
f1 (ppm)

Methyl (2-((1R,2S)-1-((4S,5R)-2-((S)-1-amino-2-methylpropyl)-5-methyl-4,5-dihydrooxazole-4-carboxamido)-2-methylbutyl)thiazole-4-carbonyl)-*D*-alaninate

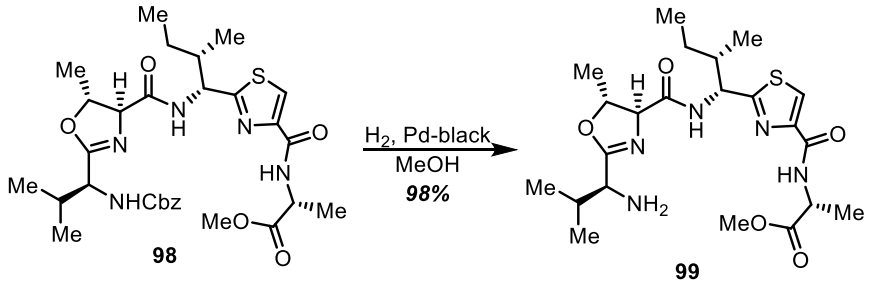

In a flask **98** was dissolved in enough solvent to bubble hydrogen gas. Palladium-black (10 eq.) was added and the system was sealed. Hydrogen gas was bubbled with a venting needle for ~10 minutes. The extra venting needle was removed, and reaction was vigorously stirred for 30 minutes. Palladium was filtered using celite and the filtrate was concentrated under reduced pressure to yield **99** quantitatively. R_f = 0.0 (3:1 ethyl acetate/hexanes): (Deprotected material retain in the baseline)

^{1}H NMR (400 MHz, Methanol-d_4) δ 8.18 (s, 1H), 5.30 (d, *J* = 6.4 Hz, 1H), 4.84 – 4.76 (m, 1H), 4.67 (q, *J* = 7.2 Hz, 1H), 4.39 (dd, *J* = 7.1, 1.1 Hz, 1H), 3.78 (s, 3H), 3.50 (dd, *J* = 5.8, 1.1 Hz, 1H), 3.21 (q, *J* = 7.3 Hz, 2H), 2.35 – 2.21 (m, 1H), 2.08 – 1.96 (m, 1H), 1.54 (d, *J* = 7.3 Hz, 3H), 1.49 (d, *J* = 6.3 Hz, 3H), 1.33 (t, *J* = 7.3 Hz, 3H), 1.29 – 1.23 (m, 1H), 1.04 – 0.96 (m, 12H).

Notebook Entries

Procedure: PKD2-411

^{1}H: PKD2-411-crude-MeOH-400N (Crude NMR)

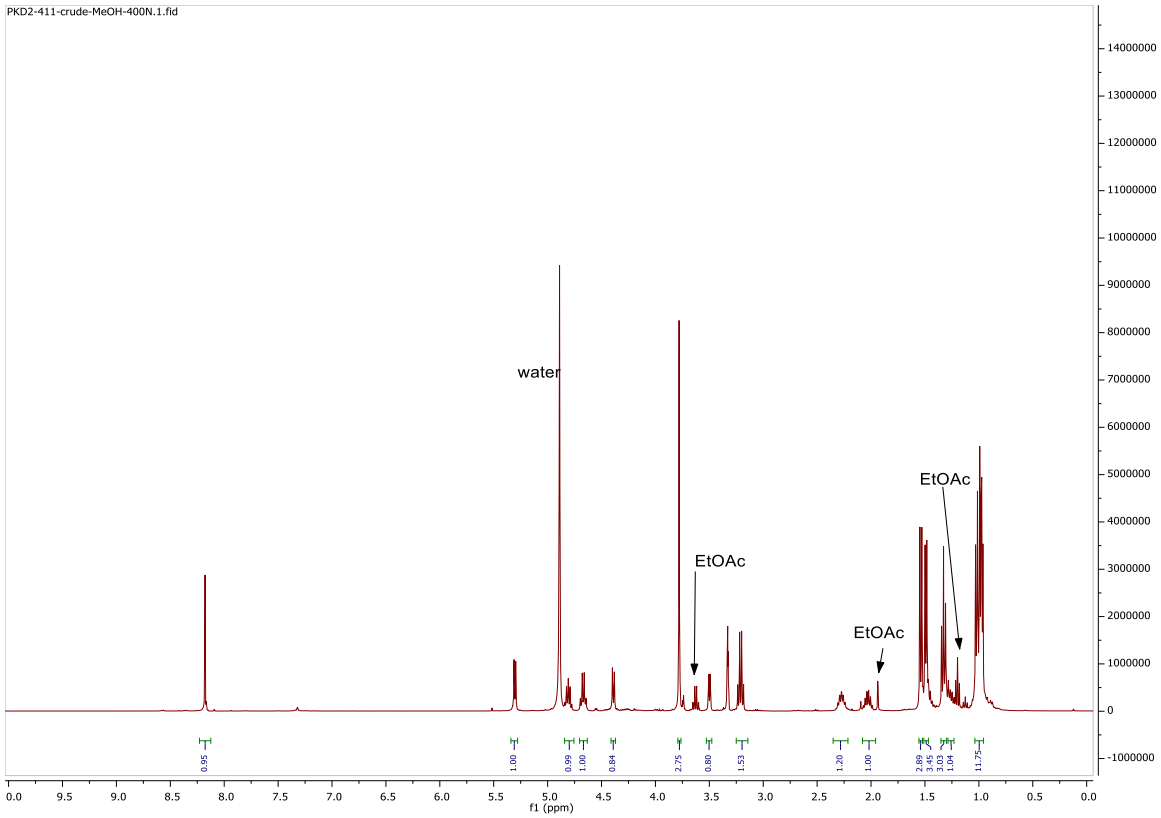
PKD2-411-crude-MeOH-400N.1.fid
water
EtOAc
EtOAc
EtOAc
f1 (ppm)

Methyl (2-((1R,2S)-1-((4S,5R)-2-((S)-1-((2S,3R)-2-(((benzyloxy)carbonyl)amino)-3-hydroxybutanamido)-2-methylpropyl)-5-methyl-4,5-dihydrooxazole-4-carboxamido)-2-methylbutyl)thiazole-4-carbonyl)-*D*-alaninate

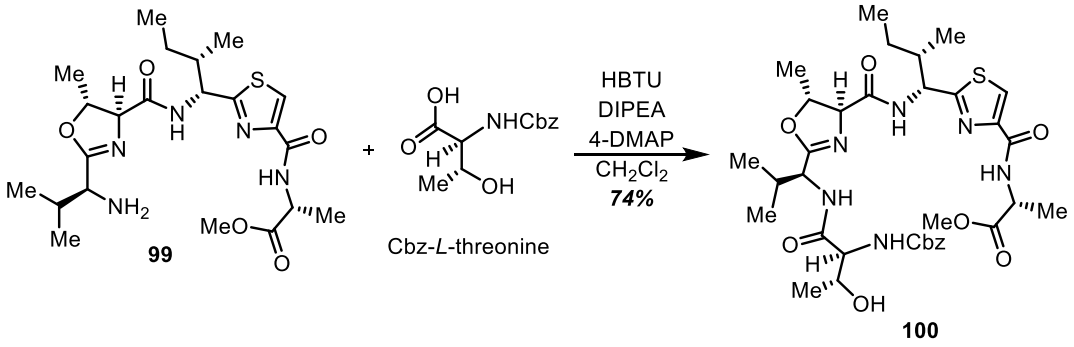

Reaction was performed using standard HBTU peptide coupling conditions. The product was afforded in 74% yield with purification by flash column chromatography with 3:1 ethyl acetate/hexanes. R_f = 0. 3 (3:1 ethyl acetate/hexanes).

^{1}H NMR (400 MHz, Chloroform-*d*) δ 8.23 (d, *J* = 8.8 Hz, 1H), 8.04 (s, 1H), 7.44 (d, *J* = 8.8 Hz, 1H), 7.36 (q, *J* = 5.0, 3.7 Hz, 5H), 5.79 (d, *J* = 8.0 Hz, 1H), 5.31 (dd, *J* = 8.9, 4.9 Hz, 1H), 5.12 (d, *J* = 1.8 Hz, 2H), 5.07 – 4.96 (m, 1H), 4.94 – 4.85 (m, 1H), 4.61 (ddd, *J* = 8.4, 4.3, 1.7 Hz, 1H), 4.44 (dd, *J* = 8.0, 4.1 Hz, 1H), 4.28 (dd, *J* = 6.6, 4.3 Hz, 1H), 4.25 – 4.20 (m, 1H), 3.82 (s, 2H), 2.25 – 2.15 (m, 1H), 2.01 (q, *J* = 6.3 Hz, 1H), 1.62 (d, *J* = 7.3 Hz, 3H), 1.54 (d, *J* = 6.2 Hz, 4H), 1.22 (d, *J* = 6.5 Hz, 3H), 1.17 – 1.09 (m, 1H), 0.97 (dd, *J* = 8.5, 6.7 Hz, 9H), 0.72 (d, *J* = 6.9 Hz, 3H).

^{13}C NMR (151 MHz, Chloroform-*d*) δ 174.96, 170.45, 169.49, 160.34, 156.06, 149.23, 136.19, 128.57, 128.22, 127.97, 123.55, 67.80, 66.97, 58.10, 54.56, 53.59, 52.91, 47.48, 41.17, 29.73, 29.17, 26.02, 21.54, 18.88, 18.60, 17.40, 16.52, 14.43, 11.68.

Notebook Entries

Procedure: PKD2-412-400N

^{1}H: PKD2-412-400N, ^{13}C: PKD3-015-C13-2nd-600N

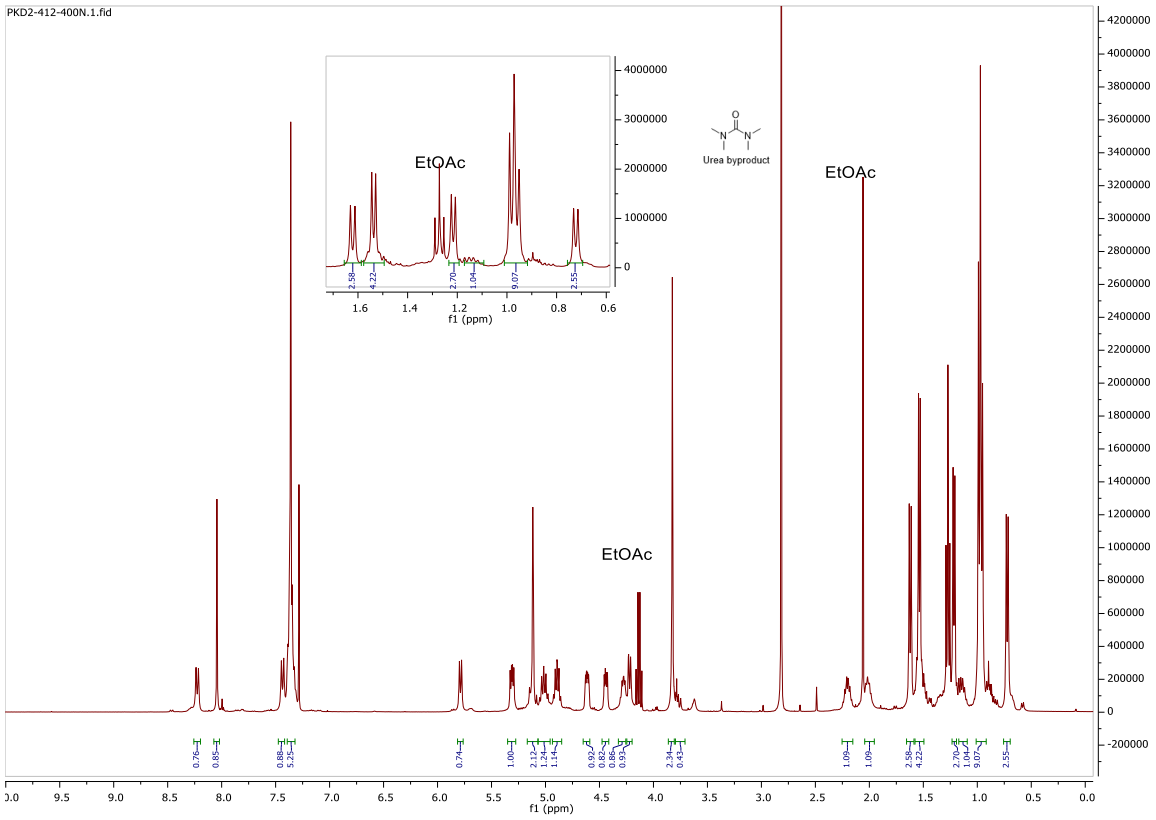

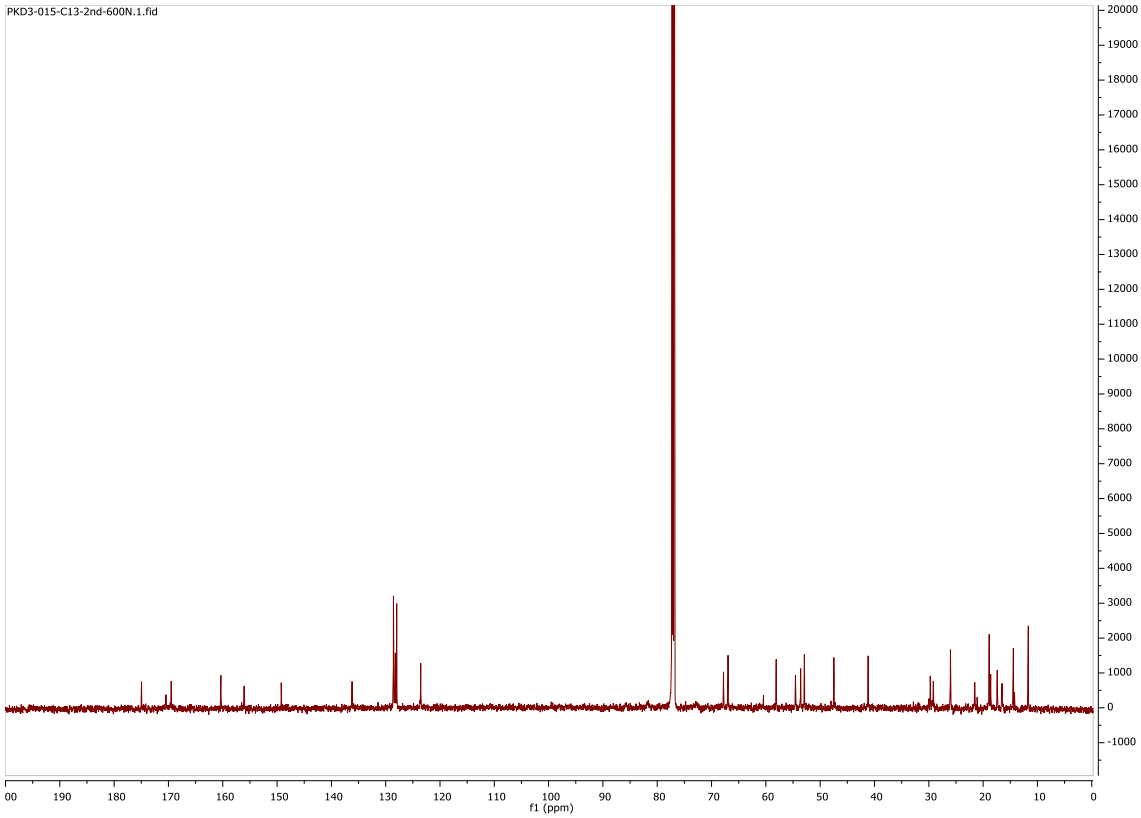
PKD3-015-C13-2nd-600N.1.fid
20000
19000
18000
17000
16000
15000
14000
13000
12000
11000
10000
9000
8000
7000
6000
5000
4000
3000
2000
1000
0
-1000
00
190
180
170
160
150
140
130
120
110
100
90
80
70
60
50
40
30
20
10
0
f1 (ppm)

(2-((1R,2S)-1-((4S,5R)-2-((S)-1-((2S,3R)-2-amino-3-hydroxybutanamido)-2-methylpropyl)-5-methyl-4,5-dihydrooxazole-4-carboxamido)-2-methylbutyl)thiazole-4-carbonyl)-*D*-alanine

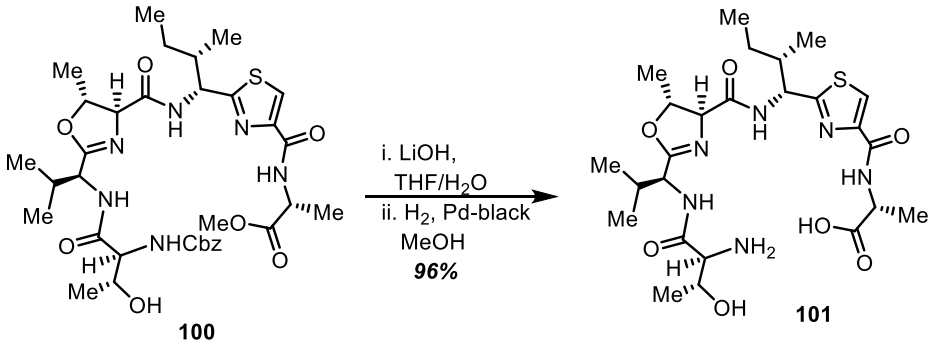

The reaction was performed using saponification conditions and proceeded to Cbz deprotection. The free carboxylic acid was dissolved in enough solvent to bubble hydrogen gas. Palladium-black (10 eq.) was added and the system was sealed. Hydrogen gas was bubbled with a venting needle for ~10 minutes. The extra venting needle was removed, and reaction was vigorously stirred for 30 minutes. Palladium was filtered using celite and the filtrate was concentrated under reduced pressure to yield **101**. R_f = 0.0 (3:1 ethyl acetate/hexanes): (Deprotected material retain in the baseline). The product **101** was obtained and proceeded to attempted macrocyclization. Rf = 0.0 (3:1 ethyl acetate/hexanes): (Deprotected material retain in the baseline)